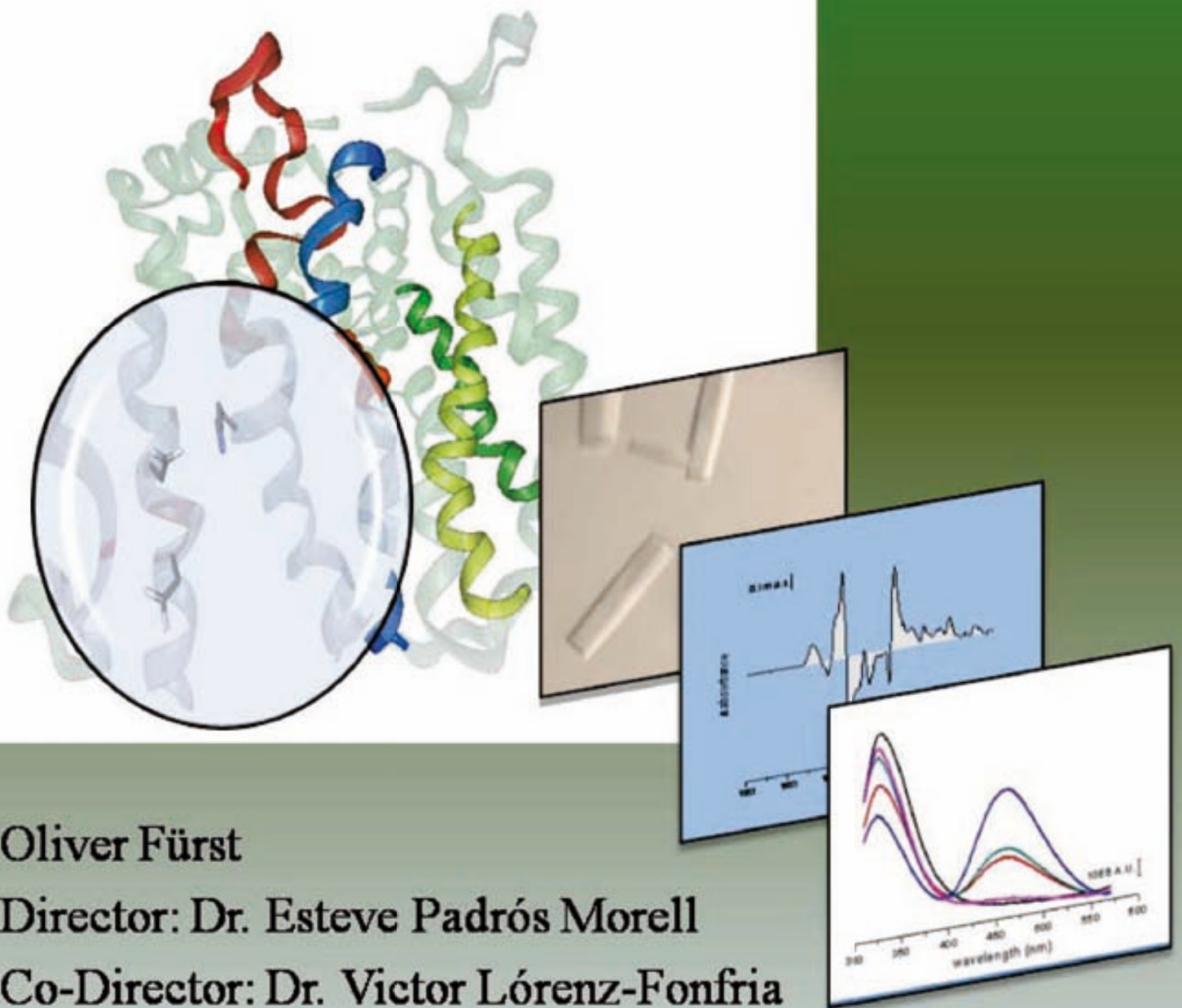


# Biophysical Studies of the C-terminal domains of the melibiose transporter from *Escherichia coli*



Oliver Fürst

Director: Dr. Esteve Padrós Morell

Co-Director: Dr. Victor Lórenz-Fonfria

CEB – Centre d'Estudis en Biofísica

Universitat Autònoma de Barcelona



**Biophysical Studies of the C-terminal  
domains of the melibiose transporter  
from *Escherichia coli***

PhD thesis presented by Oliver Fürst to obtain the

Title of doctor.

This work has been realized in the CEB-Unitat de Biofísica

in the Departament of Biochemistry and Molecular Biology

Facultat de Medicina

at the Universitat Autònoma de Barcelona,

under the supervision of Dr. Esteve Padrós Morell and Dr. Victor Lórenz-Fonfria.

read and certified by the directors

Dr. Esteve Padrós Morell

Dr. Victor Lorenz-Fonfria

Bellaterra,

July 2012



---

# TABLE OF CONTENTS

TABLE OF CONTENTS.....	3
ABBREVIATIONS .....	7
INTRODUCTION.....	9
1.    Proteins – the essentials of life.....	9
1.1.    Membrane proteins.....	9
1.2.    The major facilitator superfamily.....	13
1.3.    The Glycoside-pentoside-hexorunide (GPH) family .....	15
2.    The melibiose permease.....	16
2.1.    Melibiose permease as a model for the active sugar-cation co-transport.....	16
2.2.    Properties of the melibiose permease.....	18
2.3.    Alternating access model as source of mechanistic understanding.....	20
2.4.    MelB structural organization in 2D and 3D .....	31
2.5.    3D structure of related $\alpha$ -helical membrane transporter.....	31
3.    Biophysical insights of the melibiose carrier .....	37
3.1.    Intrinsic fluorescence by Trp excitation .....	37
3.2.    Dns <sup>2</sup> -S-Gal as external probe for FRET analyses .....	38
3.3.    Structural information of MelB by FTIR .....	39
MATERIALS AND METHODS.....	45
4.    Materials.....	45
4.1.    Chemicals.....	45
4.2.    Media for bacterial growth.....	45
4.3.    Buffers for protein Purification .....	46
4.4.    Buffers used in infrared spectroscopy experiments.....	47
4.5.    Buffer for the preparation of RSO and ISO vesicles.....	48
5.    Methods.....	49
5.1.    Preparation of Proteoliposomes .....	49

## TABLE OF CONTENTS

---

5.2.	Infrared spectroscopy .....	61
5.3.	Fluorescence spectroscopy .....	77
SCOPE AND OBJECTIVES .....		83
6.	Why to choose MelB as a raw model for the study of membrane transport.....	83
RESULTS .....		85
7.	Lys-377 – an important residue for the function of the melibiose symporter?.....	85
7.1.	Lys-377 replacement affects the substrate binding.....	85
7.2.	Fluorescence spectroscopy of the Lys-377 single mutants.....	95
7.3.	Lys-377 revertants .....	99
7.4.	Absorbance spectra of the single mutants and revertants.....	106
7.5.	Fluorescence analysis of the Ile-22 mutants.....	107
7.6.	Revertants with L326F mutation .....	109
7.7.	Is there a salt bridge between Lys-377 and aspartic acids 55 and 59?.....	118
7.8.	MIANS analysis of K377C and K377C/I22S mutants.....	121
7.9.	FRET analyses of the vesicles of the mutants related to Lys-377 .....	122
7.10.	ISO/RSO vesicles of Lys-377 revertants and selective single mutants .....	125
7.11.	Importance of the charge of residue Lys-377 .....	128
8.	Charged residues in loop 10-11 .....	130
8.1.	Na-binding of the MelB mutants of the charged amino acids of the loop 10-11	131
8.2.	The effect of melibiose binding.....	133
8.3.	Fluorescence spectroscopy .....	138
8.4.	ISO and RSO FRET data of the mutants of the loop 10-11.....	139
9.	Elucidating the importance of residues in helix XI .....	142
9.1.	IR <sub>diff</sub> triggered by the cation.....	143
9.2.	Melibiose-mediated IR <sub>diff</sub> of helix XI mutants.....	144
9.3.	Fluorescence experiments of the helix XI mutants.....	149
9.4.	Labeling of cysteines in helix XI with the fluorescent probe MIANS .....	151
9.5.	Examining the FRET in membrane vesicles of the mutants from helix XI.....	153
10.	Trp-342, a suggested participant in sugar binding.....	156
10.1.	Phenotype of W342C.....	156
10.2.	W342C – IR <sub>diff</sub> spectra .....	157

10.3. Fluorescence spectra of W342C.....	159
10.4. Fluorescence energy transfer mediated by fluorescent sugar.....	160
DISCUSSION .....	163
11. Proteoliposomes vs vesicles – chances and boundaries .....	163
12. Lys-377 – the significance of the positively charged residue.....	165
13. Lys-377 and its “revertants”.....	168
14. loop 10-11 as a functional domain? .....	173
15. Helix XI as mainly hydrophobic segment facing the aqueous channel in MelB ....	177
16. Outlook.....	181
SUMMARY OF THE THESIS.....	183
RESUMEN DE LA TESIS .....	187
BIBLIOGRAPHY .....	191
ACKNOWLEDGEMENTS .....	203



# ABBREVIATIONS

## Amino acids

A	Ala alanine	M	Met methionine
C	Cys cysteine	N	Asn asparagine
D	Asp aspartic acid	P	Pro proline
E	Glu glutamic acid	Q	Gln glutamine
F	Phe phenylalanine	R	Arg arginine
G	Gly glycine	S	Ser serine
H	His histidine	T	Thr threonine
I	Ile isoleucine	V	Valvaline
K	Lys lysine	W	Trptryptophane
L	Leu leucine	Y	Tyrtyrosine

## General Abbreviations

ATP	adenosine-triphosphate
ATR-FTIR	attenuated total reflection Fourier-Transform Infrared Spectroscopy
bp	base pairs
BSA	bovine serum albumin
C-less	MelB free of all intrinsic cysteines
cm <sup>-1</sup>	unit of FTIR (resolution)
DDM	dodecyl-maltoside
DM	decyl-maltoside
DMSO	dimethyl sulfoxide
Dns <sup>2</sup> -S-Gal, D <sup>2</sup> G	2'-( <i>N</i> -dansyl) aminoethyl-1-thio-β-D-galactopyranoside
DTT	1,4-dithio-treitol
FRET	Förster energy transfer
FTIR	Fourier-transform Infrared spectroscopy
GPH	glucoside-pentoside-hexuronide:cation symporter family
h	hour
IR <sub>diff</sub>	infrared difference
ISO	inside-out
K377R/L236F <sub>DDM</sub>	MelB mutant K377R/L236F solubilized with DDM
KPi	potassium-phosphate-buffer (K <sub>2</sub> HPO <sub>4</sub> + KH <sub>2</sub> PO <sub>4</sub> )

## ABBREVIATION

---

<i>lacY</i>	gene coding for the lactose permease from <i>E. coli</i>
LacY	lactose permease from <i>E. coli</i>
LAPAO	3-(laurylamido)- <i>N,N'</i> -dimethylaminopropylamine oxide
LB	Luria Bertani broth
mel	melibiose [ $\alpha$ -D-galactopyranosyl-(1 $\rightarrow$ 6)- $\alpha$ -D-glucopyranose]
<i>melA</i>	gene coding for the $\alpha$ -galactosidase from <i>E. coli</i>
<i>melB</i>	gene coding for the melibiose permease from <i>E. coli</i>
MelB	melibiose permease from <i>E. coli</i>
<i>melR</i>	gene of the Regulator protein for the operon activation from <i>E. coli</i>
MFS	major facilitator superfamily
MIANS	2-(4'-maleimidylanilino) naphthalene-6- sulfonic acid
min	minute
$\mu$ L	microlitre
$\mu$ M	micrometer
mL	millilitre
mM	millimolar
MTS	methanethiosulfonate
MTSET <sup>+</sup>	[2-(trimethylammonium)ethyl] methanethiosulfonate
MTSEA <sup>+</sup>	(2-aminoethyl) methanethiosulfonate
NaCl	sodium chloride
NaPi	sodium- phosphate-buffer ( $\text{Na}_2\text{HPO}_4 + \text{NaH}_2\text{PO}_4$ )
NEM	<i>N</i> -ethyl maleimide
ng	nanogram
nm	nanometer
PAGE	polyacrylamide gel electrophoresis
PCMBs	p-chloromercuribenzenesulfonate
PCR	polymerase chain reaction
psi	pressure per square inch (1 psi = 6.895 x 10 <sup>3</sup> Pascal = 68.95 x 10 <sup>-3</sup> bar)
RSO	right-side-out
s	second(s)
SDS	sodium dodecyl sulfate
TB	terrific broth
TBS	Tris-buffered saline
TDG	thio
TMG	methyl-1-thio- $\beta$ -galactopyranoside
TMRM	tetamethylrhodamine-5-maleimide
UV-VIS	ultraviolet – visible
$\alpha$ -NPG	$\rho$ -nitrophenyl- $\alpha$ -D-6-galactopyranoside

# INTRODUCTION

## 1. Proteins – the essentials of life

The greater goal for protein scientists is the elucidation of the structure-function relationship for every single protein available in all organisms. Another challenging objective is the cure of diseases linked to proteins. Thus, to extend further such possibilities the study and understanding of the proteins remains of great significance. What all organisms have in common is that their entire physicochemical appearance and functioning rely on a complex network associated to biomolecules (proteins, nucleic acids, lipids, ...). Hence, it is of absolute desire to understand life by explaining the function of the biomolecules in general and of proteins in particular. Basically, all proteins are composed of amino acids which vary not only in functional chemical groups but also in size. Proteins can be divided into two major groups considering the preferential type of amino acids they contain. On one side, there are the soluble proteins, with a high proportion of hydrophilic amino acids, which makes them soluble in aqueous solutions. The cell's biggest compartment is the cytoplasm. It is composed mainly of an aqueous solution, which delivers the perfect environment for soluble proteins.

The proteins containing large hydrophobic domains are located in cell membranes, which define the cell's compartments. Therefore, they are called membrane proteins. This group will precipitate in water, but are soluble in organic solutions. Being in the cell's membranes, membrane proteins are primarily responsible for processes involving exchange of materials and energy between the cell exterior and interior. Numerous vital assignments are attributed to these proteins, such as ejection of toxic products or signal transduction into the cells. Since their habitat is restricted to the membrane, their number is rather scarce compared to the soluble fraction. Also, their expression and purification is far from trivial, making them worth studying.

### *1.1. Membrane proteins*

The cell membrane insulates the cytosol from the outer medium. In addition, it delineates a unique compartment for the chemical reactions that sustain life. But, since no organism survives in isolation, the cell membrane must also mediate the transduction of signals from the exterior to the interior (and *vice versa*), electrical currents and the transport of chemical compounds. Ubiquitous membrane protein families are heterogeneously spread along the bilayer, serving the cell. The lipid bilayer forms a perfect host for the membrane proteins due to its hydrophobic core region. The amphiphilic character of the lipids is established as the heads dwell in aqueous surrounding. As most integral membrane proteins span the entire lipid bilayer, they mimic this attribute by consisting of hydrophobic amino acids in their bulk and hydrophilic residues in the

flanks. Membrane proteins also form complexes where the protein only partially stripes the membrane and the center is cytosol-located. In the case of the human genome, it was estimated that all proteins with membrane segments comprise when combined between 15-39% of all coded proteins<sup>1</sup>. For lower organisms with a sequenced genome, as for example the prokaryote *Escherichia coli*, the eukaryote *Saccharomyces cerevisiae* and the archaea *Pyrococcus horikoshii*, the total quantity of membrane proteins is known. The values for eubacteria and eukaryotic organisms correlated very well. In *E. coli* and *P. horikoshii* 29.9% of the whole chromosome encodes for membrane spanning proteins and in *S. cerevisiae* also 28.2% of its genome codes for this protein class<sup>2</sup>. This data in turn delivers the information that in spite of differences in the biological architecture, the amount accounting for membrane proteins seems to be stable in different organisms.

Cells have to adapt to all possible environmental changes. Thus, they use membrane proteins as a kind of antenna to sense changes in the environment. Membrane proteins are often coupled to other proteins in the cell interior, or induce metabolic adaptations through influx or efflux of chemicals or ligands. This also works to communicate with other cells, in order to adjust their anabolic and catabolic processes.

In general, membrane proteins serve as transport systems in the three domains of life: in archaea, in prokaryotes and in eukaryotic cells. Numerous tasks are assigned to membrane proteins such as: the transport of carbon-, nitrogen- and sulfur-sources, the regulation of anabolic and catabolic substances by excretion, drug extrusion and the maintenance of homeostasis. Furthermore, membrane proteins are also in charge of transporting neurotransmitters within organisms and hence allowing the organism to react upon external stimuli. Regarding the complexity of life forms, membrane proteins suit as servants in warfare as well. Antiviral and antifungal agents are just two examples to exploit cellular transport systems.

Considering the type of organism, the membrane architecture differs immensely. The class of bacteria is divided due to its envelope design. A dye, called Gram's stain, is the exclusive criteria determining the bacterium's capacity to retain the dye or not. Hence, bacteria tending to be stained with this dye are classified as gram-positive and bacteria unable to retain the dye are selected into the gram-negative group. Gram<sup>+</sup> bacteria are composed of several layers of peptidoglycan, whereas the gram<sup>-</sup> class is surrounded by a primary membrane composed of phospholipids and lipopolysaccharide molecules. Underneath, the periplasmic space harbors an additional compartment for cell nutrition, delivery or chemical modification of compounds. Finally, a secondary cell membrane encloses the cytoplasm embedding the majority of the membrane proteins.

For the gram-negative model organism *Escherichia coli*, each membrane contains an array of various membrane proteins responsible for specific assignments. Proteins embedded in the phospholipid double layer encompass all kinds of membrane protein families. Most of these polypeptides are in charge of transporting solutes or ions into or out of the cell. Relatively small substances such as oxygen or fatty acids just pass the cell membrane by diffusion without

regulating transport systems. Also, polar molecules like carbon dioxide enter the cell by simple diffusion through the phospholipid double layer. To maintain the cytosolic homeostasis, a controlled exchange of large polar and even charged molecules or ions with the external medium is required. This process is accomplished by membrane transport proteins. Depending on the size, shape or chemical properties of the molecule, these characteristic proteins help the target molecule to cross the membrane barrier.

Protein channels are one class of membrane proteins. In principle, channels act as a kind of restricted “funnel”. They open up selectively for some specific ions using a complex filter system. Only ions with the correct charge and size will pass the channel filter and being channeled through the membrane. Channels are categorized into ungated, voltage-gated, ligand-gated, mechanically-gated and temperature-gated subfamilies, depending on the event triggering the opening of the channel. Lately, ion channel proteins gain tremendous attention relating to their involvement in various diseases. Especially, the understanding of voltage-dependent channels for  $\text{Na}^+$ ,  $\text{K}^+$ ,  $\text{Ca}^{2+}$  and  $\text{Cl}^-$  ions advanced immensely during the previous decade due to the crystal structure information available<sup>3-5</sup>. Channel proteins change their states from open to close or *vice versa* in response to the membrane potential. The ligand-gated channels require an inducer molecule as the trigger event. The paradigm of this class is the acetylcholine receptor<sup>4</sup>. Either an internal or an external stimulus controls the mechanism of channels. Generally, no further energy

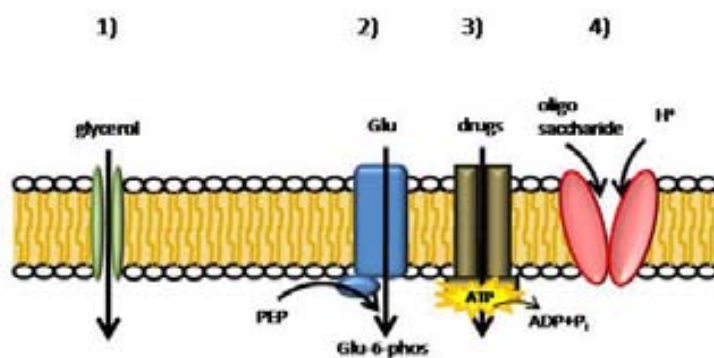


Figure 1.1 Different types of transport; 1) channels (e.g. GlpF for glycerol transport), 2) group translocators (glucose-PTS system), 3) primary transporters (ABC transporter), 4) secondary transporters (e.g. melibiose permease) ; slightly modified after Paulsen *et al.*<sup>6</sup>

input is required for this “passive” diffusion process.

A second more versatile group encompasses membrane proteins which transport molecules not by providing them through a pore, but by binding them. The process by which membrane proteins are using an energy source to transport compounds across the cell membrane is called facilitated diffusion. To classify these

membrane proteins, several terms are used namely porters, carriers, transporters or permeases. The design of the transport process differs among this second type of integral membrane proteins. A chemical modification accompanying the actual transport mechanism is exclusively executed by group translocators<sup>5</sup>. In bacteria the transport system for carbohydrates alters the ligand by phosphorylation and facilitates the uptake process. A second possibility for carrying elementary substances across the cell membrane is displayed by the termed primary transporter family. This class of transport proteins requires an external energy source. The input could be either photons, chemical or electrical energy. An ATP-binding cassette carrier has been discovered as on the most

promising drug targets among primary transport proteins for human cells. Targeting abnormalities of those diverse clustered proteins, knowledge on drug absorption and metabolism has advanced tremendously<sup>7</sup>. Thus, new methods dedicated to drug selectivity and pharmacokinetics offer substantial hope for progress in the field of membrane protein associated diseases.

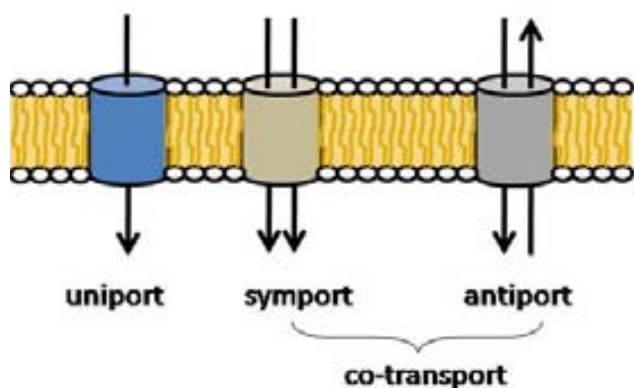


Figure 1.2 All three types of transport across the phospholipid bilayer, black arrows indicate the number of solutes and the direction of transport

Reported as secondary active transport proteins, the last subfamily of active transporters exploits the energy stored in the transmembrane ion-gradient. This class transports two substances in parallel by using the energy from the electrochemical potential. If the substrates are transported in the same direction, the process is called symport. Antiport refers to the transport of the ligands in counter direction (Fig. 1.2). These transporters are regulated by ligand

coupling or by an electrical membrane potential. As most abundant co-substrates, the proton or sodium, the selectivity is linked by a few crucial residues of the polypeptide backbone. Interestingly, solute transporters which use either  $H^+$  or  $Na^+$  as ionic partner for their primary ligand, belong to distinctive families<sup>8</sup>.

The transporter classification database (TCDB; <http://www.tcdb.org/>) includes all superfamilies of different membrane protein transporters. Consisting of over 25 distantly related families, rigorous methods mostly based on computational alignments group membrane proteins depending on specific features.

Voltage-gated ion channel (VIC) superfamily is one of the largest families recognized. This family represents one of the major drug targets nowadays<sup>9-11</sup>.

Another family categorized in the TCDB library transports amino acids, polyamines and organocations. Abbreviated as APC, this family uses monovalent cations to drive the transport mechanism.

Table 0.1 Comparison of the membrane transporter content in all three kingdoms of life. Data retrieved from Transport DB<sup>12,13</sup>.

<b>Organism</b>	<b>ion channels</b>	<b>group translocators</b>	<b>primary transporter</b>	<b>secondary transporter</b>	<b>un-classified</b>
<i>H. volcanii</i>	15 (7.6%)	7 (3.5%)	76 (38%)	100 (50%)	2 (1%)
<i>E. coli K-12 MG1655</i>	13 (3.7%)	29 (8.2%)	74 (20.9%)	235 (66.4%)	2 (0.6%)
<i>S. cerevisiae S288C</i>	20 (6.3%)	-	70 (22%)	225 (70.8%)	1 (0.3%)
<i>C. elegans</i>	234 (35.8%)	-	72 (11%)	348 (53.2%)	-
<i>H. sapiens</i>	391 (38.3%)	-	139 (13.6%)	447 (43.7%)	40 (3.9%)

## 1.2. The major facilitator superfamily

As the most investigated superfamily, the major facilitator superfamily (MFS) stands out as a prototype for all membrane transporters. Together with the ABC superfamily, MFS transporters encode for a vast majority of transporters in prokaryotes<sup>6</sup>. Nevertheless, MFS carriers are also described for mammalian cells<sup>14</sup>. Currently, this superfamily has 28 subfamilies of diverse characteristics<sup>15</sup>. These versatile families (Table 1.2) display vast ligand specificity, as for anions, carbohydrates, organo-cations, peptides and glycopeptides, siderophore iron complexes as well as drugs, neurotransmitter and hydrophobic complexes. Some of these families have not been described yet considering their substrate specificity. A few distant related groups display the ability to couple pigments, organic anions, peptides and specific sugars<sup>15</sup>.

Table 0.2 Major facilitator subfamilies (MFS) after Saier, 2000<sup>15</sup>

TC number	MFS families
2. A.1.1	Sugar porter family
2. A.1.2	Drug: H <sup>+</sup> antiporter-1 family
2. A.1.3	Drug: H <sup>+</sup> antiporter-2 family
2. A.1.4	Organophosphate:Pi antiporter family
2. A.1.5	Oligosaccharide:H <sup>+</sup> symporter family
2. A.1.6	Metabolic:H <sup>+</sup> symporter family
2. A.1.7	Fucose:H <sup>+</sup> symporter family
2. A.1.8	Nitrate/nitrite porter family
2. A.1.9	Phosphate:H <sup>+</sup> symporter family
2. A.1.10	Nucleoside:H <sup>+</sup> symporter family
2. A.1.11	Oxalate:formate antiporter family
2. A.1.12	Sialate:H <sup>+</sup> symporter family
2. A.1.13	Monocarboxylate porter family
2. A.1.14	Anion:cation symporter family
2. A.1.15	Aromatic acid:H <sup>+</sup> symporter family
2. A.1.16	Siderophore-iron transporter family
2. A.1.17	Cyanate permease family
2. A.1.18	Polyol permease family
2. A.1.19	Organic cation transporter family
2. A.1.20	Sugar efflux transporter
2. A.1.21	Drug: H <sup>+</sup> antiporter-3 family
2. A.1.22	Vesicular neurotransmitter transporter family
2. A.1.23	Conjugated bile salt transporter
2. A.1.24	Unknow facilitator family-1
2. A.1.25	Peptide acetyl-coenzyme A transporter family
2. A.1.26	Unknow facilitator family-2
2. A.1.27	Phenyl propionate permease family
2. A.1.28	Unknow facilitator family-3
2.A.2	Glycoside-pentoside-hexuronide: catio symporter family
2.A.17	Proton-dependent oligopeptide transporter family
2.A.60	Organo anion transporter family
2.A.71	Folate-biopterin transporter family
2.A.48	Reduced folate carrier family
97.7	Putative bacteriochlorophyll delivery family

The MFS classified carriers are capable of transporting their substrates in parallel or anti-parallel fashion, to or against a concentration gradient. The transport of a solute which is already accumulated to higher concentrations in the cell than outside is thermodynamically unfavorable. However, the process is empowered by an electrochemical gradient of some cation<sup>16</sup>. Although, the majority of the MFS polypeptides function as transporters, a few proteins also transmit signals to the cell interior.

Regarding the topology of MF superfamily members, almost all proteins share an architecture of 12 membrane spanning helices. This observation is in line with discoveries of the gene duplication events described by the Saier lab<sup>17</sup>. The prehistoric membrane transporter consisted of just 2 helices. Gene duplication eventually resulted in 12 transmembrane helices as the preferential number among MFS proteins.

### *1.3. The Glycoside-pentoside-hexuronide (GPH) family*

As announced in the Table 1.2 the glucoside-pentoside-hexuronide (GPH) subfamily is remotely related to the major facilitator superfamily as concluded from PSI-BLAST and hydrophathy analysis<sup>18</sup>. Membrane proteins classified within this family couple mostly oligosaccharides<sup>19,20</sup>. But noteworthy, members of the GPH family are not linked to other sugar transport families<sup>15</sup>.

Constituents of this family couple monovalent cations to drive the transport. Explicitly, either H<sup>+</sup>, Na<sup>+</sup> or Li<sup>+</sup>, are used as liganding ions by this protein family. Although the major part of the group members belong to prokaryotes, also GPH protein have been already identified in eukaryotic cells<sup>21-24</sup>.

All membrane transporters have a common size of around 400 to 500 amino acids. Usually they transport relatively small sugar molecules across the membrane. Prokaryotic GPH facilitators are linked to the group translocators. Therefore, the longer C-terminal segment is probably modulated by the PEP-PTS systems<sup>20</sup>. Although typically consisting of 12 membrane-spanning helices, the homology between the transporters is relatively low.

All recognized GPH proteins function as monomers except the LacS from *S. thermophilus*. Its dimer follows two distinctive pathways to translocate the substrate molecules<sup>25</sup>.

The melibiose permease from *Escherichia coli* is the best studied member of the GPH family.

Table 0.3 Listed TC sugar transport families after TC criteria modified from Saier, 2000 <sup>15</sup>

TC number	Family	# of members	Substrates
2.A.1.1.	SP	> 200	Glc, Fru, Man, Gal, Ara, Xyl, Mal, Lac, $\alpha$ -Gal, quinate, myoinositol
2.A.1.5.	OHS	> 20	Lac, Scr, Raf
2.A.1.7.	FHS	> 10	L-Fucose, Glc, Man, Gal
2.A.1.12.	SHS	> 10	Sialate, lactate, pyruvate
2.A.1.18.	PP	> 4	D-arabinitol, ribitol
2.A.1.20.	SET	> 10	Lac, Glc, Cel, Mal, $\alpha$ MG, IPTG, Kan, Strep, etc.
2.A.2.	GPH	>50	Mel, Lac, Scr, Raf, glucuronides, pentosides

## 2. The melibiose permease

### *2.1. Melibiose permease as a model for the active sugar-cation co-transport*

First described by Pardee<sup>26</sup> in *Escherichia coli*, the melibiose permease not only transports melibiose but also a variety of  $\alpha$ - and  $\beta$ - galactosides as well.

Due to a detailed study in 1965, the melibiose permease was entitled as a second methyl-1-thio-  $\beta$  -galactopyranoside permease (TMG II) besides the earlier established lactose permease<sup>27</sup>. Temperature sensitivity and substrate specificity were the main criteria to distinguish between TMG permease I and II. Later the names for TMG I and II permease were replaced by lactose permease (LacY) and melibiose permease (MelB), respectively. Even though related to each other, LacY and MelB display a low sequence homology. Both permeases however, have various substrates in common comprising various galactosides in  $\alpha$  or  $\beta$  configuration.

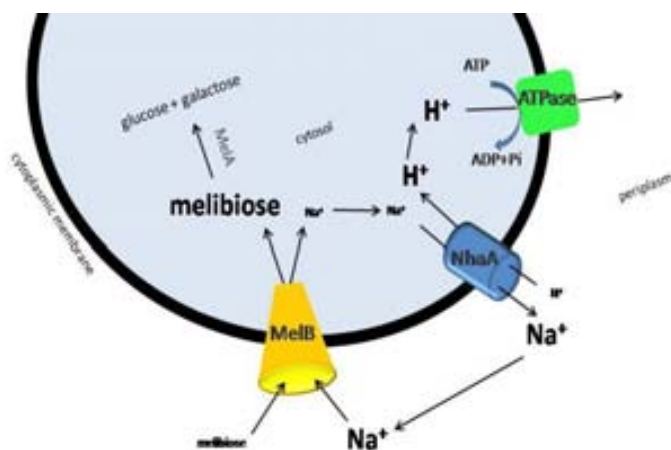


Figure 2.1 Sodium and proton cycle from cell exterior to interior mediated by the melibiose carrier (MelB in yellow), the  $\text{Na}^+/\text{H}^+$  antiporter (NhaA in blue) and the H-ATPase (in green) in *Escherichia coli*.

The concept for MelB of co-transporting the substrates arose from the work done by Stock & Roseman<sup>28</sup>. The melibiose carrier is expressed in various prokaryotic organisms like *Klebsiella pneumoniae*<sup>29</sup>, *Streptococcus thermophilus*<sup>30</sup>, *Salmonella typhimurium*<sup>31</sup> and *Escherichia coli*.

The homology between the proteins is fairly high and key residues are conserved. The melibiose carrier from *E. coli* has been extensively studied to receive functional and structural insights of the transport activity. Although possessing a relative high homology, melibiose transport proteins of different prokaryotic organisms differ in their cation specificity<sup>20</sup> (see Table 2.1).

Table 0.4 cation selectivity of the sugar transporters from *Escherichia coli* (MelB<sub>Ec</sub>, melibiose permease; LacY<sub>Ec</sub>, lactose permease), from *Salmonella typhimurium* (MelB<sub>Sy</sub>, melibiose permease), from *Enterobacter aerogenes* (MelB<sub>Ea</sub>, melibiose permease) and from *Klebsiella pneumoniae* (MelB<sub>Kp</sub>, melibiose permease), slightly modified after Poolman *et al.*<sup>20</sup> (TMG, methyl- $\beta$ -D-thiogalactopyranoside), nd implies not detected

Sugar	MelB <sub>Ec</sub>	MelB <sub>Sy</sub>	MelB <sub>Ea</sub>	MelB <sub>Kp</sub>	LacY <sub>Ec</sub>
$\alpha$ -galactosides (melibiose)	$\text{H}^+$ , $\text{Na}^+$ , $\text{Li}^+$	$\text{Na}^+$ , $\text{Li}^+$	$\text{H}^+$ , $\text{Li}^+$	$\text{H}^+$ , $\text{Li}^+$	$\text{H}^+$
$\beta$ -galactosides lactose TMG	$\text{Na}^+$ , $\text{Li}^+$	$\text{Na}^+$ , $\text{Li}^+$	$\text{H}^+$ , $\text{Li}^+$	$\text{H}^+$ , $\text{Li}^+$	$\text{H}^+$
monosaccharides (D-galactose)	$\text{Na}^+$ , $\text{Li}^+$	Nd	nd	Nd	$\text{H}^+$

Since the melibiose permease belongs to the secondary active transporters group, it requires an electrochemical gradient to drive the transport mechanism. It uses the free energy stored in the downhill transport of the co-substrate. If the membrane potential is not present, the downhill movement of the sugar delivers the required energy for the cation transfer.

First recognized as a pump translocating galactosides across the membrane bilayer by sodium and the proton as co-substrates, it was later reported that also lithium suits as a gradient-generating cation for the transport mechanism<sup>32,33</sup>. Sodium and lithium are the preferred co-substrates. Nevertheless, MelB is also able to use the proton-motive force for efficient transport<sup>34</sup>. The use of three different cations makes the melibiose carrier unique among secondary transporters. MelB has been postulated as a transition transporter between proton and sodium coupling carriers. This characteristic marks MelB for the study of versatile cation coupling.

As a major requirement for secondary transport systems, the membrane potential  $\Delta\mu_{H^+, Na^+}$  drives the mechanism. To steadily maintain the crucial  $Na^+$  and  $H^+$  homeostasis<sup>35</sup> (Fig. 2.1), the  $Na^+/H^+$  antiporter (NhaA in *E. coli*) carries protons across the bacterial membrane in exchange for sodium ions. If the electrochemical gradient is absent, the permease uses the downhill concentration gradient of the sugar to transport cations across the membrane.

## 2.2. Properties of the melibiose permease

The melibiose permease from *Escherichia coli*, as a member of the GPH subfamily, reveals details about the function and structure of secondary transporters. Although still lacking a 3D crystal structure, a combination of biophysical, biochemical and immunological studies gives a broad spectrum of information about this secondary transporter. The melibiose permease is encoded by the *melB* gene which is a part of the melibiose operon<sup>37,38</sup>. This operon is comprised of the three successive genes *mela*, *melB* and *melR*. Whereas *mela* encodes for the  $\alpha$ -galactosidase responsible for the intracellular hydrolysis of the melibiose into galactose and glucose, the regulator protein expressed by *melR* is still unnamed<sup>39</sup>. The MelB operon is similar in its organization to the lactose operon,  $\beta$ -galactosidase (*lacZ*), the lactose permease (*lacY*) and the regulator *lacX* form the lactose operon.

The melibiose permease contains 473 amino acids. The final melibiose carrier lacks the initial methionine due to cleavage after protein expression<sup>40</sup> and has a molecular weight of ~52

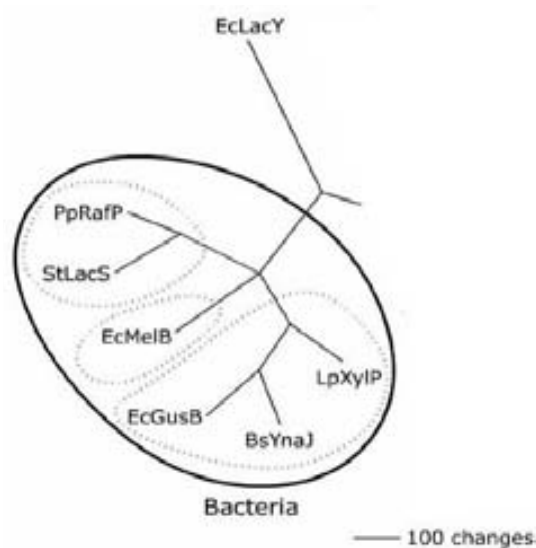


Figure 2.2 Phylogenetic tree of prokaryotic sugar transport proteins from Reinders and Ward<sup>23</sup>, altered by Geertsma<sup>36</sup>; indicating the melibiose permease from *E. coli* (EcMelB) to be closely related to the glucuronide permease from *E. coli* (EcGusB), to the pentoside permease from *B. subtilis* (BsYnaJ), to the isoprimeverose permease from *L. pentosus* (LpXylP), as well as to the raffinose permease from *P. pentosaceus* (PpRafP), to the lactose permease from *S. thermophilus* (StLacS) and to the lactose permease from *E. coli* (EcLacY)

KDa<sup>41</sup>. The protein consists of 70% non-polar residues which is a common amount among secondary transporters (LacY about 71%). Considering all charged amino acids, MelB has an excess of four positive charges, which makes it a basic protein at neutral pH. Deduced from the amino terminus of the protein, the melibiose permease does not require a signal peptide for proper membrane insertion, neither does the lactose permease nor the histidine transporter (HisQMP<sub>2</sub>). Apart from the disaccharide melibiose, MelB is capable of transporting other  $\alpha$ - and  $\beta$ -galactosides (see Fig 2.3 and Tab. 1.3). Notably, the sugar conformation dictates the coupling cation. Sugars containing a  $\alpha$ -linkage are translocated by any of the three cations, whereas  $\beta$ -galactopyranosides like lactose or methyl-1- $\beta$ -D-galactopyranoside, are co-transported by Na<sup>+</sup> or Li<sup>+</sup>, but not H<sup>+</sup><sup>42</sup>. Hence, depending on the substrate, the cation specificity changes indicating proximity of substrates recognition sites<sup>43</sup>.

Apart from the monosaccharides galactose, fucose and arabinose the broad grid of possible ligands for MelB is even supplemented by larger tri- and tetra-galactopyranosides like raffinose and stachyose<sup>44</sup>. MelB functions as a monomer and for each molecule of sugar only one cation is required to drive the transport. Hence, the stoichiometry for the sugar and coupling ion is a steady 1:1 ratio, like the related LacY<sup>45</sup>.

Based on fusion protein analysis with a phoA adapter protein and the hydrophaty analyses<sup>37,63</sup>, a topological model of the secondary structure reveals 12  $\alpha$ -helical membrane segments and rather short loops connecting the helices<sup>46</sup>. Each membrane spanning segment comprises on average 20 residues of mostly hydrophobic character. The regions located in the hydrophilic periplasm and cytoplasm contain a large number of polar residues. Remarkably, the N- and C-terminus are located in the cytoplasm. The predicted secondary structure was supported by proteolytic cleavage experiments, where mainly loop regions were marked by protease activity<sup>47</sup>.

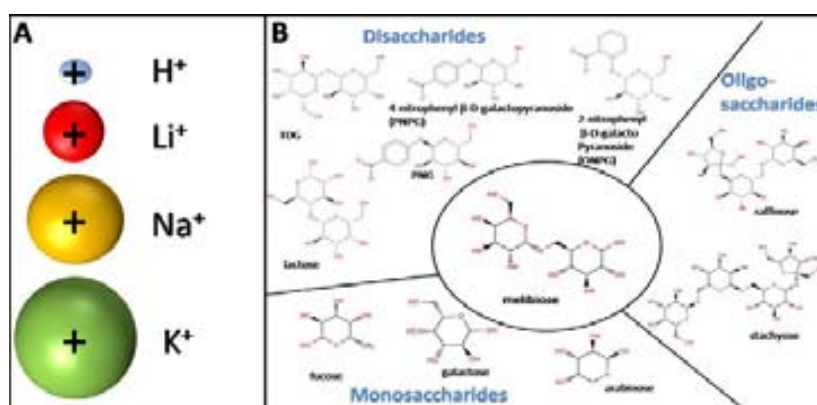


Figure 2.3 **A** comparison of the approximate cation sizes for the proton, lithium, sodium and potassium in relation to each other (unscaled); **B** different sugar ligands of the melibiose carrier (MelB) grouped after their number of molecules, centered: melibiose molecule as preferential sugar ligand

Since there is still no crystal structure available, the assumptions considering protein conformation are based on the assembly of different techniques like site-directed mutagenesis and MelB chimera<sup>48</sup>. Structural data available for MelB comprises images from cryo-electron

microscopy revealing a 3D model of the heart-shaped porter<sup>49</sup>. A two-helix bundle pseudosymmetry was proposed for MelB<sup>50</sup>. If the hypothesis of symmetrical distribution remains intact for the melibiose permease is not clear yet. The resolution of the 3D microscopy images was not sufficiently high to confirm a pseudosymmetry. Thus, asymmetrical helix distribution might arise for the sugar/cation co-transporter. An argument reinforcing the two-bundles pseudosymmetry is a relatively large loop connecting helices VI and VII<sup>15,50</sup>. This loop could anchor the two protein bundles with each other.

A projection of the helices arrangement at 8Å resolution delivers additional information about the possible proximities of  $\alpha$ -helical sub-domains. Regarding the aqueous channel, the projection map indicates a location in the core region of the protein surrounded by helices.

A threading model for MelB is the latest structural assessment of the melibiose carrier. Over other related transporters of known structure, the lactose permease gave the best score as a template. Unfortunately, the sequence of the lactose permease only shares 15% identity and 37% similarity with the melibiose permease. Although segments located in the helices resemble each other, structural details might be imperfect and give rise to biased conclusions. Therefore, further structural information is required to improve this model stepwise.

### 2.3. Alternating access model as source of mechanistic understanding

It has been postulated that the translocation of solutes from the extracellular space to the

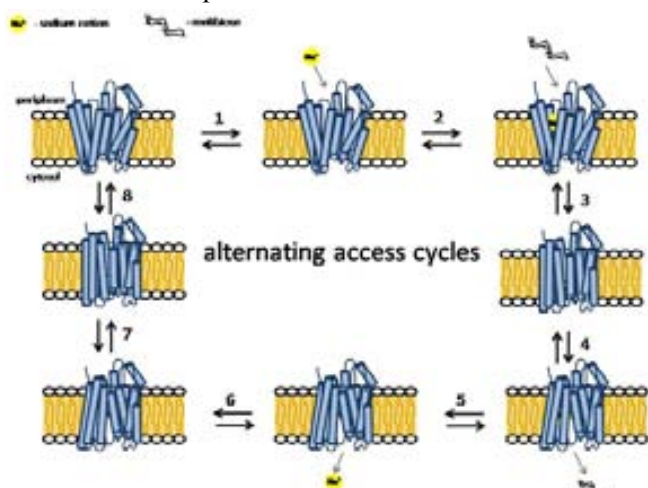


Figure 2.4 theoretical alternating access model for MelB; 1 MelB binds sodium cation, 2 MelB binds sugar 3 MelB in occluded intermediate state as transporter changes from outward-facing to inward-facing conformation, 4 MelB in inward facing state releases the sugar, 5 MelB releases sodium ion, 6 empty MelB, 7 MelB re-adapts outward-facing conformation through occluded state, 8 MelB in initial outward-facing conformation.

intracellular medium is realized by an alternating access mechanism. First hypothesized by Mitchell, the protein adopts two basic states within the transport cycle: one, where the substrate-binding site is accessible from the extracellular side and another one vice versa for the intracellular space<sup>51</sup>. In 1966, Jardetzky stated the hypothesis of the two protein states for sufficient transport across the cell membrane<sup>52</sup>. But from there it took almost four decades until the first resolved 3D protein crystal structure from the efflux pump AcrB revealed details of its structure. The proton-driven lactose permease (LacY)

and the glycerol-3-phosphate antiporter (GlpT) followed shortly thereafter. All three membrane proteins use the proton as the coupling ion. The first secondary transporter using sodium cations instead of the simpler proton appeared in 2004. The aspartate transporter GltPh, the sodium-proton-antiporter (NhaA) and the leucine transporter (LeuTa)<sup>53</sup> demonstrated similar features among membrane transporters even from distant families. Strikingly, almost all transporters retain a pseudo-two fold symmetry of the carboxy- and the amino terminus of the secondary protein structure. The multidrug pump NorM differs slightly in terms of symmetry.

NorM displays an organization based on four bundles with three helices each. Astoundingly, none of the protein bundles is traversed by a helix belonging to another subdomain<sup>54</sup>. Apparently, the composition of the four “separated” protein domains is the preferential arrangement for the transport mechanism.

Most of the membrane proteins retain  $\alpha$ -helical composition. The fewer amounts of known transporters displaying a  $\beta$ -sheet-structure might be explained with the relative flexibility of helices over sheets. The symmetry of a membrane protein defines the hydrophilic pore through which the solute passes after binding to key residues. Generally, the binding sites for the ligands are located in the centre of the protein halfway through the membrane. Also loops connecting the protein scaffold undergo conformational changes to disclose the hydrophilic passage.

For MelB, the description of the whole transport mechanism is fuzzy and based only on studies done by protein manipulation and low resolution imaging. Considering the protein to be in a conformation facing the periplasm, the transport cycle commences by binding the cation. This increases the affinity for the sugar molecule. After the sugar binds to its cavity, a helical rearrangement conceals the periplasmic entrance. Further hypothetical movement of helices discloses the cytoplasmic side. The stepwise release of the sugar and the cation triggers similar conformational changes. The protein reestablishes its original shape and the transport cycle is completed (Fig. 2.4). Intermediate steps termed as “occluded” occur after substrate binding and release. The occluded state implies that the periplasmic as well as the cytoplasmic side are sealed off. In the occluded states, the substrates cannot enter nor exit the transporter. Between each step, there exists an equilibrium depending on various parameters.

Ideally, the protein should be trapped and crystallized in each state of the transport cycle. The obtained information would ease the explanation of the function of key residues, ligand binding and translocation as well as conformation changes.

### 2.3.1. Important helices for the transport mechanism

cysteine in position 235 was substituted by valine to maintain the level of expression.

The combination of all four mutations, termed as cysteine-less (Cys-less, C-less or Cys<sup>-</sup>) was proved to be almost as active as the wild type protein. Similar binding constants and appreciable transport rates for sugar and co-substrates suggested the absence of severe changes of the structure. Interestingly, the substitution of Cys-364 by serine made the protein insensitive to inhibition by NEM (N-ethylmaleimide). This in turn indicates the loop 10-11 as a major contributor for the protein function. In conclusion the wild-type protein devoid of its natural

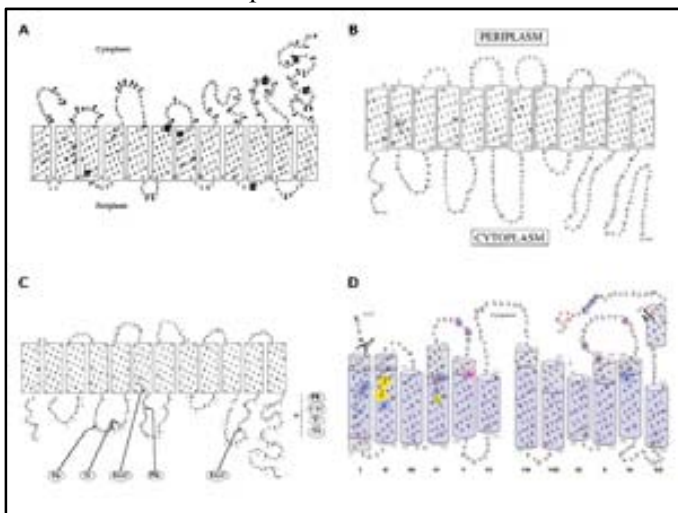


Figure 2.5 Putative helix length of the Melibiose carrier; A first MelB topology<sup>55</sup>, B topology adapted<sup>56</sup>, C topology considering the accessibility for proteases<sup>47</sup>, D latest topology model from Yousef and Guan, 2009<sup>50</sup>

cysteines served as an ideal background for site-specific modification of the permease leaving the transport parameters unaffected.

Individually substituted by cysteine, results of mutations of helix I in the MelB demonstrated that it might lie directly in the core of the aqueous channel through which the substrates are transported. The majority of the residues have a hydrophobic character. The replacement of any of three charged amino acids Lys-18, Asp-19 or Asp-35 inactivated the transport<sup>57</sup>.

Additionally, cysteine variants of glycine 17, tyrosine 32 and threonine 34 are lacking activity. The water-soluble mercurial compound PCBMS inhibits transport by interacting with the sulfhydryl group of the side chain of the cysteine and blocks the passage for the substrates. Almost half of the residues of helix I lost their activity in the presence of the inhibitor exhibiting the accessibility by the aqueous phase.

Further details of proximities of polypeptide regions were retrieved from the study of the revertants of the inactive MelB variants. K18C/D19N gave rise to the notion of a possible interaction of the charged residues since the double mutant recovers the transport by 50% in comparison to the parental melibiose permease. Amino acid replacements for the non-transporting Tyr-31 arose in helix VII indicating closeness of the hydrophobic segments. M234L and L236F compensate the sugar transport<sup>57</sup>. In another study, three residues (Asp-19, Ala-21 and Ile-22) display impaired recognition for methyl- $\beta$ -D-galactopyranoside (TMG) and insensitivity to

lithium inhibition. The mutants D19E, A21T and I22N clearly demonstrated the involvement of these residues in the process of sugar coupling<sup>58</sup>.

Computational analyses combined with previous biochemical and biophysical studies predict that the membrane-spanning helix II is composed of 31 amino acids. Since the average width of the cell membrane of *Escherichia coli* is about 30 Å, it is likely that the helix II is tilted in respect to the phospholipid bilayer. Titled helices were already described for several other transmembrane proteins<sup>59</sup>. Regarding the amino acid sequence, especially three residues seem to be crucial. Cysteine substitutions of Arg-52, Asp-55 and Asp-58 cause the loss of transport activity. Together with Ans-58, the two negatively charged residues 55 and 59 affect the cation recognition and/or coupling. Arg-52 replacements abolish the proton-coupled transport almost completely and have a negative effect on the sodium-induced melibiose accumulation<sup>56</sup>. Spontaneous mutations to recover the proton-mediated melibiose transport in Arg-52 failed and only three second-site mutations, namely W116R, S247R and N248K partially rescue the melibiose accumulation using sodium as co-substrate<sup>56</sup>. The additional introduced positive charge apparently compensates for the lost charge of Arg-52 demonstrating its significance.

In the presence of melibiose almost all residues of helix II are protected when exposed to the inhibitor PCMBS. This in turn indicates the proximity of sugar binding to the membrane spanning helix II. Similar results were obtained by cysteine scanning mutagenesis technique of the helices II and VII for the homologous transporter Glut1 from eukaryotic cells<sup>60</sup>.

The putative transmembrane  $\alpha$ -helix IV of the melibiose permease bears several highly crucial residues regarding efficient catalytic activity of the protein. The aspartic acid 124 has been investigated by IR<sub>diff</sub> spectra revealing its importance for the melibiose and sodium coupling process. The binding of both substrates is strongly affected when substituting Asp-124 with cysteine<sup>61</sup>. Although not essential for sodium binding per se, this residue might interact with the cation.

Replacing glycine in position 117 by cysteine produces a phenotypically fascinating transporter. While still transporting the substrates in a similar rate as the wild-type protein, conformational changes normally detected by intrinsic fluorescence vanish. Also charge displacements upon substrate exposure almost disappear. The active transport indicates an intact translocation, but the absence of structural responses indicate a modified protein conformation<sup>62</sup>. The tyrosine in position 120 in the helix IV might be significant for the transporter. By replacing tyrosine with phenylalanine, the melibiose affinity is massively reduced. A likewise reduction of sodium affinity strengthen the idea of tight cooperativity in between sugar and cation binding sites. Tyr-120 might act as a transition residue for coupling the interaction between sites.

The carboxy-terminal helix XI harbors several potentially essential residues for the symport mechanism. Cysteine-scanning mutagenesis revealed key evidence that helix XI render the aqueous channel<sup>63</sup>. Studies on Lys-377, the only charged amino acid in the cytoplasmic end of the helix, propose a participation in the transport mechanism. This residue influences either the cooperative substrate binding process or the stabilization of the protein by interacting with other

residues. The drastically reduced expression rate of Lys-377 mutants delivers more evidence of its significance. The positive charge in this particular position in the transporter might be significant<sup>64</sup>.

Besides the cysteine substitution, mutants K377D and K377V sustain the belief of implications of the lysine in the process of active transport. In cells containing the K377V mutant, reduced melibiose and TMG accumulation has been detected and for K377D the sugar transport was absent<sup>65</sup>. Second-site revertants for the Lys-377 display substitutions of the Phe-20, Ile-22 as well as Asp-59. The double mutant K377V/F20L rescues the downhill transport. The second double mutant K377V/D59V also transports melibiose concomitant to a proton gradient. The recovery of respectable sodium-dependent transport activities was not shown in any of the Lys-377 mutants. A charge switch between Asp-59 and Lys-377 resulted in a mutant which accumulated a substantial amount of melibiose but also failed to reconstitute sodium stimulated co-transport<sup>65</sup>. Further studies support the notion of a potential salt bridge between Lys-377 and Asp-59. Similar contributions have been implied for the pair Asp-237/Lys-358 of LacY which affects critically the symport activity<sup>66-68</sup>.

Apart from the Lys-377, five other residues display a detrimental effect of active transport by individual cysteine replacement. In MelB variants G379C, F385C and Y396C, the melibiose accumulation was totally abolished, whereas A383C, L391C and G395C had a substantially low amount of sugar transport activity. The organic compound PCMBS determine inhibitory effects on residues from the helix XI. The presence of melibiose protected almost all of these amino acids from inhibition. This suggests that at least one part of the helix XI faces the hydrophilic cavity of the protein.

Several second-site mutations suggest the proximity of the helix XI to other membrane spanning segments as helix I, II and V. Only F385C displayed second site mutations within the helix XI itself and the C-terminal loop 11-12. Surprisingly, MelB variants K377C, A383C, L391C and G395C expressed second-site mutations around the same area for the protein (Table 2.2)

Table 0.5 listed second-site revertants of parental MelB mutants in the transmembrane helix XI

MelB variant	Second-site mutation
K377C	I22S, D59A
K377V	F20L, D59V
A383C	I22S, I22N, F20L
F385C	I387M, A388G, R441C
L391C	I22T, I22N, D19E, A152S
G395C	D19E, I22N

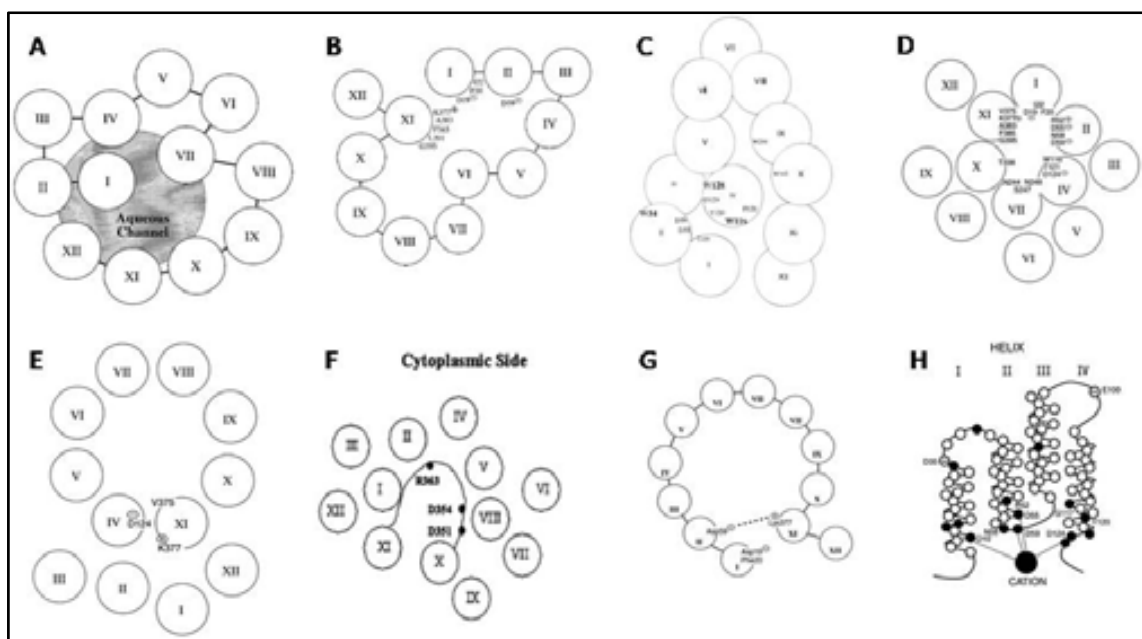


Figure 2.6 **Tertiary structure models for the 12 membrane-spanning helices**; **A** Helix I is embedded into the aqueous channel<sup>57</sup>; **B** proximity proposal between helices XI and I and II<sup>69</sup>; **C** role of helix IV as connector for sugar and cation binding<sup>70</sup>; **D** arrangement based on obtained revertants<sup>71</sup>; **E** model for potential closeness of D124 with V375<sup>72</sup>; **F** loop 10-11 lies in the aqueous channel<sup>73</sup>; **G** potential salt bridge between D59 and K377<sup>65</sup>; **H** proposed cation ligands<sup>20</sup>

### 2.3.2. Important loops for the transport process

Alkaline phosphatase assays as well as hydrophaty plots and proteolytic digestion revealed domains exposed either to the periplasm or to the cytoplasmic side<sup>48</sup>. As the phosphatase activity is only present in periplasmic regions, the assignment of cytoplasmic domains was discriminated by hydrophaty plots as well as limited proteolysis<sup>47</sup>.

The loop between the putative helices IV and V apparently plays a major role in the sodium-dependent coupling of the melibiose<sup>47</sup>. Upon sodium addition a 2-fold protection against protease cleavage indicate the proximity of the loop to the co-substrate binding site. Moreover, the sugar in the presence of sodium enhances protection. These results demonstrate not only the cooperative effect of both substrates but also that loop 4-5 participates in structural changes during substrate coupling.

Functional implication of the positive charged residues Arg-141 and Arg-149 further reinforced the notion that the loop plays a major role in the symport mechanism of MelB. These two basic residues are involved either direct in the catalysis of the transporter or in the reorientation process following the coupling and uncoupling of the substrates. Cysteine substitution of Arg-141 impairs sugar transport. For R141C still binds the substrates, but a substrate accumulation was not detected. The authors concluded that Arg-141 is involved either in the reorientation process or release of the substrate into the cytoplasm<sup>74</sup>. The positive charge of

arginine is of less importance<sup>75,76</sup>.

Among the negatively charged residues only Glu-142 exhibits impaired substrate translocation when replaced by a neutral cysteine. Like the R141C, E142C lacks conformational changes after addition of melibiose<sup>74</sup>. Both MelB mutants R141C and E142C retain the ability to bind the substrates<sup>74,76</sup>. The double mutant E142C/I22S recovers the transport activity indicating a strong link between helix I and the cytoplasmic structure 4-5<sup>74</sup>.

The second significant arginine in the loop 4-5, Arg-149 demonstrated deficiency of transport activity when measured in right-side-out vesicles. The authors concluded impaired binding as the reason for the lack of transport activity<sup>75</sup>. The positive charge this arginine seem to be of less importance, since a second-site revertant R149C/V343G restore catalytic activity with C-less-like substrate affinity<sup>75</sup>. The second site obviously compensates for a structural deficiency imposed by the mutation to cysteine.

The exact location of Arg-149 is still pending. Just lying at the interface between the loop 4-5 and the helix V, several MelB models predicted the Arg-149 to be part of the cytoplasmic loop whereas the recently published model based on the structure of the lactose permease positions the residue in the helix V. Unpublished results of our group hypothesize Arg-149 as an essential residue for the reorientation mechanism of the transporter. R149C clearly binds its substrates in proteoliposomes as well as in inside-out-vesicles (unpublished results). Conclusively, the loop 4-5 may act as a hinge region which dictates broader conformational changes upon the transporter during the transport mechanism.

The loop between helices X and XI is a putative cytoplasmic loop as well. There are controversial data available<sup>20,47</sup> predicting that the loop may enter partially into the aqueous pore. Those structural domains are termed as re-entrant loops. As a common characteristic of re-entrant loops of other transport proteins, the in-pore conformation serves as a kind of scaffolding for the substrate moiety<sup>77-80</sup>. Hydrophobicity is another characterizing parameter of those loops. Usually re-entrant loops possess their lowest hydrophobicity half-way of the hairpin structure<sup>81</sup>. The interhelical loop 10-11 might as well impose major structural modification on the symporter.

All residues forming the putative loop 10-11 were consecutively replaced by cysteine. Several mutants exhibit a reduced expression rate and additionally five of those residues lost the ability to transport<sup>82</sup>. The authors imply the importance of the loop 10-11 during the transport mechanism. Special attention rests on the charged residues Asp-351, Asp-354 and Arg-363. Cysteine mutation of these residues abolishes the transport<sup>82</sup>. Whereas D351C affects the sugar binding, the cysteine mutation of Asp-354 provokes an alteration of sodium recognition<sup>64</sup>. Arg-363 is supposed to be involved in the translocation process<sup>64</sup>.

Charged thiol-reagents could not restore the transporter activity in transport-deficient mutants D351C, D354C and R363C<sup>73</sup>. Until now their role regarding the transport mechanism remains unknown. Furthermore, several spontaneous mutations of the interhelix loop display altered recognition for  $\beta$ -galactosides, like lactose. The MelB mutants Q372C and V376C exhibited an increase in  $\text{Li}^+$ -dependent co-transport whereas the melibiose accumulation mediated

by sodium was largely reduced. Both amino acids might participate in the cation recognition.

Revertants of transport deficient residue A350C demonstrate the potential proximity of this functional loop to membrane spanning loops I and VII. Ile-22 and Phe-268 were the second sites causing spontaneous amino acid substitutions.

### 2.3.3. Proximity of important domains

Based on the highly dynamic process of solute transport, protein domains change their location during the individual stages of substrate coupling, translocation and the final release. Considering the alternating access model, the proximities between helices might change during the transport cycle. But since there is still no three-dimensional structure of MelB available, details about helix interactions are based primarily on topological models and second-site revertants. Especially, the second-site revertants suggest proximities. In the literature are mutants described which compensates for a transport-deficient first-site mutation by replacing another amino acid. These mutants could suggest a dependency between two protein domains based on their position. Several publications describe revertants deduced from first-site mutations.

List of interactions between the helices:

- Interactions of helix I with: helix II, IV, VII, X, XI<sup>57,82</sup>
- Interactions of helix II with: helix IV, VII, X, loop 10-11, XI<sup>56,65</sup>
- Interactions of helix IV with: helix X, XI<sup>72</sup>
- Interaction of loop 4-5 with: helix I<sup>74</sup>
- Interaction between helix VIII with helix X<sup>82</sup>
- Interaction of helix X with: helix VIII<sup>82</sup>
- Interaction of helix XI with helix V<sup>69</sup>

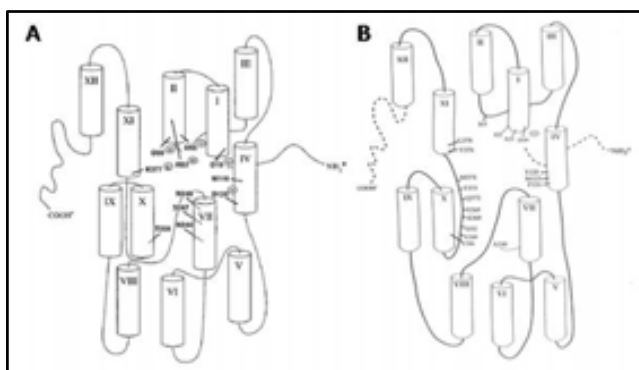


Figure 2.7 proposed helical arrangement based on interaction of residues (revertants), **A** after Franco and Wilson<sup>56</sup>. **B** after Ding<sup>58</sup>

Spontaneous double mutants recovering cation-dependent transport as well as cross-linking events indicate a potential proximity between membrane-spanning helices I and XI. Cross-linking of double mutant V36C/G395C verifies the proximity of helix I and XI at the periplasmic end of both helices<sup>83</sup>. The same approach failed for the cytoplasmatic side. Sodium supplementation elucidates that neither helix I nor helix XI undergo drastic structural changes induced by co-substrate binding<sup>84</sup>. Lys-18 located in helix I might interact

with residues Thr-118 and Met-123 in helix IV emphasizing that the helices I and IV are in contact with each other<sup>56</sup>.

A proximity between helix IV and XI reinforce the possibility that both membrane-spanning segments form part of the cation and/or the sugar binding sites, like the potential pairs Asp-59/Lys-377 and/or Asp-55/Lys-377<sup>65</sup>.

Deduced from the latest MelB model, a potential Tyr-120/Arg-141 pair highlights that loop 4-5 is in direct contact to the putative helix IV<sup>50</sup>. The idea of proximity between helix I and II was suggested by a spontaneous double mutant containing substitutions at Arg-52 and Asp-19. The replacements of the charged residues indicate a potential salt bridge between both residues. Arg-52 replacement provokes various second-site revertants in different domains of MelB. The authors highlight the interaction of helix I with helices IV and VII<sup>56</sup>.

Loop 4-5 residues also point out their implication in either the protein stability or functionality by acquiring second-site revertants located in the N-terminal helix I<sup>82</sup>. Both loop 4-5 and helix XI are linked directly to the N-terminal helix I indicated by revertants<sup>69,74</sup>.

### **2.3.4. A possible cation binding site**

The putative binding site for the cations in MelB may vary because the three cations differ in size. Although sharing a mutual coupling site<sup>32,85,86</sup>, differences in the binding process are apparent. The majority of the publications of MelB rely on the sodium as the co-substrate due to the highest affinity over lithium and the proton. Site-directed mutagenesis indicated the involvement of four aspartic acids (Asp-19, Asp-55, Asp-59 and Asp-124) in the coupling of the sodium cations<sup>46,87-89</sup>. Latest studies however refined the hypothesis of these participating aspartates. FTIR experiments done on the MelB mutants confirmed the participation of Asp-55 and Asp-59 in the sodium binding. Asp-19 was excluded as a potential ligand for the cation since the mutant D19C demonstrates c-less-like binding in infrared spectroscopy. Asp-124 was confirmed as non-essential residue for the sodium binding, but apparently Asp-124 triggers structural changes in the carrier upon cation binding<sup>61</sup>. Proven by Hama *et al.*, Asn-58 affects sodium binding as well.<sup>90</sup> The asparagine is located adjacent to Asp-55 and Asp-59. It is likely that other residues still not identified are contributing to the translocation of the sodium ion.

### 2.3.5. Synopsis of the putative sugar binding site

Although the melibiose carrier is one of the best studied prokaryotic sodium/solute transport protein, information about the sugar binding site is still scarce. A review of the available data indicates that domains from the N- and C-terminus are involved in the coupling of the sugar molecule. As stated repeatedly, the substrates bind to the protein in cooperative fashion meaning that one substrate increases the affinity for the other<sup>91</sup>.

Data from our lab indicates that the arginine in position 149 affects the reorientation mechanism of the transporter. The Arg-149 residue could also be involved in sugar recognition<sup>75,92</sup>.

Helix IV participates in the sugar binding process through several side chains. Gly-117 seems to be a key residue for cooperative ion and sugar binding, although direct binding can be ruled out<sup>93</sup>. Helix IV residues Tyr-120 and Asp-124 might connect the cooperative coupling of the cation and the melibiose. Tyr-120 is in a similar position as Ala-122 from LacY<sup>94</sup>. Among orthologues of secondary sugar symporters, charged amino acids similar to Asp-124 and Arg-149 are conserved and proposed to form charged pairs stabilizing the binding pocket like Glu-126 and Arg-144 in LacY<sup>95</sup>. Modeling data predicts the serine 153 as a potential ligand of the sugar molecule as well<sup>62</sup>.

Helix I definitely participates in the liganding of the sugar. IR<sub>diff</sub> and fluorescence spectroscopy on D19C confirmed that manipulation of this residue abolishes sugar binding but the binding of the cation remains unaffected.

In helix II, mutation of the amino acid Arg-52 uncouples proton translocation from active transport. But the activity mediated by a sodium gradient is not affected. Docking simulations proposes hydrogen bonding of the melibiose galactosyl ring with Arg-52, Arg-149 and the Lys-377. The lysine residue additionally is predicted to form a potential salt bridge with either Asp-55 or Asp-59<sup>65,69,84</sup>.

Previously, lysine residues have been described to form either H-bonds directly with the substrate as in the oxalate transporter<sup>96</sup> or develop charged pairs with negative charged residues<sup>97</sup>. The docking also revealed that the supposed loop 4-5 might be involved in binding of the sugar. Helix IV may contain a hinge half-way through the membrane. This could impose a region of high flexibility twisting upon the bound substrate and disclosing the cytoplasmic path.

The connection of the cation and the sugar binding site is presumably realized by a network of charged and H-bonding amino acids of the helices I, II, IV, V, XI as well as loops 4-5 and 10-11<sup>41,73,88,98</sup>.

### 2.3.6. Possible symport mechanism for MelB

During the last decade, several membrane transporter structures underline possible mechanisms of transport. Two theoretical transport scenarios have been described in the literature.

In the “gated-pore” mode, the protein blocks the extracellular space by thick gate after the ligands have entered the internal cavity. Merely a few amino acid side chains, called a “thin gate”, hinder the ligands from directly entering the intracellular compartment. This gate only opens upon ligand binding and allows ligand influx.

Although the gated-pore mechanism is mostly described for channel proteins, transporters have been published accomplishing substrate translocation via the gated-pore mode<sup>99,100</sup>.

The second postulated transport mechanism is termed “rocker-switch”. The lactose permease suits as a prototype underlining the extensive structural changes occurring in this mechanism.

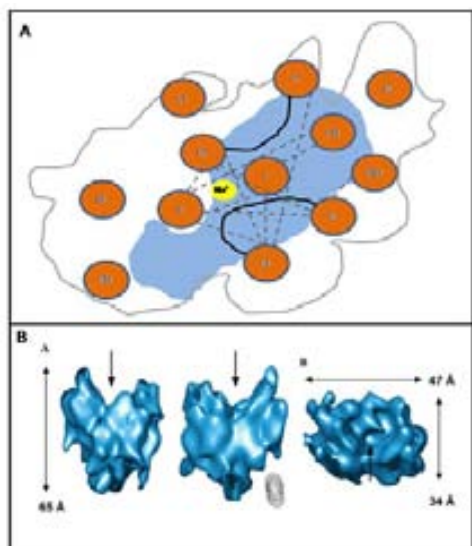


Figure 2.8 **A** 2D projection map of the putative helix arrangement of the melibiose carrier after Hacksell *et al.*<sup>101</sup>, numbered helices (in orange), loops 4-5 and 10-11 (in black) aqueous channel (in blue), sodium cation (in yellow) potential interaction between helices indicated by a dashed line (in red) ; **B** 3D cryo-EM images of MelB<sup>49</sup>

Carriers are usually composed of 2 intertwined pseudo-symmetrical helix bundles. Ligand binding to the interface drives the closure of the formerly accessible extracellular side. Simultaneously, rigid-body movements of protein domains expose the ligands to the opposite side of the membrane. Hence, structural rearrangements in the rocker-switch mode are more complex and each step is considered to be highly dynamic.

The mechanism for the transport of MelB remains unclear so far. A more superficial transport mechanism for MelB evidentially consists of at least 8 uniform steps. Like LacY, the proposed mechanism relies on the alternating access model<sup>52</sup>. As hypothesized in the thesis of Dr. Kerstin Meyer-Lipp, the empty carrier adopts an inward facing conformation as the initial step of the transport cycle<sup>102</sup>. The cation binding triggers structural changes which increase the affinity for the sugar molecule. The latter imposes an intermediate occluded state and additionally induces a transition of the protein to the intracellular membrane site. After opening the intracellular access, the protein releases stepwise the substrates into the cytosol beginning with the sugar. Eventually, the empty carrier seals off the cytoplasmic site and reorients towards the outward-facing membrane site.

As the mechanism was describes for the influx of the substrates, the efflux undergoes the same steps regarding the inward-facing conformation as the starting point of the transport cycle

## 2.4. MelB structural organization in 2D and 3D

A 8 Å resolution projection map and three-dimensional cryo-electron microscopy images at 10 Å categorize MelB as a  $\alpha$ -helical membrane carrier.

The projection map (Fig. 2.8 A) indicates membrane segments lining the aqueous pore. Almost 70% of all transmembrane helices of MelB present an inclination which is in line with predictions made for the sodium-proton antiporter and the oxalate/formate antiporter<sup>103,104</sup>. If the helices of MelB are ordered in an asymmetrical fashion, is not clear yet. The NhaA antiporter displays a asymmetrical order of its helices, unlike many other membrane proteins<sup>101</sup>.

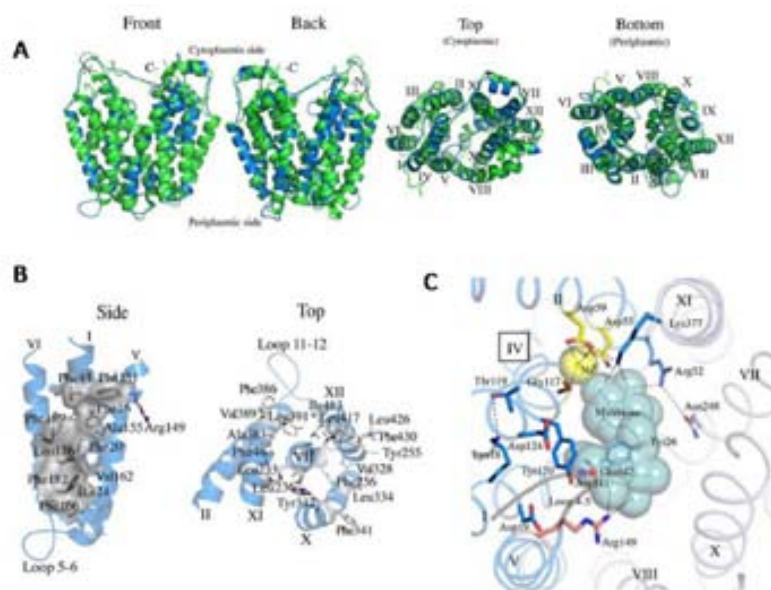


Figure 2.9 MelB model based on the crystal structure of lactose permease, as proposed by Yousef and Guan; **A** overall tertiary structure of melibiose permease (blue) and the superimposed LacY (green); **B** proximity of important residues of MelB retrieved from the model; **C** docking of the melibiose molecule in proposed sugar cavity model<sup>50</sup>.

The low-resolution images from a cryo-electron microscopy (Fig. 2.8 B) show an asymmetrical molecule. It resembles a V-shape typical for a transporter open to one side of the membrane. Dissimilar electron densities between the putative domains confirm the asymmetry of MelB. In regard of the structural resemblance, MelB harbors a more condensed arrangement than the lactose/proton symporter or the glycerol-3-phosphate antiporter<sup>49</sup>.

## 2.5. 3D structure of related $\alpha$ -helical membrane transporter

In 1984 the bacterial photosynthetic reaction center was the first published membrane protein structure<sup>105</sup>. From this point on, the number of known structures increased constantly. Unfortunately, the amount of solved structures did not grow as fast as for soluble proteins. This is understandable considering that the hydrophobic character of membrane proteins usually interferes with its purification and crystallization processes.

### 2.5.1. MFS transporters

The lactose permease was the first ever published secondary membrane transporter. Many conclusions drawn nowadays rely on the benchmarks set by the lactose permease. The thermostability as basic requirement for the crystallization of a highly dynamic carrier was introduced into LacY by the point mutation of C154G. Crystals obtained from this stable mutant protein in the presence of the high affinity substrate TDG elucidated the binding mechanism of the transporter.

The proton coupling site of the related lactose permease is composed of several mainly charged amino acids located in the carboxy end of the transporter. Given that LacY data relies on a 3D-crystal structure, refinement of the available data indicates that the glutamate 269 coordinates the coupling of the proton and the sugar simultaneously. The residue Glu-325 is required for deprotonation, whereas His-322 is responsible for proton translocation<sup>45</sup>. Additionally, Arg-302 and Tyr-236 also affect the proton binding of the lactose permease<sup>106</sup>.

The mechanism of sugar binding is theorized with the high affinity  $\beta$ -galactoside derivative TDG. It is postulated that by disrupting the charged pair Glu-126/Arg-144 the process is initiated. Arg-144 is irreplaceable. Even by conserving the positive charge (R144K), the substrate binding is absent. Glu-126 is less sensitive to substitutions, but also exhibits a severe loss of transport. Glu-269 is the residue responsible for cooperativity of proton and sugar binding sites in LacY. Deduced from spectroscopic results, the Trp-151 participates in the formation of the ternary complex consisting of the protein, proton and the sugar.

Emerging almost simultaneously to the lactose permease, the 3D structure of the GlpT antiporter from *Escherichia coli* added valuable insights of membrane protein structure arrangement of the MF superfamily. The intracellular phosphate concentration drives the accumulation of glycerol-3-phosphate. Arginine 45 and 269 are the key residues for transport mechanism of GlpT because their substitution highly affects the transport activity.

Another MFS-member, the oxalate/formate antiporter OxlT, was modeled by using the low resolution cryo-electron microscopy image as a template and refine the data of the 3D structure by using the homologous antiporter GlpT and the lactose symporter LacY<sup>107</sup>. The residues lysine 355 in helix XI and arginine 272 in helix VIII evidentially conduct the substrate binding as it was demonstrated by replacements with neutral amino acids which eliminate the protein activity.

The structure of the Fucose permease (FucP) from *Escherichia coli* has been published recently. Crystallographic data of the pH-dependent MFS-symporter demonstrates an outward facing conformation. Earlier examples from LacY and GlpT always adopted the inward-facing conformation. For FucP, the polypeptide bundles turn as a whole over a considerable angle to orient between one membrane site to the other<sup>108</sup>. Glu-135 and Tyr-365 interact via H-bonding to stabilize the outward faced protein conformation. The initial steps of the active transport are mediated by the sequential protonation and deprotonation of aspartate 46 and subsequently of glutamate 135. Asp-46 is responsible for the proton-mediate transport of fucose whereas

glutamate is involved in direct substrate recognition.

The H<sup>+</sup>/multidrug pump EmrD from *E. coli* defines a specific structural arrangement where the internal cavity is mostly loaded with hydrophobic residues in contrast to the majority of MFS members<sup>109</sup>. The aromatic acids Tyr-52 and 56 as well as Trp-300 and Phe-249 are responsible for the coupling of different ligands. Moreover, the valine 17 mediates substrate recognition. Helix IV contains several charged residues and thus is likely to participate in the substrate recognition. The protein crystal appeared in an unbound intermediate state.

As the latest model structure of the MFS transporter family, the peptide-proton symporter emphasizes the relevance of hairpin loops 4-5 and 10-11 as potential regulatory elements for the transport mechanism<sup>110</sup>. The symporter displays the two-helix bundle repeat motif which is common for MFS proteins. Interestingly, the carboxy domain is suggested to function as the hash motif.

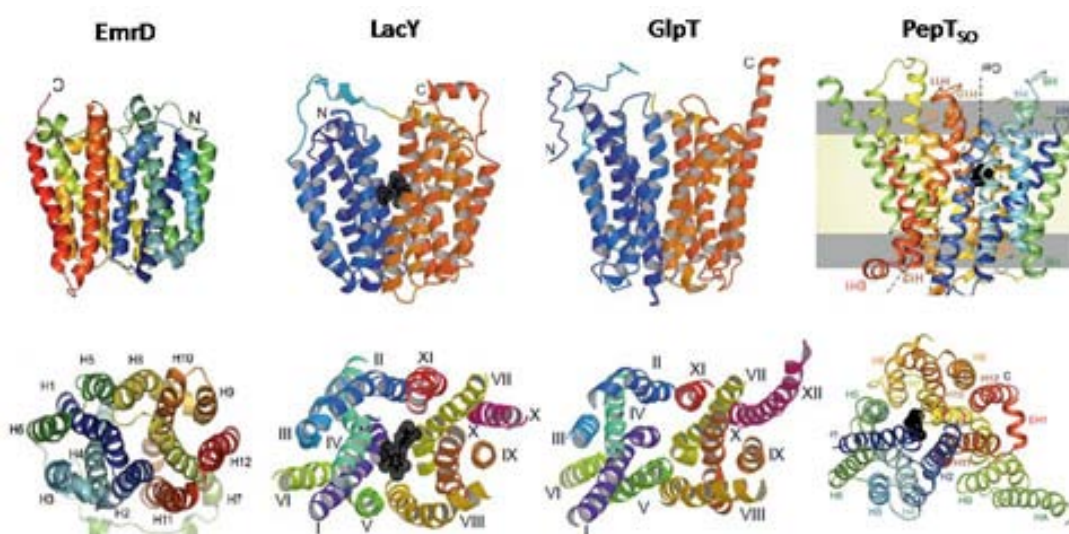


Figure 2.10 **Ribbon presentation of 3D-MFS transporter structures**; upper panel: side view of the structures, lower panel: view along the membrane normal either from periplasm (EmrD<sup>109</sup> and PepT<sub>so</sub><sup>110</sup>) or cytoplasm (GlpT and LacY<sup>111</sup>) showing the two-fold pseudo-symmetry between N- and C-terminal part of the MFS members.

## 2.5.2. Sodium-dependent transporters

Although sodium seems to be the major cation involved in active secondary transport, the structural requirements are still unclear and rely only on a few known structures. A comparison of the binding and translocation mechanisms could illustrate similarities and improve general understanding.

As an important transporter for the maintenance of the intracellular homeostasis, the Na<sup>+</sup>/H<sup>+</sup> antiporter regulates the intracellular ion level by transporting Na<sup>+</sup> or Li<sup>+</sup> for protons in 1:2 stoichiometric ratio. Extreme ion concentrations activate the antiporter. Studies on the antiporter from *E. coli* provided the idea that although the monomer is functional, the dimer is preferred in terms of stability<sup>112</sup>. The cation binding site is located in the assembly of the two interrupted transmembrane segments IV and XI<sup>113</sup>. Both helices consist of a helix-chain-helix motif. The

cytoplasmic end of helix IV and the periplasmic end of helix XI are partially positively charged. Aspartate 133 counteracts the alkaline character by applying an equilibrating negative charge. The positive-charged lysine in position 300 emulates the charge equilibrium for the periplasmic helix IV section and the cytoplasmic part of helix XI which are negatively charged. Similarly to MelB, the translocation of the cations is mediated by two aspartic side chains (Asp-163 and Asp-164) which are essential for the protein.

The authors of the recently published calcium/sodium exchanger NXC describe a mechanism involving the sequential exchange of four cations. As high intracellular calcium concentrations are disadvantageous, the protein binds calcium in a high affinity cavity and reorients towards the external side. A downhill sodium gradient mediate the binding of three sodium ions which gradually reduce the affinity in the calcium binding side and result in the  $\text{Ca}^{2+}$  release. After conformational changes the transporter liberates stepwise the sodium ions and enhances the affinity for calcium. This model elucidates the cooperativity of cation binding and release<sup>114</sup>.

Extracted from the crystallographic data, the hydantoin symporter MhpI suggests a transport mechanism based on the “gated-pore” theory. Two large helical domains termed as hash and bundle, move relatively to each other and change the orientation of the transporter from outward- to inward-faced. A “thin” gate closes the access from the extracellular space whereas a “thick” gate blocks the access of the cytoplasm<sup>115</sup>. The central cavity for substrate interaction is considerably large and composed of the membrane-spanning helices I, III, V, VI and VIII. Hypothetically, the sodium ion interacts with residues from helices I and VIII, whereas the substrate hydantoin is H-bond coordinated by the side chains of Trp-117 and 220, Gln-121 and Asn-318<sup>115</sup>.

The physiologically important neurotransmitter transporter group (NSS) also links the transport mechanism with the concomitant uptake of sodium ions. The bacterial leucine-transporter  $\text{LeuT}_{\text{Aa}}$ , a neurotransmitter homologue, is able to transport a variety of amino acids across the membrane using the sodium-motive force. The amino acid alongside two sodium ions are bound in the centre of the  $\text{LeuT}$  carrier as it is common feature among membrane transporter. Evidences considering the width of the gates of the intra- and extracellular compartments point out that  $\text{LeuT}_{\text{Aa}}$  transport could easily interpreted as a gated-pore mechanism. Only a charged pair hinders compounds from entering into the extracellular space of the protein, whereas a substantial amount of several residues block the entrance into the cytoplasm. The binding site for leucine is organized by residues mainly located in helix I and VI. The accompanying  $\text{Na}^+$  cations interact with amino acids from helix I and VIII. Strikingly,  $\text{LeuT}$  crystals have been obtained in three different states; the substrate-bound occluded state, the occluded state with competitive inhibitors (tricyclic antidepressants) and the open-to-outward state by using a competitive inhibitor<sup>116</sup>.  $\text{LeuT}$  exhibits a broad substrate specificity which eventually uncovered a second substrate binding site.

Belonging to the solute-sodium-symporter family (SSS), the sodium-galactose symporter (vSGLT) from *Vibrio parahaemolyticus* exhibits a secondary structure which consist of 14

transmembrane helices including a quasi symmetry between helix bundles II-VI and VII-XI (inverted). The structure resides in an inward-facing conformation. The transport mechanism relies primarily on the data for the galactose binding site since the significant residues for cation coupling were modeled with data from the related LeuT<sub>Aa</sub> transporter. As confirmed by functional assays, the alanine 61 and 361 as well as the isoleucine 65 form hydrogen bonds with the cation<sup>117</sup>.

The pyranose ring of the galactose molecule interacts with Gln-69, Tyr-87, Glu-88, Lys-294, Ser-365 and Gln-428<sup>118</sup>. Moreover, Tyr-263 alongside with adjacent hydrophobic amino acids Tyr-262 and Trp-364 inhibit the ligands from slip directly through to the cytosol. As postulated by Faham *et al.*, the bound sodium cation causes structural rearrangements in transmembrane helix II and facilitates therewith the sugar coupling. The galactose molecule induces conformational rearrangements causing the switch from outward-faced to inward-faced. The quick release of the sugar modifies the protein and results in the escape of the cation to complete the transport cycle.

The 2009 published betaine transporter BetP from *Corynebacterium glutamicum* relies on the sodium-motive-force of the cytoplasmic membrane. This symporter resembles to other cation-depnt membrane proteins using sodium as the co-ion, like vSGLT, LeuT<sub>Aa</sub> and MhpI. BetP consists of 12 membrane traversing segments from which helices III, IV, VIII and IX represent the core region of the substrate coupling. Aromatic residues located in helix IV and VIII mediate the substrate binding<sup>119</sup>. The transporter uses a 2:1 stoichiometry (Na<sup>+</sup>:betaine). The first Na<sup>+</sup> is coordinated by betaine as well as Met-150 and Ala-148. The second cation binds to Ala-147 from helix IV and Ser-306 plus Met-310 from helix IX. As an interesting feature, an entire BetP transporter is organized as a trimer where each monomer triggers the activity of the adjacent one.

### 2.5.3. Other exemplifying transporter structures

Similar to the sodium-coupled transport, the amino acid antiporter AdiC exchanges intracellular agmatine for extracellular arginine in a pH dependent manner. Considering the binding process, residues from helix I, II, VI, VIII and X interact with the substrate<sup>120</sup>. In the proposed model Trp-293 blocks the cytoplasmic gateway for arginine. Upon substrate binding translocation of Trp-202 and 293 allow arginine to further enter the substrate moiety with Glu-202. The protein orientation alters to the cytosol faced state and agmatine replaces arginine after tyrosine 93 and 365 translocate.

Another mutant was reported last year displaying altered characteristics as the previously crystallized N22A AdiC mutant. The substitution of Asn-101 to alanine generates a transition state of AdiC with a much lower  $v_{\max}$ , but with an almost unaffected binding constant  $K_m$ <sup>121</sup>.

The sodium-independent amino acid transporter ApcT catalyses the intracellular uptake of various amino acids from which alanine and glutamine are preferential. An alkaline lysine residue in position is responsible for proton-coupled transport activity<sup>122</sup>. When Lys-158 is protonated, it governs structural alterations of transmembrane segments I and VI and by that closing in the important side chains of Ile-22, Ser-283 and Ser-286.

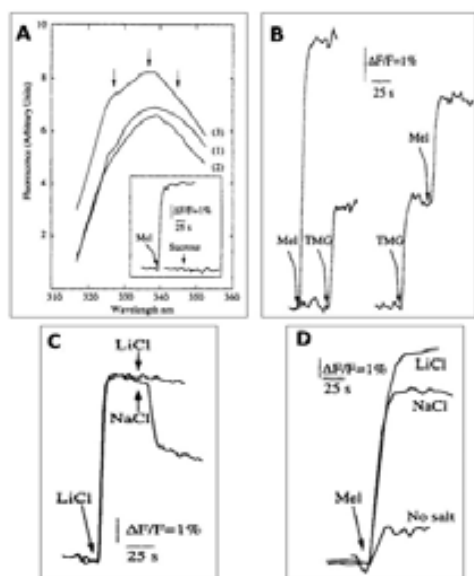


Figure 3.1 A fluorescence spectra of MelB (1), with NaCl (10 mM) (2), with NaCl and melibiose (both 10 mM); B kinetics with different sugar ligands in the presence of sodium (10 mM) - competitive replacement; C fluorescence increase by supplementing lithium (10 mM) in the presence of melibiose (10 mM) - competitive replacement by sodium (10 mM); D comparison of fluorescence increase induced by melibiose (10 mM) in the presence of different salts. From Mus-Veteau *et al.*<sup>86</sup>

### 3. Biophysical insights of the melibiose carrier

#### 3.1. Intrinsic fluorescence by

#### *Trp* excitation

The intrinsic fluorescence of a protein is a powerful tool to analyze the activity and stability of the reconstituted transporter<sup>123</sup>. The fluorescence signal of proteins is primarily dictated by emission of the tryptophans at a excitation wavelength of 290 nm. The contribution from tyrosines is much lower and that from phenylalanines is negligible. As published by Mus-Veteau *et al.*, the melibiose porter respond to its substrates in a characteristic fashion<sup>86</sup>. For the wild-type protein the addition of 10 mM lithium or sodium as coupling ion quenches the fluorescence signal by around 2 %<sup>86,124</sup>.

The formation of the ternary complex, consisting of the cation, the sugar and the protein, produces a characteristic increase in the fluorescence emission (Fig. 3.1 B and D). This increase indicates a change of the protein conformation due to the coupling of the sugar. The effect of the sugar is much stronger in the presence of sodium or lithium than for the proton (Fig. 3.1 D). Simultaneously, this result demonstrates that the substrates bind to the protein in a cooperative mode. The amplitude of the fluorescence signal also depends on the type of the sugar.  $\alpha$ -galactosides induce a bigger change than sugars with  $\beta$ -conformation.

The cation-induced signals also differ in their intensities confirming a slightly different protein conformation depending on the substrate. The peak of Trp emission at 337 nm defines an apolar environment as expected from a membrane protein with several membrane spanning segments<sup>125</sup>.

The major challenge for a detailed assignment of signal variations is the amount of intrinsic tryptophans. The melibiose permease possesses 8 tryptophanyl residues. Only the Trp-73 lies in a

connecting loop, whereas the rest are embedded in hydrophobic membrane segments.

Trp-299 and Trp-342 in the C-terminal part of the protein were substituted by site-specific mutagenesis for phenylalanine. The sugar recognition parameters remained unchanged, although

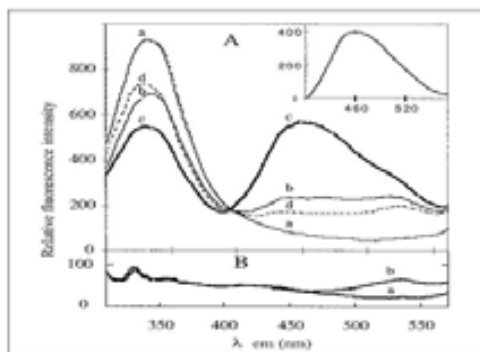


Figure 3.2 FRET of the melibiose permease wild type protein, A FRET of MelB, a only protein, b MelB with 15  $\mu$ M Dns<sup>2</sup>-S-Gal, c MelB with 15  $\mu$ M Dns<sup>2</sup>-S-Gal with 10 mM NaCl, d MelB with 15  $\mu$ M Dns<sup>2</sup>-S-Gal, 10 mM NaCl and 150 mM melibiose – competitive replacement of fluorescent sugar; B negative control with *E. coli* lipids in the presence of 10 mM NaCl (a) and after addition of Dns<sup>2</sup>-S-Gal (b)<sup>126</sup>.

the maximum of fluorescence signal for the W342F mutant slight shifted about 15 nm. This signal displacement reflects a more polar environment of the mutant in the sugar binding moiety. This result corroborates that Trp-342 lines the aqueous channel of the transport and is concomitantly located at or close to the substrate binding sites. Furthermore, the analysis elucidate that the C-terminal tryptophan residues Trp-299 and Trp-342 are the main contributors of the melibiose-induced signal of the melibiose carrier<sup>124</sup>.

The same approach has been made for the tryptophans located in the carboxy terminus of the membrane symporter. The six tryptophans were genetically manipulated and assess regarding their impact on the transport activity<sup>70</sup>. As already mentioned, sodium quenches the fluorescence emission intensity by 2% which could be assigned to three specific trp's. Trp-54 results in a quenching of the intensity of around 7%. An enhancement of 5% is provoked by the tryptophans Trp-116 and Trp-128 located in the transmembrane helix IV. The result of both effects cause a signal decrease of around 2%. Furthermore, replacements of tryptophan 128 impair the  $\beta$ -sugar recognition.

Trp-116 and Trp-128 influence the selectivity of the sugar leading to the assumptions of a proximity to both binding sites.

### 3.2. Dns<sup>2</sup>-S-Gal as external probe for FRET analyses

The galactosyl analog Dns<sup>2</sup>-S-Gal (2'-(N-5-dimethylaminonaphthalene-1-sulfonyl)-aminoethyl-1-thio- $\beta$ -D-galactopyranoside or D<sup>2</sup>G) carrying a fluorescent dansyl group, is a ligand of the melibiose permease<sup>126,127</sup>. Apart from the ethyl linked D<sup>2</sup>G, two other dansylated sugar analogs have been derived possessing a propyl (Dns<sup>3</sup>-S-Gal) or hexyl (Dns<sup>6</sup>-S-Gal) connector molecule. Originally utilized for the lactose permease<sup>128</sup>, this effective probe was established to test binding conditions in the MelB carrier. It has been used for vesicles as well as

proteoliposomes. The D<sup>2</sup>G probe is an indicator of polarity changes occurring in its proximity<sup>127</sup>. The validation of the energy transfer (FRET) between the intrinsic Trp's and the dansylated sugar bears the possibility to examine residues potentially close to the sugar binding site. The polarity of the melibiose binding site alters the fluorescence emission. Consequently, MelB mutations can be assessed for their impact on the polarity and evaluate its participation in structural rearrangements. The sugar acts as a competitive inhibitor as it blocks the transport activity of MelB and binds with a much higher affinity than the physiological  $\alpha$ -galactoside melibiose<sup>127</sup>. Protein samples in the presence of the fluorescent sugar can be examined either by exciting the intrinsic tryptophans at 290 nm or by directly evaluating the signal of D<sup>2</sup>G by exciting at 335 nm. Like melibiose, D<sup>2</sup>G couples to MelB in a sodium-dependent fashion. This result argues in favor of a potentially shared binding site for D<sup>2</sup>G and melibiose.

The maximum of emission at 465 nm for the alkylated reporter predicts a hydrophobic surrounding by evaluating the dielectric constant. The theory of a hydrophobic microenvironment agrees with the idea that the sugar binding site lies about half way through the plasma membrane enclosed by  $\alpha$ -helical domains. The amplitude of the D<sup>2</sup>G mediated signal at 465 nm is relatively small in the presence of the proton (Fig. 3.2). The signal increases strongly when sodium is added. This enhancement of energy absorption leads to the impression of further changes induced by the sodium cations.

By manipulating sequentially all eight tryptophans from the melibiose permease, the residues in position 64 and 299 are the main contributors of the energy resonance effect (Fig 3.3). By calculating the Förster distance, W64 and W299 are situated about 20 and 14Å respectively away from the alkylated fluorophore<sup>126</sup>.

Although contributing less to the FRET signal, the tryptophan in position 342 is apparently located close to the sugar binding site. The supporting information was obtained from the sodium-dependent FRET signal. As the maximum shifted towards a higher wavelength, the mutation is exposed to a more polar environment. Overall, the external probe D<sup>2</sup>G suits for specific assessment of Trp residues considering the sugar binding site for MelB mutants.

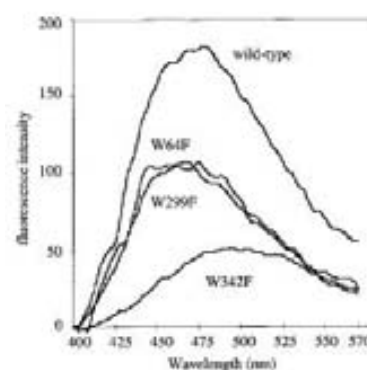


Figure 3.3 FRET contribution of different intrinsic Trp residues in the MelB carrier mediated by Dns<sup>2</sup>-S-Gal<sup>126</sup>.

### 3.3. Structural information of MelB by FTIR

FTIR spectroscopy delivers useful insights on the structure and on the structural changes induced by binding of substrates of MelB. In comparison to other spectroscopic techniques, the major advantage is the response of the entire protein without adding any external probes. Hence, sample and reaction interference are reduced to a minimum. The structure-sensitive bands amide I and II elucidate conformational changes of the protein upon interaction with ligands.

### 3.3.1. Secondary structure determination by FTIR

FTIR data revealed the secondary structure composition of the MelB symporter. The protein consists of 50%  $\alpha$ -helical content (bands at 1660 and 1653  $\text{cm}^{-1}$ ),  $\beta$ -sheets (bands at 1640, 1634 and 1628  $\text{cm}^{-1}$ ) account for 20%, and the remaining 30% include  $3_{10}$ -helices and unordered domains (bands at 1683, 1676, 1669 and 1647  $\text{cm}^{-1}$ )<sup>129</sup>. These values are in line with other membrane proteins such as LacY, the human erythrocyte glucose transporter and numerous ion channels<sup>59,130</sup>. The fact that the secondary structure of MelB is governed foremost by  $\alpha$ -helices confirms the topological prediction based on hydrophobicity and fusion proteins. The amide bands I and II account for almost the entire amount of the  $\alpha$ -helices spanning the plasma membrane. Moreover, the functional status of the protein can be assessed since bands around 1628  $\text{cm}^{-1}$  are indicative of protein aggregation<sup>131</sup>. Sodium and/or melibiose mediate changes of amide I and II associated to conformational arrangements of MelB upon substrate binding<sup>132</sup>.

H <sub>2</sub> O			D <sub>2</sub> O		
Wavenumber* ( $\text{cm}^{-1}$ )	% area*	Assignment	Wavenumber* ( $\text{cm}^{-1}$ )	% area*	Assignment
1683	17	Rev. turns	1683	16	Rev. turns
1676			1678		
1669			1671		
	1665				
1660	49	$\alpha$ , unordered	1660	42	$\alpha$
1653			1653		
1647	12	$3_{10}$ , open loops, $\alpha$	1646	13	Unordered, $\alpha$
1640	20	$\beta$ -sheets	1638	29	$\beta$ -sheets, $3_{10}$ , open loops
1634			1629		
1628					

\*These values were rounded off to the nearest integer.

Figure 3.4 Secondary structure assignment of *E. coli*'s melibiose carrier deduced from FTIR spectra in normal water and in the presence of deuterium water from Dave et al.<sup>129</sup>.

#### 3.3.1.1. Exchange of H/D in MelB

Proton/deuterium exchange experiments elucidate the accessibility of the protein's backbone. In a saturated D<sub>2</sub>O atmosphere, the melibiose carrier exchanges within 24 h 60% of its hydrogen atoms for the heavier deuterium. In comparison to other transporter this amount is relatively low (85% for LacY and 95% for ADP/ATP mitochondrial transporter)<sup>59,133</sup>.

As in the presence of the substrates this exchange rate is reduced, the protective implications of the substrates are evident. Moreover, since deuteration of MelB in the presence of both cations (sodium 50%, proton 46%) are very similar in the presence of the sugar, the protein compactness should be equal as well. The sugar molecule seems to have additional shielding or stabilizing effects. This fact was already corroborated from the protein purification<sup>40</sup>.

An additional feature is the protonation/deprotonation state of carboxylic residues. By infrared difference spectroscopy, IR<sub>diff</sub>, it has been proven that the peak around 1576  $\text{cm}^{-1}$

assigned to aspartic acids alters upon cation binding. This fact implies the involvement of the negatively charged residues in the coordination of the sodium cation confirming the earlier biochemical data about the C-terminal aspartates<sup>41</sup>. The negative peaks  $1725\text{ cm}^{-1}$  and  $1403\text{ cm}^{-1}$  as well as the positive peak at  $1384\text{ cm}^{-1}$  demonstrate possible changes in the protonation and deprotonation of the symporter.

The binding of the sugar causes changes in the asymmetrical stretching of the carboxylic side chains illustrated by the peaks at  $1591\text{ cm}^{-1}$  and  $1567\text{ cm}^{-1}$ . An alteration of the aspartic acids after melibiose binding occurs due to proposed breaking of a potential charged pair formed with a lysine or an arginine residue and the formation of hydrogen bonds directly with the sugar molecule<sup>134</sup>.

$\beta$ -sheet structures are the primary target for deuterium insertion for hydrogen atoms<sup>132</sup>. Although the membrane porter foremost consists of  $\alpha$ -helical membrane spanning segments, a substantial amount of  $\beta$ -sheet structure can be assigned to the cytoplasmic loops 4-5 and 10-11. This is consistent with suggestions that the two loops as possible re-entrant loops are involved in substrate translocation<sup>74,82</sup>.

The MelB mutant R141C exhibits a lower  $\beta$ -sheet content compared to the wild-type<sup>135</sup>. Cytoplasmic loops 4-5 and 10-11 are believed to form major parts of the entire  $\beta$ -sheets content of MelB. The higher H/D exchange rate in all conditions (MelB·Na<sup>+</sup>; MelB·melibiose; MelB·Na<sup>+</sup>·melibiose) indicates a MelB mutant better accessible and therefore less compact.

In orientation experiments structural titling events can be detected corresponding to polypeptide movements upon ligand binding. The main bands examined for the dichroism of the wild-type are the amide A ( $3296\text{ cm}^{-1}$ ), amide I ( $1660\text{ cm}^{-1}$ ) and amide II ( $1543\text{ cm}^{-1}$ ). By comparing the orientation of the R141C MelB mutant with the wild-type protein, the helix tilt has almost vanished and is not oriented with respect to the membrane plane<sup>135</sup>.

The wild-type melibiose permease reorients by  $26^\circ$  in the presence of only the proton or in combination with the sugar. In the presence of the sodium ion, the helices are even more inclined; about  $30^\circ$  for the sugar-sodium·MelB - complex and  $36^\circ$  for the MelB and the coupled sodium ion<sup>136</sup>.

### 3.3.2. ATR- infrared difference spectra of MelB mutants

The attenuated total reflectance difference spectra ( $IR_{diff}$ ) permits the study of membrane protein with an alternating flux of buffer solution containing the protein ligands. A stable protein film on top the reflecting material (crystal) is an essential requirement<sup>134</sup>.

Other crucial parameters are the ionic strength and the pH of the buffer solutions, the absorption of the ligands and the effect of the lipid on the protein.

For the ionic strength, even small variations in the buffer system (sample buffer and reference buffer) could cause an inflation of the proteoliposome layers. This swelling of the proteoliposomes contributes to the absorbance spectrum and is not associated to the ligand effect. The pH difference between sample and reference buffer should not exceed 0.5 units. Any pH variation above this margin results in distortion of film thickness and protonation of side chains which are incorrigible during the data processing.

Fortunately for the  $IR_{diff}$  spectrum of the melibiose permease, the substrates melibiose and sodium do not introduce additional absorbance bands in the amide region between 1700 and 1500  $cm^{-1}$ .

Each difference spectrum is the result of all detected changes after the subtraction of two successive absorbance spectra in different conditions. In the case of the cation, the difference spectrum demonstrates the structural changes imposed on the protein by the formation of a sodium-MelB intermediate complex at the expense of the preceding proton-MelB complex. The cation alone is not transported. The acquired  $IR_{diff}$  of the protein in the presence of the sodium exhibits arrangements within the protein due to binding. Sodium induces tilting of transmembrane segments<sup>134</sup>, changes in sheets, reverse turns and in unordered structural matter as well<sup>132</sup>. For the  $IR_{diff}$  of the sugar the process is repeated by changing only the composition of the buffer solution.

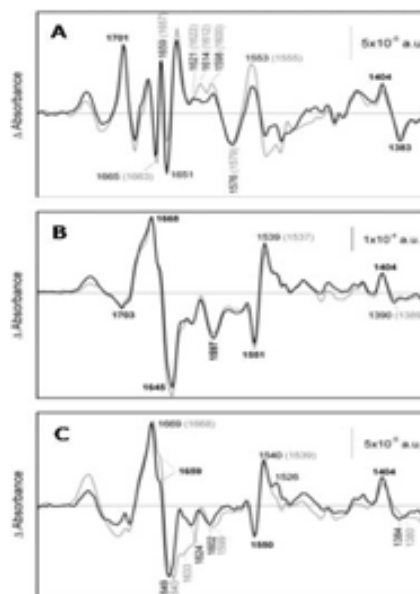


Figure 3.5  $IR_{diff}$  of R141C (black) compared to WT (grey); **A** sodium-induced difference spectrum of R141C and Wt; **B** melibiose-induced difference spectrum of R141C and Wt in the presence of sodium (10 mM); **C** melibiose-induced difference spectrum of R141C and Wt in the presence of proton. General Buffer composition consist of 20 mM MES, 100 mM KCl, pH 6.6 supplemented by either 10 mM NaCl (A), 10 mM melibiose + 10 mM NaCl (B) or 50 mM melibiose (C). Leon *et al.*<sup>135</sup>

### 3.3.2.1. C-less

The MelB transporter devoid of its natural cysteines (C-less) demonstrates almost identical difference spectra compared to the wild-type transporter. The results from the infrared difference spectra were extensively discussed in Leon *et al.*<sup>134,137</sup>. For the IR<sub>diff</sub> spectra the deconvolution method using the maximum entropy<sup>138</sup> reveals peaks similar to the wild-type transporter.

For the sodium-dependent difference spectrum of C-less, the peaks at 1649, 1657 and 1663 cm<sup>-1</sup> are assigned to  $\alpha$ -helix structures. The peaks at 1553 and 1539 cm<sup>-1</sup> respectively belong to the amid II region. The detected peak at 1724 is assigned to the vibration of the protonated carbonyl group of aspartates or glutamates.

The melibiose-induced spectra in the presence of the proton or the sodium are more intense than the sodium-induced IR<sub>diff</sub>; more than 2 fold for the proton but almost 5 fold for the sodium. Peaks related to  $\alpha$ -helix structures are detected at 1666, 1659 and 1652 cm<sup>-1</sup>. The  $\beta$ -structure peaks are at 1695, 1688, 1680 and 1672 cm<sup>-1</sup>. Leon *et al.* described the peak at 1641 cm<sup>-1</sup> as a reversed turn or  $3_{10}$  helix or even loop structure<sup>134,139</sup>.

### 3.3.2.2. R141C

For the R141C MelB protein, the IR<sub>diff</sub> spectrum for sodium binding almost overlaps with the wild-type spectrum. This result indicates that the sodium binding is unaffected by the replacement of the arginine 141 confirming earlier FRET studies<sup>102</sup> and electrogenic clamp measurements<sup>74</sup>. The half saturation constant of sodium is unaffected<sup>102</sup> as it is the case for the activation constant of the binding in presence of the sugar-derivative  $\alpha$ -NPG<sup>64,75</sup>.

Sugar-induced absorbance spectrum alterations are observed when MelB forms the ternary complex (mel·Na<sup>+</sup>·MelB or mel·H<sup>+</sup>·MelB) at the expense of the cation-bound intermediate.

The spectrum indicates wild-type like sugar binding reflected by the variety of positive and negative peaks.

### 3.3.2.3. Aspartic acids 19, 55, 59 and 124

The proposal that the aspartic acids 19 (helix I), 55, 59 (both helix II) and 124 (helix IV) are sodium ligands stimulated the detailed examination of their substrate binding as the elementary requirement for the transport mechanism. The profound study done by Granell *et al.* revealed that the melibiose permease mutant D55C and D59C completely lost their ability to couple with the sodium cation even at a saturating concentration of 50 mM (Fig 3.6)<sup>61</sup>. D19C, formerly described a potential ligand for co-substrate coupling, exhibit C-less like binding. Therefore, this residue can be excluded from the list of possible residues forming the cation binding site. The IR<sub>diff</sub> of D124C shows an alternative issue. Clearly the distinctive peaks in the amide I and II region are significant even though with much lower intensity. By multiplying the spectrum with a factor of 3.5, peaks of the amide I and amide II region are comparable to the reference of the C-less.

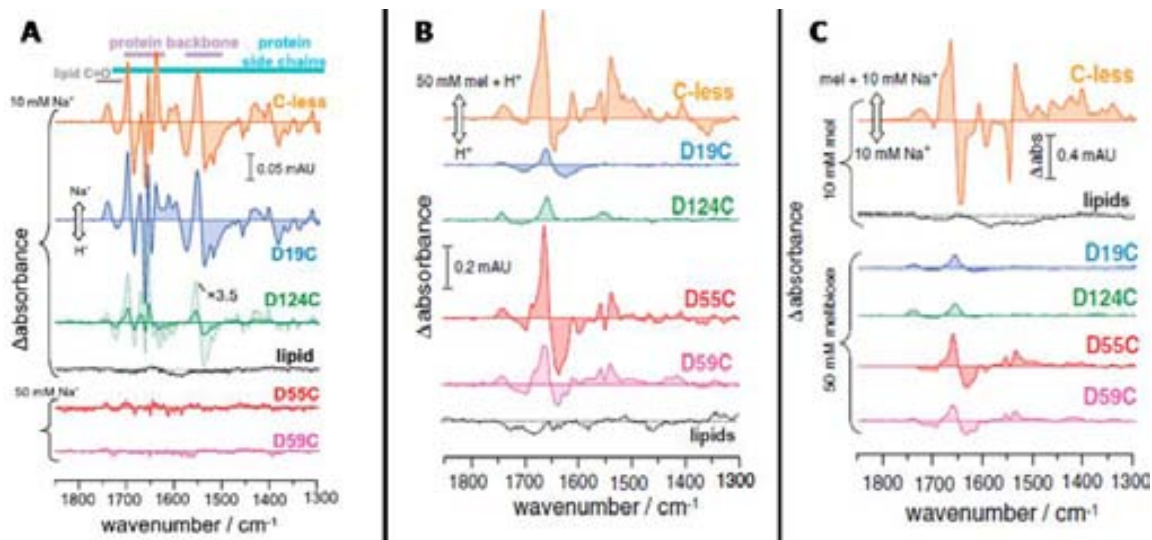


Figure 3.6 IR<sub>diff</sub> for MelB mutants D19C (blue), D124C (green), D55C (red) and D59C (pink) in comparison to C-less (orange, positive control) and lipids (black, negative control). **A** sodium-induced IR<sub>diff</sub>; **B** melibiose-induced IR<sub>diff</sub> in the presence of the proton; **C** melibiose-induced IR<sub>diff</sub> in the presence of sodium. Figures taken from Granell et al.<sup>61</sup>

For the melibiose, the aspartates 55 and 59 present a melibiose-induced IR<sub>diff</sub> spectrum. The replacements of Asp-55 and Asp-59 by cysteine do not change the binding of melibiose in the presence of the proton. But for the sodium-induced IR<sub>diff</sub><sup>139</sup> the spectral intensity declines immensely, primarily for the D59C mutant. This is in accordance to the results of Zani et al.<sup>46</sup>. For the D19C mutant, IR<sub>diff</sub> evidently point out its importance for the binding of the sugar. The absence of a melibiose-induced IR<sub>diff</sub> in the presence of either the sodium or the proton as coupling ion indicates that Asp-19 might be involved in direct binding of the sugar molecule<sup>139</sup>. D124C displays a defect in melibiose binding. The melibiose-induced IR<sub>diff</sub> of this mutant in the presence of either cation does not provoke any conformational changes in the protein, as shown from the extremely low spectral intensity (< 5% with respect to the C-less).

# MATERIALS AND METHODS

## 4. Materials

### *4.1. Chemicals*

If not else stated, all commercially available chemicals were bought from Sigma-Aldrich (St. Louis, MO, USA).

### *4.2. Media for bacterial growth*

#### **LB (Luria Bertani) broth**

1% (w/v) tryptone

0.5% (w/v) yeast extract

1%(w/v) NaCl

#### **M9 minimal medium**

42 mM Na<sub>2</sub>HPO<sub>4</sub>·2H<sub>2</sub>O

22 mM KH<sub>2</sub>PO<sub>4</sub>

8.5 mM NaCl

18.7 mM NH<sub>4</sub>Cl

54 mM glycerol

1 mM MgSO<sub>4</sub>

0.1 mM CaCl<sub>2</sub>

1 mM thiamine-HCl

0.2% (w/v) casaminoacid

0.3 mM ampicilin

pH 7.5

### 4.3. Buffers for protein Purification

#### Resuspension Buffer

50 mM Tris-HCl  
50 mM NaCl  
5 mM  $\beta$ -mercaptoethanol

#### Buffer I (2x)

20 mM Tris-HCl  
1.2 M NaCl  
10 mM  $\beta$ -mercaptoethanol  
20% (v/v) glycerol  
pH 8.0

#### Buffer 9/10 (2x)

20 mM Tris-HCl  
600 mM NaCl  
5 mM  $\beta$ -mercaptoethanol  
10% (v/v) glycerol  
10 mM imidazol  
10 mM melibiose  
pH 8.0

#### Buffer A

20 mM Tris-HCl  
600 mM NaCl  
5 mM  $\beta$ -mercaptoethanol  
10% (v/v) glycerol  
10 mM imidazol  
10 mM melibiose  
0.2% (w/v) LAPAO  
pH 8.0

#### Buffer B

20 mM Tris-HCl  
600 mM NaCl  
5 mM  $\beta$ -mercaptoethanol  
10% (v/v) glycerol  
10 mM imidazol  
10 mM melibiose  
0.1% (w/v)  $\beta$ -DDM  
pH 8.0

#### Buffer C

20 mM Tris-HCl  
100 mM NaCl  
5 mM  $\beta$ -mercaptoethanol  
10% (v/v) glycerol  
10 mM imidazol  
10 mM melibiose  
0.1% (w/v)  $\beta$ -DDM  
pH 8.0

Buffer D

20 mM Tris-HCl  
 100 mM NaCl  
 5 mM  $\beta$ -mercaptoethanol  
 10% (v/v) glycerol  
 100 mM imidazol  
 10 mM melibiose  
 0.1% (w/v)  $\beta$ -DDM  
 pH 8.0

*4.4. Buffers used in infrared spectroscopy experiments*Stock Buffer (W)

20 mM MES  
 100 mM KCl  
 pH 6.6

Washing Buffer (W1)

20 mM MES  
 110 mM KCl  
 pH 6.6

Washing Buffer (W2)

20 mM MES  
 150 mM KCl  
 pH 6.6

Buffer Na<sup>+</sup> 10 mM

20 mM MES  
 100 mM KCl  
 10 mM NaCl  
 pH 6.6

Buffer Na<sup>+</sup> 50 mM

20 mM MES  
 100 mM KCl  
 50 mM NaCl  
 pH 6.6

Buffer Mel 50 mM

20 mM MES  
 100 mM KCl  
 50 mM melibiose  
 pH 6.6

Buffer Na<sup>+</sup> + mel 10 mM

20 mM MES  
 100 mM KCl  
 10 mM NaCl  
 10 mM melibiose  
 pH 6.6

Buffer Na<sup>+</sup> + mel 50 mM

20 mM MES  
 100 mM KCl  
 10 mM NaCl  
 50 mM melibiose  
 pH 6.6

#### 4.5. Buffer for the preparation of RSO and ISO vesicles

To generate membrane vesicles for either the wild-type or any mutated form of the MelB protein, cells have been grown as described under 2.1.4.

##### 4.5.1. Inside-out vesicles (ISO)

###### Washing Buffer

20 mM Tris-HCl

pH 8.0

###### Storage Buffer (ISO)

100 mM  $KP_i$

10 mM EDTA

##### 4.5.2. Right-side-out vesicles (RSO)

###### Washing Buffer

20 mM Tris-HCl

pH 8.0

###### Sucrose Buffer

20 mM Tris-HCl

30%(w/v) Sucrose

###### Storage Buffer (RSO)

100 mM  $KP_i$

10 mM  $MgSO_4$

pH 7.5

## 5. Methods

### 5.1. Preparation of Proteoliposomes

#### 5.1.1. Bacterial strains

The *E. coli* strain DW2-R<sup>140</sup> (*melA*<sup>+</sup>  $\Delta$ B,  $\Delta$ lacZY) has been used primarily throughout the whole study. This strain is a *recA* depleted version of the maternal DW2 strain, in which its endogenous genes of the melibiose (*melB*) and lactose permeases are deleted. The gene *recA* encodes for the recombinase A which prevents homologue recombination and therefore any inserted plasmid remains extra chromosomal. Competent cells for transformation were prepared by calcium and rubidium chloride method after Hanahan<sup>141</sup>.

The pK95 $\Delta$ AHB plasmid, used throughout the whole procedure, is derived from the commercially available pKK 223-3 (Pharmacia, Uppsala, Sweden). Plasmid purification was accomplished by using the Qiaprep® Miniprep Kit (Qiagen, Hilden, Germany). The plasmid pK95 $\Delta$ AHB contains the *melB* gene with a genetically engineered His-Tag, as well as a deleted part of the *melA* gene. *melB* encodes for the melibiose carrier and *melA* for the  $\alpha$ -galactosidase from *Escherichia coli*. The presence of the *melA*-gene leads to an increased expression of the melibiose symporter<sup>40</sup>. The vector also harbors an ampicillin resistance marker to reduce the risk of contamination and to maintain the selection pressure. The expression of the *melB* gene is controlled by a *tac*-promoter<sup>40</sup>.

An additional *E. coli* strain, DH5 $\alpha$ , has been only used as a shuttle strain for transformation of the pK95 $\Delta$ AHB plasmid after PCR reaction due to its higher transformation efficiency compared to the DW2-R strain.

#### 5.1.2. Site-directed mutagenesis

In-vitro amino acid substitutions were carried out by the usage of the Quik-Change Site-Directed Mutagenesis (Stratagene) combined with the protocol used by Edelheit et al.<sup>142</sup>. The *melB* gene already contains point mutations of its natural cysteines. Cys-110, Cys-310 and Cys-364 have been mutated to serine and Cys-235 has been exchanged to valine. In the forthcoming chapters, the abbreviation C-less refers to the wild-type protein devoid of its cysteines.

The polymerase chain reaction for single residue substitution (Fig. 2.1) was performed by the protocol of Kushner and Mandel & Higa, respectively<sup>143,144</sup>. A PCR-reaction was performed by just using one oligonucleotide primer at a time, resulting in a linear amplification of the matrix. Hence, two reactions were placed simultaneously, one with only the forward and the other with the reverse primer. The primers were

designed and shipped from Invitrogen, Carlsbad, CA, USA, and composed of 27 to 35 nucleotides. The initial DNA quantity required for the PCR was quite large (~500 ng) since the amplification process was not exponential. 0.2 mL tubes (Deltalab, Rubi, Barcelona, Spain) were used for a 25  $\mu$ L reaction volume containing 1X buffer solution (20 mM Tris-HCl (pH 7.5), 8 mM MgCl<sub>2</sub>, 7.5 mM DTT, 50  $\mu$ g/mL BSA), 0.1 mM of dNTP's (dATP, dGTP, dCTP and dTTP), 0.75 mM MgSO<sub>4</sub>, and 0.5  $\mu$ M of forward or reverse primers. Shortly before starting the PCR reaction 0.02 units of KOD polymerase (Novagen, Merck KGaA, Darmstadt, Germany) was added and hot-start activated. Samples were subjected to the PCR thermocycler (VWR, Radnor, PA, USA) following a programmed cycling: 1) initial 95°C hot start polymerase activation and template denaturation for 5 min; 2) 30 cycles composed of DNA denaturation for 30 sec at 95°C, primer annealing at 55°C for 30 sec, and a product elongation step at 70°C for 7.5 min; 3) DNA elongation step at 70°C for 10 min.

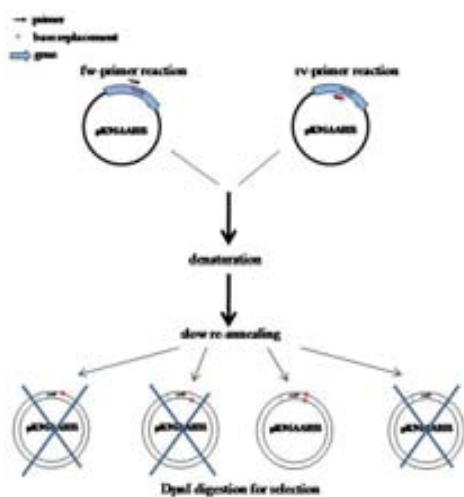


Figure 5.1 PCR flow chart technique

After the amplification both solutions with the different primers were combined. The DNA product mixture was once again denaturated at 95°C for 1 min and a slow temperature decrease terminating at 37°C re-anneals the products arbitrarily. The final mixture is composed of four different types of plasmids. Only one contains the mutation introduced on both strands of the DNA. Two plasmids contain the mutation only on one strand and the one contains no substitution at all.

To successfully select the product containing the desired base substitution, the DNA solution was purified using the Qiagen PCR purification kit and furthermore incubated with the enzyme DpnI to digest undesired methylated maternal plasmid DNA. Eventually, the DH5 $\alpha$  *E. coli* strain was transformed

with the plasmid to receive a nick-free MelB-expression vector. The *E. coli* strain DH5 $\alpha$  was used as a “shuttle-strain” to enlarge the plasmid quantity on the one side, and to methylate the plasmid DNA on the other, before transformation of the strain DW2-R. Direct transformation and growth of the strain DW2-R was highly inefficient for PCR-generated plasmid DNA.

For preliminary screening of successfully transformed cells, colonies were cultured in small volumes of 10-15 mL in LB medium, adding plasmid-purified with the Qiaprep® Miniprep Kit afterwards. The plasmid was subjected to endonuclease digestion. Fortunately, the *melB* gene contains unique restriction sites every 250 bp offering the possibility to scrutinize the plasmid for contingent abnormalities in product size. The plasmid size was determined by agarose gel electrophoresis using 1%-agarose gels (Sigma-Aldrich, St. Louis, MO, USA) in TAE buffer (pH 8.0). To verify the desired nucleotide substitution, samples were sequenced with *melB* specific primers binding approximately 100 bp upstream and downstream the *melB* gene at the local Genomics Service of the *Universitat Autònoma de Barcelona*.

Throughout the thesis, the MelB mutants will be designated by an abbreviation composed of a single letter corresponding to the amino acid in a one-letter code followed by the position of the residue in the

wild-type protein and the final letter indicating the amino substitution.

Primer	Sequence	Comments
K377V	5'-CAGACTATGGTGGTG <b>GTG</b> GGCGGTTTCAGCCTT-3'	Lys to Val at position
	5'-AAAGGCTGAACCGCC <b>CAC</b> CACCACCATAGTCTG-3'	377
K377H	5'-CAGACTATGGTGGTG <b>CAT</b> GGCGGTTTCAGCCTTTC-3'	Lys to His at position
	5'-GCAAAGGCTGAACCGCC <b>ATG</b> CACCACCATAGTCTG-3'	377
K377R	5'-ACTATGGTGGTG <b>CGT</b> GGCGGTTTCAGCCTTTC-3'	Lys to Arg at position
	5'-GCAAAGGCTGAACCGCC <b>ACG</b> CACCACCATAGT-3'	377
K377D	5'-ACTATGGTGGTG <b>GAT</b> GGCGGTTTCAGCCTTTC-3'	Lys to Asp at position
	5'-GCAAAGGCTGAACCGCC <b>ATC</b> CACCACCATAGT-3'	377
L236F	5'-ACGATCAGCTTTCAGTC <b>TTC</b> TTGGGTATGGCTCTTGC-3'	Leu to Phe at position
	5'-GCAAGAGCCATACCCAA <b>GAA</b> ACTGAAAGCTGATCGT-3'	236
I22S	5'-GGAAGGATTTTTCG <b>AGC</b> GGCATTGTGTATATG-3'	Ile to Ser at position 22
	5'-CATATACACAATGCC <b>GCT</b> CGCAAAATCCTTCC-3'	
I22A	5'-GGGAAGGATTTTTCG <b>GCC</b> GGCATTGTGTATATG-3'	Ile to Ala at position 22
	5'-CATATACACAATGCC <b>GCC</b> CGCAAAATCCTTCCC-3'	
Q372C	5'-GTATCGCTTACTCCGT <b>TGC</b> ACTATGGTGGTGAAGG-3'	Gln to Cys at position
	5'-CCTTCACCACCATAGT <b>GCA</b> CACGGAGTAAGCGATAC-3'	372
D55K	5'-GGTGGCGAGGATCTGGA <b>AAG</b> GCTATTAACGATCCG-3'	Asp to Lys at position
	5'-CGGATCGTTAATAGC <b>CTT</b> CCAGATCCTCGCCACC-3'	55
D59K	5'-GGGATGCTATTAAC <b>AAA</b> CCGATTATGGGATGG-3'	Asp to Lys at position
	5'-CCATCCCATAATCGG <b>TtT</b> GTTAATAGCATCCC-3'	59
G379V	5'-GTGGTGAAGGGCG <b>TtT</b> CAGCCTTTC-3'	Gly to Val at position
	5'-GCAAAGGCTGAA <b>ACG</b> CCCTTCACCAC-3'	379
G379C	5'-GGTGGTGAAGGGC <b>TgT</b> CAGCCTTTC-3'	Gly to Cys at position
	5'-CAAAGGCTGAAC <b>AGC</b> CTTCACCACC-3'	379
A383C	5'-GGGCGGTTTCAGCCTT <b>TTC</b> GCTTTTTTCATTGCGG-3'	Ala to Cys at position
	5'-CCGCAATGAAAAAAGC <b>GCA</b> AAAAGGCTGAACCGCCC-3'	383
F385C	5'-GCCTTTGCGGCT <b>GtT</b> TTCATTGCGGTTG-3'	Phe to Cys at position
	5'-CAACCGCAATGAA <b>CA</b> AGCCGCAAAGGC-3'	385
L391C	5'-CTTTTTTCATTGCGGTTGTGT <b>GC</b> GGGATGATTGGCTATGTACC-3'	Leu to Cys at position
	5'-GGTACATAGCCAATCATCCC <b>GC</b> ACACAACCGCAATGAAAAAAG-3'	391
G395C	5'-GTTGTGTTAGGGATGATT <b>TG</b> CTATGTACCGAATGTTG-3'	Gly to Cys at position
	5'-CAACATTCGGTACATAGC <b>AA</b> ATCATCCCTAACACAAC-3'	395
Y396C	5'-GTTAGGGATGATTGGCT <b>GC</b> TACCGAATGTTGAAC-3'	Tyr to Cys at position
	5'-GTTCAACATTCGGTAC <b>GC</b> AGCCAATCATCCCTAAC-3'	396

Figure 5.2 Primer sequences of the site-directed mutations of MeIB (first column describes the abbreviated name of the residue replacement, e.g. K377V ( lysine in position 377 was substituted by valine; second column lists the sequence of the primer in 5'→ 3'

direction, upper sequence for the forward primer, lower sequence for the reverse primer; third column explains residue replacement). Substituting bases are framed in bold and italic. Primers were generated by [http://www.bioinformatics.org/primerx/cgi-bin/DNA\\_1.cgi](http://www.bioinformatics.org/primerx/cgi-bin/DNA_1.cgi) and validated for self-dimer and hetero-dimer by <http://eu.idtdna.com/analyzer/Applications/OligoAnalyzer/>. All other single amino acid substitutions listed in the result section were made by the lab of Dr. Gerard Leblanc (Laboratoire J. Maetz, Département de Biologie Cellulaire et Moléculaire/CEA, Villefrance sur Mer, France).

### 5.1.3. Transformation

*E. coli* DW2-R or DH5 $\alpha$  competent cells were transformed with the pK95 $\Delta$ AHB-plasmid containing wild-type or mutated *melB* gene following the heat shock protocol by Mandel and Higa<sup>144</sup> or Inoue<sup>145</sup>, respectively. Therefore, aliquots of cells were incubated with approximately 100 ng of plasmid-DNA for 30 min on ice, then incubated for 3 min at 42°C (water bath), and finally kept for 5 min on ice. After adding 2 mL of LB medium cells were incubated at 37°C, and either plated on a MacConkey-agar plate containing 100 mg/mL ampicillin, 10 mg/mL tetracycline and 10 mM melibiose for the DW2-R strain, or on a LB agar plate with just 100 mg/mL ampicillin as selection marker for the DH5 $\alpha$  strain. The MacConkey plates contain a pH indicator which responds to acidification of the surrounding medium<sup>146,147</sup>. The decrease in pH is caused by the metabolisation of the melibiose disaccharide into glucose and galactose by the  $\alpha$ -galactosidase encoded by *melA*. White Colonies of the DW2-R strain indicate absence of melibiose metabolism and thus melibiose uptake, in turn implying for a *melB* gene encoding for a nonfunction MelB permease.

### 5.1.4. Bacterial culture

After spreading an aliquot of the cell stock on an agar plate, a desired colony was selected and grown overnight in 12 mL of LB medium supplemented with 100 mg/mL ampicillin and 10 mg/mL tetracycline at 30°C and 200 rpm. After 12 hour growth the bacterial culture was used as *inoculum* in 400 mL of M9 minimal medium (pH 7.5) containing glycerol as the sole carbon source supplemented with 1 mM thiamine-HCl as well as ampicillin in the usual concentration. Glycerol is relatively cheap and maintains the pH value better than other C-sources<sup>148,149</sup>. Tetracycline has not been added anymore since the ampicillin is sufficient to avoid the risk of contamination and as a selection marker for the strain to express the proteins from the pK95 $\Delta$ AHB plasmid including MelB. After incubation for 6 hours, the pre-culture was further diluted 20-fold into the final M9 expression medium consisting of 8 liters, and grown overnight reaching an optical density between 1.0 and 1.5 in OD<sub>600nm</sub> depending on the MelB mutant. Cell cultures normally were grown at 30°C since some MelB mutants were reported to be temperature sensitive<sup>150</sup>. For cell cultivation the cells were harvested by centrifugation at 10.000 g by means of a Beckman centrifuge (Beckman Coulter,

Brea, CA, USA), washed twice with the Resuspension buffer, and frozen at  $-80^{\circ}\text{C}$  until further use.

### 5.1.5. Selection of second-site revertants

MelB variants displaying a white color on Mac-Conkey-Agar plates were further incubated at  $30^{\circ}\text{C}$  for 5-8 days, to look for a second mutation that could restore the transport ability. Several dark red areas within the initial white colonies appeared and were selected. Re-streaking on plates containing the same agar composition, prevented possible contaminants. The pK95 $\Delta$ AHB plasmid was isolated and sent for sequencing to verify an intact melB gene. In the final control the purified plasmid-DNA was re-transformed into competent DW2-R cells to prove the effect of mutation on the phenotype.

### 5.1.6. Protein purification

#### 5.1.6.1. Preparation of inverted vesicles

Frozen cells of a wet weight of approximately 15-20 g were thawed at  $25^{\circ}\text{C}$  in a water bath. After centrifugation to remove broken DW2-R cells, the pellet was resuspended in 50 mM Tris-HCl (pH 8.0), 50 mM NaCl and 5 mM  $\beta$ -mercaptoethanol and incubated in the cold room ( $4^{\circ}\text{C}$ ) with 10 mg/mL lysozyme and 15 mM EDTA for 30 min to destabilize the outer membrane. From this step onwards, the procedure was either be carried out in the cold room or in ice. Shortly before cell lysis, RNase and DNase (Roche Diagnostics, Basel, Switzerland) have been added at a final concentration of 50  $\mu\text{g}/\text{mL}$  and activated by 15 mM  $\text{MgSO}_4$ . For cell disruption purposes, the cells have either been subjected for three times to a

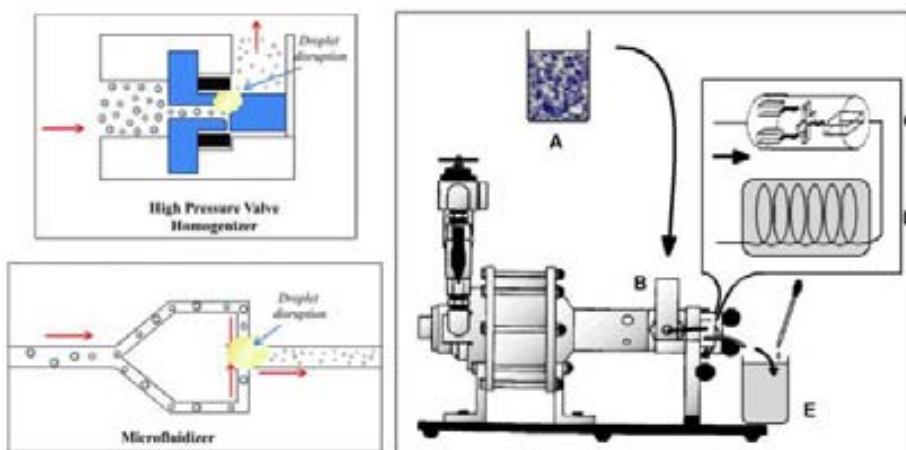


Figure 5.3 assortment of cell disruption techniques; upper left panel: high pressure method to break cells (similar to French press); lower left panel: microfluidizer method; right panel: side view of the microfluidizer

microfluidizer (Microfluidizer 110S) or to a French press (American Instruments Company, Silver Spring, Maryland, USA) with a maximal pressure applied of 1,200 psi for the French press and 20,000 psi for the Microfluidizer. A centrifugation step at 1,000 g sedimented the unbroken cells and debris, whereas the vesicles still present in the

supernatant were sedimented using an ultracentrifuge (Sorvall, DJB labcare Ltd., England) at a centrifugal force of 146,000 g for 35 min at a temperature of 4°C and rinsed several times with the Resuspension buffer. At this point the possibility existed to either continue with the protocol or store the ISO vesicles at -80°C. Preferentially, the vesicles were solubilized immediately with detergent and not frozen. Eventually, this yielded in a higher outcome which was critical for some low expression MelB mutants.

### 5.1.6.2. Solubilization and elution of MelB

The ISO vesicles-containing pellet was mixed with Buffer I (2X) in a volume-ratio of 1:1 and distributed into ultracentrifugation tubes again. Each tube was filled up to the top (~25 mL) with Buffer I (1X) to avoid a collapsing of the tube during ultracentrifugation. Once centrifuged (see previous section for the conditions), the supernatant was discarded, and the pellet was resuspended in Buffer 9/10 and solubilized by adding 1% of 3-(Laurylamido)-N,N-dimethylaminopropylamine oxide (LAPAO)<sup>151</sup> which is

$$\text{concentration (mg/mL)} = \frac{\text{absorbance at 280nm}}{\text{extinction coefficient of MelB}}$$

approximately 20-fold the critical micellar concentration (cmc) (cmc<sub>LAPAO</sub>=0.052%). Moreover, the protease

inhibitor 4-(2-Aminoethyl) benzenesulfonyl fluoride hydrochloride (AEBSF, Sigma-Aldrich) was added to prevent the cleavage of the protein.

The solubilization was carried out incubating the protein for 30 min in the cold room on an orbital shaker. In the following centrifugation, the sediment merely consists of remnants from the former membrane vesicles. Almost all membrane proteins are solubilized in forms of micelles, visually apparent by a yellow color of the supernatant. To separate the MelB protein from other solubilized proteins, Ni-nitrilotriacetic acid (NTA) resin was added to the detergent protein mix. The genetically engineered histidine tag forms a

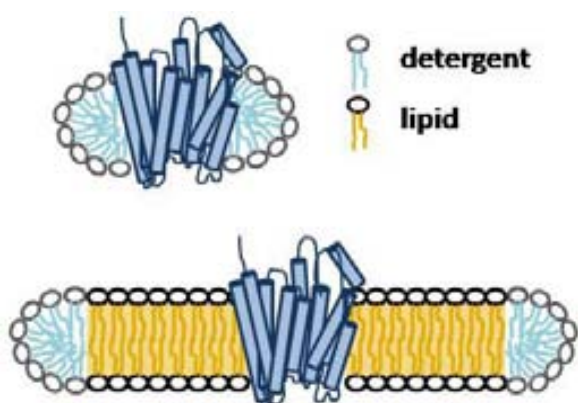


Figure 5.4 solubilized protein either in detergent micelle (upper image) or in a micelle composed of detergent and lipid (lower image)

complex with the resin and attaches the MelB protein. Previous to its use, the nickel-NTA resin was washed three times with distilled water and three times with Buffer I (1X), and kept in buffer A to equilibrate the resin with LAPAO. After 1 h in the cold room with smooth agitation, the sample was centrifuged using no more than 4,000 g, and the sedimented resin was washed twice with buffer A.

Next, the Ni-resin-bound protein was loaded onto a 15 mL-chromatography column (Biorad, Hercules, CA, USA) and washed thoroughly with on column volume of buffer A containing 0.2% LAPAO still well above the cmc value for LAPAO. At this point, the detergent solubilizing the protein was

exchanged by replacing LAPAO with 0.1% n-dodecyl- $\beta$ -D-maltoside ( $\beta$ -DDM) in the washing buffer, and rinsing with 5 column volumes. Then, using 5 column volumes of buffer C the sodium concentration was reduced to 100 mM. Finally, the protein was eluted from the columns by using 5-15 mL of buffer D, containing 100 mM imidazole and 100  $\mu$ M of AEBSEF, and the elutant was collected in 1.5 mL fractions. The amount of protein in each fraction was estimated measuring the absorbance of 280 nm on a quartz cuvette (Hellma GmbH & Co. KG, Germany), in an UV/VIS-spectrophotometer (Varian Cary 3Bio UV-Vis spectrophotometer, Varian, CA, USA). Fractions containing sufficient amount of protein ( $> 0.15$  mg/mL) were pooled. The protein concentration of each fraction was calculated as shown in more detail below, considering that the extinction coefficient for MelB is  $1.5 \text{ L}\cdot\text{mol}^{-1}\cdot\text{cm}^{-1}$ . Furthermore, an aliquot of 20  $\mu$ L was collected to check the protein purity on a 12% Coomassie-stained SDS-PAGE-gel. The entire protein solution was, depending on the circumstances, shock-frozen by liquid nitrogen and stored at  $-80^\circ\text{C}$ , or directly reconstituted into liposomes. The above described protein solubilization protocol was also used in other instance with a few modifications. For the solubilization of inverted membrane vesicles  $\beta$ -DDM was added instead of LAPAO. In this case the exposure time to the detergent to ensure adequate protein extraction was extended, from the 30 min used for LAPAO, to 2 hours for the gentler detergent  $\beta$ -DDM. Since  $\beta$ -DDM was used in this case as the unique detergent throughout the whole procedure, the exchange of detergent in the affinity chromatography was skipped.

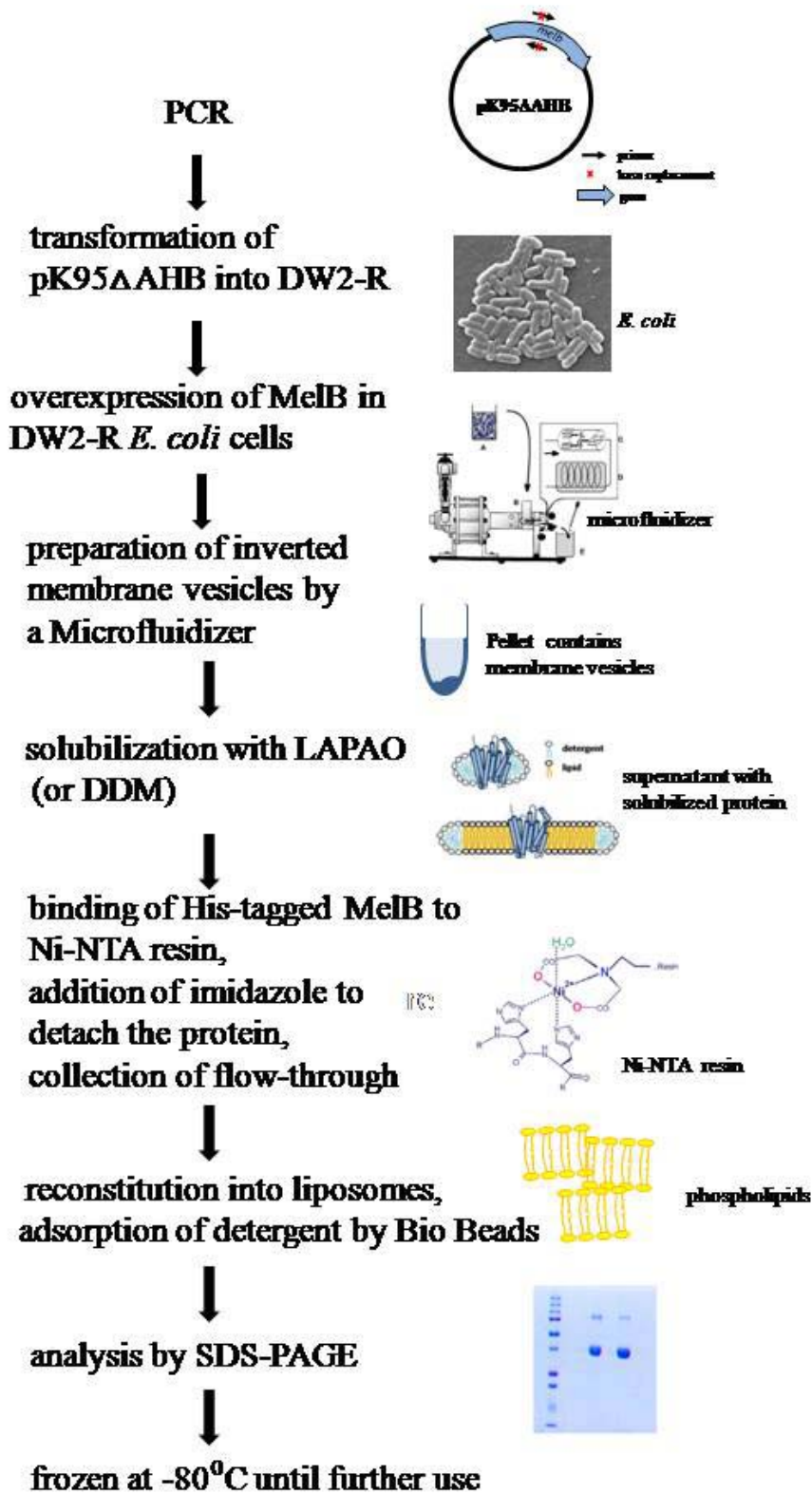


Figure 5.5 Flow chart of the MelB purification

To prepare proteoliposomes, natural solid *E. coli* total lipids (Avanti Polar lipids Inc., Alabaster, AL, USA) were weighed on a microbalance according to the amount of protein to be reconstituted. For every mg of MelB protein, 2 mg of solid *E. coli* total lipids is required. *E. coli* lipids were kept constantly in a nitrogen-enriched atmosphere and dissolved rapidly in chloroform to prevent any event of hydration and/or oxidation of the lipids. Usually, the *E. coli* total lipids were prepared at 10 mg/mL. Evaporation of chloroform in a rotary evaporator (Heidolph, Germany) yielded in a very thin lipid film. Upon addition of the reconstitution buffer (20 mM MES, 100 mM KCl, pH 6.6) the lipid-buffer mix was vortexed for at least 5 min at room temperature to form large multilamellar vesicles. Those vesicles were first disrupted by extrusion using 1  $\mu\text{m}$  pore-size polycarbonate filters to prefilter (Whatman, GE Healthcare, UK) and thereafter a 0.1  $\mu\text{m}$  pore-size filter to downsize the vesicle diameter and receive homogeneous unilamellar vesicles. To the previously purified MelB protein solubilized in detergent, lipid vesicles were added to a ratio of 2:1 of lipid:protein (w/w). The mixture was incubated for 10 min in the cold room. Bio-beads SM-2 (BioRad, Hercules, CA, USA) washed with 50 mL MilliQ-H<sub>2</sub>O and 50 mL washing buffer (20 mM MES, 100 mM KCl, pH 6.6) were added in three aliquots to a final concentration of 150 mg/mL. For efficient detergent adsorption and protein insertion into the vesicles, the mixture was incubated overnight at 4°C<sup>152</sup>. With the help of a polypropylene column the Bio-beads were separated, allowing only the liquid phase containing the proteoliposomes to flow through. The proteoliposomes (Fig. 2.4) were sedimented three times at approximately 310,000 g. After each centrifugation step the proteoliposomes were resuspended in the stock buffer (20 mM MES, 100 mM KCl, pH 6.6) and sonicated in the Ultrasonic cleaner (Fungilab, Keyland Court, NY, USA) twice for 20 sec for proper buffer exchange of the vesicles interior. Under these circumstances any contamination with sodium or melibiose can be excluded. In the final step the proteoliposomes were resuspended in stock buffer to obtain a MelB protein concentration of 5-8 mg/mL. 1  $\mu\text{L}$  of the reconstituted protein was diluted into 19  $\mu\text{L}$  of dialysis buffer for further analyzing its purity with a 12% - SDS-PAGE gel. The sample was aliquoted and frozen at -80°C for subsequent use.

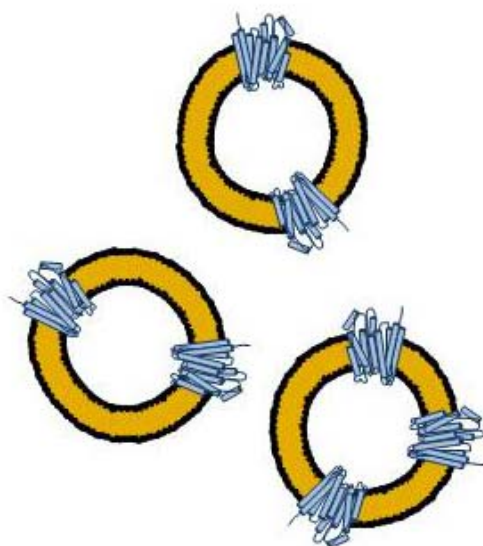


Figure 5.6 Reconstituted membrane protein into natural *E. coli* lipids

### 5.1.7. Preparation of vesicles

To prepare membrane vesicles (Fig. 5.7) for either the wild-type or any mutated form of the MelB protein, DW2-R cells have been grown under the same condition as described in the section 5.1.4. ISO- and RSO- vesicles were prepared from the same batch cultivation to warrant equal condition for the expression of the membrane protein.

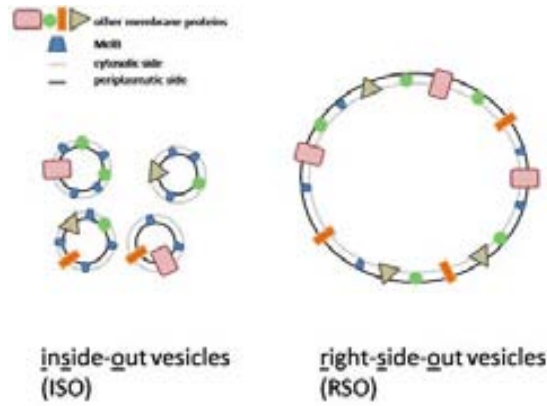


Figure 5.7 Types of membrane vesicles retrieved after cell disruption with osmotic shock or high pressure method

### 5.1.7.1. Inside-out vesicles (ISO)

The protocol is based on the French press procedure<sup>153,154</sup>. Frozen cells were thawed rapidly at 25°C and washed twice with 10 mM Tris-HCl (pH 8.0). Each time the cells were pelleted by a centrifugation step using a centrifugal force of 10,000 g for 5 min at 4°C. EDTA and lysozyme were added at a concentration of 15 mM and 1 mg/mL respectively, and incubated at 4°C for 30 min. In addition, 20 µg/mL of DNase and RNase were added and activated by 15 mM MgSO<sub>4</sub>. By means of a French press or by a Microfluidizer, which is similar to the French press procedure<sup>40</sup>, cells were broken to form inverted membrane vesicles. In these vesicles the inner membrane side is expected to be turned inside-out, giving it its name. The entire volume of the cell suspension was passed three times either through the Microfluidizer or the French Press. Successive centrifugation at 800 g for 30 min clears the unbroken cells and the remaining debris from the ISO vesicles. The vesicles were washed at least three times by ultracentrifugation of 146,000 g with 100 mM KPi (pH 7.5), 10 mM EDTA. Finally, the vesicles were resuspended in the same buffer at a concentration between 10-20 mg/mL and frozen at -80°C until further use.

### 5.1.7.2. Right-side-out vesicles (RSO)

Right-side-out vesicles preparation differs from the high pressure method used to generate the inverted variants. Basically these vesicles expose the natural side of the membrane to the surrounding environment. RSO vesicles are produced based on an osmotic shock protocol<sup>155,156</sup>. Therefore, cells from the same preparation used to prepare the ISO vesicles were washed twice with 50 mM Tris-HCl (pH 8.0) and the cells were pelleted at 4°C by centrifugation at 10,000 g for 10 min. Upon resuspension of the pellet using 80 mL per 1g DW2-R in a buffer containing 50 mM Tris-HCl (pH 8.0) and 30% (w/v) sucrose, the cells were incubated at room temperature under vigorous stirring for 1 h. To destabilize the membrane, lysosome and potassium-EDTA (pH 7.0) at a concentration of 0.5 mg/mL and 10 mM, respectively were added simultaneously. Followed by a centrifugation at high speed (13,000 g) the cells sedimented and were resuspended using a glass syringe in the smallest possible volume (3-5 mL) of KPi-buffer (pH 6.6) containing 30% (w/v) sucrose and 20 mM MgSO<sub>4</sub>.

1 mg/mL of DNase and RNase was added to the sedimented cells. For cell rupture, the small volume (3-5 mL) of the cells was released in 0.5 L KPi-buffer (pH 6.6) pre-equilibrated at 37°C. After 15 min incubation under vigorous stirring, the protoplasts generation is enhanced by addition of first 10 mM K-EDTA (pH 8.0) followed by 15 mM MgSO<sub>4</sub> after another 15 min. To precipitate unbroken cells, the lysate was centrifuged at low speed (800 g, 4°C) for 1 h leaving only RSO vesicles in the supernatant. A further centrifugation at higher speed (16,000 g) resulted in the sedimentation of the right-side-out vesicles. Finally, the vesicles were washed at least three times using the KPi-buffer (pH 7.0) harboring 20 mM MgSO<sub>4</sub>. Until further experiments, the RSO vesicles were adjusted to a concentration of 10 - 20 mg/mL. Preferably, the FRET signal for

RSO vesicles (see below) was measured directly without freezing the sample because every freezing/thawing cycle will convert a part of the RSO vesicles into the inverted form (ISO). The signal for right-side-out vesicles would then be merged with a background response from the ISO vesicles. If the measurement was not possible, the RSO vesicles were straightaway frozen with liquid nitrogen and kept until further use at -80°C.

### **5.1.8. Protein purity and quantification**

As aforementioned, during the purification process of the MelB protein, either C-less or mutated variant, the samples were mixed with dialysis buffer and subjected to a 12% - SDS-PAGE<sup>157</sup> gel. The collected samples were always compared to a protein standard loaded as a reference onto the same gel. By Coomassie-blue staining, the level of oligomer formation as well as possible contaminants of the MelB protein occurring during solubilization and after membrane insertion could be easily verified.

Before setting up any experiments, the assumed protein concentration has been determined by an assay according to the instruction given by the manufacturer (Bio-Rad DC Protein Assay, Bio-Rad, Hercules, CA, USA). This assay is based on the Lowry assay<sup>158</sup> and has been modified to measure protein concentrations in the presence of lipids. Bovine serum albumin was used to obtain the required standard curve.

### **5.1.9. Labeling with His**

As mentioned for the proteoliosomes, the membrane vesicles were also tested for their content of MelB protein. Depending on the MelB mutant, between 1 and 30 ug of total protein was loaded in a 12 % - SDS-PAGE gel. After the electrophoresis the proteins were transferred on a nitrocellulose membrane for 1 hour at 100 volts. To reduce the background, the membrane was blocked for another hour with TBST buffer containing BSA at a concentration of 25 mg/mL. The Histiding-Tag-specific reagent His-Probe<sup>TM</sup>-HRP was prepared at a concentration of 1:2500 in TBST + BSA buffer and incubated with the membrane for 1 h at room temperature. Three washing steps with TBST of 10 min were applied to reduce unspecific interaction of the probe. The final development was carried out by using the developer from MilliQ.

## 5.2. Infrared spectroscopy

Infrared spectroscopy (IR) is a technique which is frequently used to study the structure of proteins<sup>159-162</sup>. Its primary advantage over other spectroscopic techniques is the absence of problems related to light scattering. Normally, IR does not require any external probe nor the introduction of an isotopic marker which makes it an easy applicable research tool. Nowadays, the infrared spectrometers are using Fourier-transformation for the detected infrared signal. The Fourier-transformed infrared spectroscopy is a versatile technique which permits the study of a protein in different conditions: like reconstituted in liposomes<sup>129,133</sup>, in dry films<sup>163</sup>, in organic solutions<sup>164</sup> or in detergent<sup>129,133</sup>. The technique also suits well for the study of the protein backbone<sup>165</sup>. Furthermore, FTIR makes fingerprint detection of protonation and deprotonation of aspartic and glutamic acids feasible<sup>166,167</sup>.

In infrared spectroscopy light is used in the infrared region of the electromagnetic spectrum (14,000 to 10  $\text{cm}^{-1}$ ) and is associated with much lower energy in comparison to the visible or ultraviolet light.

The infrared region can conventionally be subdivided into the near-infrared, the mid-infrared and the far-infrared spectrum.

The fundamental apparatus relies on the Fourier-Transform Infrared technique which uses an Interferometer as well as a moving mirror to guide light towards the sample and then to the detector.

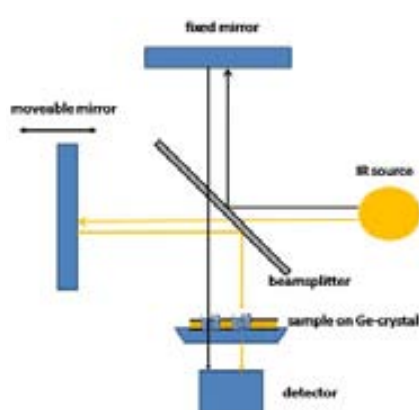


Figure 5.8: Michelson interferometer - basic arrangement for IR

Figure 2.8 presents the habitual way to record a spectrum using an interferometer. The light emitted by a typical infrared source is divided into two parts by a beam splitter. The optical path of one path is constant, whereas the second varies due to a moving mirror. After reflection in adequate mirrors, both light paths recombine in the beam splitter giving rise to an interference and the resulting light is conducted to the detector. For monochromatic light this design causes a sinusoidal oscillation of the energy which reaches the detector. Herewith, the relation between the signal intensity and the distance of the moveable mirror is

recorded. Fourier transformation converts it into the relation of the signal intensity to wavenumbers.

In an ideal situation, the mirror should move to an infinite position which after Fourier-transformation results in a well-defined wavenumber in the interferogram. But since the mirror movement is limited, the interferogram is called “Boxcar” and represents the data set which is lost due to the limited displacement of the mirror. The more applicable form of interferograms for biological samples is the triangle form. After Fourier-transforming this triangle interferogram, the spectrum was received which was further transformed into the absorbance

spectrum. (see below)

$$\text{sample absorption} = -\log \frac{\text{sample transmittance}}{\text{transmittance without sample}} \quad (\text{eq. 2.1})$$

### 5.2.1. Attenuated total reflection FTIR

The physiological and structural evaluation of membrane proteins is rather tricky. Because of their amphiphilic character, the samples of membrane proteins either contain surfactants or the proteins are embedded into liposomes. The main advantage of ATR is the possibility to easily exchange the solvent. Therewith the protein can be assessed regarding its functions in alternative conditions. For structural determination of proteins ATR-FTIR delivered valuable information<sup>159,168,169</sup>. A major asset of this special FTIR technique is the possibility to probe the membrane protein directly in a solvent environment meaning to be physiologically adequate. Under these circumstances, the protein could be examined in the various media like the different pH or reaction with potential ligands.

Studies reveal also the remarkable opportunity to determine the proton exchange of sample exposed to heavy water<sup>132</sup> where the required amount of deuterium is a crucial cost-affecting factor. Basically, a crystal represents the major contributor of this technique. The material of such a crystal is limited to elements, like germanium or zinc selenide, having a higher refraction than the probed sample, because the general principle relies on the Snell law (eq. 2.2), where  $n_1$  and  $n_2$  are the refractive indices of the two media and  $\Theta_1$  and  $\Theta_2$  are the angle of incidence and refraction with respect to the interface of the two media.

$$n_1 \sin \Theta_1 = n_2 \sin \Theta_2 \quad (\text{eq. 2.2})$$

Infrared light entering the crystal is almost totally reflected on the surfaces of the crystal. After several reflections the beam is focused on the detector. By reaching the surface of the crystal a fraction of the light beam penetrates its surrounding. This part of the light is entitled by evanescent wave. By placing the sample onto the crystal the light beam enters marginally the protein and is absorbed. The reflected light conveys information about the sample to the detector. The evanescent wave alters only in amplitude, whereas the frequency remains the same<sup>170</sup>. The number of reflections of the light beam within the reflecting material depends on the length and thickness of the crystal and on the angle. Therefore, ATR has been utilized on various occasion to

study membrane proteins under different conditions<sup>171</sup>.

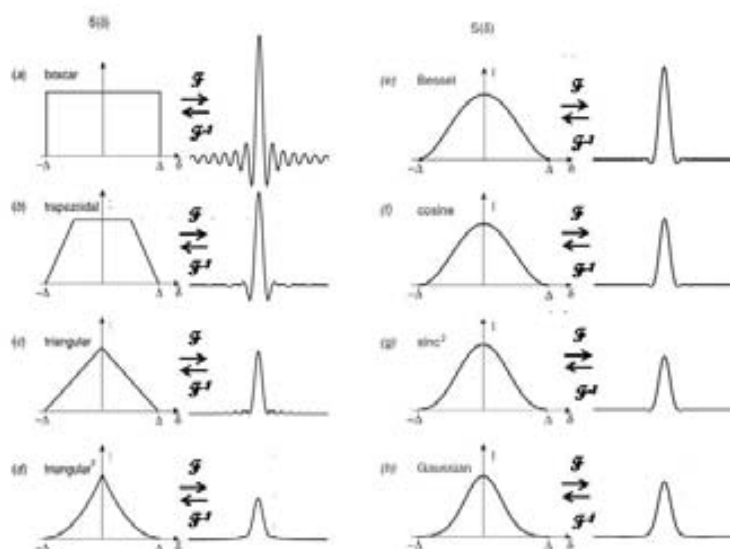


Figure 5.9 Fourier-transformed spectra from Griffiths and de Haseth<sup>172</sup>.

coming in close contact with the sample. In ATR many parameters affect the final spectrum. This is related to the wavelength of the light, the effective path length, the depth of penetration, the refraction index of the crystal and the sample, the angle of incidence of the light beam, the quality of the sample-crystal contact and the amount of internal reflections as well as the sample itself<sup>173</sup>.

One reason for the use of ATR is the opportunity to the exchange surrounding conditions of proteins. The hydration of protein is an interesting aspect considering its effect on the structure<sup>174</sup>. Apart from that, water subtraction is also crucial since water in proximity of charged residues behaves differently from bulk water. Heavy water could serve as a solution, but sample deuteration varies in time which makes its effect unpredictable<sup>175-177</sup>. All these parameters eventually influence the appearance of an ATR absorbance spectrum. Especially, the thickness of the film is worthwhile considering. In films larger than the sample penetration of the evanescent wave, the absorbance spectrum behaves differently. Those films were rated as “infinite”. Under these circumstances, the absorbance depends not only on the evanescent beam penetration distance but also on the average concentration of the sample in the penetration of the evanescent wave. Noteworthy, in ATR the absorbance spectrum has a greater absorbance at lower wavenumbers than in the equivalent transmittance spectrum.

The thickness of the evanescent wave weakens inversely to the wavenumber. Also a distortion in the shapes of bands is visible in regions with a strong signal absorbance which is due to a difference in the refractive index. Those distortions would be appreciable in bands with large absorption coefficients which is not the case with proteoliposomes.

Considering thin films where the bulk height is small relative to the penetration distance of the evanescent wave, the absorbance does not depend on the wavenumber. Additionally, the band distortion will be much less intense compared to the effect in thick films. The main problem for thin film is the sample distribution. Merely, a monolayer of sample ought to represent this

The trapezoidal crystal used throughout this study was made of germanium (Harrick Scientific Products Inc., New York, USA) having a length of approximately 5 cm and 2 mm in thickness and a critical angle of 22°. The angle of incidence was 45° realizing 25 internal reflections thereof 13

condition, which implies a very low absorbance signal and therefore an intolerable low signal-to-noise ratio. The sample film, in our case proteoliposomes, is another crucial factor to be considered for ATR data acquisition. For the experiments done with MelB variants reconstituted in proteoliposomes, the film thickness was considered to be infinite. This hypothesis implies several advantages as the sample absorbance is maximized and the film thickness remains constant. It is true that absorbance intensities change with the wavenumber but on the other side this does not cause any distortion in the spectrum. Also highly concentrated samples with high absorption coefficients or an angle of incident close to the critical angle provokes distortions of the absorbance bands which have been avoided in the experimental procedure.

The sample orientation is another important aspect to be taken into account<sup>178,179</sup>. Since the reconstituted membrane protein is accommodated in a buffer solution and spread on the ATR crystal, before setting up the experiment, the sample has to be semi-dried to ensure close crystal contact. Arbitrarily, the sample will adsorb to the surface and remains on the crystal avoiding the risk of undesired loss of sample. Furthermore, the lipid bilayer will also establish an orientation parallel to the refractive element<sup>180</sup>. Even though only a small fraction of the sample is in contact with crystal surface, the validity of the data are unquestionable<sup>180</sup>. To probe the sample under physiological conditions, the film was rehydrated. On the downside, the water entry decreases the spectral intensities because it causes the swelling of the proteolipidic layers.

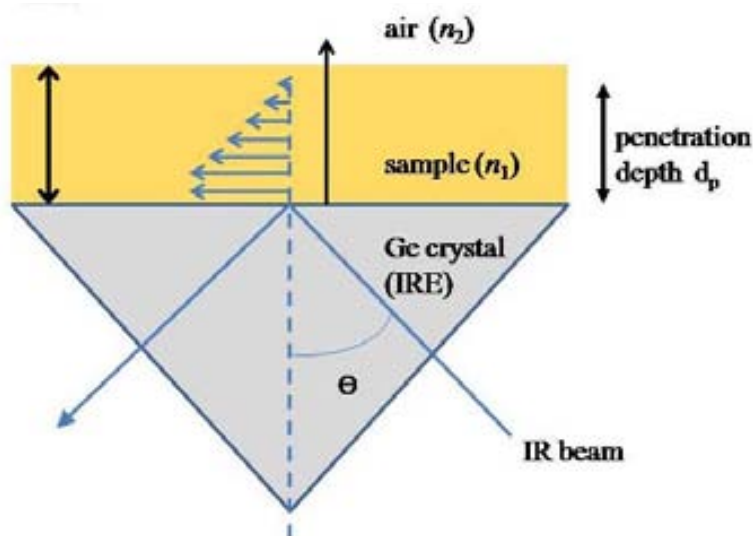


Figure 5.10 Evanescent wave at the interface of two media, under conditions of total reflection

### 5.2.2. Molecular vibrations caused by IR

Infrared light possesses longer wavelengths with lower frequencies than the visible part of the electromagnetic spectrum. Therefore, the energy content is much lower. This spectroscopic technique causes molecules to absorb energy of specific frequencies from the IR light. Those frequencies are characteristic and forces chemical groups to vibrate. Those vibrations of the bonds are detected and can be explicitly linked to chemical groups or entire compounds. In the mid-infrared region between 4000 and 1000  $\text{cm}^{-1}$  many functional groups are responding to the absorbed frequencies. The position of an infrared absorption band depends on the vibrating mass of the molecule, the type of bonding between atoms and coupling effects to other vibrations.

Those functional groups manifest the chemical properties of all molecules. Above and below this range only minor interactions take place which hardly allow the elucidation of structural impact.

Vibrations of molecules are ubiquitous and range from the simplest case, where only two atoms connected by a bond are vibrating, to a very complex macromolecule with different chemical groups responding by specific vibrations. A molecule with  $N$  atoms has  $3N$  degrees of freedom in the  $x$ -,  $y$ - and  $z$ -axis. Since 6 motions can be excluded due to translational and rotational motion, there are still  $3N-6$  different modes in which the atoms can vibrate.

For linear molecules the rotation about the axis does not lead to any displacement. Vibrations of molecules are provoked by the absorption of a quantum of energy which corresponds to the frequency of the vibration best interpreted by,

$$E = h \cdot \nu \quad (\text{eq. 2.3})$$

where  $h$  is the Planck's constant and  $\nu$  is the frequency. Every molecule has a unique vibration pattern which facilitates its detection. Nowadays, libraries of known spectra create new possibilities of molecule identification. The absorption of IR light principally excites molecular vibrations referred to as vibrational modes. Each mode has a characteristic frequency which corresponds to the energy applied to the atoms. As a result, the atoms move from its configuration equilibrium in specific manner<sup>181</sup>.

For proteins the most abundant bond which gives rise to vibrational changes is the amide group of the peptidic bond (Fig. 2.9). This functional group has many vibrational states, but the most important ones are represented by amide A, I and II. Vibration modes are usually divided into bending and stretching. Both modes are further subdivided into numerous vibrational patterns.

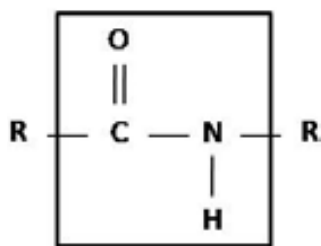


Figure 5.11 Amide group

The amide A signal corresponds to the NH stretching, and is detected at wavenumbers from 3310 to 3270  $\text{cm}^{-1}$ . Amide I (1610 – 1695  $\text{cm}^{-1}$ ) is associated to the vibration of C=O with minor contributions of out of phase stretching from CN and deformation of CCN. The frequency of this vibration depends largely on the hydrogen bonds and therefore is influenced by the secondary protein structure. The amide I is highly sensitive to any kind of conformational change in the protein. Unfortunately, the region of the amide I is also contaminated by signals from amino acid side chains<sup>182</sup>. The spectral interpretation is more complex.

The second specific protein band is amide II which is located in the region from 1510 to 1575  $\text{cm}^{-1}$ . The corresponding vibrations come from the in-plane bending of the NH and the CN stretching. Moreover, CC and NC stretching as well as CO in-plane bend also affect the amide II mode. Overall, the amide II sensitivity is less important than amide I.

Other important vibrations caused by amino acid side chains could elucidate conformational changes of the protein. The most interesting modes from aspartic and glutamic acids are distributed in three distinctive vibrations at 1400  $\text{cm}^{-1}$  caused by  $\text{COO}^-$ , at 1574 to 1579  $\text{cm}^{-1}$  for the aspartic acid and at 1556 to 1560  $\text{cm}^{-1}$  for the glutamic acid associated to anti-symmetric stretching. The final vibration can be categorized for the negatively charged amino acids at 1712 to 1788  $\text{cm}^{-1}$ , where the C=O absorbs.

In another subgroup of important side chain vibration mode can be observed between 1678 and 1704  $\text{cm}^{-1}$  for the C=O vibration of glutamine and for asparagine between 1668 and 1687  $\text{cm}^{-1}$ . Stretching of the  $\text{NH}_2$  can be detected for Asn at 1612 to 1622  $\text{cm}^{-1}$  and for Gln at 1586 to 1610  $\text{cm}^{-1}$ .

Another fingerprint amino acid visible in spectroscopy is tyrosine. Having a vibration giving a narrow band between 1516 and 1518  $\text{cm}^{-1}$ , tyrosines can be extracted from the spectrum.

The main problem deriving from infrared spectroscopy is the extraction of valuable information. Its rather intensive and broad bands, foremost in the absorbance spectra contain a mixture of vibration signals deduced from numerous peptide bonds. Since proteins are polymers, fingerprint analysis is even harder, because of the number of IR signals.

### 5.2.3. Experimental set-up for difference spectrum acquisition

For the ATR-FTIR difference spectrum ( $IR_{\text{diff}}$ ) acquisition, a Bio-Rad FTS 6000 (Bio-Rad, Hercules, CA, USA) was used. The crystal for the reflection experiments was made of germanium and possesses the dimensions of 50 mm x 10 mm x 2 mm (length, width, depth) realizing an area of 4 cm<sup>2</sup>. The beam enters the crystal at an angle of 45° surpassing the critical angle for total reflection. To guarantee the proper temperature control of the sample, a custom-made casing (Fig. 2.10) was connected to a thermal circulating bath (Haake, ThermoFisher Scientific, MA, USA). This allows a steady temperature of the sample casing and of the buffer solutions for sample probing. This casing consists of four nozzles, two for convenient temperature control as well as further two for solution influx and efflux. Throughout the studies the temperature of the room and of the circulation thermal bath was set to 25°C.

For every single protein film, 20 µL of proteoliposomes corresponding to 100-150 µg of protein, was pipetted and then gently distributed onto the crystal surface. This “thick” proteoliposome (Fig. 2.10) film was air-dried for 10 min. After another 5 min of under a stream of nitrogen gas ensured complete water evaporation.

To examine the hydration level of the MelB sample, the absorption band at 3400 cm<sup>-1</sup> gives a clear indication of residual water.

An absorbance spectrum of the dry protein film was recorded determining several sample aspects. This spectrum indicates the insertion of the protein into the proteoliposomes, but also emphasizes possible aggregation of the protein. At 1620 cm<sup>-1</sup> a typical band is located in the infrared spectrum indicating intermolecular  $\beta$ -sheets<sup>183,184</sup>. Furthermore, the spectrum indicates the correct protein-to-lipid ratio enhancing its importance as a benchmark in the sample validation.

The absorbance spectra were acquired by using a mercury-cadmium-telluride detector cooled by liquid nitrogen. Each absorbance spectrum was recorded at a resolution of 4 cm<sup>-1</sup> accumulating either 500 or 1000 scans.

To validate the effect of the substrates on each MelB variant, infrared difference spectra with the ATR- technique was recorded. The proteoliposomes formed a multilamellar ordered film on the ATR-crystal surface by strong hydrophobic interactions.

The relatively stable protein film allows the manipulation of the surrounding buffer. For the MelB mutants, the dried protein film was probed by different buffers containing its ligands in various concentrations to verify interactions between MelB and the substrates. Preferentially, melibiose and sodium were measured in different concentrations to obtain infrared difference spectra.

The flux was set to 1.5 mL/min to guarantee a constant hydration of the protein film and the complete release of the ligands after the spectrum acquisition.

The washing buffer (**W or W1 or W2**) was applied to the sample for equilibration. In the case for 10 mM substrate, 10 min was sufficient, whereas for buffer containing 50 mM substrate

30 min of sample washing was applied prior to the acquisition of the absorbance spectrum.

A two-way magnetic valve controls the on-time switch between the two different buffers. The magnetic valve is controlled by a home-made software in Visual Basic. After completing the washing cycle, an absorbance spectrum was collected accumulating 500 scans for 10 mM sodium or 1000 scans for any other condition.

The valve then changes the influx between the washing buffer and the difference buffer. For 2-4 min the protein film was equilibrated with the difference buffer containing the substrate. The melibiose binding was tested in the presence of sodium. Hence, the washing buffer (**W1** or **W2**) also contained the same concentration of sodium as the difference buffer for equilibration purposes.

A second absorbance spectrum was acquired after equilibrating the protein film. The difference spectrum from the two absorbance spectra was automatically calculated for each cycle. For each MelB mutant the spectrum accumulation lasted in between 7 to 24 hours depending of the substrate concentration and generated 25 difference spectra composed in total of 12,500 (for 10 mM sodium) or 25,000 accumulated scans respectively.

These 25 differences were averaged and subtracted. For every MelB mutant the final difference spectrum for  $\text{Na}^+\cdot\text{H}^+$ ,  $\text{Mel}\cdot\text{H}^+$  or  $\text{Mel}\cdot\text{Na}^+$  consists of at least two independent experiments.

The experimental procedure was first designed by Dr. X. León (extensively described in his thesis 2006) and further optimized by Dr. M. Granell (thesis 2009). The exposure times regarding the washing buffer and difference buffer are listed in the table below.

<i>Difference spectra</i>	<i>Washing buffer</i>	<i>Ligand buffer</i>
$\text{Na}^+$ 10 mM vs H	10 min buffer <b>W1</b>	2 min buffer $\text{Na}^+$ 10 mM
$\text{Na}^+$ 50 mM vs H	30 min buffer <b>W2</b>	4 min buffer $\text{Na}^+$ 50 mM
Mel 10 mM $\text{Na}^+$ vs $\text{Na}^+$	10 min buffer $\text{Na}^+$ 10 mM	4 min buffer $\text{Na}^+$ + mel10 mM
Mel 50 mM $\text{Na}^+$ vs $\text{Na}^+$	30 min buffer $\text{Na}^+$ 10 mM	4 min buffer $\text{Na}^+$ + mel 50 mM
Mel 50 mM vs $\text{H}^+$	30 min buffer <b>W</b>	4 min buffer mel 50 mM

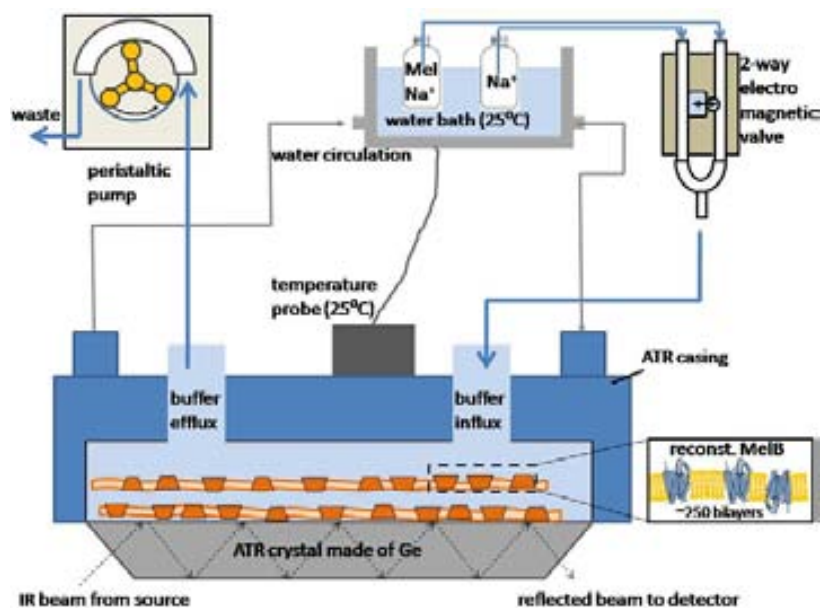


Figure 5.12 Scheme of the experimental design for the ATR-IR difference spectra acquisition

In Figure 5.12 the experimental set-up is illustrated with the ATR casing at the centre. The MelB proteoliposome sample is deposited on the germanium crystal and perfused constantly with buffer solution. The buffer composition changes from no substrate to either 10 mM sodium or 50 mM melibiose to test the coupling in the presence of the proton (or hydronium,  $\text{H}_3\text{O}^+$ ). The condition of 10 mM melibiose was examined in the presence of 10 mM sodium in both buffers to check the coupling of the sugar mediated by sodium.

Before setting up ATR-IR difference spectra experiments, the germanium crystal was cleansed with a mild detergent, washed with distilled  $\text{H}_2\text{O}$  and dried carefully before acquiring a background spectrum.

As mentioned in the previous chapters, a sample was deposited on the crystal and first air dried and then subjected to a constant nitrogen stream to evaporate residual free water molecules. Nevertheless, the protein still retains some water<sup>133</sup>. All this benefits to a close protein-crystal contact ensuring a stable film for the successive perfusion with substrate-containing buffers.

For data acquisition the ATR casing was combined with a probe controlling the temperature by a thermostatic water bath (see Fig. 5.12). This bath also equilibrates the buffers at a constant temperature of 25°C because temperature variations could provoke spectral abnormalities difficult to eliminate.

The different buffers were perfused with a speed of 1.5 mL/min to the ATR-flow chamber.

As stated in the materials section, the general buffer for the infrared difference spectra acquisition were composed of 20 mM MES (pH 6.6) and 100 mM KCl. This buffer was furthermore divided into a washing buffer and a substrate buffer. For sodium difference spectrum, the washing buffer was adjusted for the ionic strength by supplementing 10 mM KCl since the substrate buffer contained 10 mM NaCl. To measure the difference spectrum for the sugar in the presence of sodium, the stock buffer contained 10 mM NaCl. Then this buffer was divided into a

part without the substrate and a second to which either 10 mM or 50 mM melibiose was added. For proper subtraction, the difference spectra of the buffers were frequently recorded.

The spectrometer parameters remained unchanged throughout the whole measurement. The intensity was set to 1.5 and the aperture indicated an open status. The difference spectra acquisition for each new sample was always accompanied by a collection of a water vapor spectrum for convenient subtraction

#### 5.2.4. Corrections of the infrared spectra

Each new acquisition requires the calculation of the mean of the absorbance and the difference spectrum. The two averaged spectra are corrected for the effect of the buffer, the swelling of the protein film and the influence of the water vapor. To remove the effect of the buffer efficiently, difference and absorbance spectra were recorded regularly for the different buffer compositions (as seen in Fig. 5.13).

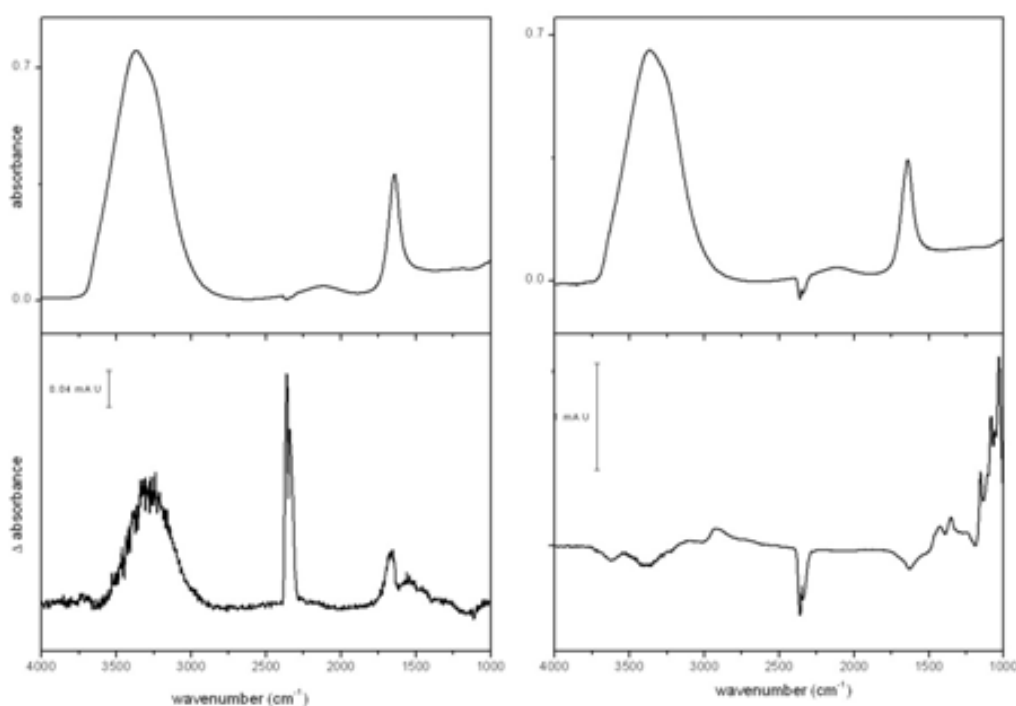


Figure 5.13 Averaged buffer spectra; on the right side: upper panel, absorbance spectrum from 10 mM Na<sup>+</sup>, lower panel difference spectrum for 10 mM Na<sup>+</sup>; left side upper panel: absorbance spectrum from 10 mM melibiose, lower panel difference spectrum from 10 mM melibiose in the presence of 10 Mm Na<sup>+</sup>.

The absorbance spectrum of the sample was collected indicating the quality of the protein film (Fig 5.14). As mentioned in previous chapters, the absorbance and difference spectra of the protein sample were averaged. To further validate the spectra for each MelB mutant, several contributions had to be removed. The absorbance spectrum is mainly dominated by the water

absorption band at approximately  $3300\text{ cm}^{-1}$  (Fig. 2.12) coming from the OH stretching. To subtract this band successfully, the average absorbance spectrum of the buffer was used under the same conditions (composition, temperature, etc.). The subtraction factor varied between 0.89 and 0.84 leaving a spectral uncertainty.

The main focus of the subtraction of the absorbance spectra rests on the region between  $1900$  and  $1300\text{ cm}^{-1}$ . There the protein-associated vibration modes amide I and II were examined to disclose additional structural details from the protein. The abovementioned subtraction factor also implies that  $\sim 84\%$  (for a subtraction factor of 0.84) of the signal consists of buffer. This in turn implies that the protein-lipid mixture contributes for 16% to the recorded signal. The sample consisted of stacks of lipid patches which were hydrated by the buffer system and herewith made the protein accessible for its substrates.

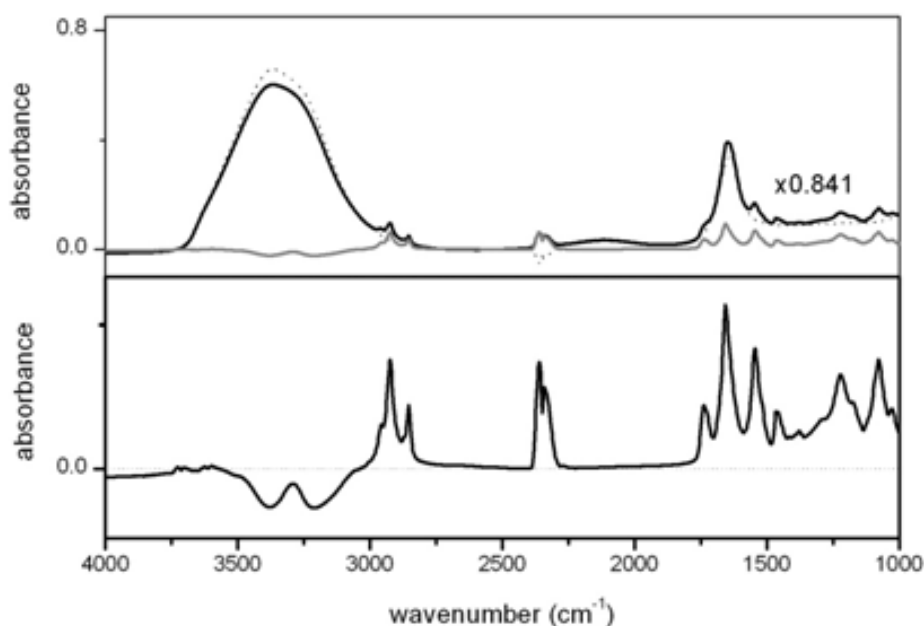


Figure 5.14 Absorbance spectrum correction of the reconstituted MelB variant applied to the Ge crystal. Upper panel: absorbance of the hydrated protein film (black line); also illustrated, absorbance spectrum of the plain buffer (dotted line); the corrected absorbance spectrum of the proteoliposomes of the MelB sample (in grey) using a subtraction factor of 0.841. Lower panel: scaled absorbance spectrum of the protein film after subtraction of water bands.

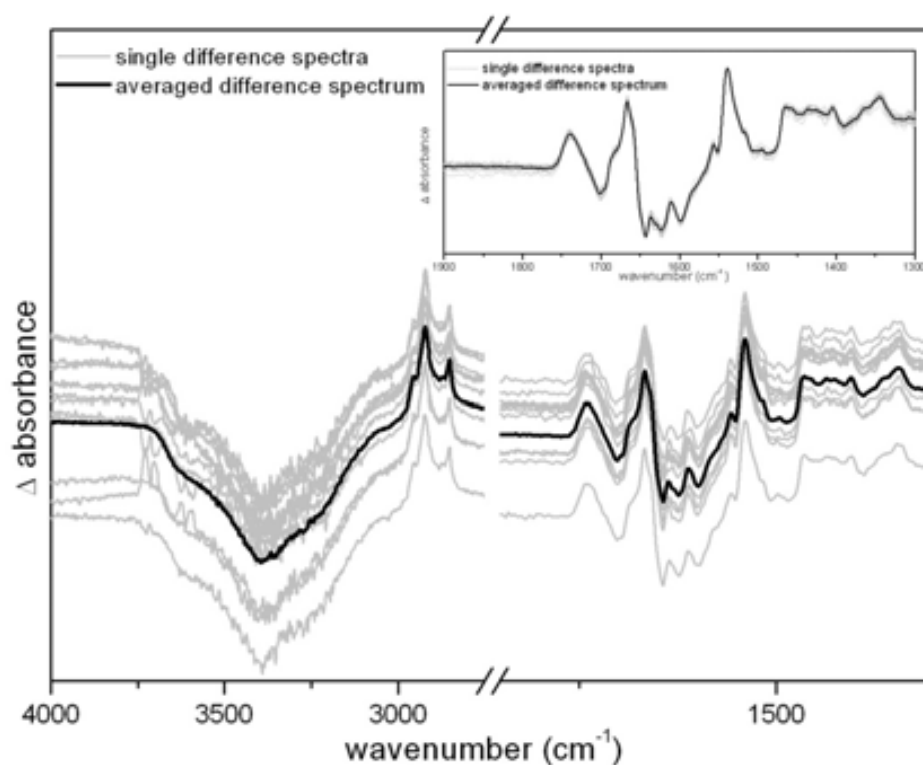


Figure 5.15 Averaged difference spectrum for 10 mM melibiose in the presence of 10 mM  $\text{Na}^+$ , in grey single difference spectra acquired, in black the mean of the difference spectrum after averaging 25 single difference spectra (before subtraction), in the top right corner normalized difference spectra before subtraction indicating the important region between 1900 and 1300  $\text{cm}^{-1}$ . The averaged absorbance spectrum is not shown since the mean hardly differs from the single absorbance spectra.

Usually the difference spectrum has low signal intensity and the various parameters affect the recorded spectrum. The subtraction depends on the buffer composition. Whereas in the substrate-induced  $\text{IR}_{\text{diff}}$  only minor substrate-specific absorption occurs for 10 mM sodium, the  $\text{IR}_{\text{diff}}$  provoked by the melibiose clearly indicated sugar absorption in the range from 1200 to 1000  $\text{cm}^{-1}$  (Fig. 2.16 upper panel).

The effect of the water (3400 – 3300  $\text{cm}^{-1}$ ) and melibiose (1200 – 1000  $\text{cm}^{-1}$ ) were corrected simultaneously using the reference  $\text{IR}_{\text{diff}}$  of the buffer containing melibiose (Fig. 5.16 A). Since the correction might have been imperfect considering the absorbance of the water, the difference spectra was additionally corrected by using the absorbance spectra of the buffer. Then the swelling of the protein film was eliminated (Fig. 5.16 B). The absorbance spectra might change over time and hence is useful as an indicator of the film swelling. And additionally the  $\text{CH}_2$  bands from the lipids at 2900  $\text{cm}^{-1}$  were eliminated (Fig. 5.16 B). Finally, the difference spectrum was corrected for the water vapor, concluding in the final melibiose-induced  $\text{IR}_{\text{diff}}$  spectrum between wavenumbers 1900 and 1300  $\text{cm}^{-1}$ . (Fig 5.16 A)

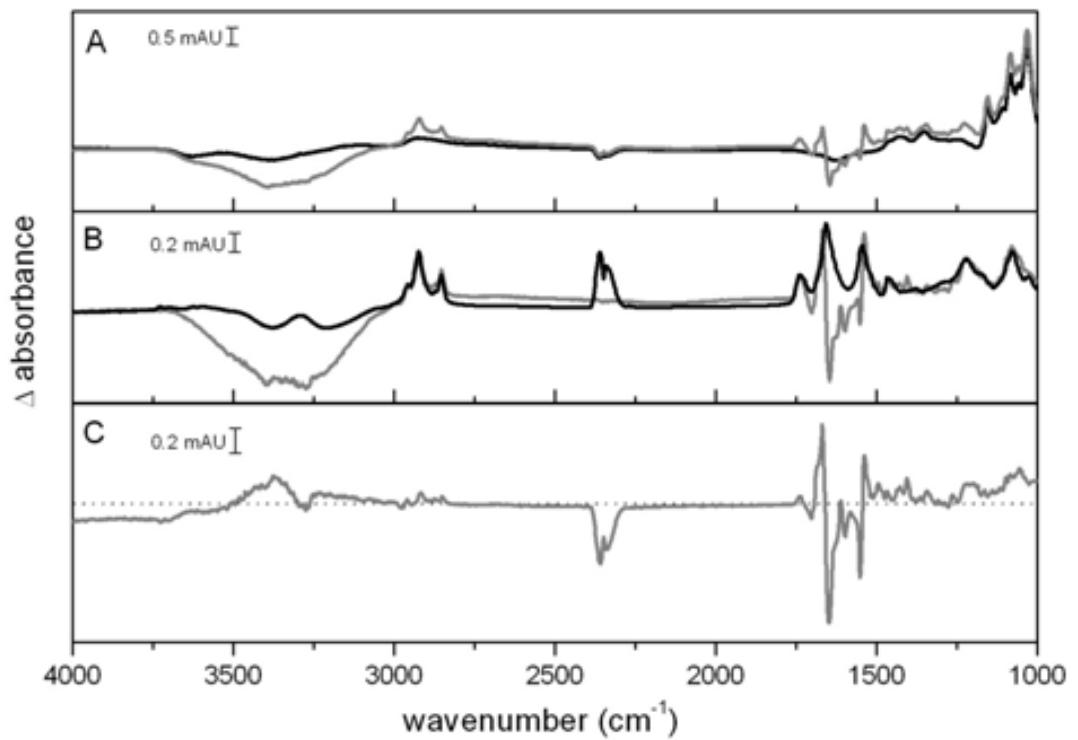


Figure 5.16 Corrected melibiose-induced  $IR_{diff}$  spectrum for the C-less melibiose permease; **A** in grey averaged  $IR_{diff}$  of 25 single difference spectra and in black averaged  $IR_{diff}$  of the buffer; **B** melibiose induced- $IR_{diff}$  and in black  $Abs_{sample}$  used to eliminate the effect of the lipid; **C** final melibiose-induced  $IR_{diff}$

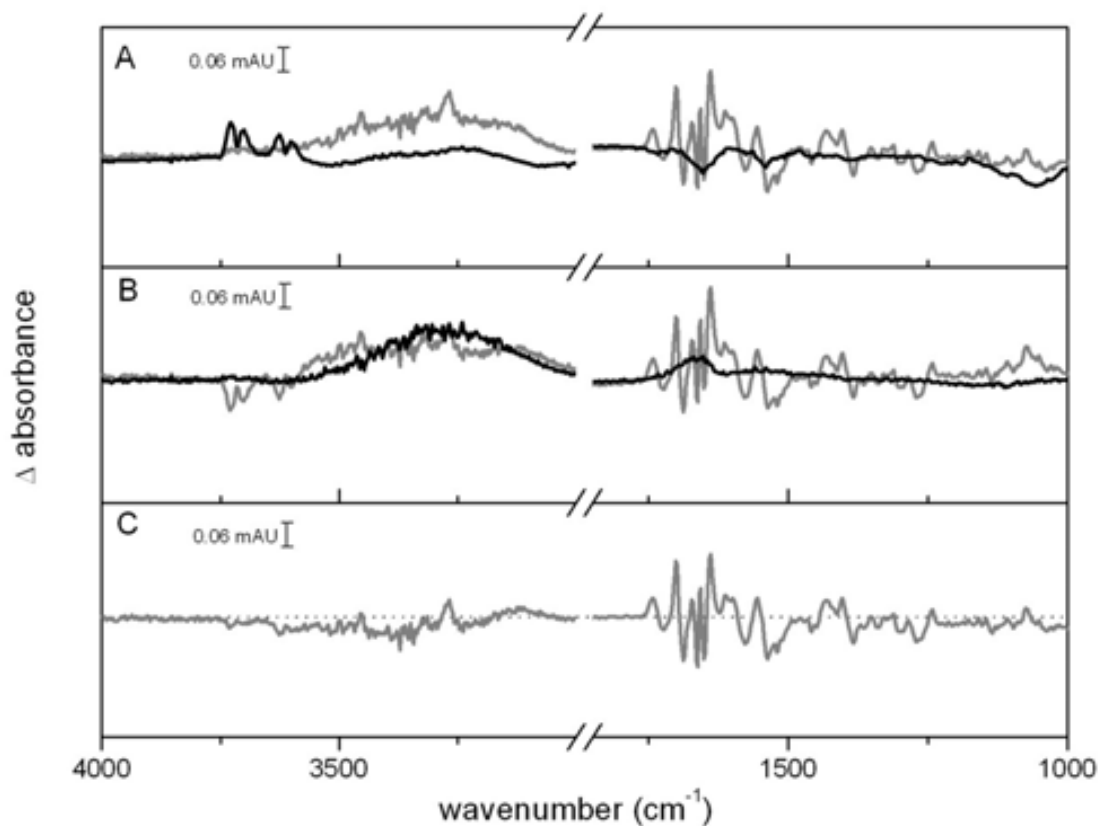


Figure 5.17 Correction for the 10 mM  $Na^+$ -induced difference spectrum of C-less MelB variant; **A** obtained

average difference spectrum (grey) corrected for swelling of the protein film (black) (absorbance spectrum variation during the buffer perfusion); **B** IR<sub>diff</sub> (grey) corrected for the buffer effect on the sample; **C** final Na<sup>+</sup>-induced IR<sub>diff</sub> spectrum.

The protocol for the correction of the difference spectrum induced by sodium binding was similar to the previously described sugar-induced difference spectrum. The positive charged ion is non-IR active and therefore has no direct contribution on the spectrum, although it partially influences the water band. This influence increases with higher sodium concentration which complicates the subtraction process. The following steps remain unchanged to the previously explained melibiose-induced spectrum. The final difference spectrum for sodium as MelB ligand was obtained as seen in Fig 5.18 **B**.

The buffer composition of the IR<sub>diff</sub> was changed depending on the MelB mutant, however a change in the concentration does not change the subtraction protocol. Higher concentrations of the two substrates had no further effect on the spectral correction.

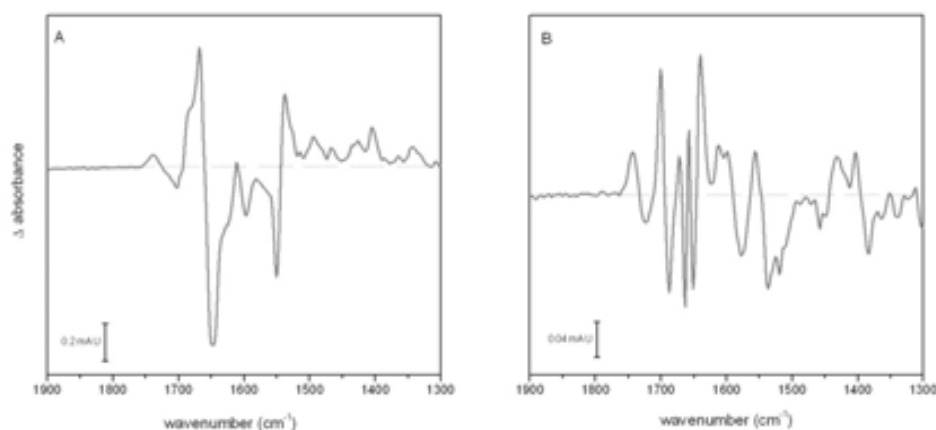


Figure 5.18 Final IR<sub>diff</sub> spectra for C-less MelB; **A** melibiose-induced IR<sub>diff</sub> in the presence of Na<sup>+</sup>, **B** Na<sup>+</sup>-induced IR<sub>diff</sub> in the presence of H<sup>+</sup>

The difference spectra data were treated with Varian Resolution Pro 4.0 (Agilent Technologies, Santa Clara, CA, USA). Subsequent analysis has been performed by the Origin 8.0 Pro software (Northampton, MA, USA) and Matlab v5.3 and v7.0 (MathWorks Natick, MA, USA). The difference spectra were deduced of the buffer effect by subtracting the plain buffer measured under the same conditions as the sample.

### 5.2.5. Analysis of the absorbance and the IR<sub>diff</sub> spectra by derivation

The interpretation of IR<sub>diff</sub> spectra of the various MelB mutants is complex and the conclusions are not straightforward. The IR<sub>diff</sub> spectra revealed only qualitatively the effect of the substrates on the melibiose carrier protein. To aid the data assessment, the obtained spectra were compared in intensity and similarity to the reference spectrum of the C-less protein. Also the absorbance spectra were combined and analyzed systematically.

At least two independent difference spectra from the same conditions were averaged and normalized. To diminish unspecific background absorption that does not change with the wavenumber, the first-derivative to the IR<sub>diff</sub> was utilized for the analysis.

Additionally, the absorbance spectra's derivation revealed detailed structural information from the MelB variants. Hidden peaks in the broad amide I and II vibration mode were exposed by the second derivative.

The quantitative comparisons were performed by a linear regression method for the difference spectra in the region of 1710 to 1500 cm<sup>-1</sup> and for the absorbance spectra similarly from 1700 to 1500 cm<sup>-1</sup>. In this specific range of wavenumbers, the protein-explicit peaks amide I and amide II absorb the infrared light and give rise to interpretation of the conformational changes in the protein. The linear regression analysis provided two outcomes, the slope, *m*, and the correlation coefficient, *R*<sup>2</sup>. The correlation coefficients determined the similarity of the spectrum with respect to a reference spectrum, usually the C-less protein, and the slope correlates the relative intensity of the spectral features to the reference spectrum as well.

For both cases, similarity and intensity, the level of uncertainty was calculated as the standard deviation of the independent experimental repetitions. For the absorbance spectra, the slope determines the different quantities of protein deposited on the ATR-crystal. This in turn is useful for the normalization of the IR<sub>diff</sub> spectra since the contributing amount of the protein films varies for each new film. The spectra were analyzed with MATLAB v7.0 and Origin 8.0 Pro. The first and second derivative were calculated with a cut point of 0.125 (4 cm<sup>-1</sup>) for the phase corrected Fourier spectra using a Sinc<sup>2</sup> filter<sup>185</sup>. Furthermore, a correlation matrix for the IR<sub>diff</sub> and absorbance spectra was calculated from all possible combinations of inputs and reference spectra. This matrix used the value obtained for the similarity in between the spectra of the MelB variants, calculated as *R*<sup>2</sup> x 100 (Fig. 5.19).

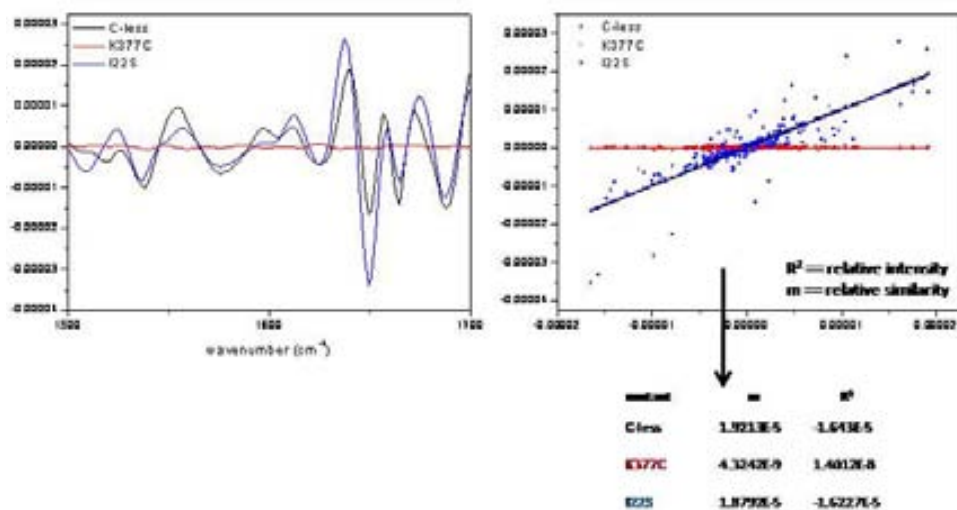


Figure 5.19 Linear regression analysis of the IR's relative intensity and similarity compared to the C-less reference spectrum. In the left panel difference spectra Na 10 mM vs H of C-less (black), K377C (red) and I22S (blue) between wavenumbers 1500 and 1700  $\text{cm}^{-1}$ . In the right panel: linear regression using the slope (m) as the relative intensity and the  $R^2$  value as relative similarity.

### 5.3. Fluorescence spectroscopy

During the last two decades fluorescence spectroscopy and time-resolved fluorescence were basic tools just used in biophysics and biochemistry. Nowadays a much broader field of application for this technique exists. Especially because of its sensitivity, fluorescence is a highly desirable tool for environmental monitoring, clinical chemistry and genetic analysis like DNA sequencing.

Basically, fluorescence is a special form of light emission, called luminescence. Depending on the state of the electron, energy emission is regarded as fluorescence or phosphorescence. In fluorescence the electron releases energy in form of photons much faster ( $\sim 10^8$   $s^{-1}$ ), whereas electrons in the triplet state emit light much slower ( $10^3$ - $10^0$   $s^{-1}$ ).

The fundamental principle which occurs between absorption and

emission of light was initially discovered by Alexander Jablonski. Principally, a fluorophore, which is a molecule capable of being excited, goes to a higher energy state after the absorption of light. This excited state of the fluorophore decays over time and the molecule emits the excess of energy in form of light. There are multiple higher energy levels the molecule can attain depending on the wavelength of the excitation. Since higher energy states are unstable the molecules eventually adapts to the lowest excited state which is semi-stable. To reach the basic low energy state, the fluorophore emits the excess of energy in the form of light. This light referred to as fluorescent light has a lower energy than the excitation light. Therefore, the color of the excited lights differs from the emitted light.

This process can be repeatedly applied to the fluorophore which is very useful for techniques like fluorescent microscopy. Considering that the emitted light has lower energy content than the absorbed light, there will be always a shift visible in the spectrum. Fluorescent dyes characteristically absorb energy over a range of wavelengths, called excitation spectrum.

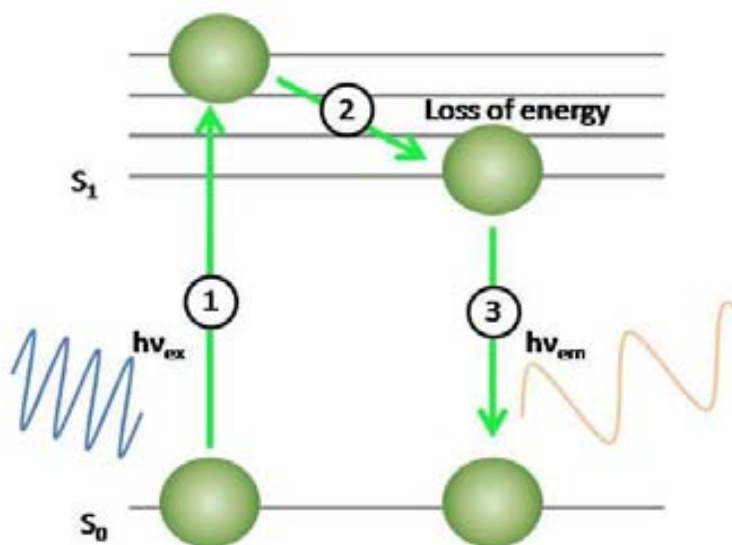


Figure 5.20 simplified Jablonski diagram explaining the molecular basis of the fluorescence phenomena

However, each fluorophore specifically absorbs the highest amount of energy at its excitation maximum. The same principle adapts for the light emission. Every fluorophore has also a range of wavelengths in which the light emission occurs, therefore it is called the emission spectrum. The light emission peaks in the fluorophore emission maximum and detection of the light at this specific wavelength leads to the highest fluorescence signal.

Fluorescence probes are generally divided into two major groups. Whereas extrinsic fluorophores have to be added to samples to generate fluorescence, intrinsic fluorochromes are naturally available.

Intrinsic fluorescence is associated to the chemical properties of the indol group from the amino acid tryptophan. Fortunately, tryptophan is an essential amino acid and suits therefore as an internal marker. Like the other aromatic acids phenylalanine and tyrosine, tryptophan emits fluorescent light after excitation. The quantum yield for tyrosine is lower than that of tryptophan, and in native proteins the signal is frequently quenched either by the protein backbone interaction or energy transfer to tryptophans<sup>186</sup>. Phenylalanine has a very low quantum yield and is rarely used.

Extrinsic fluorescent molecules are used if the molecule of interest does not emit fluorescent light, as in the case with DNA. Lately, the number of available extrinsic probes exploded and nowadays many assays for different purposes make use of external fluorophores.

Another fluorescence method which gained rising importance in various applications is the Förster energy transfer (FRET). In this case, the emission spectrum of the excited fluorophore, called donor, overlaps with the absorbance spectrum of another molecule called acceptor. This process does not involve an intermediate photon transfer because donor and acceptor are usually connected via dipole-dipole interactions. The major influential factor is therefore distance between both molecules and the orientation of their dipoles. This offers a superb possibility to measure distances between two macromolecules of interest. One of the widely used interactions is the energy transfer between the aromatic acid tryptophan and the dansyl molecules serving as acceptor.

### **5.3.1. Intrinsic tryptophan fluorescence**

All Trp-fluorescence experiments were carried out in a UV-visible QuantaMaster<sup>TM</sup> spectrofluorimeter at 20°C and the data was processed with the Felix32 software (Photon Technology International Inc., Birmingham, NJ, USA). Trp fluorescence spectra were obtained by setting the excitation wavelength to 290 nm, with a half-bandwidth of 5 nm. The emission spectra were collected in a range of 310 to 400 nm. For the kinetic fluorescence measurement, the samples were excited at a wavelength of 290 nm with a bandwidth of 8 nm and the emission wavelength was set to 325 nm as the emission maximum for intrinsic fluorescence of the Trp's. Approximately, 35 µg of MelB proteoliposomes were suspended into 1.5 mL of 0.1 M KPi (pH

7.0) resulting in a final protein concentration of 23  $\mu\text{g}/\text{mL}$ . Before acquisition, the samples were sonicated (Ultrasonic cleaner, Fungilab, Keyland Court, NY, USA) twice for 20 seconds to ensure homogenization of the proteolipsomes.

For each mutant, initially an emission scan was acquired to certify the convenient protein concentration of the sample with low background noise. A time-course acquisition was recorded successively at 325 nm while exciting at 290 nm. During the first 50 seconds, the sample was measured without ligand addition to ensure the steady sample equilibrium. Thereafter, either 10 mM or 50 mM NaCl was added to the cuvette depending on the MelB mutant. After another 50 seconds melibiose was added at concentrations up to 50 mM to facilitate binding to MelB mutants with reduced substrate affinity.

For a convenient data analysis, equal volumes of the non-substrate sucrose or KCl were added to the cuvette as well. These volumes serve as subtraction factors according to dilution effect of the added solutions. The dilution effect of NaCl could be minimized by adding the smallest possible volume of a NaCl stock solution of 5 M. In this way, the cuvette volume changed only by 0.2%.

The impact of melibiose supplementation was more significant. The solubility of melibiose in water is limited to 1.7 M at 25°C. In our case, the melibiose solution was prepared at 1.5 M. The change of the sample volume was a considerable 3% when working with a final concentration of 50 mM in the cuvette. However, the same volume changes occurred when adding 50 mM sucrose to the sample, and this served to correct for the dilution. Consequently, an emission spectrum after NaCl and melibiose addition corroborates the effect of the substrates on the protein fluorescence. In all cases, the emission spectra were subtracted with the plain buffer spectra.

### 5.3.2. FRET with Dns<sup>2</sup>-S-Gal

For the resonance energy transfer experiments (FRET) of MelB, the fluorescent sugar 2'-(n-dansyl)aminoethyl-1-thio- $\beta$ -D-galactopyranoside (Dns<sup>2</sup>-S-Gal or D<sup>2</sup>G) was utilized. This sugar was kindly delivered by Dr. Gerard Leblanc.

The sugar analog D<sup>2</sup>G contains a fluorescent dansyl-group which has its excitation maximum at 335 nm where no amino acid absorbs. Thus, this compound can serve as an acceptor of the Trp fluorescence signal emitted by the MelB. The emission spectrum of the dansyl-sugar is sensitive to its surrounding and peaks usually at 520 nm. Advantageously, the fluorescent sugar binds to the sugar binding site and moreover this molecule inhibits active sugar transport. Therefore it suits as a perfect spectroscopic tool for analyzing the sugar-protein interaction with the associated FRET signal<sup>127</sup> occurring between the Trp's and the dansyl group of D<sup>2</sup>G.

Förster energy transfer (FRET) is depends on various factors. This makes the data analysis more complex to interpret. Not only the overlaps of the donor emission spectrum with the

absorption spectrum of the acceptor, but also the quantum yield of the donor (normally Trp's) affect the FRET efficiency<sup>186</sup>. Furthermore, the relative orientation of the dipoles of both participants and the distance of acceptor and donor contribute to the energy transfer.

The distance calculation is an interesting characteristic and has been used extensively in the last decade. For instance, unfolding and refolding events of proteins analyzed by FRET gave rise to new interpretations in proteomics. By using FRET, highly complex biological structures like multi-domain proteins reveal new perspectives by obtaining detailed information about arrangement of subunits upon ligand binding or inhibition.

#### **5.3.2.1. FRET in proteoliposomes**

For the FRET experiments on the MelB transporter, approximately 50 µg of the reconstituted proteoliposomes was suspended into 1.5 mL of 0.1 M KPi-buffer (pH 7.0). The solution was sonicated (Ultrasonic cleaner, Fungilab US, Keyland Court, NY, USA) twice while maintained in ice prior to the measurement. The fluorescence experiments with the fluorescent sugar were carried out at 20°C in the UV-visible QuantaMaster<sup>TM</sup> spectrofluorimeter (Photon Technology International, Inc., Birmingham, NJ, USA) and the samples were shielded from light. Data were obtained by exciting the Trp's at 290 nm and recording the emission spectra from 310 to 570 nm. To obtain the direct fluorescence signal of the D<sup>2</sup>G sugar, the excitation was set at 325 nm and the emission spectra was recorded from 400 to 570 nm.

After acquiring the protein emission spectrum, 16 µM of D<sup>2</sup>G was added to the MelB protein suspension. Either 10 mM NaCl or 50 mM NaCl was added to the sample, depending on the mutant. Finally, to displace the fluorescent sugar from the MelB binding site, first 10 mM and consecutively 150 mM melibiose were added to the quartz cuvette (Hellma GmbH & Co. KG, Germany). Each MelB spectrum is the average of at least two independent scans.

#### **5.3.2.2. FRET in inside-out and right-side-out vesicles**

The FRET measurements in both types of vesicles, RSO and ISO, were carried out similarly as for the MelB proteoliposomes. Differing from the proteoliposomes and ISO vesicles, RSO were not sonicated before starting the measurement. A sonication step will not only homogenize the sample, but also break giant liposomes which adopt the inverted form (ISO). For RSO vesicles homogenization was realized by cautiously pipetting the emulsion into the 0.1 M KPi-buffer (pH 7.0). Since the total protein concentration is much higher than for the reconstituted MelB and the Trp signal reached signal saturation, the emission spectrum was set from 400 to 570 nm in order to detect specifically the D<sup>2</sup>G emission.

The total protein concentration used was 0.1 mg/mL. The excitation wavelength was set to 290 nm. After acquiring the spectra for the Trp's, 10 µM D<sup>2</sup>G was added to the fluorescence

cuvette. Furthermore, the samples were subjected to different NaCl concentration starting from 10 mM until 50 mM. Fluorescent sugar displacement was realized by stepwise adding of 10, 50 or even 150 mM melibiose. Each spectrum for the vesicles of a MelB mutant is the average of at least two independent scans.

### 5.3.3. Alkylation with the extrinsic probe MIANS

The cysteine-scanning mutagenesis method reveals on the one hand important residues for protein activity. Secondly this method offers the flanking possibility to chemically modify the cysteine. Cysteine possesses some advantageous features like its average size and its relative hydrophobicity. Another asset as replacing residue is the possibility to be modified through the thiol group.

In fluorescence experiments single cysteine MelB mutants were specifically marked by 2-(4'-maleimidylanilino)-naphthalene-6- sulfonic acid (MIANS, Molecular Probes, Eugene, OR, USA) (Fig 2.23). This probe was used to validate the accessibility of the single cysteine replacements. Only when MIANS interacts with thiol group it fluorescents.

Therefore, this probe is a powerful tool to study specific protein environments around single cysteines. Preferable, MIANS reacts in hydrophobic surroundings<sup>187</sup>. This fluorescent marker is only soluble in organic solution. In our case MIANS was solubilised in DMSO at a final concentration of 24 mM. Labeling experiments with reconstituted MelB mutants were carried out with approximately 50 µg of protein. The proteoliposome samples were diluted into 1.5 mL 0.1 M KPi-buffer adjusted to a pH of 7.0 and sonicated (Ultrasonic cleaner, Fungilab US, Keyland Court, NY, USA) twice for 20 seconds. The solution was excited at 325 nm (the maximum excitation wavelength of MIANS). An emission spectrum was collected from 350 to 570 nm. Subsequently, fluorescence kinetics was measured exciting the protein sample at 325 nm. After 30 seconds of steady fluorescence, 16 µM MIANS was added to the MelB samples and the emission was recorded at 415 nm for at least 1500 seconds. Since the extrinsic probe is sensitive to light, the experiments were performed in cuvettes shielded from light. The proteoliposomes were preincubated without substrates, with 20 mM sodium, 10 mM sodium and 10 mM melibiose, or 50 mM melibiose. The resulting plots were analysed with Origin 8.0 Pro.

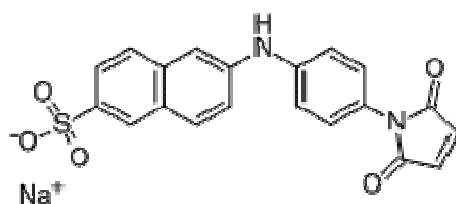


Figure 5.21: structure of the MIANS probe

MIANS data were analysed in the Origin 8.0 Pro software. Normally, the recorded curves were extrapolated with the bi-exponential equation:

$$\Delta F = F_{max} + A_1 e^{-(t-t_0)/\tau_1} + A_2 e^{-(t-t_0)/\tau_2} \quad (\text{eq. 2.10})$$

where  $\Delta F$  is the change in fluorescence,  $F_{max}$  is the ultimate fluorescence intensity,  $A_1$  and  $A_2$  are the amplitudes and  $\tau_1$  and  $\tau_2$  are the time constants. The fits were based on at least two independent measurements.

## SCOPE AND OBJECTIVES

### 6. Why to choose MelB as a raw model for the study of membrane transport

Cellular transport is basic principle for living organisms to obtain crucial inorganic and organic substances for the maintenance for all required processes. Also, transport systems continuously excrete toxic dissimilation products and serve as the cells communication system with its surrounding environment. As transport vehicles for those solutes, cells are using various membrane proteins.

The protein that forms the topic of this thesis is the secondary active sugar transporter melibiose permease (MelB) from the prokaryote *Escherichia coli*. MelB transports a variety of sugars into the cell catalyzed by an ion-motive-force. Interestingly, this carrier is capable of using three different cations which makes it much more versatile compared to members of the same glucoside-pentoside-hexuronide (GPH) family.

MelB also shares common features with highly important sodium/solute-transporters, which have been numerously recognized as potential drug targets. Information based on the study of membrane transporters such as MelB might as well be useful to understand the mechanism behind multidrug resistance transporters which also cover a vast spectrum for potential pharmacological applications.

For our purpose, the interest is more fundamentally based on the general transport mechanism processed by MelB. The transport mechanism consists of several steps including substrate binding, translocation and release accompanied by conformational changes of different transporter domains. Our study of MelB focuses on the binding characteristics of the symporter.

The scope of this thesis lies on important domains in the cytoplasmic half of MelB. It contributes insights in the ligand coupling of the secondary transporter from the Major Facilitator Superfamily by applying a mixture of biochemical and biophysical techniques. Normally the study of membrane proteins is a major bottleneck and requires the development of special techniques since their characteristics vary from soluble proteins. The attenuated-total reflection FTIR spectroscopy offers the possibility to characterize membrane protein interacting with its ligands. Therefore, this technique is a welcomed opportunity to probe the substrate binding of the melibiose carrier.

One way to receive distinct information about MelB is the site-specific replacement of amino acids. Several residues have been already identified which play a key role for the MelB transport mechanism. Our spectroscopic techniques were used to characterize amino acids substitutions which influence the interaction of MelB with its ligands. Apart from ATR-FTIR, fluorescence

spectroscopy further elucidates the properties of those residues in terms of accessibility and interaction with external probes.

In **the first section** of the results, the focus lies on the important residue Lys-377. Several studies outlined the loss of transport activity when replaced by a neutral cysteine<sup>63,69</sup>. Apart from cysteine, we replaced Lys-377 with four other amino acids. The main objective was to prove whether the impaired transport is due to the loss of substrate binding.

The next aspect addressed in the first chapter is the potential of spontaneously obtained secondary mutations of the Lys-377 mutants to recover the binding in the symporter. Moreover, since the Lys-377 is the only charged amino acid in the transmembrane helix XI, we assessed the significance of the charge by alkylation with positively charged thiol reagents.

In the **second section**, charged amino acids of the interhelical loop between helices X and XI were substituted by cysteine. Previous studies already marked mainly charged amino acids in this loop structure as main effectors of a functional sugar transport in MelB. It has been hypothesized that the loop might act as a scaffolding structure potentially affecting the substrate binding sites<sup>82</sup>. Those charged amino acids were characterized in terms of binding ability of the substrates. Since several residues cause the loss of sugar accumulation, revertants which restore the transport mechanism would aid in elucidating potential interaction of MelB subdomains.

Especially interesting appears to be the putative transmembrane segment XI. In **third section** of the results, the main objective is to outline the binding properties of cysteine mutants reported as transport-defective.

The final part of the result section (**fourth section**) is dedicated to the amino acid Trp-342. Cordat *et al.* indicate the relevance of the Trp-342 for the FRET signal contribution and emphasized that the residue might indirectly be involved in the sugar binding<sup>70</sup>. In that study the Trp-342 was replaced by phenylalanine which conserves the aromatic side chain character. Moreover, this residue apparently resides in a more polar environment interpreted as a potential residue lining the aqueous channel. During our study, the Trp-342 was replaced by cysteine which particularly alters the character of the side chain. Our primer objective was to prove if the mutant W342C affects the coupling of MelB with its ligands since the change from Trp to Cys is relatively severe. A second aim is to prove the accessibility of W342C by the alkylating reagent MIANS. Since this residue lines the aqueous channel, substrate coupling might induce some changes in the accessibility owing to helical movement.

## RESULTS

### 7. Lys-377 – an important residue for the function of the melibiose symporter?

A target residue of the transmembrane segment XI of the melibiose carrier is the lysine in position 377. This residue is the only charged amino acid in the putative transmembrane helix XI which suggests its importance for protein function and/or stability. Normally, charged residues are thermodynamically unfavorable when located in hydrophobic microenvironments, but they are partially stabilized when forming salt bridges with other charged residues. Further hydrogen bonding will eventually ensure the stability of charged residues even in the hydrophobic  $\alpha$ -helical segments. An alignment using the sequence of the melibiose transporter from several prokaryotic organisms indicated a high conservation of this charged residue.

#### 7.1. Lys-377 replacement affects the substrate binding

Lysine 377 has been replaced by neutral and charged amino acids to test how essential the positive charge at position 377 is to retain normal substrate binding. Valine and cysteine, with

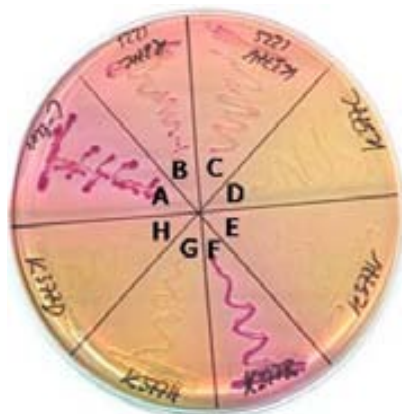


Figure 7.1 *Escherichia coli* strains DW2-R containing MelB mutants on a MacConkey agar plate supplemented with 10 mM melibiose, 10 mg/mL tetracycline and 100 mg/mL ampicilin. 8 segments: each segment for one MelB mutant, **A** C-less, **B** K377C/I22S, **C** K377V/I22S, **D** K377C, **E** K377V, **F** K377R/I22S, **G** K377H, **H** K377D

neutral (nonpolar and polar) side-chains, are expected to lead to significant alterations when inserted at position 377. In contrast, arginine and histidine replacements should mimic the positive charge of lysine, being conservative mutation in terms of charge. Finally, the extreme mutation to aspartate was used to switch to a negative charge at position 377. Combined with a second mutation to revert the negative charge of aspartates 55 and 59, this mutation was designed to test the presence of a salt bridge between Lys-377 and Asp-55 or Asp-59 suggested by current structural models.

Results of earlier publications focused on sugar transport properties confirmed the detrimental effect of the cysteine replacement, whereas lysine or valine substitution retained active transport in the presence of the proton to wild-type levels and 25% by using sodium<sup>65</sup>. The effect of these two mutations in the sugar and cation binding was not assessed

though. Information about the substrate binding and transport properties of the arginine and histidine mutants, chosen to conserve the positive charge at position 377, is still lacking, and it is for the K377D mutant

A common feature observed in all Lys-377 mutants is the tremendously reduced expression level of no more than 10% with respect to normal levels. Unknown expression levels for the mutants K377R and K377H does not allow a direct validation of their expression. The calculation of the protein expression level for each Lys-377 mutant based on purification yields are not accurate enough since preparations vary from one to another. However, compared to other mutants or the C-less control, larger culture volumes were required for Lys-377 mutants to purify sufficient amount of functional protein.

We tested qualitatively the sugar transport properties of the different mutant strains by growing in MacConkey agar plates.

The strain DW2-R expressing the C-less MelB protein exhibits red colonies on a MacConkey agar plate which contain melibiose as the main C-source (Fig. 7.1). The colored bacterial cells indicate a pH change of the media due to metabolisation of the melibiose. After its transport, the melibiose is cleaved intracellularly into the monosaccharides glucose and galactose by the  $\alpha$ -galactosidase. This reaction provokes the acidification of the media that is indicated by the pH indicator which stains the colonies. However, a red colored bacterial colony cannot necessarily be interpreted as intracellular transport of the melibiose. Since the concentration of melibiose in the surrounding medium is higher than in the cytoplasm, melibiose could enter the cell passively, until equilibrium is established between the melibiose concentration inside and outside of the cell.

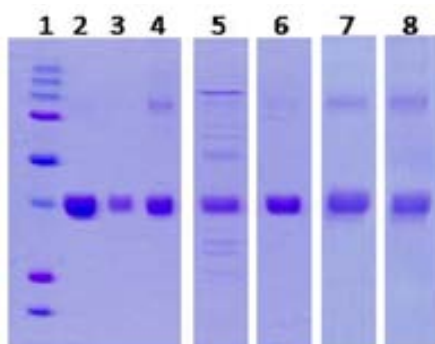


Figure 7.2 SDS-PAGE of reconstituted Lys-377 mutants and reference MelB proteins. lane1: protein marker (Bio-Rad), lane2: C-less, lane3: MelB wt, lane4: K377C, lane5: K377V, lane6: K377R, lane7: K377H, lane8: K377D. All proteins reconstituted in *E.coli* total lipids (ratio 2:1 lipid to protein). 12% SDS-gels in all cases.

A white colony on the other hand illustrates the absence of sugar transport since the sugar does not enter into the cell, no metabolizing activity exists, and the media retains its pH. In Figure 7.1 the *E. coli* strains expressing the MelB mutant transporters exhibit different phenotypes. The mutants K377C, K377H, K377D and K377V clearly demonstrate a white phenotype due to the lack of the sugar accumulation into the cells, indicating a defect in sugar transport. Although implying sugar up-take, it cannot be taken as a proof of active sugar transport. Given the high sugar concentration in the MacConkey agar plate, passive sugar transport could also occur in the mutants displaying red colonies.

The mutants K377C/I22S, K377R/I22S and K377V/I22S as part of the Figure 7.1 will be described in detail in section 7.2 of the results. The double mutants indicate a pink to red color of their cells.

### 7.1.1. Sodium-induced difference spectra of Lys-377 mutants

The MelB transporter was purified, solubilized in detergent, and reconstituted in proteoliposomes, better mimicking its native environment. In this lipid-reconstituted form the binding of substrates to the MelB transporter was assessed by infrared difference spectroscopy ( $IR_{diff}$ ) using buffers supplemented with MelB's substrates in different concentrations.

In Figure 7.3 the listed spectra were acquired in the presence of the co-substrate sodium only, to illustrate conformational changes of the MelB transporter mediated by the cation binding. The C-less  $IR_{diff}$  spectrum colored in black displays different positive and negative peaks. The difference spectrum is the subtraction between the absorbance spectrum in the presence of the proton and the absorbance spectrum in the presence of the sodium. A feature-less spectrum visible as a nearly straight line would imply an absence of interaction of the cation with MelB. The positive and negative peaks indicated vibrational differences between the two absorbance spectra. This in turn can be interpreted as structural changes of the MelB transporter when replacing the proton with sodium.

The C-less transporter possesses almost identical properties as the wild-type carrier. Throughout the study we used C-less as a control for  $IR_{diff}$  spectra.

Although acquiring the difference spectrum in broad range from 4000 to 800  $cm^{-1}$ , the most important part of a spectrum is the amide region. This region contains the protein-sensitive bands amide I and II. Therefore, for interpretation purposes we focus on the vibrational changes appearing in the amide I ( $\sim 1650\text{ cm}^{-1}$ ) and II ( $\sim 1550\text{ cm}^{-1}$ ) region. The lower wavenumbers from 1400 to 1300  $cm^{-1}$  can be crucial for fingerprint analyses of certain side chains. For a detailed assignment of peaks, see the introduction or Léon et al.<sup>135</sup>. For instance, the peaks at 1598-1600  $cm^{-1}$ , 1576-1579  $cm^{-1}$ , 1404  $cm^{-1}$  and 1383  $cm^{-1}$  are assigned to carboxylic acids<sup>134</sup>.

By assessing the  $IR_{diff}$  spectra qualitatively, the Lys-377 single mutants display feature-less difference spectra. No signal has been obtained for any of the MelB mutant in Figure 6.3. The mutants have lost the  $Na^+$  cation binding *per se*.

The evaluation of the difference spectra was further improved by using a quantitative approach. The spectra were compared quantitatively to the C-less reference spectrum. All the information of a difference spectrum were reduced to only two parameters, the spectral intensity and the spectral similarity, using the C-less spectrum as the reference. For a detailed description of how the calculation was done see the "materials and methods" section.

In all five single amino acid replacements, the relative spectral intensity and similarity between wavenumbers 1700 and 1500  $cm^{-1}$  is lower than 5% which is not significant. Therefore, it can be concluded that sodium does not interact with any of the Lys-377 single site mutants.

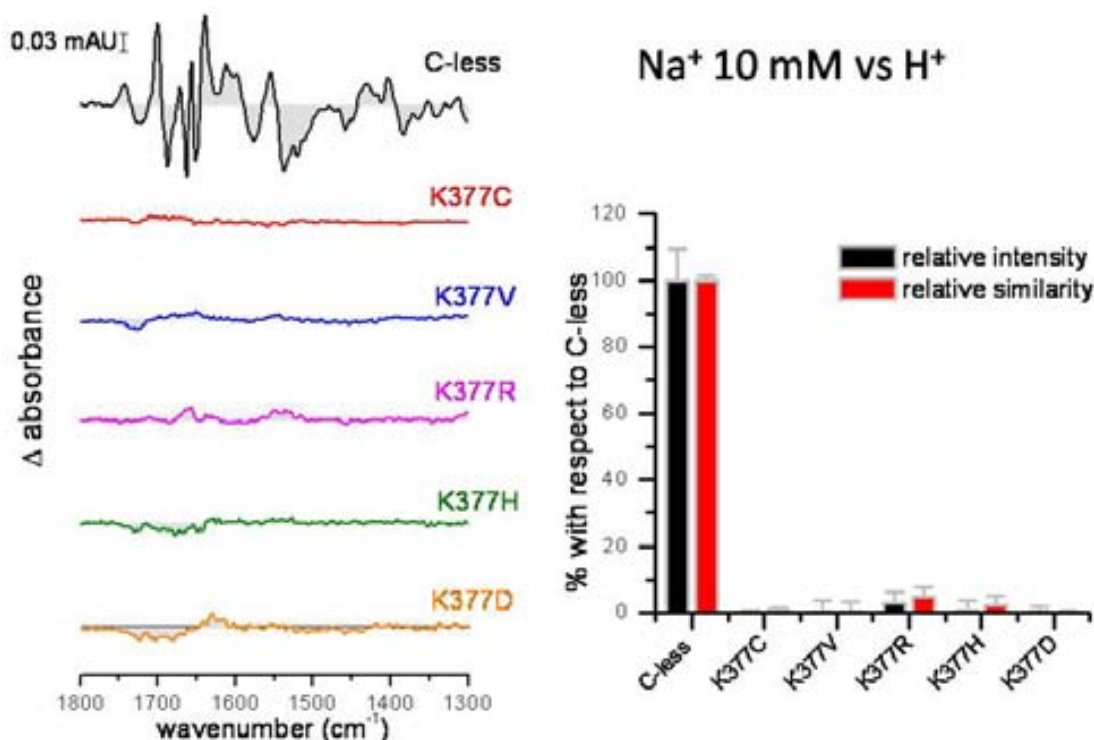


Figure 7.3 IR<sub>diff</sub> spectra of the Lys377 mutants. In the left panel: difference spectra of the MelB variants, in black: C-less as reference spectrum, in red: K377C mutant, in blue: K377V mutant, in pink: K377R mutant, in green: K377H mutant, in orange: K377D mutant, in the right panel: comparison using the first derivative of K377-mutant spectra using C-less as reference spectrum. The error bars indicate the variation depending on at least three independent data acquisitions.

To further confirm that mutation of Lys-377 mutations generate a reduced affinity for sodium, a cation-induced difference spectrum was acquired also at 50 mM sodium, 25 times the  $K_{0.5}$  of the wild-type transporter<sup>76</sup>. It is clearly seen that K377C, K377V, K377H, K377R and K377D MelB mutations provoke a defect in cation binding of MelB (Fig. 7.4) since even a high sodium concentration could not induce any clear signal in the IR<sub>diff</sub> spectra of these mutants. However, after a quantitative analysis K377R points out a tiny but significant changes ( $5\% \pm 1\%$ ) induced by  $\text{Na}^+$ .

Although significant changes in the protein-sensitive regions amide I and II are absent in the Lys-377 mutants, all mutants display a negative peak around  $1720\text{ cm}^{-1}$ . This peak can be assigned to COOH vibration and maybe a contribution from the lipids<sup>134</sup>.

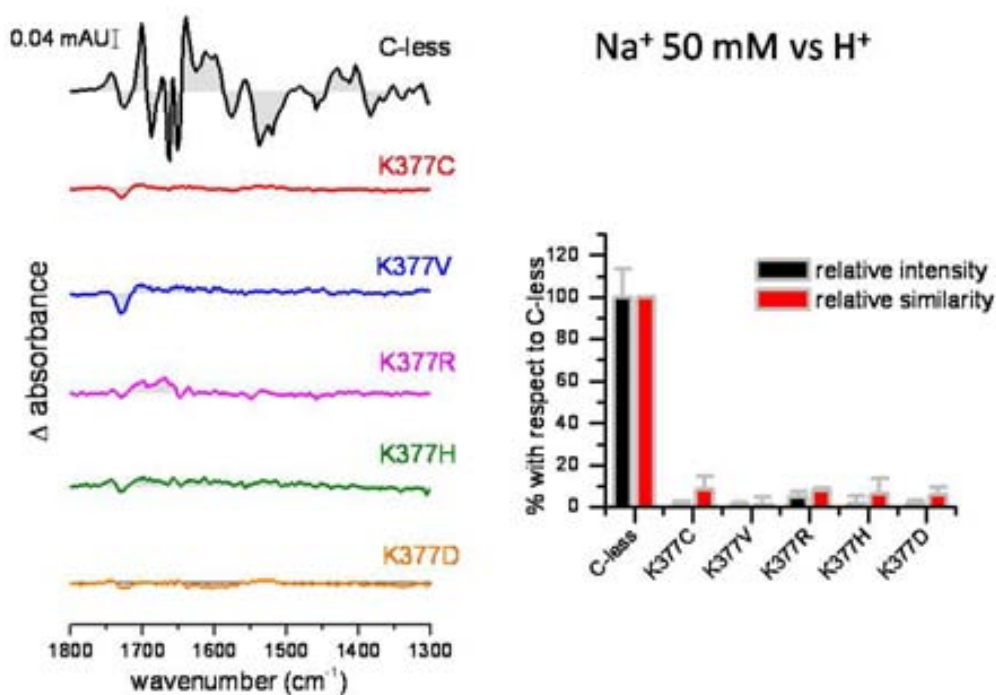


Figure 7.4 Na-induced IR<sub>diff</sub> of the Lys377 mutants (50 mM sodium). In the left panel: difference spectra of the MelB variants, in black: C-less as reference spectrum, in red: K377C mutant, in blue: K377V mutant, in pink: K377R mutant, in green: K377H mutant, in orange: K377D mutant, in the right panel: comparison using the first derivative of K377-mutant spectra using C-less as reference spectrum. The error bars indicate the variation depending on at least three independent data acquisitions.

### 7.1.2. Melibiose-induced difference spectra of Lys-377 mutants

As for the sodium-induced difference spectrum, the same technique has been used to acquire difference spectra in the presence of the melibiose. The sugar-induced difference spectrum for the C-less transporter differs in its characteristics from the cation-mediated difference spectrum.

The C-less transporter was again used as the reference displaying all necessary structural changes of the functional MelB transporter to drive the transport mechanism.

The melibiose-induced difference spectrum in the presence of the sodium displays a variety of different positive and negative peaks. From the deconvoluted spectrum several peaks could be assigned to secondary protein structures. The peak at 1703 cm<sup>-1</sup> is caused by the vibration of aspartic and glutamic acids, as well as turns and asparagines. The peaks at 1693, 1688, 1680 and 1674 cm<sup>-1</sup> are primarily provoked by β-sheet structure. The consecutive peak at 1668, 1659 and 1652 cm<sup>-1</sup> define α-helix structures. At 1643 and 1631 cm<sup>-1</sup> β-sheets cause further peaks in the melibiose difference spectra in the presence of the sodium. Aromatic side chains display characteristic peaks at 1620 and 1611 cm<sup>-1</sup>, but these peaks might have a contribution of other

## RESULTS

secondary structures as well. Tyrosine vibrations are displayed by the peaks at 1518 and 1513  $\text{cm}^{-1}$ .

Melibiose-induced  $\text{IR}_{\text{diff}}$  for the MelB mutants were consecutively acquired in the presence of the unavoidable proton and the sodium cation. Whereas the difference spectrum  $\text{Mel}\cdot\text{H}^+$ , only requires melibiose addition, the buffer for the  $\text{Mel}\cdot\text{Na}^+$  difference spectra was also supplemented with sodium chloride. Sodium increases the affinity for the sugar which can be observed by higher spectral intensity compared to the spectrum in the presence of the proton.

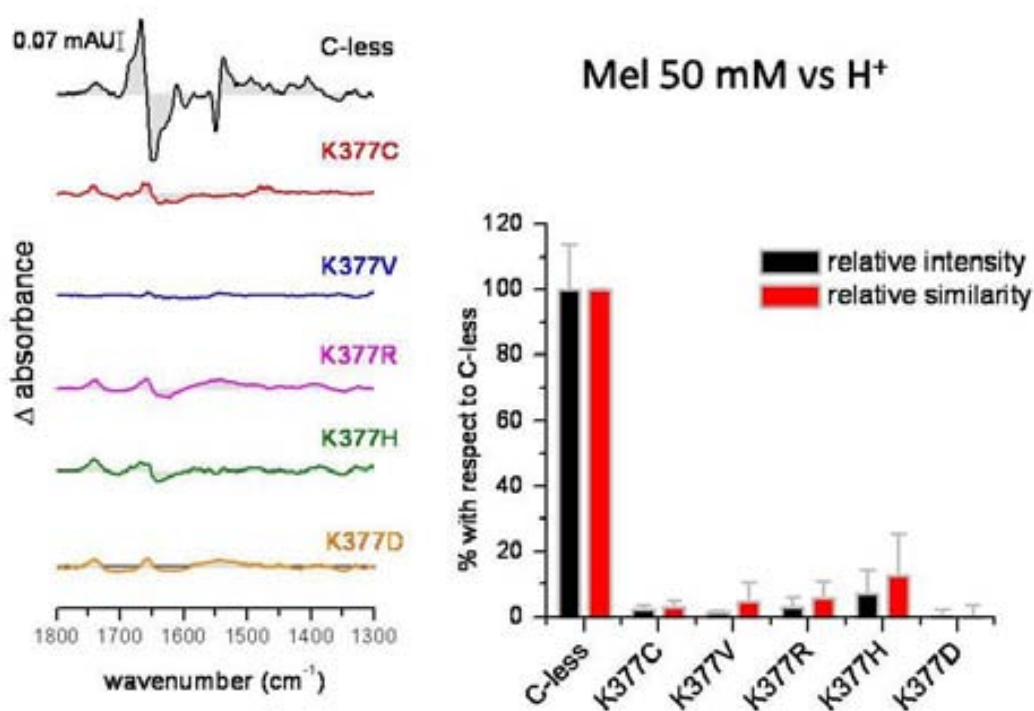


Figure 7.5 Melibiose-induced  $\text{IR}_{\text{diff}}$  (50 mM melibiose) in the presence of proton of the Lys377 mutants. In the left panel: difference spectra of the MelB variants, in black: C-less as reference spectrum, in red: K377C mutant, in blue: K377V mutant, in pink: K377R mutant, in green: K377H mutant, in orange: K377D mutant, in the right panel: comparison using the first derivative of K377-mutant spectra using C-less as reference spectrum. The error bars indicate the variation depending on at least three independent data acquisitions.

Melibiose-induced  $\text{IR}_{\text{diff}}$  in the presence of  $\text{H}^+$ . - The melibiose-induced difference spectra of MelB in the presence of the proton were recorded by using 50 mM melibiose as substrate concentration, since the half saturation constant  $K_{0.5}^{\text{mel}}$  is 22 mM in the presence of the proton, whereas  $K_{0.5}^{\text{mel}}$  is 3 mM in the presence of sodium<sup>188</sup>.

The difference spectra suggest a highly decreased sugar binding for most of the Lys-377 mutants (Fig. 7.5). K377R and K377H obviously bind the disaccharide with immensely reduced

affinity. The analysis of K377C, K377D and K377V indicate that cysteine, valine and aspartate substitutions eliminate the interaction between MelB and the sugar, whereas in the arginine and histidine mutant, the tertiary complex (MelB/H<sup>+</sup>/mel) still can be formed (Fig. 1.6) although with highly reduced affinity.

To verify if the presence of the sugar generates structural changes in the Lys-377 mutants in the presence of the co-substrate sodium, the difference spectra was acquired by supplementing 10 mM sodium to the buffer. The reference spectrum from C-less melibiose permease determines the spectral variation detected between the tertiary complex (MelB·Na<sup>+</sup>·sugar) and the cation-bound protein.

None of the lysine mutants show melibiose-induced conformational rearrangements similar to those of the C-less, and concluded by the flat melibiose-induced IR difference spectra. The quantitative comparison of the region between 1500 and 1700 cm<sup>-1</sup> with the C-less confirms the loss of sugar binding in the MelB mutants of the Lys-377 (Fig. 1.7). The single mutant K377R displays a relative high spectral similitude of about 22% compared to the C-less reference. But mutations might preserve the binding ability but affect the affinity constant of the transporter, requiring an elevated concentration to stimulate binding events. Therefore, as done when testing for Na<sup>+</sup> binding, the Lys-377 mutants were also exposed to higher melibiose concentrations (50 mM), still in the presence of 10 mM sodium.

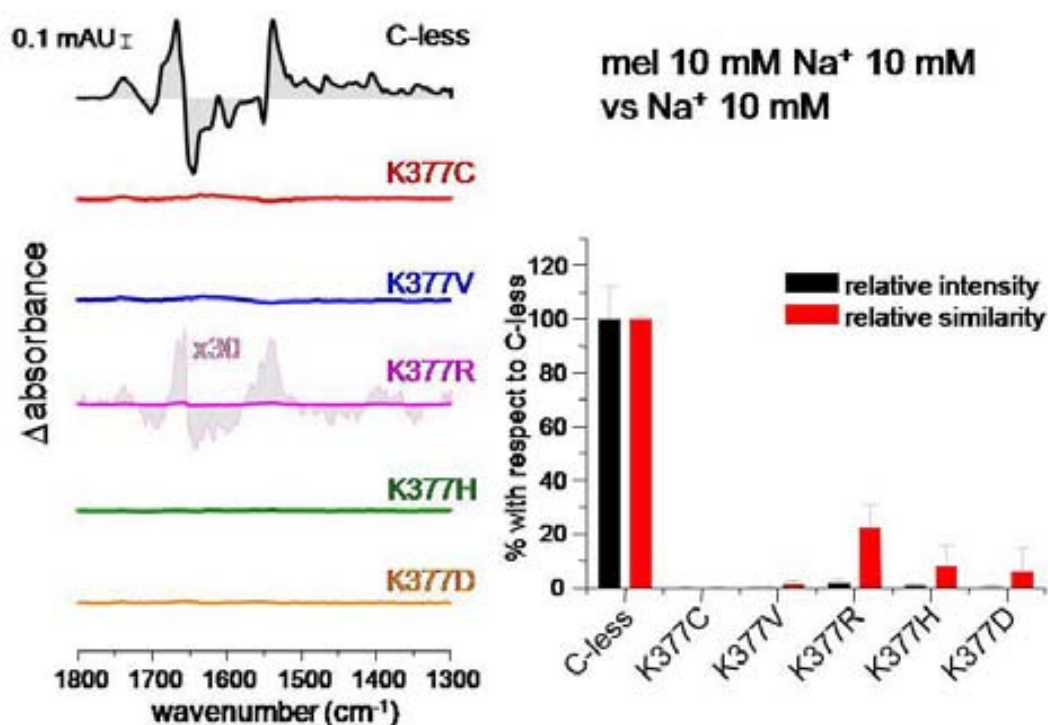


Figure 7.6 Melibiose-induced IR<sub>diff</sub> (10 mM melibiose) in the presence of sodium (10 mM) of the Lys377 mutants. In the left panel: difference spectra of the MelB variants, in black: C-less as reference spectrum, in red: K377C mutant, in blue: K377V mutant, in pink: K377R mutant (shaded spectrum: K377R multiplied by the factor 30), in green: K377H mutant, in orange: K377D mutant, in the right panel: comparison using the first derivative of K377-mutant spectra

## RESULTS

---

using C-less as reference spectrum. The error bars indicate the variation depending on at least three independent data acquisitions.

Small  $IR_{diff}$  spectra intensity can mean either a reduced affinity or a reduced structural effect of the substrate binding. The intensity will increase with the substrate concentration, whereas the structural effects remain unchanged. At a concentration of 50 mM melibiose, the Lys-377 mutants generate also a feature-less difference spectrum after subtracting background noise, the effect of the buffer and of the substrate. This result indicates the lack of melibiose-induced structural changes of the transporter. Only the arginine substitution, which maintains a positive charge of the side chain, presents a partial difference spectrum. Although the spectral intensity of just 2% compared to C-less is exceedingly reduced. Spectrum amplification by the factor 12 strengthens the notion of melibiose binding for the mutant K377R with highly reduced affinity. The factor 12 was lower than for the difference spectrum induced by only 10 mM melibiose, where the spectrum was multiplied by factor 30 to reach similar C-less intensities. K377R might outline a potential significance of the charge of the residue. By multiplying the difference spectrum with the factor 30, K377R suggests remnants of melibiose binding.

The C-less transporter demonstrates a higher signal intensity for the melibiose-induced difference spectrum in the presence of sodium compared to the difference spectrum using the proton as co-substrate. The binding is enhanced after adding sodium. This result is reasonable because the sodium induces further structural changes in MelB which leads to a tighter sugar binding.

Since in the Lys-377 mutants the binding of the sodium is lost, the sugar induces the same changes in the difference spectra with and without sodium supplementation.

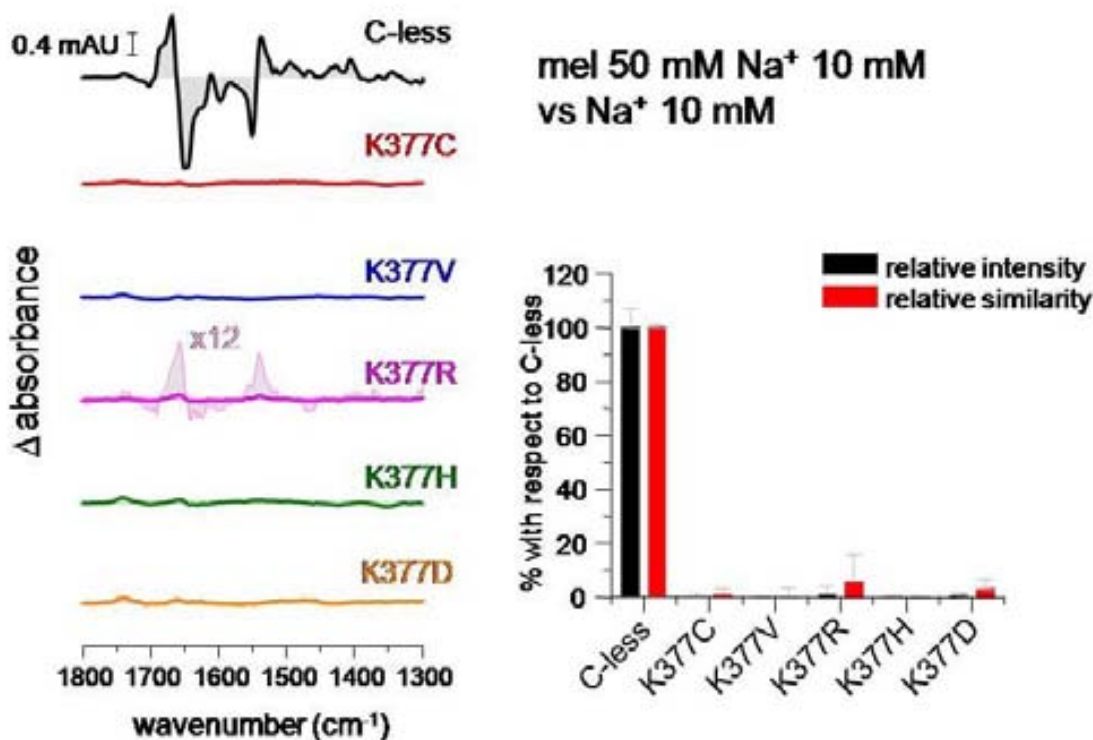


Figure 7.7 Melibiose-induced  $\text{IR}_{\text{diff}}$  (50 mM melibiose) in the presence of sodium (10 mM) of the Lys-377 mutants. In the left panel: difference spectra of the MelB variants, in black: C-less as reference spectrum, in red: K377C mutant, in blue: K377V mutant, in pink: K377R mutant (shaded spectrum: K377R multiplied by the factor 12), in green: K377H mutant, in orange: K377D mutant, in the right panel: comparison using the first derivative of Lys-377-mutant spectra using C-less as reference spectrum. The error bars indicate the variation depending on at least three independent data acquisitions.

### 7.1.3. Evaluation of the absorbance spectra of the Lys-377 mutants

Since the replacement of a single amino acid in position 377 tremendously alters the binding characteristics for both substrates, either this residue is essential for the binding of both substrates, or more likely the mutation might affect directly or indirectly the protein structure. To check the later hypothesis we analyzed the IR absorption in the protein backbone sensitive 1700 - 1500  $\text{cm}^{-1}$  region for each mutant and compared to the reference C-less transporter (Fig. 7.8). The main structural information is contained in the rather broad bands amide I and II, mostly C=O stretching and N-H bending coupled with C-N stretching of the peptide bond, respectively. Furthermore, the lipid-to-protein ratio can be deduced from the relative intensity of the C=O stretching of the phospholipids ester. A low ratio might report a failure of the reconstitution process of the solubilized protein into liposomes and lead to an inactive sample. The ratio of 2:1 (w/w) between lipids and purified MelB protein delivers an active wild-type transporter and is therefore a crucial parameter affecting the protein function and stability<sup>136</sup>. Secondly, the absorbance spectrum offers the option, as already commented, to attest for changes in the protein secondary structure of the protein caused by the mutation. At first view, the absorbance spectra of

the Lys-377 mutants are similar in the amide I-II region to the reference spectra of the fully functional MelB transport protein of C-less and wt (Fig. 7.8). But since the protein structure sensitive amide I and II bands are relatively broad, hidden patterns cannot be easily distinguished from the absorbance spectrum.

The second derivative of the absorbance spectrum of all MelB proteins was computed to resolve changes caused by the single amino acid replacement. The second derivative could give insights in conformational changes of protein or peptides. Usually, the derivation of the absorbance spectrum is used to enhance the selectivity of spectral motives. The first derivative usually clears background absorbance that occur independent of the sample, whereas the second derivative discriminates sharp pattern from a broader spectral motive<sup>189</sup>. The first derivative of the difference spectra has been used for quantitative analysis of the intensity and similarity, since it excluded the noise from the evaluation, but still maintains the spectral characteristics.

As a control we compared the second derivative spectra of two functional MelB variants: wild-type and C-less. Both spectra overlap perfectly indicating their conserved structural identity. For the mutants K377C, K377V, K377R, K377D and K377H, the second derivative spectra demonstrate small but significant spectral difference with C-less, used for the comparison (Fig. 7.8). Most remarkable, in all Lys-377 mutants the amide I peak at  $1658\text{ cm}^{-1}$  (assigned to transmembrane  $\alpha$ -helices) is shifted to  $1655\text{ cm}^{-1}$ . Moreover, the peak at  $1630\text{ cm}^{-1}$  has a pronounced height. This wavenumber has been attributed to  $\beta$ -sheets. The mutation of the lysine seems to cause some structural alterations in MelB which could be transmitted to the substrate binding site, and be the cause of the defective cation binding and only partial sugar binding in the mutants K377H, K377R and K377C. The structural alterations in the transmembrane  $\alpha$ -helices seem not to be correlated with the mutated residue, but those assigned to formation of  $\beta$ -sheets are apparently smaller in K377R and K377H than in the other mutants.

The structural changes are very similar to the mutants D55C, D59C and D124C where the sodium coupling is lost or in the case of D124C, in which it is critically reduced<sup>61</sup>. Apparently, a correlation exists between the absorbance spectra alterations and the loss of sodium binding and perhaps the melibiose binding as well. The Lys-377 mutants all lost the ability to couple the sodium, like the D55C and D59C. All of these mutants show a slight shift in the peak to  $1655\text{ cm}^{-1}$  and simultaneously the increase of the shoulder at  $1630\text{ cm}^{-1}$ .

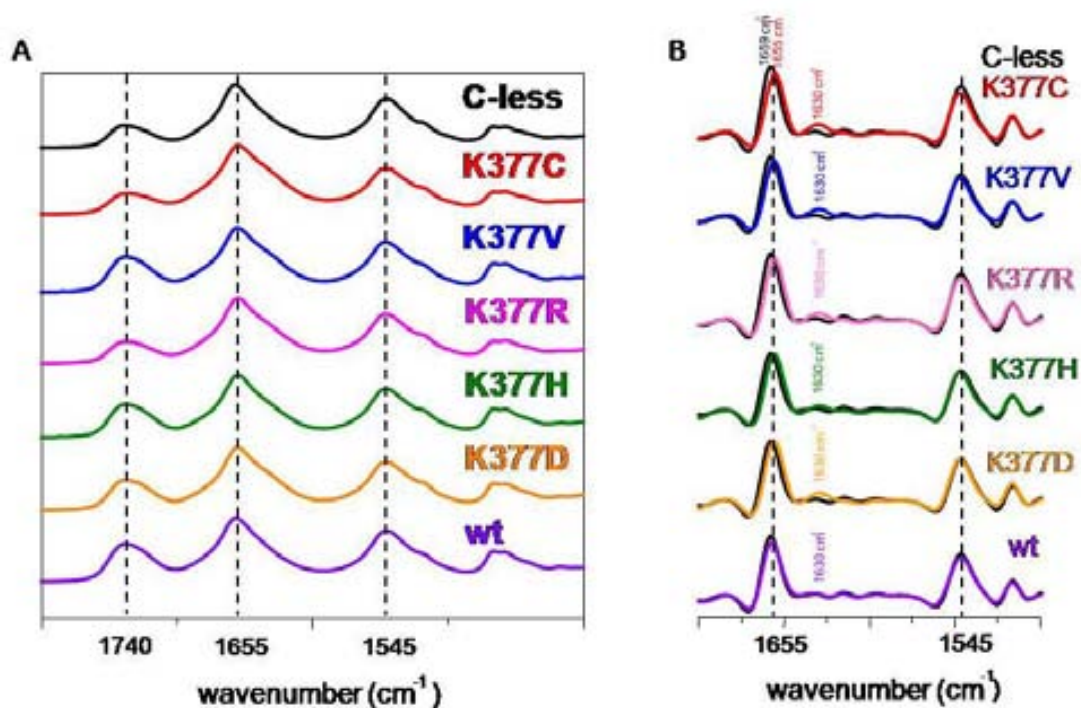


Figure 7.8 **A** comparison of absorbance spectra of the Lys377 mutants in comparison in the left panel, **B** second derivative of the absorbance spectra in the right panel. The dashed lines mark the maximum of the lipid C=O ( $1740\text{cm}^{-1}$ ), the maximum of the amide I ( $1655\text{cm}^{-1}$ ) and the amide II ( $1545\text{cm}^{-1}$ ) band.

## 7.2. Fluorescence spectroscopy of the Lys-377 single mutants

The interaction of the sugar with the protein increases the intrinsic fluorescence of MelB, while interaction with the either sodium or lithium quenches the fluorescence by 2% in the absence of the sugar, and increases it in the presence of the sugar, as described by Mus-Veteau *et al.*<sup>124</sup>. The changes of Trp fluorescence relies on three Trp residues. Whereas Trp-54 quenches the signal by 7% , the helix IV located Trp-116 and Trp-128 cause an increase of the sodium-induced fluorescence of 5%<sup>126</sup>. The combination of both occurrences results in the overall signal decrease of 2% upon  $\text{Na}^+$  binding.

The fluorescence spectroscopy is a convenient and simple method to detect substrate binding to the melibiose permease. Moreover, the intrinsic fluorescence spectroscopy is a complementary technique to confirm the results provided by  $\text{IR}_{\text{diff}}$  spectroscopy. In addition, the use of external fluorophores, as fluorescent sugars, can provide further insights.

The time course experiments were carried out by first adding the sugar. The presence of the sugar molecules induces the sugar-binding in the presence of the proton. When the sugar is bound to its moiety, the intrinsic fluorescence of MelB increases. The consecutive addition of the sodium quenches fluorescence on one side but more importantly increases also the affinity for the melibiose. The latter aspect increases further the sugar binding using the sodium as the co-substrate and eventually increases the intrinsic fluorescence as well.

For control purposes, the experiments were repeated by changing the order of the substrates,

which leads first to a decrease and then to a large increase of the fluorescence. But since the fluorescence quenching caused by the sodium and lithium binding is small, it is difficult to detect.

### 7.2.1. Intrinsic Trp fluorescence

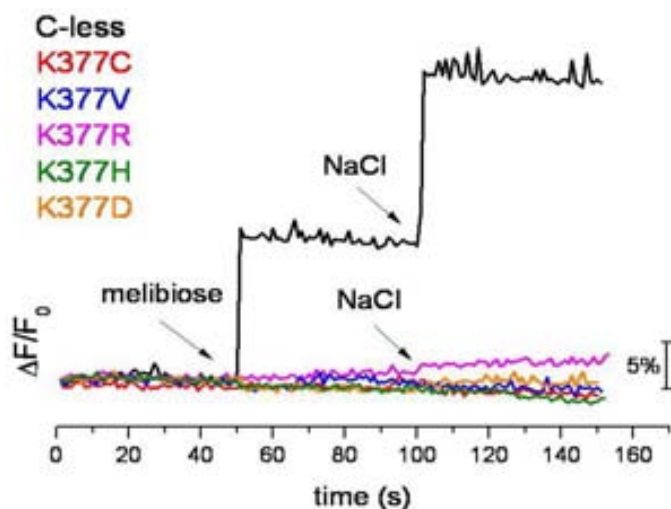


Figure 7.9 Trp fluorescence spectroscopy of the Lys377 mutants; buffer is composed of 100 mM KPi and 100 mM KCl, pH 7.0. melibiose and NaCl were supplemented at a concentration of 50 mM for the Lys377 mutants and at 10 mM for C-less. black line: C-less, red line: K377C, blue line: K377V, pink line: K377R, green line: K377H, orange line: K377D. after 50 sec supplementation of 50 mM melibiose (first black arrow), after 100 sec supplementation of 50 mM NaCl. All spectra were corrected for the dilution effect of the added volumes of the substrates.

The changes in the intrinsic Trp fluorescence confirm the results retrieved from the IR<sub>diff</sub> spectroscopy. The ligands do not produce fluorescence changes of the tryptophans as they do in the C-less control (Fig. 7.9). Only the K377R mutant exhibits a minuscule fluorescence increase of around 1% after adding both substrates. The substrates sodium and melibiose were added at 50 mM to foresee the saturation of the transporter. For the K377R, 10 mM of both substrates were sufficient to provoke a fluorescence increase of around 1%. This value agrees with the

result of the IR<sub>diff</sub> of 10 mM melibiose in the presence of 10 mM sodium. The K377R is the only mutant which demonstrates a stimulation of the protein structure in the presence of its substrates.

### 7.2.2. FRET analysis with the sugar derivative D<sup>2</sup>G

The fluorescent sugar D<sup>2</sup>G (2'-N-5-dimethylaminonaphthalene-1-sulfonyl)-aminoethyl 1-thio-β-D-galactopyranoside), a β-galactoside-derivative, binds to MelB. Moreover, it shares the binding site with melibiose, since both sugar show competitive binding, with the D<sup>2</sup>G displaced by melibiose in excess. Once bonded, the D<sup>2</sup>G allows for FRET experiments with energy transfer from the intrinsic tryptophans to the dansyl-group of the D<sup>2</sup>G.

The fluorescent galactoside analog D<sup>2</sup>G has been widely used to study the related sugar transporter LacY<sup>190-192</sup>. Its fluorescence depends on the solvent polarity. For energy transfer between the bound D<sup>2</sup>G and MelB, the dansyl group from D<sup>2</sup>G absorbs the emitted light from Trp residues located in proximity.

Maehral *et al.* reported a much higher affinity of MelB for D<sup>2</sup>G ( $K_d^{D^2G} = 1.4 \mu\text{M}$ ) compared to the physiological melibiose sugar ( $K_d^{\text{mel}} = 0.5 \text{ mM}$ )<sup>127</sup>. The authors also stated that the polarity of the acceptor environment changes in a sodium-dependent fashion. Without sodium cations the substrate binding site is more polar. This indicates a tighter substrate binding in the presence of sodium. The fluorescent sugar allows insights into the physiochemical properties of the substrate binding site of the melibiose symporter.

We recorded the fluorescence spectra for the MelB proteoliposomes in an interval from 310 – 570 nm. The experiments using the D<sup>2</sup>G sugar as a substrate were acquired using light excitation at 290 nm. The wavelength is absorbed by the intrinsic Trp. The overlap of the D<sup>2</sup>G excitation spectrum with the Trp emission spectrum enables the FRET phenomenon.

Using the C-less proteoliposomes (Fig 7.10 upper panel on the left), the spectrum displays the typical Trp peak with the maximum around 325 nm (black line). After the addition of 16  $\mu\text{M}$  D<sup>2</sup>G (red line), the signal of the Trp residues decreases due to an inner filter effect and quenching of the fluorescent sugar in the medium<sup>127</sup>. Simultaneously, a small peak appears between 420 and 540 nm. The addition of sodium (blue line) results in a further quenching of the Trp fluorescence around 325 nm. But in parallel, the peak from 420 – 570 nm increases in intensity. The maximum of this peak is around 465 nm. An addition of melibiose (cyan line) reverses the effects by decreasing the D<sup>2</sup>G FRET signal at 465 nm and increasing the Trp fluorescence.

Finally, an excess of melibiose (150 mM – magenta line) replaces the majority of the remaining D<sup>2</sup>G molecules. The Trp fluorescence at 325 nm recovers its signal intensity and the fluorescence signal between 420 – 540 nm almost vanishes. This indicates that the D<sup>2</sup>G is

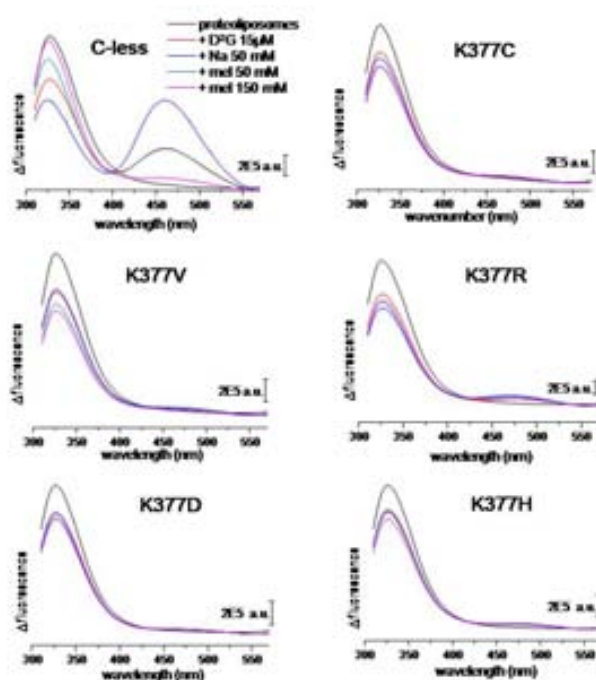


Figure 7.10 FRET analysis of the Lys-377 single mutants, for all fluorescence spectra: excitation wavelength at 290 nm and emission wavelength from 310 to 570 nm; upper left corner: C-less, center left: K377V, lower left corner: K377D, upper right corner: K377C, center right: K377R, lower right corner: K377H.

gradually replaced by the physiological substrate melibiose. D<sup>2</sup>G behaves as a competitive inhibitor for the melibiose permease. The sugar analog binds to the MelB substrate binding site indicated by the energy transfer between the Trp and the indole ring of the D<sup>2</sup>G.

Apart from the K377R mutant, none of the Lys-377 mutants demonstrate energy transfer. Even though very minuscule, the lysine-to-arginine replacement rescues partially the FRET signal between the indole ring of the tryptophanyl residue and the dansylated sugar.

In Fig. 7.12 the D<sup>2</sup>G was directly excited to probe the fluorescence emission maximum of the protein-bound D<sup>2</sup>G. The acceptor molecule is sensitive to the binding site surrounding.

Excitation at 335 nm produces a relatively small fluorescence signal. The spectrum for the C-less transporter (fig. 7.10 upper panel on the left) displays similarly to the spectrum acquired at 290 nm and increase after the addition of sodium (red line). This signal intensity is then gradually decreased by the addition of melibiose (blue and cyan line). The results of the direct excitation of D<sup>2</sup>G match the results from the Trp → D<sup>2</sup>G FRET spectrum (Fig. 7.10 upper panel on the left).

The direct excitation of the sugar molecule agrees with the excitation of the intrinsic Trp residues (Fig. 7.11). The sodium-dependent stimulation of the energy transfer between the intrinsic tryptophans and the D<sup>2</sup>G molecule is absent in all Lys-377 mutants. The slight signal increase with the maximum at 500 nm might be attributed to unspecific D<sup>2</sup>G binding. The reasons for this hypothesis are that in the presence of sodium the fluorescence signal does not increase. And furthermore, if in these mutants the tertiary complex consisting of the proton, D<sup>2</sup>G and MelB has been formed, the melibiose addition would decrease the signal at 465 nm. After adding an excessive amount (150 mM) of melibiose the signal remains unchanged. This result indicates the impaired D<sup>2</sup>G binding in the Lys-377 mutants.

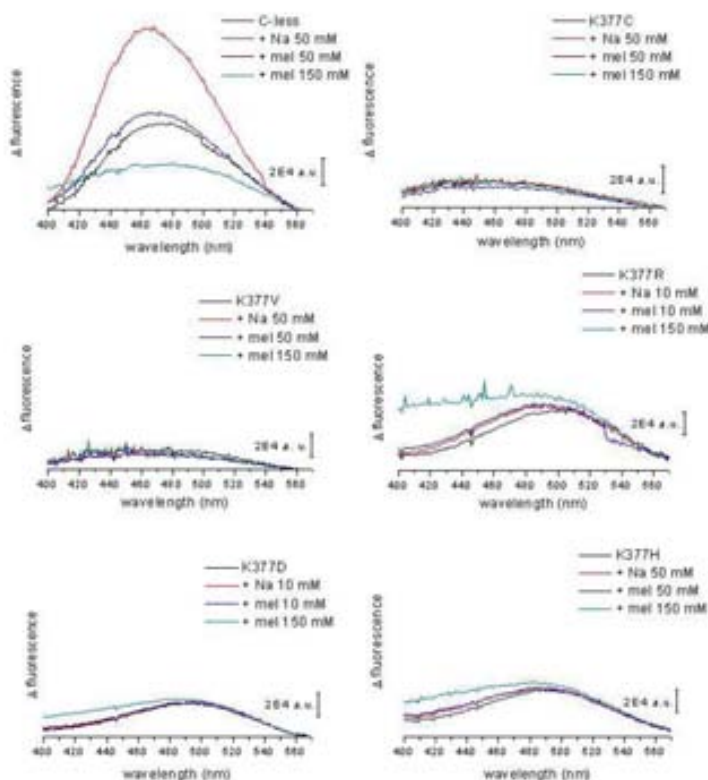


Figure 7.11 Direct excitation of D<sup>2</sup>G. For all fluorescence spectra: excitation wavelength at 325 nm and emission spectra were collected from 400 to 570 nm; upper left corner: C-less, center left: K377V, lower left corner: K377D, upper right corner: K377C, center right: K377R, lower right corner: K377H.

### 7.3. *Lys-377 revertants*

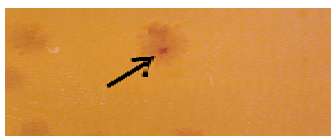


Figure 7.12 image of K377C on a MacConkey plate after 8 days at 30°C. The black arrow points to a red sub-colony with the bacteria colony.

In the past, revertants have been obtained by incubating mutants where the transport was highly reduced or completely absent on a MacConkey agar plate. A variation of the colony color, usually from white to red, witnesses a different phenotype, separating the melibiose-metabolising clones easily from colonies unable to uptake the sugar.

The same approach was performed for the *Lys-377* mutants. After 5-10 days incubating the strain containing the mutated *MelB* gene on a MacConkey agar plate, small red colonies appeared (Fig. 7.12) which were picked and re-streaked on a new agar plate to verify the phenotype change. Those colonies were inoculated into liquid medium and cultivated for plasmid preparation. The plasmid DNA was purified with commercially available kits and sequenced on location. The plasmids containing the parental *Lys-377* mutation and a second site substitution were transformed into competent cells from the same DW2-R *E. coli* strain. Colonies grown on MacConkey agar plates finally exclude the possibility of chromosomal mutation responsible for the colored phenotype.

#### 7.3.1. Revertants with I22S mutation

The mutants K377C, K377V, K377R and K377H incubated on MacConkey agar plates between 5-10 days exhibiting all red colonies. Those sequence changes could be assigned almost

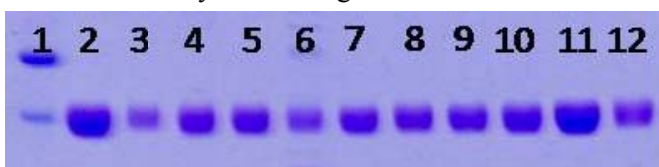


Figure 7.13 SDS-PAGE of *MelB* mutants. lane1:protein marker, lane2: C-less, lane3: *MelB* wt, lane4: K377C, lane5: K377C/I22S, lane6: K377V, lane7: K377V/I22S, lane8: K377R, lane9: K377R/I22S, lane10: K377R/L236F, lane11: I22S, lane12: D59K/K377D

exclusively to the second-site mutation I22S. The original apolar Ile-22 was replaced by a polar serine located in the transmembrane helix I of the transporter.

Strikingly, this isoleucine at position 22 is a hotspot for the generation of second site revertants in combination with several amino acids in the C-terminal part of *MelB*. Previous publications already revealed the replacement of Ile-22 by threonine, serine or glutamine for the residues *Lys-377*, *Ala-383*, *Leu-391* and *Gly-395*<sup>69</sup>. In our case, all *Lys-377* replacements present I22S as the second site mutation. Previous work already shown that the double mutant K377C/I22S improves the expression level, but hardly improves the transport activity in comparison to the parental single site replacement<sup>69</sup>.

The red-phenotype indicates clearly sugar transport compared to the defective parental strain with its white colony. However, the affinity of the double mutants is very poor but simultaneously displaying a high  $v_{\max}$  explaining the red-colored mutant. Figure 7.13 displays the SDS-PAGE of the purified MelB mutants after the elution from nickel-affinity chromatography.

### 7.3.1.1. ATR-FTIR of the mutants containing Ile-22 replacement

In this chapter, infrared difference spectra of the spontaneous double mutants K377/I22S point out the substrate binding in these MelB proteins. As mentioned beforehand, the revertants K377/I22S were obtained by spontaneous mutation. As a control to study this revertant, the Ile-22 alone was replaced by serine as well as to alanine to maintain the apolar character of the amino acid. Particularly interesting is the fact that this isoleucine is in proximity of the important residues Asp-19 and Phe-20<sup>57,65</sup>. Asp-19 was formerly considered as a part of the cation binding site, but studies made by Granell et al<sup>61</sup>., denied the idea of interaction with the cation but instead pointed out the involvement in the binding of the sugar<sup>139</sup>. The Phe-20 residue is another target residue possibly involved in the translocation of the substrates<sup>69</sup>.

The sodium dependent infrared difference spectra of the I22S and I22A single mutants show that the cation induces similar conformation changes in the transporter as in the cysteine-less transporter (Fig. 7.14). The most recognizable difference between Ile-22 mutations and C-less is the pronounced negative peak at 1650  $\text{cm}^{-1}$ , absent in the later. For the double mutants K377C/I22S, K377V/I22S and K377R/I22S the changes induced by 10 mM sodium are close to negligible. The K377V/I22S and K377R/I22S difference spectra are feature-less which corresponds to the absence of interaction between the protein and its ligand. The K377C/I22S however, points to some spectral response to sodium, which might suggest sodium binding but of strongly reduced affinity.

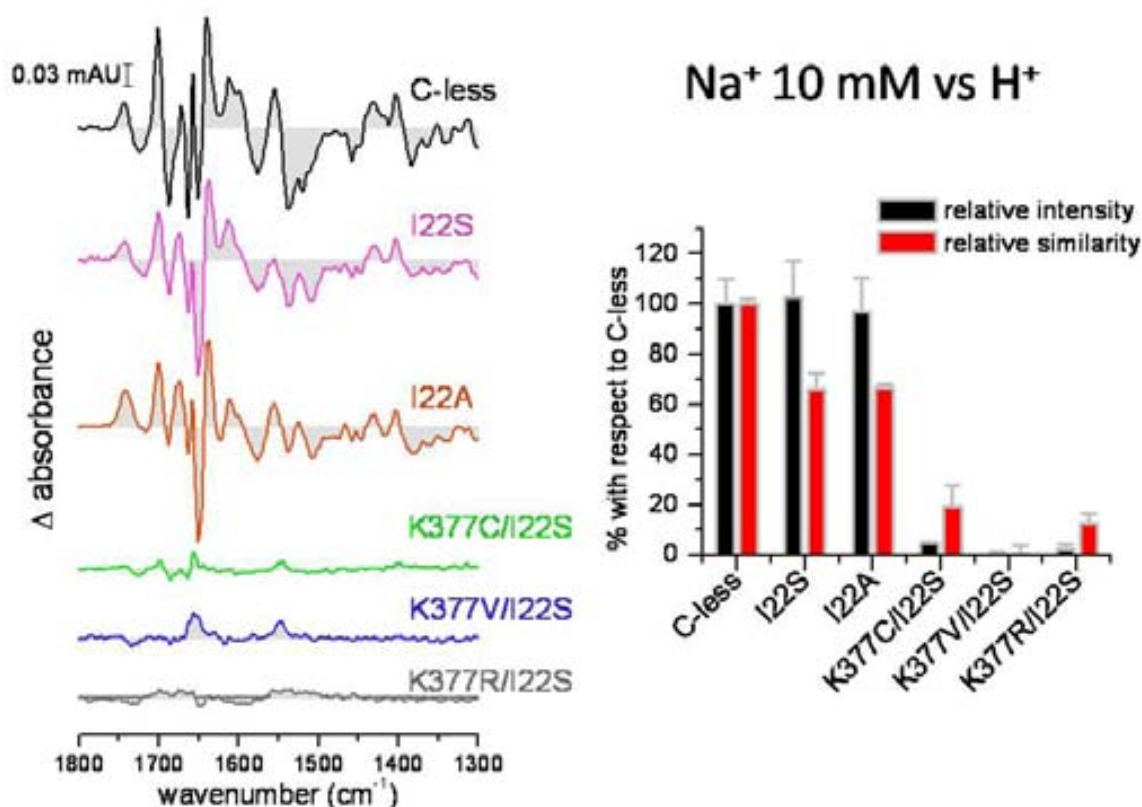


Figure 7.14 Sodium-induced IR<sub>diff</sub> spectra (using 10 mM NaCl) of the double mutants containing the second site I22S replacement in conjunction with two Ile-22 mutants. In the left panel: difference spectra of the MelB variants, in black: C-less as reference spectrum, in pink: I22S mutant, in brown: I22A mutant, in light green: K377C/I22S mutant, in marine: K377V/I22S mutant, in dark grey: K377R/I22S mutant, in the right panel: comparison using the first derivative of mutant spectra using C-less as reference spectrum. The error bars indicate the variation depending on at least two independent data acquisitions.

In the presence of a higher sodium concentration (50 mM), the difference spectra of the Ile-22 single mutants conserve the same spectral characteristics as already seen at the lower sodium concentration.

For the I22S mutant, the higher intensity compared to C-less indicates, that with 10 mM sodium the saturation has not yet been reached. But, overall the replacement of the isoleucine in position 22 does not affect the interaction with the co-substrate. Considering the spectra of the three double mutants carrying the Lys-377 replacement in combination with the I22S second site, at a saturating sodium concentration of 50 mM the K377C/I22S mutant demonstrates a slight increase in spectral intensity which can be explained by the extraordinarily reduced affinity for the cation (Fig. 7.15). The double mutants K377V/I22S and K377R/I22S exhibit a feature-less difference spectrum for the larger concentration of sodium as well.

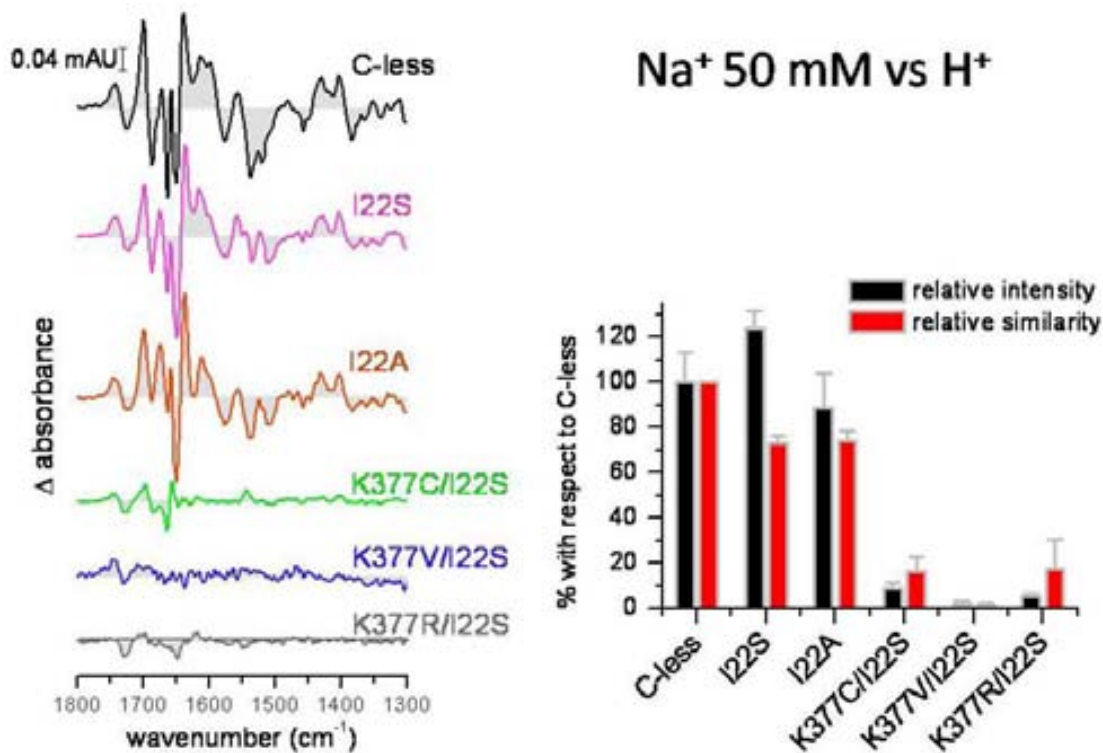


Figure 7.15 Sodium-induced  $\text{IR}_{\text{diff}}$  spectra (using 50 mM NaCl) of the double mutants containing the second site I22S replacement in conjunction with two I22 mutants. In the left panel: difference spectra of the MelB variants, in black: C-less as reference spectrum, in pink: I22S mutant, in brown: I22A mutant, in light green: K377C/I22S mutant, in marine: K377V/I22S mutant, in dark grey: K377R/I22S mutant, in the right panel: comparison using the first derivative of mutant spectra using C-less as reference spectrum. The error bars indicate the variation depending on at least two independent data acquisitions.

The red colored colonies on the MacConkey agar plates indicate sugar metabolism in the bacteria. Therefore we expect these double mutants to restore melibiose binding. Surprisingly, in the revertants the sugar binding is still absent when probed in the presence of the proton. Even more astoundingly, the single residue replacements of isoleucine to serine completely lost the ability to interact with the sugar molecule. The substitution with alanine retains a minute interaction with the sugar. The spectral quantification indicates an intensity of less than 5%. The results of the Ile-22 single mutants might explain also the absence of detectable melibiose binding in the double mutants. Also Ding *et al.* failed to demonstrate sugar transport in the same double mutant K377C/I22S obtained likewise<sup>69</sup>.

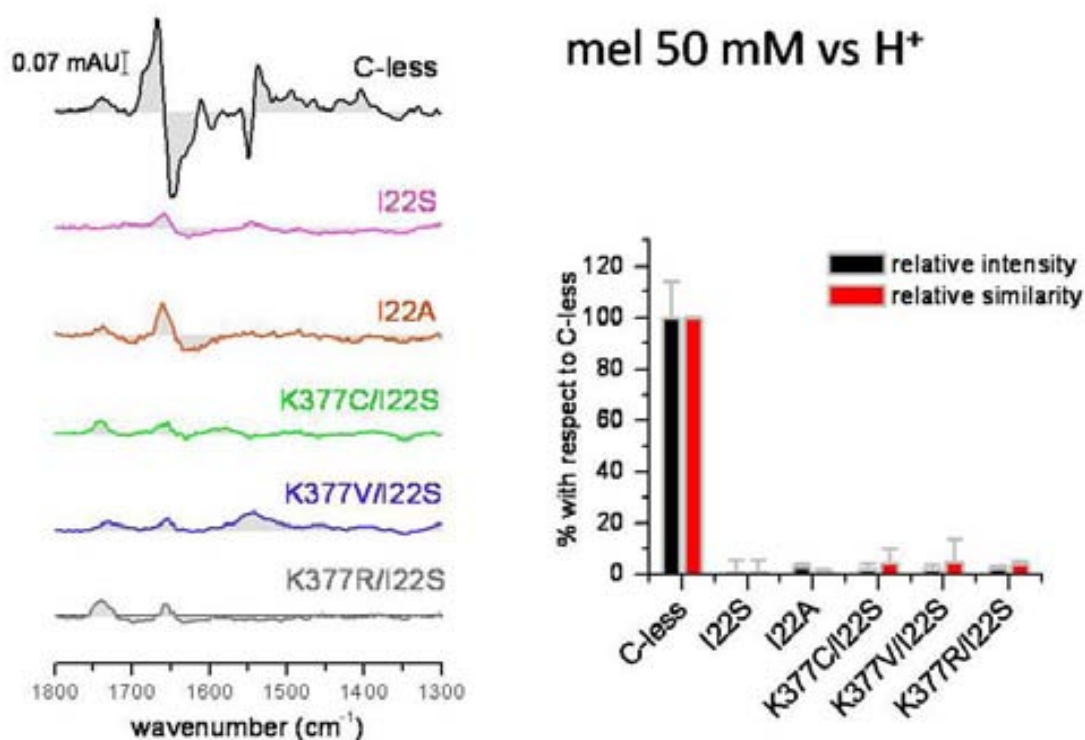


Figure 7.16 Melibiose-induced IR<sub>diff</sub> of the revertants of the Lys-377 mutants combined with I22S and I22A replacements in the presence of the proton. In the left panel: difference spectra of the MelB variants, in black: C-less as reference spectrum, in pink: I22S mutant, in brown: I22A mutant, in light green: K377C/I22S mutant, in marine: K377V/I22S mutant, in dark grey: K377R/I22S mutant, in the right panel: comparison using the first derivative of mutant spectra using C-less as reference spectrum. The error bars indicate the variation depending on at least two independent data acquisitions.

The melibiose-induced difference spectra in the presence of sodium indicate further structural changes in the C-less transporter, in which the spectral intensity exceeds the intensity of the sugar-mediated spectrum using just the proton as co-ion. For the revertants, the supplementation with sodium does not induce any melibiose-induced difference spectrum (Fig. 7.16).

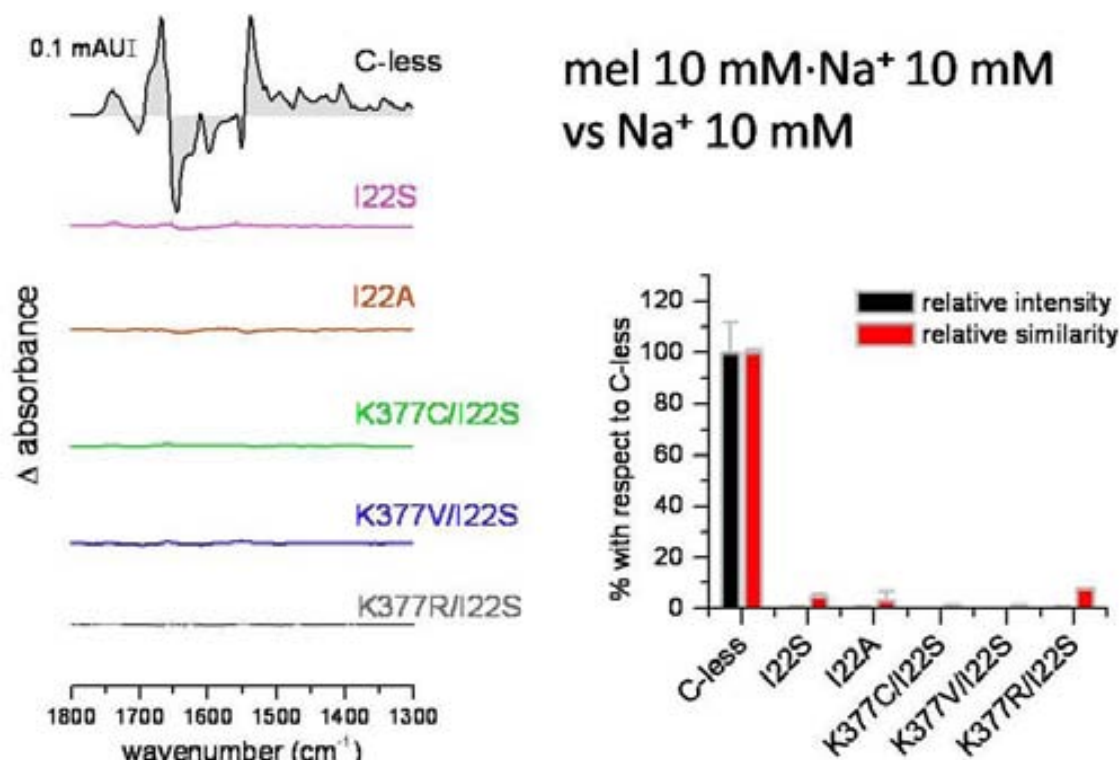


Figure 7.17 Melibiose-induced  $IR_{diff}$  of the revertants of the Lys-377 mutants combined with I22S and I22A replacements. In the left panel: difference spectra of the MelB variants, in black: C-less as reference spectrum, in pink: I22S mutant, in brown: I22A mutant, in light green: K377C/I22S mutant, in marine: K377V/I22S mutant, in dark grey: K377R/I22S mutant, in the right panel: comparison using the first derivative of mutant spectra using C-less as reference spectrum. The error bars indicate the variation depending on at least two independent data acquisitions.

Also a higher concentration of melibiose (Fig. 7.18) does not induce any conformational changes in the Lys-377 revertants. It demonstrates that the loss of interaction is not only a matter of reduced substrate affinity. The substrate-induced  $IR_{diff}$  spectra of the mutants I22A and I22S are quite similar to the recorded data from D19C. Since Asp-19 and Ile-22 are relatively close to each other based on the primary sequence, a potential interaction site of the sugar with MelB might be conFigured by both residues.

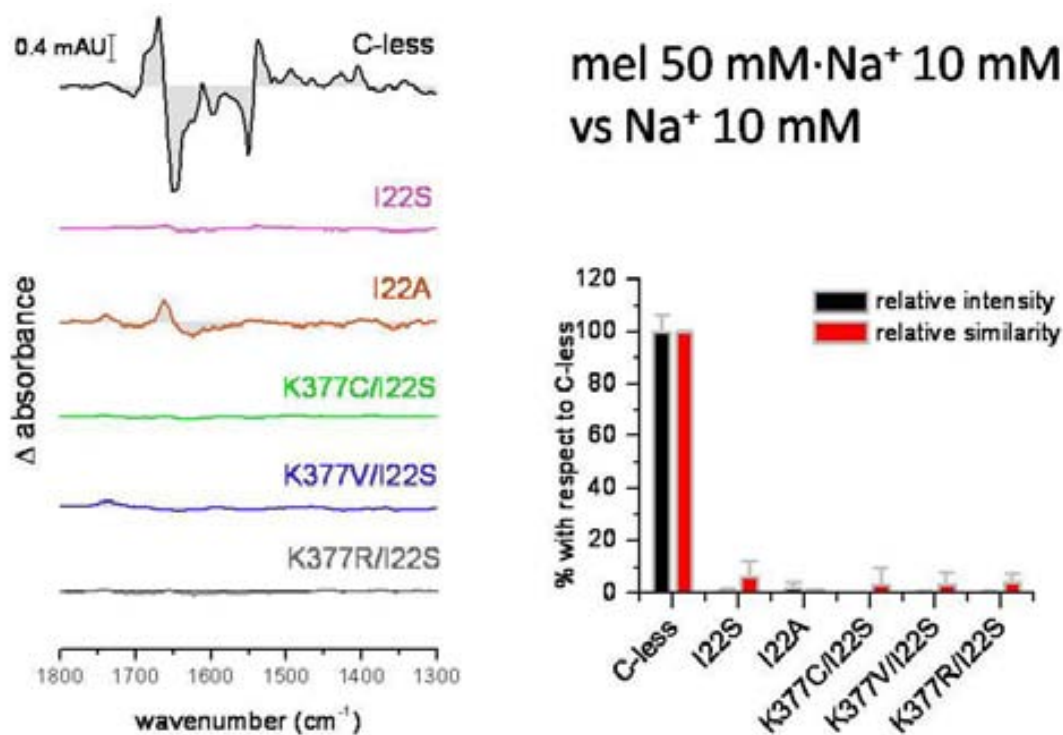


Figure 7.18 Melibiose-induced  $IR_{diff}$  of the revertants of the Lys-377 mutants combined with I22S and I22A replacements using a saturating concentration of 50 mM melibiose. In the left panel: difference spectra of the MelB variants, in black: C-less as reference spectrum, in pink: I22S mutant, in brown: I22A mutant, in light green: K377C/I22S mutant, in marine: K377V/I22S mutant, in dark grey: K377R/I22S mutant, in the right panel: comparison using the first derivative of mutant spectra using C-less as reference spectrum. The error bars indicate the variation depending on at least two independent data acquisitions.

Only I22A demonstrates remnants of melibiose binding at higher concentrations of 50 mM melibiose in the presence of either the proton or Na<sup>+</sup> as co-substrates. Whether the difference spectrum is triggered by melibiose binding or due to unspecific interactions is not clear yet. The featureless difference spectra of the majority of the Ile-22 mutants reveal the absence of co-substrate interaction with the transporter. Obviously, the I22S substitution does not conserve the sugar binding of the transporter mediated by cation coupling. The absence of proton- or sodium-dependent  $IR_{diff}$  spectra demonstrated the absence of conformational changes upon substrate interaction. By replacing the Ile-22 with serine, the sugar transporter fails to couple the melibiose.

#### 7.4. Absorbance spectra of the single mutants and revertants

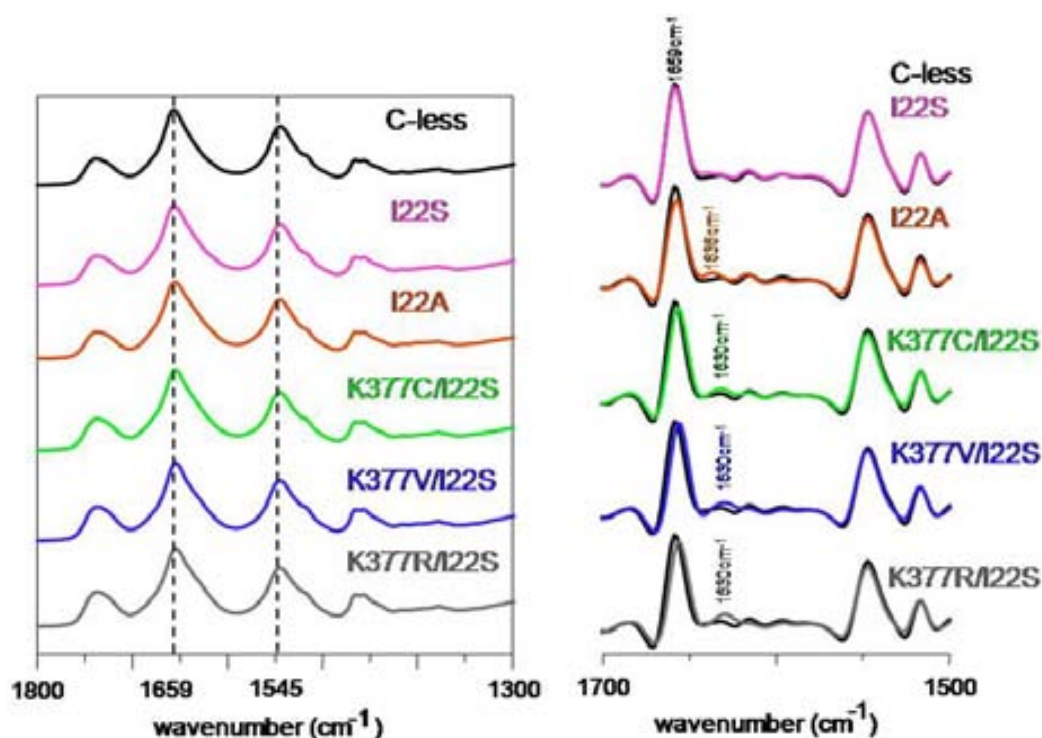


Figure 7.19 Absorbance spectra comparison between K377/I22S double mutants as well as isoleucine 22 single mutants to C-less reference spectrum. Left panel: absorbance spectra of the wet protein film between 1900 and 1300  $\text{cm}^{-1}$ , right panel: second derivative of the same absorbance spectra in the amide region between 1700 and 1500  $\text{cm}^{-1}$ .

By comparing the absorbance spectra (Fig. 7.19) of the wet protein film, the results correlate well with the data accomplished from the infrared difference spectra. The Ile-22 single mutants' second derivative of the absorbance spectra almost perfectly overlaps with the spectrum of C-less. The only small incoherence was found for the I22A mutant that displays a small shoulder with the maximum at 1636  $\text{cm}^{-1}$  which is similar to the detected peak at 1630  $\text{cm}^{-1}$  for the defective Lys-377 mutants (see chapter 7.1). I22S and I22A mutants bind the sodium cation as C-less but fail to deliver a difference spectra induced by melibiose. The Ile-22 mutants conserve the structure of the melibiose permease

Considering the absorbance spectra of the double mutants, the outcome differs from the single mutants. As in the lysine single replacements, the most significant difference compared to C-less occurred around 1630  $\text{cm}^{-1}$ . This shoulder is related to an elevated amount of  $\beta$ -sheet structure. Remarkably also the peak assigned to  $\alpha$ -helices is shifted to lower wavenumbers indicated by the peak at 1655  $\text{cm}^{-1}$ .

The K377C/I22S is the only mutant demonstrating partial co-substrate binding. For correlation purposes, it is the double mutant with the smallest shoulder at 1630  $\text{cm}^{-1}$ . It might indicate the structural implications for the substrate binding.

## 7.5. Fluorescence analysis of the Ile-22 mutants

### 7.5.1. Intrinsic fluorescence

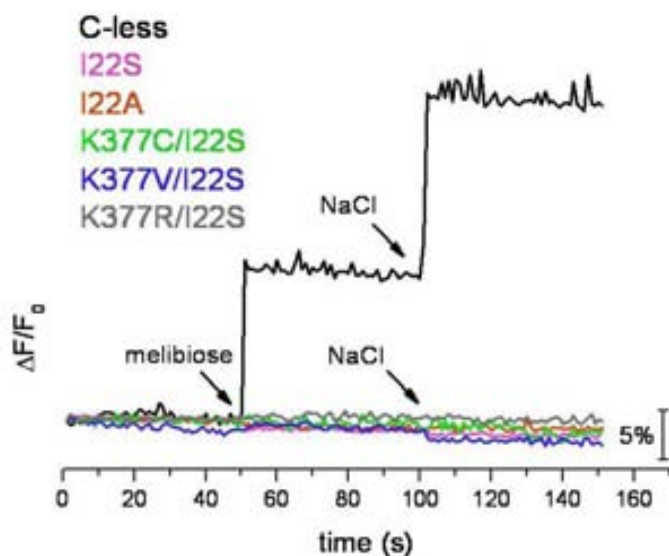


Figure 7.20 trp fluorescence of the MelB variants carrying the mutation of isoleucine 22. Black line: C-less, pink line: I22S, brown line: I22A, light green line: K377C/I22S, marine line: K377V/I22S, dark grey line: K377R/I22S. melibiose and sodium are added in saturating concentration of 50 mM. The spectra were corrected for the diluting effects of the ligand containing solutions.

substrates which automatically dilutes the sample.

The fluorescence spectroscopy of the five mutants encompassing the group of mutations of the helix I residue Ile-22 exhibits the expected lack of fluorescence increase upon substrate addition (Fig. 7.20).

The result is in agreement with the infrared analysis where the sugar fails to induce conformational changes in the transporter similar to the single mutants carrying the mutation of the lysine in position 377. On the downside, the results do not enlighten sodium binding of the carrier mutants. Usually, the cation provokes a signal quenching of around 2%, which is considerably small and difficult to extract after the addition of

### 7.5.2. FRET analysis in proteoliposomes

The FRET data of the dansylated sugar are in agreement with previous analyses. The intensity of the tryptophan fluorescence decreases stepwise. This quenching effect occurs in the proteoliposome samples missing the interaction with the sugar-analogue. The Ile-22 single mutants do not bind the fluorescent  $\beta$ -sugar analog and neither do the K377/I22S mutants. Neither alpha nor beta sugar confirmation is recognized by the carrier. Hence, the sugar conformation is not decisive for the binding.

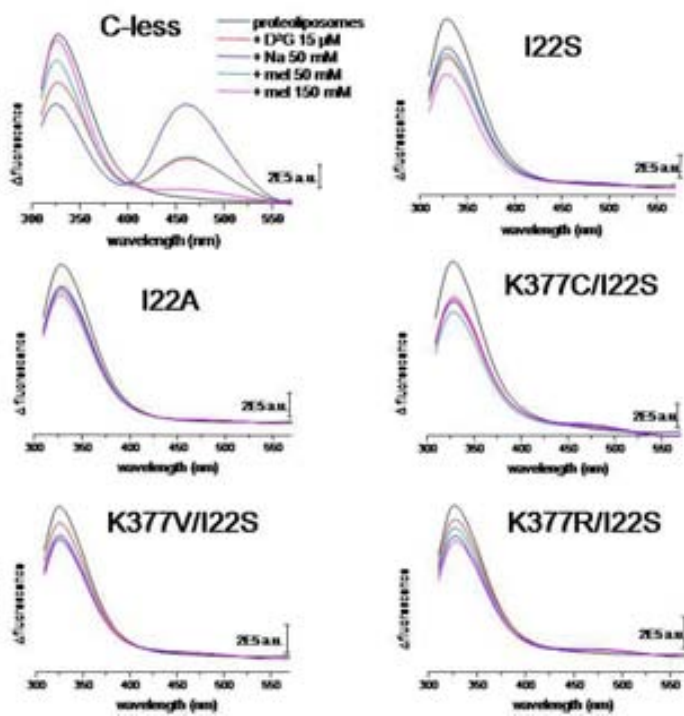


Figure 7.21 FRET analysis of the K377/I22S double mutants in comparison to I22 single mutants and C-less as reference spectrum, for all fluorescence spectra: excitation wavelength at 290 nm and emission wavelength from 310 to 570 nm; upper left corner: C-less, center left: I22A, lower left corner: K377V/I22S, upper right corner: I22S, center right: K377C/I22S, lower right corner: K377R/I22S.

## 7.6. Revertants with L326F mutation

### 7.6.1. First spectroscopic analyses of K377R/L236F

Additionally to the earlier announced second site revertants composed of the Ile-22, the incubation of the single mutant K377R brought about another mutation generating a red colony in the colorless bulk after several days of incubation. In this revertant the leucine in position 236 is replaced by a phenylalanine. This second site mutation was published already in combination with another first site mutation, the Tyr-31<sup>57</sup>.

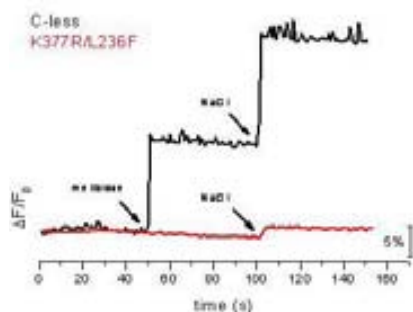


Figure 7.22 Trp fluorescence of the LAPAO-purified K377R/L236F MelB double mutant. Black line: C-less, red line: K377R/L236F. melibiose and NaCl were added in final concentrations of 10 mM.

Located in the transmembrane segment VII, the apolar residue leucine is exchanged for an aromatic amino acid conserving the apolar character. The much larger aromatic side change indicates severe alteration of its surrounding.

The double mutant K377R/L236F was purified under normal condition and characterized for its substrate binding ability by spectroscopic methods. The inevitable question appears whether this second site mutation recovers the substrate binding unlike the earlier described I22S double mutants. The detection of a melibiose-mediated increase in fluorescence intensity (Fig. 7.22) indicated persistently an intensity

increase of no more than 2%. This small but significant fluorescence change demonstrated tryptophan changes of the MelB transporter. The FRET data obtained from the proteoliposomes reinforced similar change of the double mutant mediated by the dansyl-sugar analog. The  $\beta$ -sugar derivative D<sup>2</sup>G binds to the MelB mutant with lower affinity (Fig. 7.23). Furthermore, the FRET data point out that the fluorescence increases in the presence of the cation.

Considering the results from the infrared difference spectra induced by the substrates, the double mutant demonstrates the binding of sodium, although with a very low intensity. However, the infrared difference spectrum does not resemble much with the reference spectrum from the C-less transporter. The same conclusions were drawn from

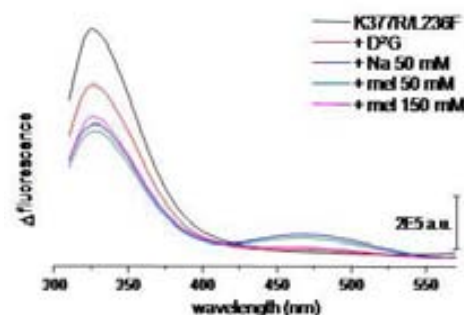


Figure 7.23 FRET data from the K377R/L236F double mutant.

the difference spectrum triggered by melibiose (Fig.7.24 B).

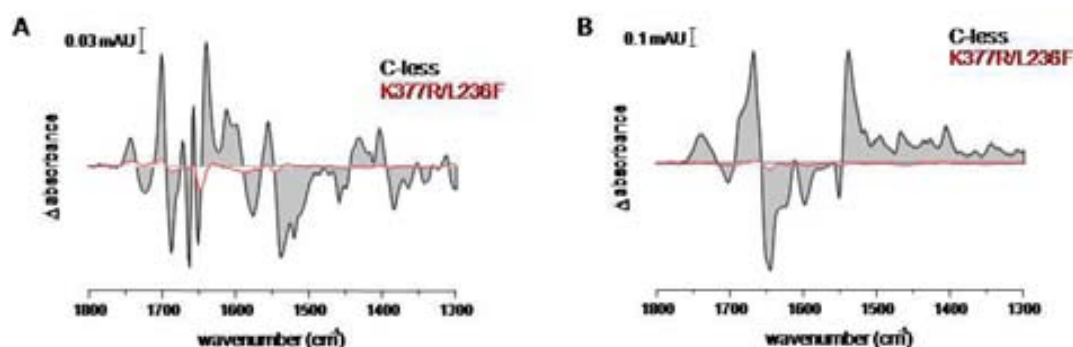


Figure 7.24 IR<sub>diff</sub> spectra of K377R/L236F. **A** sodium-induced difference spectra of C-less (black line and grey pattern), and K377R/L236F (red line and light grey pattern). The sample buffer contained 10 mM NaCl. **B** melibiose-induced difference spectra of C-less (black line and grey pattern), and K377R/L236F (red line and light grey pattern). The sample buffer contained 10 mM melibiose and 10 mM NaCl, whereas the reference spectrum was acquired in the presence of 10 mM NaCl

### 7.6.2. FRET-discrepancy of ISO vesicles and the purified transporter

A much simpler method without purifying the MelB transporter offers the preparation of membrane vesicles. Before the solubilization by detergent extended the opportunity to characterize membrane proteins, the preparation of membrane vesicles enabled a reliable way for membrane protein analysis.

For the first time the study of the lactose-proton symporter, LacY, made use of membrane vesicles more than four decades ago<sup>156</sup>. Ever since, the fragmentation of the bacterial membrane suited as a fast and easy-applicable method to gain insights of membrane protein function. The major advantage is the absence of manipulation by surfactant. This way the protein remains in its original habitat and is not artificially solubilized by amphiphilic reagents. In general, two types of vesicles can be generated. Right-side.out vesicles, abbreviated as RSO, are generated by an osmotic shock procedure in which the cells are loaded with a high-concentrated sugar solution. The release into a hypotonic buffer conducts the bursting of the cells and the cleansing of the cytosol. The efficiency is relatively low. The RSO vesicles stabilize their orientation with the periplasmic side outside-faced.

The second form of vesicles is termed ISO for inside-out-vesicles. A high-pressure method applied by a French press or a Microfluidizer generates much smaller membrane fragments. These vesicles are usually one order of a magnitude smaller compared to the RSO vesicles<sup>193</sup>. As the name already states, in those vesicles, the cytosolic membrane side is facing the outside, whereas the outer membrane surface is turned outside-in. As the vesicles are composed of the

cells' phospholipid bilayer and all the integral membrane proteins, the analysis has to be discriminated for the specific MelB protein.

The fluorescence energy transfer (FRET) of the fluorescent sugar, Dns<sup>2</sup>-S-Gal or D<sup>2</sup>G, represents an exclusive approach to minimize background signals from other membrane proteins still present in the vesicles.

Already issued for LacY vesicles, this sugar derivative is versatile and interacts with the sugar binding site. This feature is advantageous for the vesicles containing apart from MelB the entire bulk of membrane-attached polypeptides and proteins.

For the K377R/L236F mutant, the results obtained from the FRET experiments of the vesicles were incongruent to the result from spectroscopy based on the purified and liposome-reconstituted K377R/L236F mutant.

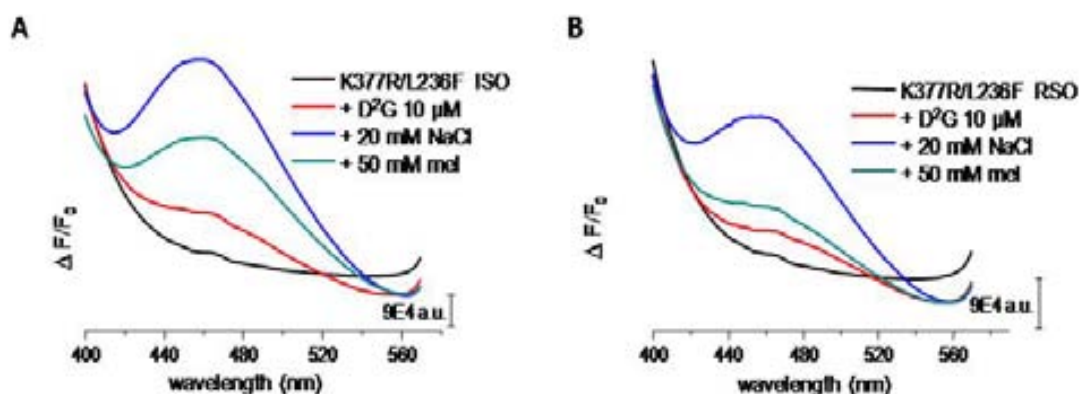


Figure 7.25 FRET data of the K377R/L236F vesicles. A ISO B RSO. D<sup>2</sup>G was added at a final concentration of 10  $\mu$ M.

In Fig. 7.25 the fluorescent sugar without doubt induces a much larger energy transfer signal than earlier shown for the proteoliposomes of the purified transporter. This result suggests that during the purification process the protein undergoes structural alterations.

During the reconstitution into liposomes, the MelB mutant hypothetically does not recover the original conformation. Especially, the solubilization of the protein with the rather harsh detergent 3-(Laurylamido)-N'-N-dimethylaminopropylamine (LAPAO) could be considered as an influential factor for keeping the characteristic protein conformation. The detergent LAPAO for extracting this particular mutant from the membrane bilayer was substituted for the milder  $\beta$ -dodecyl maltoside ( $\beta$ -DDM or DDM). This detergent is already applied in the latter stages of the purification protocol. Because of solubilization efficiency, DDM was replaced by LAPAO in the initial stages of solubilization from the membrane.

### 7.6.3. K377R/L236F purified with dodecyl-maltoside

Apart from the removal of LAPAO for extraction, the purification protocol remained unchanged. The vesicles in the presence of DDM were incubated for a larger time span for up to 3 h to ensure the highest solubilizing efficiency. The reconstitution of protein continued as usual. In the upcoming Figures appears the control mutant K377C/L236F which also was purified in the presence of DDM for comparison with the K377R/L236F mutant.

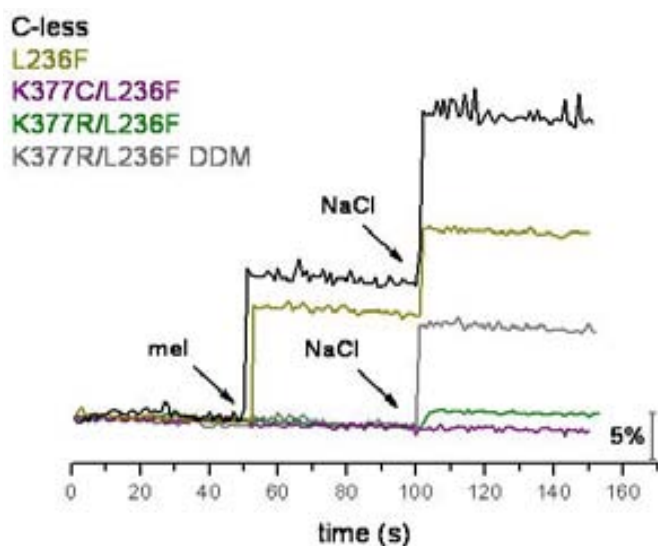


Figure 7.26 comparison of the K377R/L236F mutant purified with two different detergents. Black line: C-less, dark yellow line: L236F, purple line: K377C/L236F, olive line: K377R/L236F, grey line: K377R/L236F DDM purified. The spectra were corrected for the dilution effects of the substrates. Melibiose and NaCl were added after 50 sec and 100 sec, respectively at final concentrations of 10 mM each.

Since K377R was the only Lys-377 mutant displaying the second site mutation L236F spontaneously, phenylalanine mutation was introduced into K377C by polymerase chain reaction (PCR) to examine whether the effects of the second site are ubiquitous or only related to the positive charged side chain of the arginine. The K377C/L236F was also entirely purified with  $\beta$ -DDM.

The single mutant L236F was obtained by PCR reaction as well to assess the effects of the substrates. The single mutation of Leu-236 to phenylalanine was formerly described as a MelB mutant resistant to lithium concentration above 10 mM. The L236F demonstrated higher transport activity using sodium as a coupling ion<sup>194</sup>. The fluorescence changes of K377R/L236F<sub>DDM</sub> are much larger compared to the LAPAO-solubilized sample. The DDM-purified mutant clearly exhibits an increase in fluorescence upon melibiose supplementation of around 10%. The MelB

For other proteins of the melibiose permease, the exchange to another detergent was never an issue since normally under high sodium concentration the carrier conserved its function after reconstitution<sup>40</sup>.

In general, the effect of different detergents on the three-dimensional structure is understudied leaving a space for speculation. Different detergents might cause delipidisation which consequently triggers conformational changes in the carrier even in the presence of amphiphilic micelles. For the double mutant K377R/L236F, the exchange of the detergent definitely altered the characteristics of the protein (Fig. 7.26-31).

variant consisting of the two mutations K377C and L236F does not demonstrate a rise in fluorescence. The single mutant L236F behaves similar to the C-less. These data conclude that the double mutant K377R/L236F alters its helical conformation upon melibiose binding in the presence of sodium ions relying on the cooperativity of the binding sites.

Under these circumstances, it was interesting to examine, if the purification not only affect the melibiose interaction with the carrier but also affect the sodium binding. The infrared difference spectra of mutants carrying the mutation of L236F were compared for their ability to bind sodium at a concentration of 10 mM.

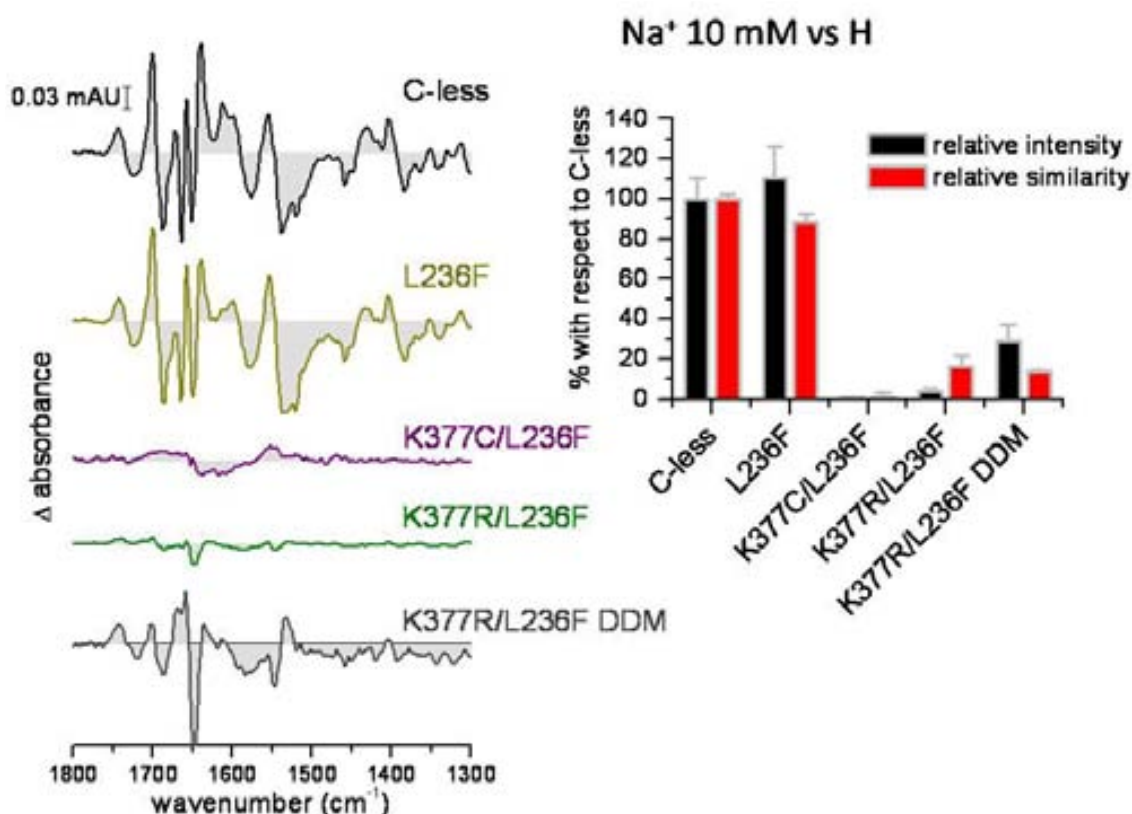


Figure 7.27 IR<sub>diff</sub> spectra of the L236F mutants. In the left panel: difference spectra of the MelB variants, in black: C-less as reference spectrum, in dark yellow: L236F mutant, in purple: K377C/L236F mutant, in olive: K377R/L236F mutant (purified with LAPAO), in grey: K377R/L236F mutant; in the right panel: comparison using the first derivative of mutant spectra using C-less as reference spectrum. The error bars indicate the variation depending on at least two independent data acquisitions.

The sodium binding in the double mutant is apparent although it differs from the spectrum obtained from C-less. The similarity between C-less and the DDM-purified K377R/L236F mutant amounts to just around 20%. The mutant obviously recovers partially the binding of the cation as in the K377C/I22S mutant but with much higher affinity. The LAPAO purified form of the double mutant also suggests some binding of Na<sup>+</sup> although with much lower affinity than in the DDM counterpart. The control protein K377C/L236F failed to demonstrate similar binding of the sodium. As the intrinsic fluorescence already manifested, the sugar induces evidently structural changes in the transporter which are enhanced in the presence of the cation. Experiments with the second site mutation I22S failed to substantiate same evidences for restored sugar binding.

## RESULTS

Extracted from the Figures 7.28 and 29, the DDM-treated MelB revertant couples the sugar with higher affinity than the mutant purified using LAPAO. The solubilization with DDM particularly has an effect for this double mutant which recovers the sugar binding. The difference of spectral intensity of 40% of the DDM sample to 4% for the LAPAO sample describes well the difference of the two preparations.

The K377C/L236F mutant purified under similar conditions (DDM) does not exhibit a melibiose-induced difference spectrum which confirms the results from the fluorescence spectroscopy. The single mutant L236F however demonstrates a C-less like interaction with the substrates.

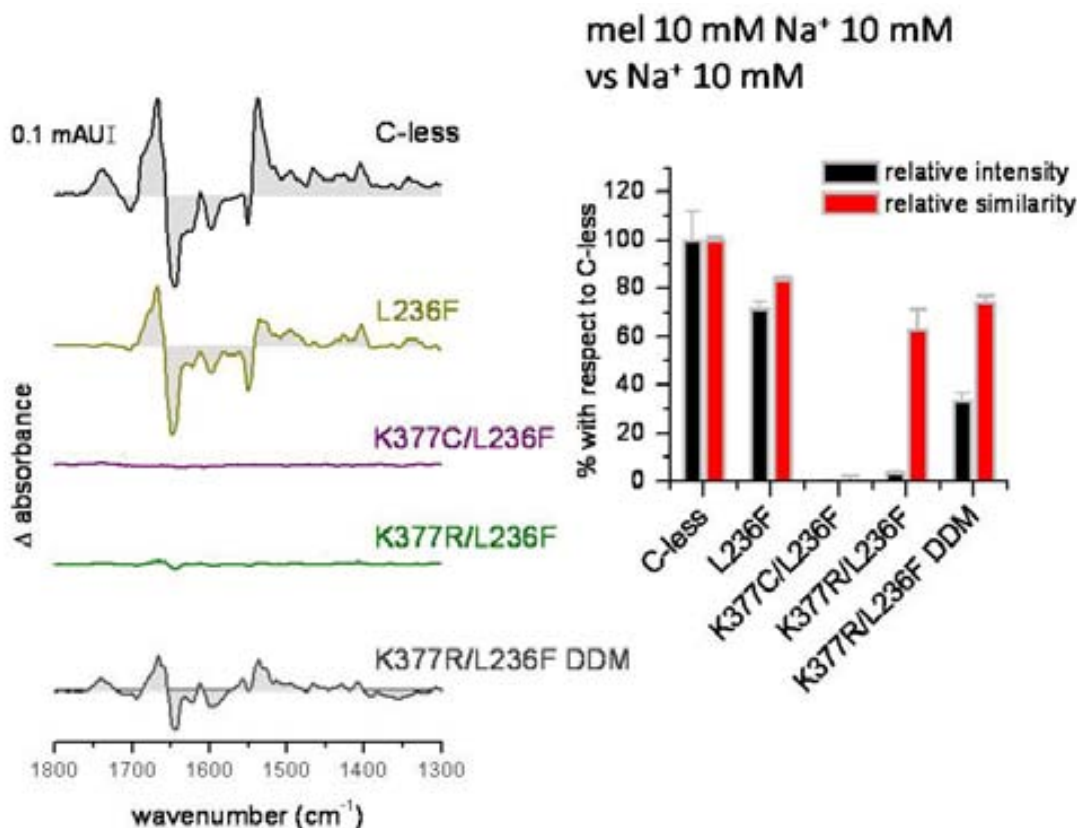


Figure 7.28 melibiose-triggered IR<sub>diff</sub> spectra of the L236F mutants in the presence of sodium (10 mM). In the left panel: difference spectra of the MelB variants, in black: C-less as reference spectrum, in dark yellow: L236F mutant, in green: K377C/L236F mutant, in purple: K377R/L236F mutant (purified with LAPAO), in grey: K377R/L236F mutant; in the right panel: comparison using the first derivative of mutant spectra using C-less as reference spectrum. The error bars indicate the variation depending on at least two independent data acquisitions.

The sugar-induced difference spectrum in the presence of the proton confirms previous results for K377R/L236F. The solubilization of the carrier by DDM stabilizes the binding site much better than the LAPAO-preparation. Strikingly, the intensity of the difference spectrum of the single mutant L236F is almost twice as high as for the C-less reference spectrum meaning that this mutant binds the sugar with higher affinity.

The melibiose-induced difference spectrum of the K377R/L236F mutant in the presence of

the proton displays resemblance majorly in the region of amide I. The amide II bands differ from the C-less reference which explains in turn the relatively low similarity of ~20%.

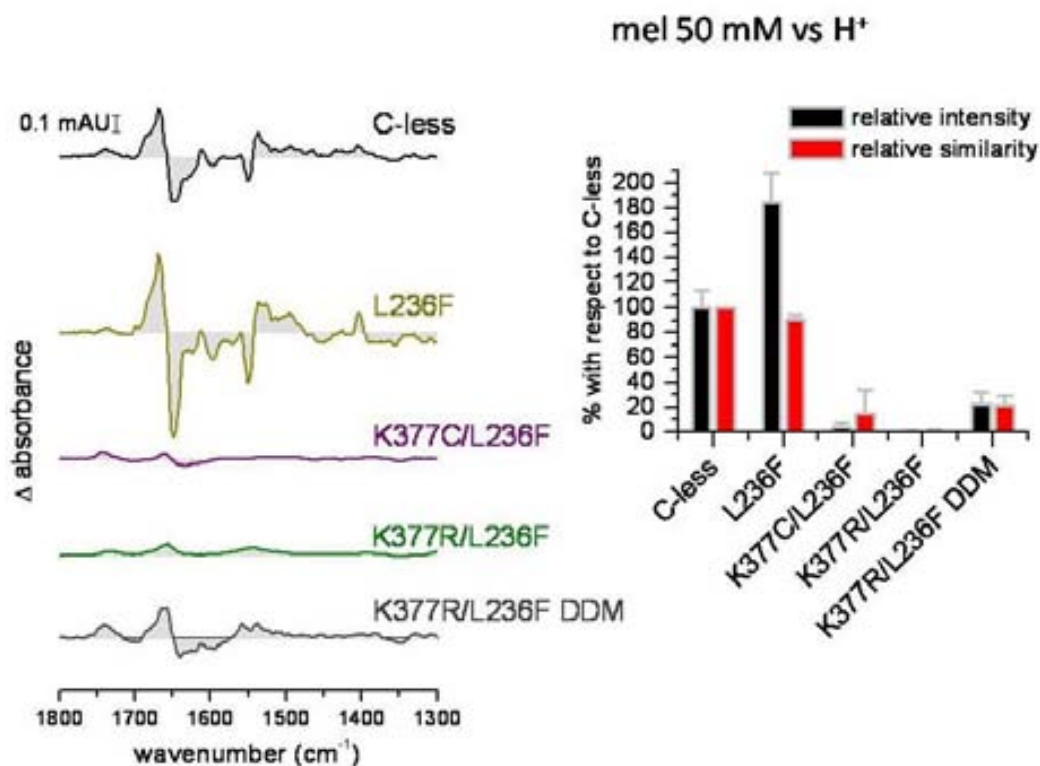


Figure 7.29 melibiose-triggered IR<sub>diff</sub> spectra of the L236F mutants in the presence of the proton. In the left panel: difference spectra of the MelB variants, in black: C-less as reference spectrum, in dark yellow: L236F mutant, in purple: K377C/L236F mutant, in olive: K377R/L236F mutant (purified with LAPAO), in grey: K377R/L236F mutant; in the right panel: comparison using the first derivative of mutant spectra using C-less as reference spectrum. The error bars indicate the variation depending on at least two independent data acquisitions.

Conclusively, the second site L236F in the mutant K377R exhibits a difference spectrum for both substrates. But the mutation seems not to be ubiquitous, since the difference spectra of the mutant K377C/L236F is seemingly feature-less, manifesting the absence of substrate coupling in this MelB mutant.

## 7.6.4. FRET data of the L236F mutants in proteoliposomes

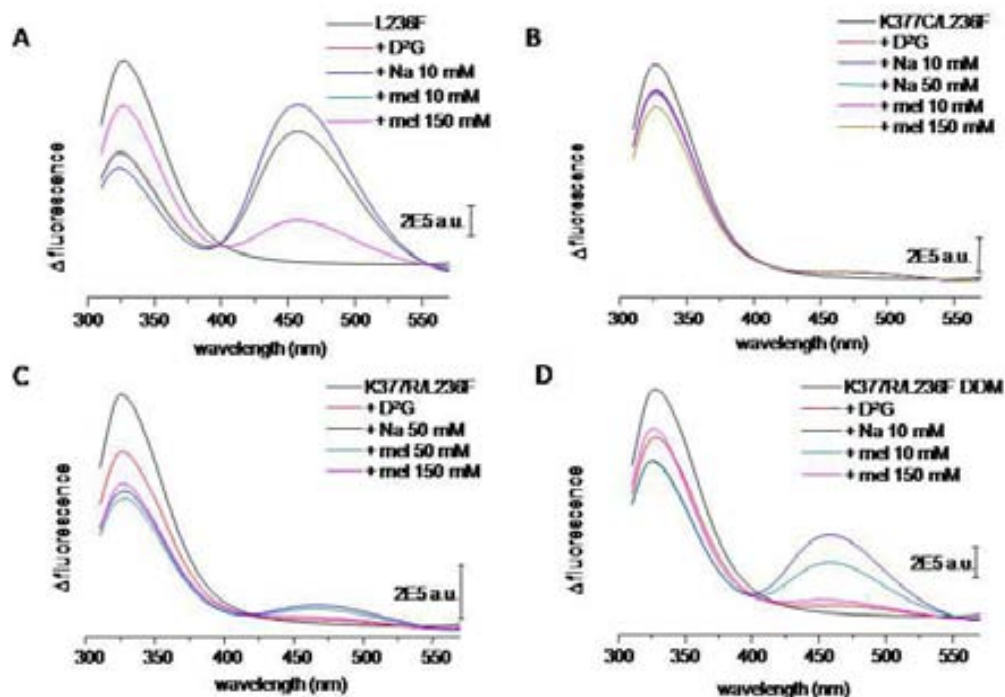


Figure 7.30 FRET data of the L236F mutants. **A:** L236F mutant; **B:** K377C/L236F mutant; **C:** K377R/L236F mutant (LAPAO purified), **D:** K377R/L236F (DDM purified). Each scan is the average of at least two independent scans. D2G was added to the proteoliposomes at a final concentration of 16  $\mu\text{M}$ .

The L236F mutant also continues to bind the high affinity sugar analog D<sup>2</sup>G better than C-less as it was shown for the mel/H<sup>+</sup>-difference spectrum. In Fig. 7.30 in the lower panel, the FRET spectra for the two different forms of solubilization of the mutant K377R/L236F with LAPAO (right) and DDM (left) confirm the better conservation of the binding sites of the transporter in the case of the maltoside detergent. The double mutant K377C/L236F is not able to interact with the fluorescent sugar suggesting the importance of the positive charge in position 377 of MelB.

Considering the rescue of the sugar/sodium binding, the double mutant K377R/L236F seems to preserve the binding sites of MelB. Obviously structural aspects are present conserving the binding sites of the substrates in combination with the use of different detergents. By assessing the protein film of the L236F mutants for structural integrity, a structural significance could be concluded.

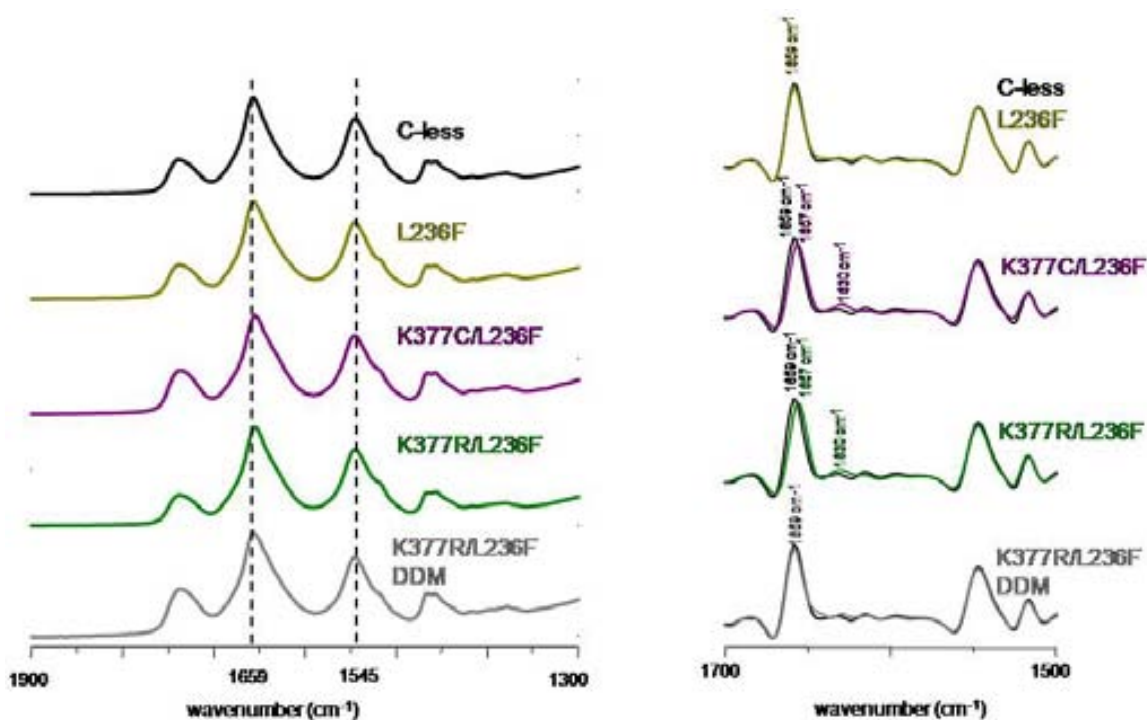


Figure 7.31 Absorbance spectra comparison between K377/L236F double mutants as well as L236F single mutant to C-less reference spectrum. Left panel: absorbance spectra of the wet protein film between 1900 and 1300  $\text{cm}^{-1}$ , right panel: second derivative of the same absorbance spectra in the amide region between 1700 and 1500  $\text{cm}^{-1}$ . color scheme: C-less in black, L236F in dark yellow, K377C/L236F in purple, K377R/L236F in green and K377R/L236F DDM in grey.

In Fig. 7.31, a recognizable tendency is apparent in the double mutant K377R/L236F purified with different detergents. The DDM-solubilized mutant conserves the C-less-like structure whereas the purification with LAPAO displays a slightly higher amount of  $\beta$ -sheet structure indicated by the elevated shoulder at 1630  $\text{cm}^{-1}$ . Moreover, the peak assigned to  $\alpha$ -helices is significantly shifted in K377C/L236F and K377R/L236F. Only L236F and K377R/L236F DDM preserve the similar position at 1659  $\text{cm}^{-1}$  as the C-less reference. Even though relatively few and small changes occur, those alterations seem to be crucial for the coupling of the substrates. The binding is the basic requirement for active transport of the permease.

## 7.7. Is there a salt bridge between Lys-377 and aspartic acids 55 and 59?

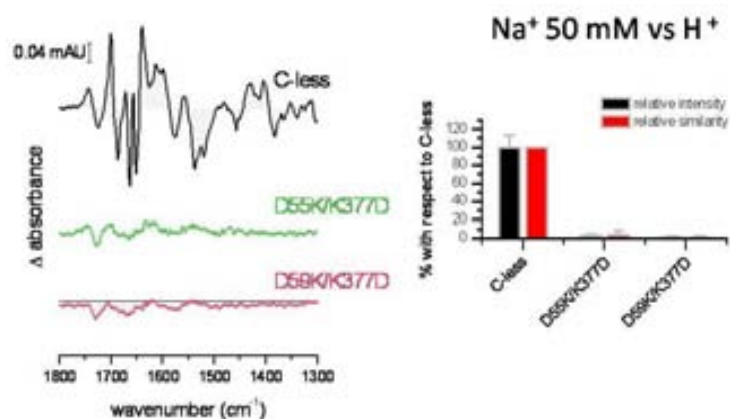


Figure 7.33 sodium-induced IR<sub>diff</sub> spectra (using 50 mM NaCl) of the double mutants D55K/K377D and D59K/K377D. In the left panel: difference spectra of the MelB variants, in black: C-less as reference spectrum, in green: D55K/K377D mutant, in red: D59K/K377D mutant, in the right panel: comparison using the first derivative of mutant spectra using C-less as reference spectrum. The error bars indicate the variation depending on at least two independent data

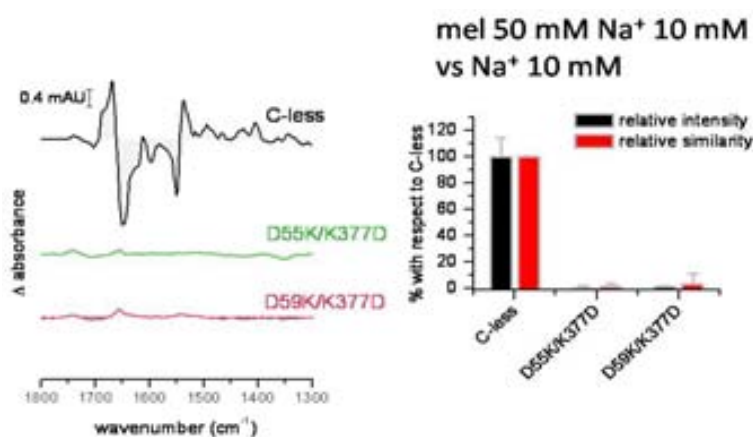


Figure 7.32 melibiose-triggered IR<sub>diff</sub> spectra of the double mutants D55K/K377D and D59K/K377D in the presence of sodium (10 mM). In the left panel: difference spectra of the MelB variants, in black: C-less as reference spectrum, in green: D55K/K377D mutant, in red: D59K/K377D mutant; in the right panel: comparison using the first derivative of mutant spectra using C-less as reference spectrum. The error bars indicate the variation depending on at least two independent data acquisitions.

Previous studies implied the idea of a potential charged pair formation of the Lys-377 with the negatively charged amino acids Asp-55 and/or Asp-59. A construction of two double mutants D59K/K377D and D55K/K377D should either challenge this hypothesis. In the case of the co-substrate the charge switch between the aspartic acids and the lysine does not cause a difference spectrum meaning the absence of interaction between the transporter and ligand. For the double mutant D59K/K377D Franco *et al.* detected transport activity<sup>65</sup>. Because of this finding, the disaccharide melibiose was supposed to trigger a signal measurable by ATR-FTIR. But Fig. 7.32 and 33 indicate the absence of a difference spectrum in the presence of a saturating concentration of 50 mM melibiose with and without sodium. Hence, the double mutants with the charge switch lack detectable signals in infrared spectroscopy.

Using the FRET as a second spectroscopic method, the D<sup>2</sup>G sugar emits a partial FRET signal in the D59K/K377D mutant. This potential binding of sugar in a beta conformation gives the impression of D<sup>2</sup>G binding with a reduced affinity for the sugar derivative. 10 mM sodium provokes a slight increase in the FRET envisioning a possible scenario of cooperativity of the binding sites.

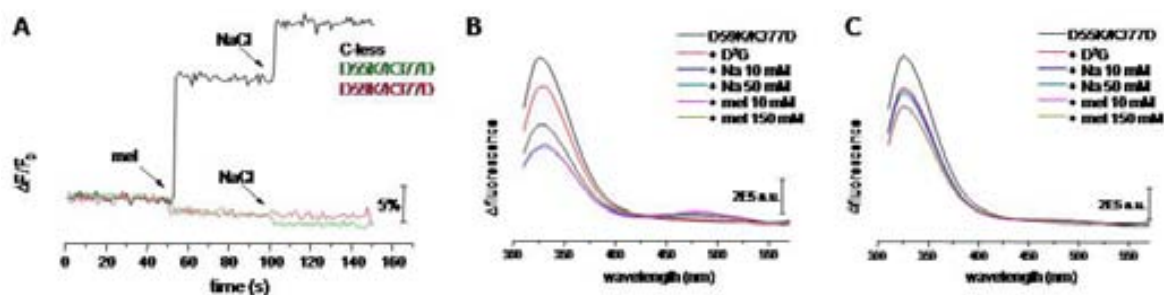


Figure 7.34 Fluorescence spectroscopy results of the double mutants D55K/K377D and D59K/K377D in proteoliposomes. **A** intrinsic Trp fluorescence after the addition of melibiose (50 mM) and NaCl (50 mM). black line: C-less, green line: D55K/K377D, red line: D59K/K377D; **B** FRET of D59K/K377D; **C** FRET of D55K/K377D.

The tiny D<sup>2</sup>G-mediated FRET signal indicates an interaction between the fluorescent sugar and the adjacent Trp's. Nevertheless, the conclusions drawn from the other data do not suggest the possibility of charge switch possibility between either Asp-59 or Asp-55 in combination with Lys-377. Although a potential salt bridge cannot be excluded from our data.

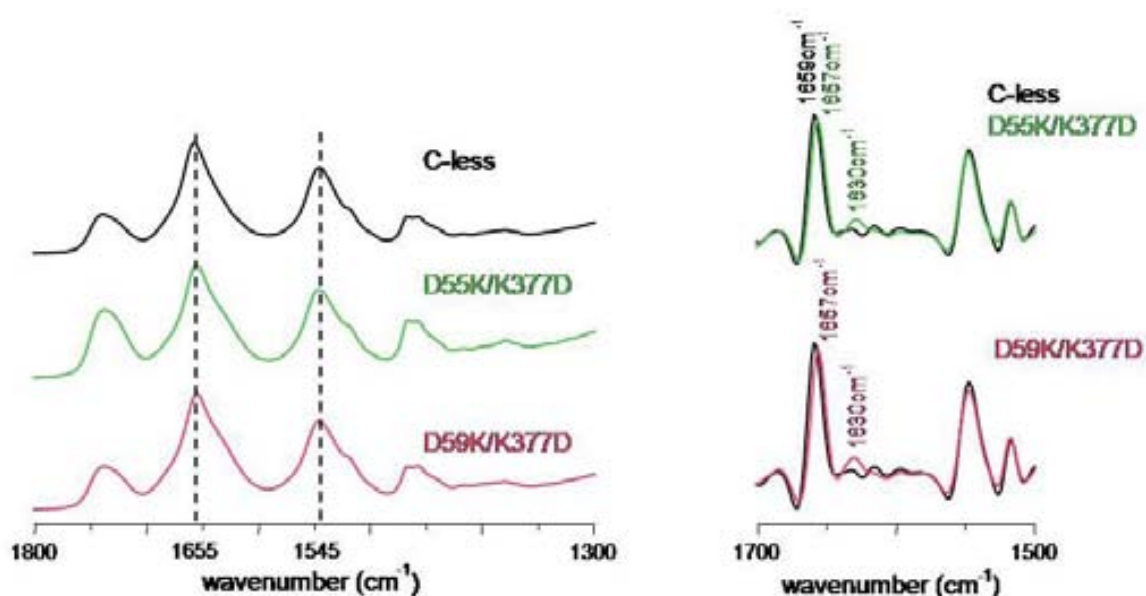


Figure 7.35 Absorbance spectrum analysis of the double mutants D55K and D59K/K377D. left panel: mean of absorbance spectra of all conditions, right panel: mean of the second derivative of the absorbance spectra.

The second derivative of the double mutants compared to C-less emphasizes the alteration considering the ratio between  $\alpha$ -helices and  $\beta$ -sheets as main structural features within the transporter. Evidently, mutations with a severe effect on the substrate coupling simultaneously display alterations of the absorbance spectrum between 1660 and 1620  $\text{cm}^{-1}$ .

On first sight, the peak at 1630  $\text{cm}^{-1}$  possesses a higher intensity than in the functional cysteine-less control. Apparently, this feature is accompanied by a parallel shifted maximum from 1659 to 1657  $\text{cm}^{-1}$  respectively in the binding-defective mutants. It can be interpreted as an increase in  $\beta$ -sheet structure. During the previous chapters already emphasized, the absorbance spectra analysis gives hints about the effect of the mutation on the entire transporter. Especially, the second derivative of the absorbance spectrum enlightens hidden patterns, mostly conformational alterations that possibly influence the function of the melibiose permease.

By assessing the absorbance spectrum of all acquired mutations considering the residue Lys-377, the quantitative analysis concludes perfectly changes in the protein structure manifested by the mutations (Fig. 7.36).

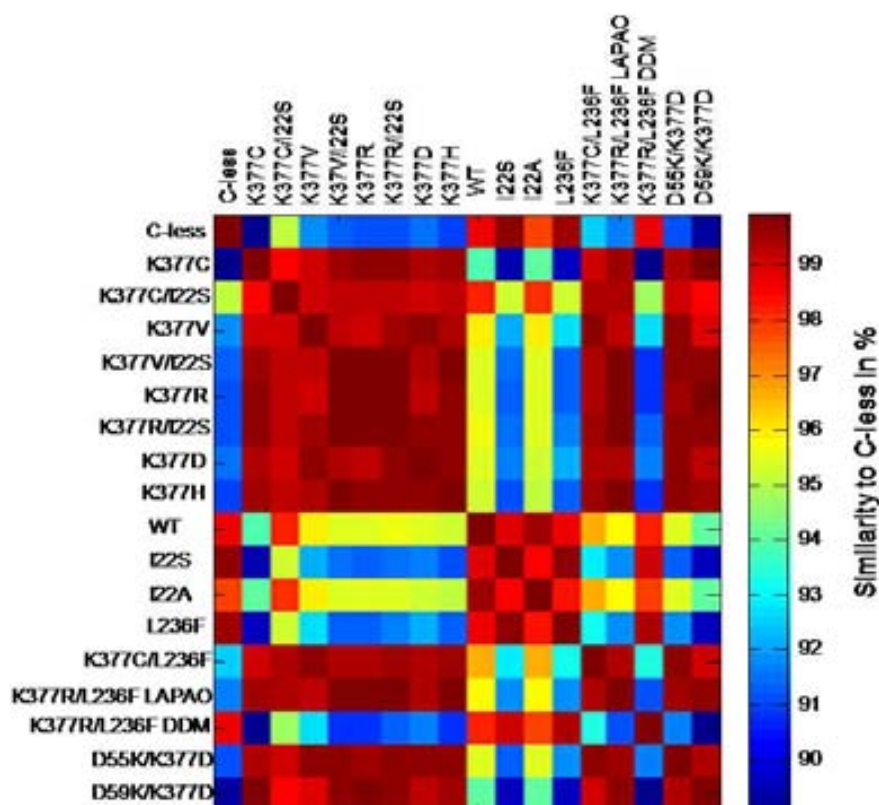


Figure 7.36 Secondary derivative of the absorbance spectrum of the mutants involving the mutations of the Lys-377 calculated as  $(1-R^2) \times 100$ .

Fig. 7.36 emphasizes the similarity of the absorbance spectrum compared to the control C-less spectrum. By regarding the color scheme and evaluating each square with the legend bar to the right, the Lys-377 single mutants entirely differ from its genetic background C-less. The similarity of only around 90% mostly depends on the changes occurring in the region between

1660 and 1600  $\text{cm}^{-1}$ .

Among the spontaneous double mutants, K377C/I22S recovers partially the original conformation of the transporter, whereas K377V/I22S and K377R/I22S do not establish the equal structural improvements.

The second revertant accomplished during the study is K377R/L236F. Purified by two different detergents, the usual protocol using LAPAO as extracting surfactant does not conserve the structure of the transporter indicated by a resemblance of only 91%. The second trial using DDM as detergent improves drastically the composition of the reconstituted carrier demonstrated by a structural similarity of 98% to the reference absorbance spectrum.

The double mutants carrying a charge switch project a low similarity as it was expected from the  $\text{IR}_{\text{diff}}$  data. Both double mutants lost the ability to bind sodium and melibiose explaining the low amount of structural resemblance to the C-less MelB transporter.

### 7.8. MIANS analysis of K377C and K377C/I22S mutants

By interacting with the target protein, the unbound non-fluorescent reagent MIANS (2-(4'-maleimidylanilino) naphthalene-6- sulfonic acid) allows specific detection of the carrier protein. The maleimide group of this chemical compound interacts exclusively with the thiol group of cysteines.

Since the mutants of the MelB comprises either no cysteine (as C-less

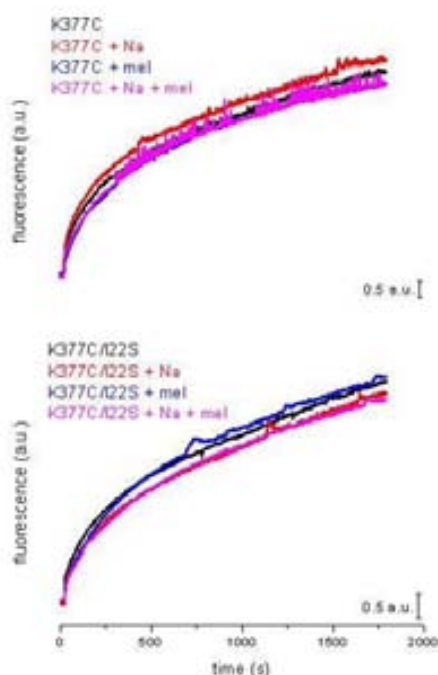


Figure 7.38 K377C and K377C/I22S MIANS reactivity.

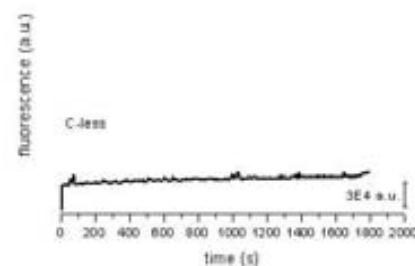


Figure 7.37 MIANS reactivity in the C-less reference.

reference in Fig. 7.37) or only one cysteine (majority of the generated MelB mutants), the detection of MIANS delivers interesting results. By exploiting the fluorescent characteristics of the probe, the fluorescent data can be used directly without further subtraction.

In the first place, this probe was chosen because of its sensitivity for the aqueous surrounding.

Usually MIANS prefers a hydrophobic over a polar environment. Apart from that its absorbance spectrum partially overlaps with the spectrum of the intrinsic tryptophans<sup>187</sup>.

For experimental purposes, the probe was added in the fluorescence cuvette already containing the

resuspended proteoliposomes in 0.1 M  $\text{KPi}$  buffer (pH 7.0) and 0.1 M KCl. The reaction between the probe and the intrinsic cysteines was recorded as a function of time.

Considering the result, the control spectrum of the C-less transporter displays an almost steady signal interpreted as background interaction of MIANS with protein and the buffer solution. Since the control sample does not contain intrinsic cysteines, a specific coupling between the thiol and the maleimide groups can be excluded as a signal contributor. MIANS time course experiments were acquired in four different conditions to assess if the substrates affect the reactivity of the fluorescent probe and the transporter; without substrates, with just the one of the substrates and finally in the presence of sodium and melibiose.

Considering the MIANS reactivity of the K377C and K377C/I22S mutants, both mutants display equal accessibility of the fluorescent in all tested conditions. From recent results it is likely that the substrates have no effect on the conformation of the MelB mutants since binding has not been detected. However, the cysteine of two displayed Lys-377 mutants (Fig. 7.38) is easily accessible for the probe and obviously embedded in a less polar environment.

The second site mutation I22S has no effect on the accessibility of the cysteine, because the reactivity remains like in the single mutant. MIANS experiments for the other lysine substituents were not performed because of the absence of an intrinsic cysteine.

## *7.9. FRET analyses of the vesicles of the mutants related to*

### *Lys-377*

The general idea behind this experimental approach is to use the fluorescent sugar analog for the MelB binding capacity evaluation embedded in vesicles.

In the vesicles the protein is still localized in its natural compartment without solubilization. The protein conserves the original conformation after the expression and insertion into the membrane. The following experiments are dedicated to the two types of membrane vesicles, inside-out and right side-out vesicles, which were generated to examine if the purification process biases the interaction with the sugar. Especially, the solubilization by detergents might affect the membrane transport protein as it has been shown earlier for the revertant K377R/L236F.

By assessing the vesicles by FRET, the different expression levels prohibit a direct comparison between the different mutants. However, it is feasible to make assumptions of  $\text{D}^2\text{G}$  interaction in the mutants without purifying MelB. Both vesicle types were always prepared from the same batch of cell culture allowing assumptions about the reactivity of the mutant with the sugar derivative and indirectly about the accessibility of the sugar molecules in the MelB variant.

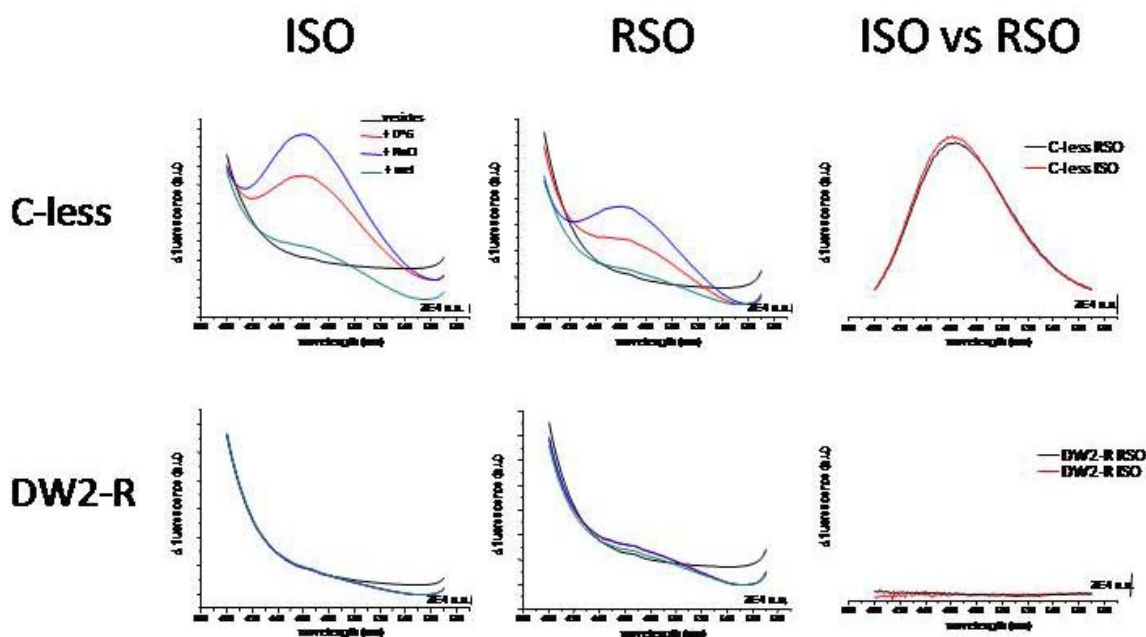


Figure 7.39 C-less and DW2-R vesicles measured by Förster energy transfer with the dansyl sugar analog  $D^2G$ . A C-less vesicles, left: FRET of the ISO vesicles (black line: vesicles, red line: + 10  $\mu\text{M}$   $D^2G$ , blue line: + 20 mM NaCl, cyan line: + mel 150 mM), centre: FRET of the RSO vesicles, right:  $\Delta$  fluorescence after adding 10 mM NaCl minus before in both types of vesicles ; B DW2-R vesicles (strain without MelB expressing plasmid; used as a negative control). Order as in C-less described. FRET experiments were carried out in 0.1 M KPi-buffer pH 7.0 supplemented with 0.1 M KCl.

Figure 7.39 illustrates the experimental results for the control vesicles. The C-less vesicles (ISO and RSO) demonstrate a significant fluorescence increase after the addition of 10 mM NaCl to the sample in the presence of 10  $\mu\text{M}$  dansylated fluorescence acceptor  $D^2G$ . The comparison of the signal increase should be similar if the transporter is accessible from both sides of the membrane. For C-less ISO the rise in fluorescence equals the signal obtained from the right-side-out form with verifies the hypothesis of accessibility of the binding sites from both sides of the membrane. Simultaneously, it manifests the alternating access mechanism postulated for MelB.

In the negative control, the DW2-R *E. coli* strain, the fluorescent sugar does not provoke an augmentation of the signal in the two types of vesicles. The lack of signal is evident since the chromosomal melibiose permease and the lactose permease which specifically interact with the galactoside analog are deleted in DW2-R. Additionally, the strain was not transformed with the MelB expressing plasmid. The comparison of the signal is therefore not necessary and was only illustrated as reference.

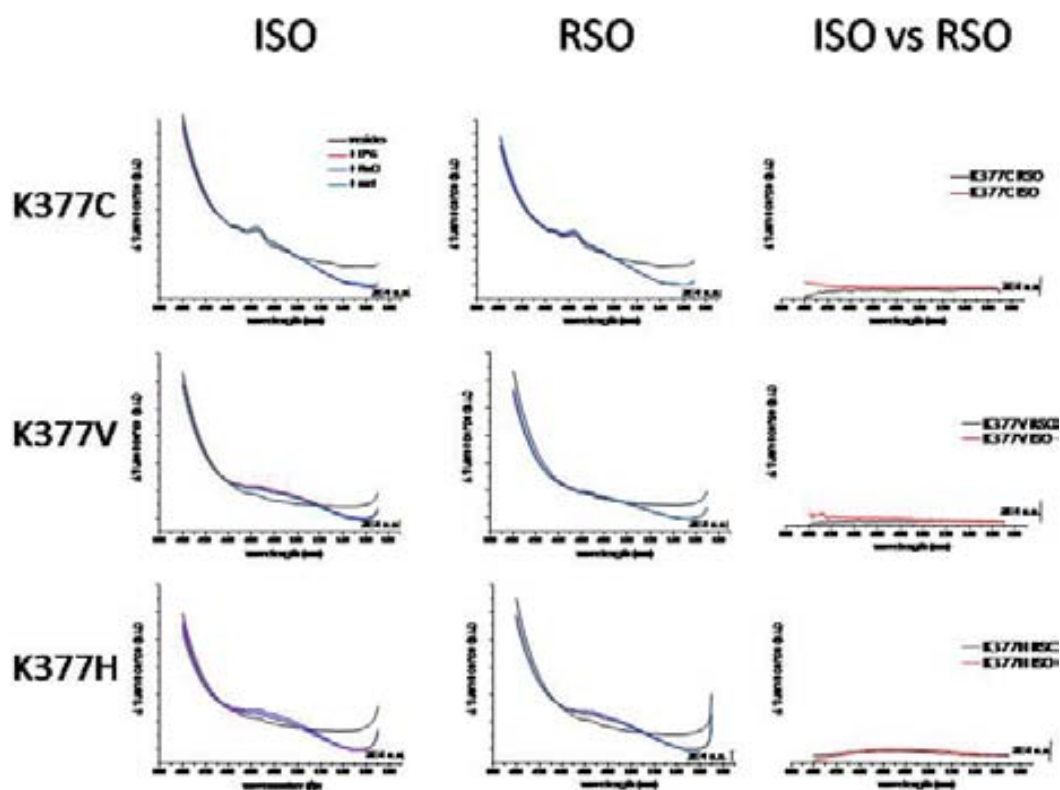


Figure 7.40 Inside and right-side-out vesicles of the lysine replacements with cysteine, valine, arginine and histidine. Left column: inside-out vesicles of the indicated single mutant (black line: vesicles, red line: + 10  $\mu$ M D<sup>2</sup>G, blue line: + NaCl, cyan line: + melibiose), centre column: right-side-out vesicles of the indicated single mutant (black line: vesicles, red line: + 10  $\mu$ M D<sup>2</sup>G, blue line: + NaCl, cyan line: + melibiose), right column: graph of fluorescence difference of the RSO (Black line) and ISO (red line) vesicles, obtained by subtracting sodium-induced fluorescence from the D<sup>2</sup>G-mediated fluorescence. Excitation wavelength: 290 nm, wavelength of the emission spectra: 400 - 570 nm. Buffer during data acquisition 0.1 M KPi, 0.1 M KCl, pH 7.0.

The results from the Figure 7.40 confirm the spectroscopic data from proteoliposomes of the mutants of the position 377 in MelB. The FRET data from the ISO and RSO vesicles of the K377C mutant agree with the purified protein in a way that the fluorescent sugar does not bind to the protein and therefore also the co-substrate sodium does not induce further increase of the fluorescence signal because of the absence of close interaction of the dansyl-group and the intrinsic tryptophanyl residues.

The mutant K377V deemed as a sugar accumulator<sup>65</sup>, exhibits a small increase of the fluorescence in the ISO form of the vesicles which can be interpreted as unspecific D2G binding because the excessive amount of melibiose does not mediate a signal reduction which could assigned to the replacement of D2G by melibiose. Moreover, sodium cations lead to no further induction of a fluorescence increase. The K377H mutation suggests binding between the ligands and the MelB variant since the supplemented sodium provokes a rise in the tryptophan fluorescence in the ISO as well as in the RSO vesicles.

### 7.10. *ISO/RSO vesicles of Lys-377 revertants and selective single mutants*

As shown in earlier parts of the thesis, two selective site mutations were detected that were responsible for the generation of revertants of the Lys-377 mutations. The Ile-22 was replaced by serine and the Leu-236 was substituted by an aromatic phenylalanine. The I22S mutation occurred in all mutants of the Lys-377, whereas the L236F second site revertant only appeared in combination with the K377R mutation. To validate the binding characteristics of the unpurified transporter, ISO and RSO vesicles were prepared and analyzed in the presence of the fluorescent dansyl-sugar D<sup>2</sup>G.

As shown in previous graphics (Fig. 7.41), D<sup>2</sup>G interacts with the C-less vesicles by presenting an increase of the D<sup>2</sup>G-fluorescence which is concomitant with a decrease of Trp fluorescence. The obtained data from the vesicles correlate with the analysis done on the purified MelB mutants. The FRET of the vesicles from the spontaneous double mutant K377C/I22S confirms the absence of binding as indicated by the FTIR difference spectra. Furthermore, the cation does not induce additional conformational changes since the fluorescent at 465 nm remains unchanged. The single mutant containing the replacement I22S also lacks the interaction with the substrates. Markedly, the double mutant K377R/I22S conserves the interaction with the fluorescent sugar D<sup>2</sup>G (Fig. 7.41). Apparently, the positive charge of the arginine in combination with the I22S replacement is important for the binding of the  $\beta$ -sugar D<sup>2</sup>G. The K377R/I22S conversely to K377C/I22S demonstrates a clear FRET between the D<sup>2</sup>G and the intrinsic tryptophans. Considering the results of the proteoliposomes of the K377R/I22S mutant, the extraction of the protein from the membrane obviously influences the coupling of transporter. Most likely the arrangement of the helices is perturbed and less rigid or less compact. Once reconstituted into a lipid bilayer, the protein does not recover the substrate binding like the C-less mutant.

The data of the K377R/L236F vesicles have been described in one of the previous chapters. The ISO and RSO vesicles of PCR-generated mutant K377C/L236F obviously bind the fluorescent sugar unspecifically as exhibited in Fig. 7.41. The reason to believe in unspecific binding is that the co-substrate does not induce similar changes as seen for the spontaneous K377R double mutants. Moreover, the addition of melibiose does not reduce the fluorescence around 465 nm indicating a replacement of the competitive inhibitor D<sup>2</sup>G by a larger concentration of melibiose. The substitution L236F however behaves like the K377R/L236F mutant in the presence of the co-ligand sodium. The cation induces a larger conformational change in the permease. The vesicles of the charge switch mutant D59K/K377D suit as a control of the purified and reconstituted sample. Earlier results indicated lack of binding of the substrates in the double mutant. The FRET of the vesicles confirms the data accomplished from the purified transporter. The data indicate the absence of any substrate binding. Thus, the sugar-transporter

MelB loses its function by switching the charges of the crucial residues of the Asp-59 and Lys-377.

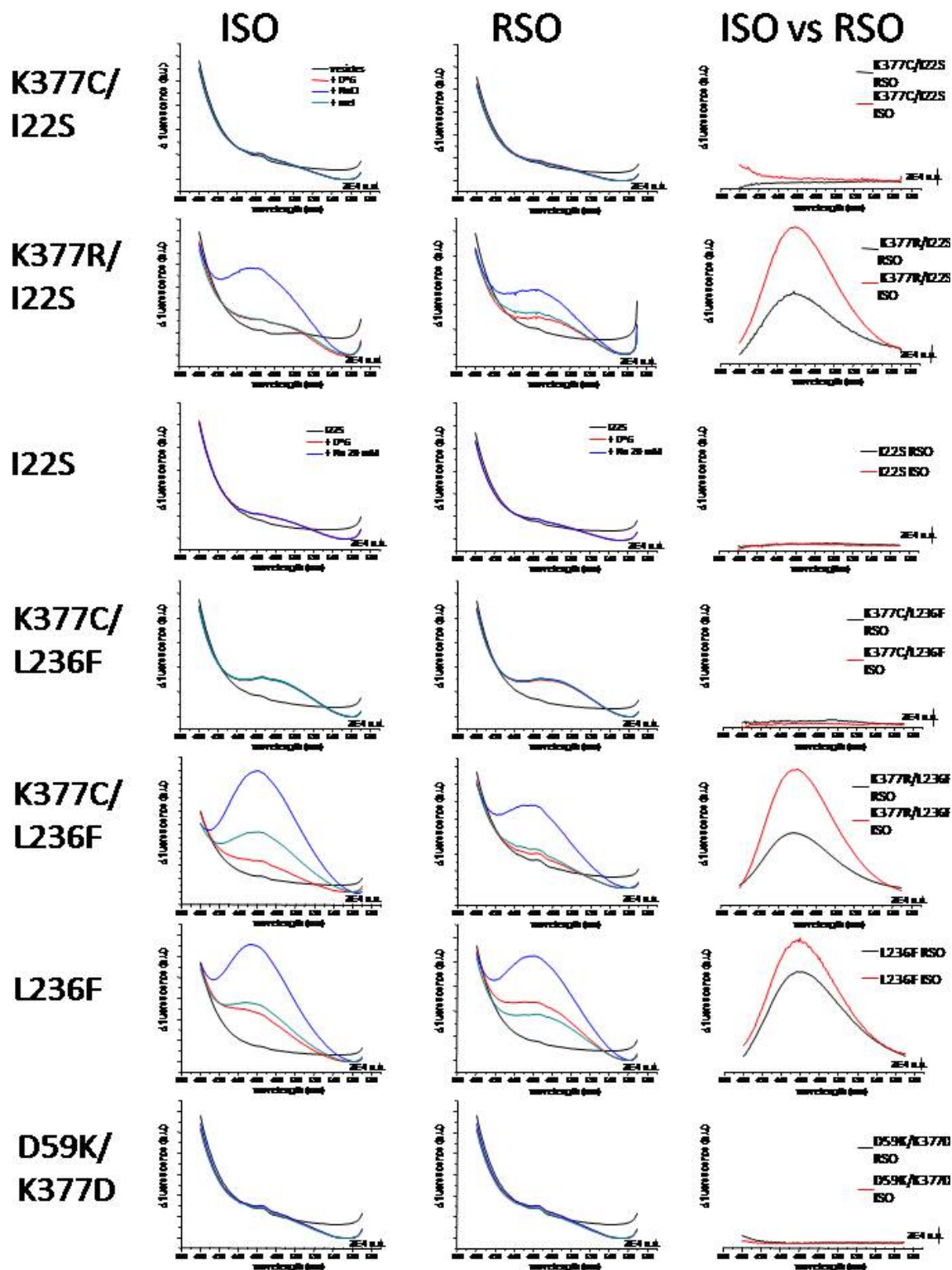


Figure 7.41 Inside-out and right-side-out vesicles of the MelB mutants. Left column inside-out vesicles of the indicated single or double mutant (black line: vesicles, red line: + 10  $\mu$ M D<sup>2</sup>G, blue line: + NaCl, cyan line: + melibiose), centre column: right-side-out vesicles of the indicated single or double mutant, right column: graph of fluorescence difference of the RSO (Black line) and ISO (red line) vesicles, obtained by subtracting sodium-induced fluorescence from the

D<sup>2</sup>G-mediated fluorescence. Excitation wavelength: 290 nm, emission spectrum: 400 - 570 nm. Buffer during data acquisition 0.1 M KPi, 0.1 M KCl, pH 7.0. I22S vesicles exceptionally were not probed in the presence of melibiose, because the sodium did not induce the signal increase around 465 nm.

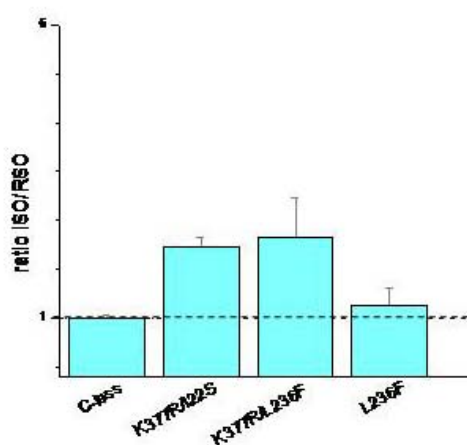


Figure 7.42 ratio ISO/RSO of the Lys-377 revertants + L236F compared to C-less reference.

K377R/I22S display a ISO-FRET signal change that is twice the change in the right-side-out vesicles (Fig. 7.42). All other listed mutants demonstrate the expected ratio of ~1. In Fig. 7.43 the MelB presence in the Lys-377 mutant vesicles was verified by labeling with the reagent His-Probe<sup>TM</sup>-HRP. In the vesicles of single mutants K377C, K377V and K377H, the MelB transporter was detected more initial quantity of the vesicles was needed to label MelB. This is related to a reduced expression of MelB in the Lys-377 mutants.

The mutant D59K/K377D expresses much more MelB compared to the Lys-377 single mutant (Fig. 7.43). However, D59K/K377D is not able to bind the substrates in a co-dependent manner as shown in the section 7.7 of the results. It can also be concluded that the revertants of Lys-377 are expressed at higher levels than their parental single mutants. The western blots demonstrated a more intense signal of the revertants by using less total protein.

The ratio between the ISO and RSO vesicles was only calculated for the mutants demonstrating a FRET signal (Fig. 7.42). This ratio could be used to make assumptions about the accessibility of the binding sites in the mutants. K377C/I22S, I22S and D59K/K377D were not included in the assessment since the FRET data either entirely failed to indicate substrate binding or in the case of the mutant K377C/L236F the cation did not enhance the signal intensity.

The ratio of the spontaneous K377R revertants indicate that K377R/L236F as well as that is twice the change in the right-side-out

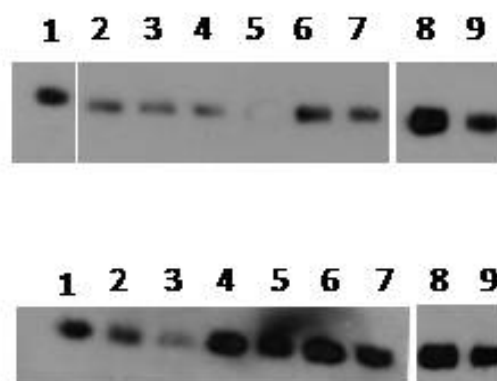


Figure 7.43 Vesicles of Lys-377 mutants; **A** in lane 1: C-less proteoliposomes control (250 ng), lane 2: K377C ISO (15 µg total protein), lane 3: K377C RSO (15 µg), lane 4: K377V ISO (15 µg), lane 5: K377V RSO (15 µg), lane 6: K377R/I22S ISO (5 µg), lane 7: K377R/I22S RSO (5 µg), lane 8: D59K/K377D ISO (5 µg), lane 9: D59K/K377D RSO (5 µg); **B** in lane 1: C-less proteoliposomes control (250 ng), lane 2: K377C ISO (15 µg total protein), lane 3: K377C RSO (15 µg), lane 4: K377V ISO (15 µg), lane 5: K377V RSO (15 µg), lane 6: K377R/I22S ISO (5 µg), lane 7: K377R/I22S RSO (5 µg), lane 8: I22S ISO (5 µg), lane 9: I22S RSO (5 µg).

### 7.11. Importance of the charge of residue Lys-377

The previous chapters announced the arginine as the only potential amino acid for partially rescuing the substrate binding in vesicles and to a far lesser extent in proteoliposomes. The same effects have not been observed in the mutant carrying a cysteine, a charge-less, polar residue. The question remains if chemical modification with thiol reagents combined with the cysteine enables liganding of the substrates.

MTSET (2-(trimethylammonium) ethyl methanethiosulfonate) and MTSEA 2-aminoethyl methanethiosulfonate are two distinct thiol reagents carrying a positive charge and therefore mimic the amino acids' charge of histidine (pH-dependent), arginine and lysine. These reagents have a short half life at room temperature but remain active when attach to a ligand like the sulfhydryl groups of a cysteine.

Surprisingly, the double mutant K377C/L236F could restore parts of the FRET signal increase in the presence of the thiol reagent MTSEA. Similar outcomes were not observed for MTSET. Even though containing a positive charge, either structural impediments or stability issues negate a restoring of the sugar binding.

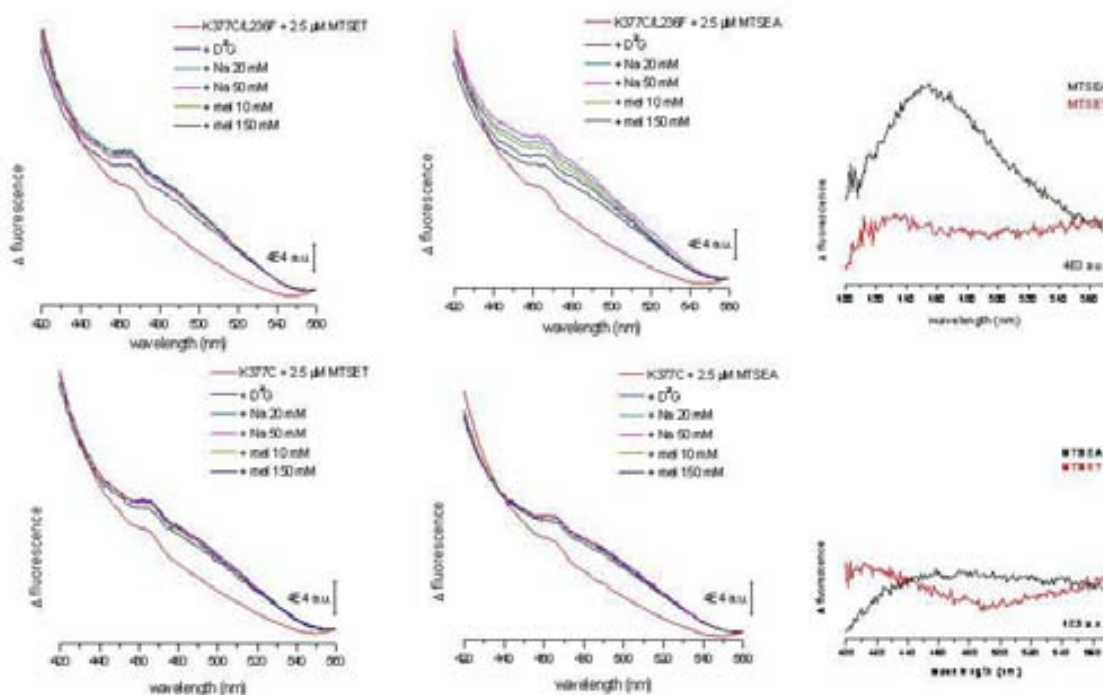


Figure 7.44 MTS reagents and FRET in vesicles. Upper panel: K377C/L236F mutant, on the right: FRET analysis in the presence of MTSET, in the centre: FRET in the presence of MTSEA, on the left: sodium-triggered FRET signal in the presence of the indicated MTS reagents (in red: MTSET, in black: MTSEA). Lower panel: K377C mutant, on the right: FRET analysis in the presence of MTSET, in the centre: FRET in the presence of MTSEA, on the left: sodium-triggered FRET signal in the presence of the indicated MTS reagents (in red: MTSET, in black: MTSEA).

The Figure 7.44 points out the significance of a positive charge in position 377 in combination with the second site mutation L236F of MelB transporter. Nevertheless, a sole positive charge does not necessarily restore the binding capacity of the transporter as seen by the absence of D<sup>2</sup>G binding in the presence of the thiol reagent MTSET which delivers a positive charge. The results strengthen the tendency of a necessity of a positive charge in position 377, but this charge might not liberate the entire functionality of the transporter. The K377C mutant failed to demonstrate similar FRET signals in the presence of the positively charged thiol- reagents.

## 8. Charged residues in loop 10-11

The loop located between C-terminal helices X-XI is reported as participant during the



Figure 8.1 MacConkey agar plate displaying the mutants from loop 10-11 plus Lys-377 double mutants. A: D351C, B: R363C, C: K377R/L236F, D: D59K/K377D, E: D55K/K377D, F: K377C/L236F, G: D354C

transport mechanism of the melibiose carrier. Relying on an array of data, the loop was classified as a so-called re-entrant loop transversing the membrane half-way and penetrating the watrous channel close to the substrate binding sites. Over the years, the proposed topology of the protein changed depending mostly on fusion protein and hydropathy analyses. The loop 10-11 remained relatively steady in composition and can be seen as the largest cytoplasmic loop. Single cysteine site-replacement reinforces the idea of possible participation during membrane transport. Besides the more  $\alpha$ -helical structured membrane segments, loops, especially 4-5 and 10-11 are stated to possess some  $\beta$ -sheet content. Typical for the extramembrane parts of membrane proteins, the amount of

charged amino acids is much higher than in the transmembrane segments. Especially interesting are two aspartic acids 351 and 354 as well as the arginine 363. Cysteine scanning revealed these residues as potentially crucial amino acids for the transport mechanism. Transport assays done by Ding *et al.* concluded a completely loss of activity in those MelB mutants<sup>82</sup>.

Two glutamic acids were also included in our list of MelB mutants of the loop 10-11. Glu-357 and Glu-365 showed only a minor reduction in transport activity when replaced by cysteine. Nevertheless, those negatively charged amino acids might have a peripheral significance for the transporter. Glu-365 for instance is crucial residue regarding the temperature sensitivity of the protein<sup>64,102</sup>. The expression rates compared to the K377C reference are higher although still less than 50% which can be interpreted that these charged amino acids are basic requirements for the MelB transporter.

Visible in Fig. 8.1 is the phenotype of each probed mutant of the cytoplasmic loop 10-11. The transport defective mutants also demonstrate no metabolization of melibiose on MacConkey agar plates indicated by their white colonies. E357C and E365C on the other hand demonstrate a pH change in their red-colored phenotype.

### *8.1. Na-binding of the MelB mutants of the charged amino acids of the loop 10-11*

All MelB mutants of the putative charged residues in the cytoplasmic loop interact with the co-substrate sodium (Fig. 8.2) although D354C shows a very low signal. The intensity of the difference spectrum demonstrates the grade of affinity between the mutated transporter and the cation. As mutants with less impact on the transport activity, E365C and E357C are simultaneously the MelB variants displaying the sodium-induced  $IR_{diff}$  spectrum with the highest intensity. Displaying the formation of white colonies on the MacConkey agar plates, the transport-defective mutants D351C, D354C and R363C were subjected to seek for second-site revertants like the formerly described Lys-377 mutant.

These revertants are attractive because they could help to emphasize intramolecular interactions of the residues, like H-bonding of salt bridges. Second site mutations could restore the catalytic activity of defective carriers. Understanding the impact of a second site mutation further elucidates the transport mechanism of MelB. Therefore, those MelB mutants were incubated for 5-10 days on MacConkey agar plates as described earlier for the Lys-377 mutations (see part 1 of the result) or in the materials and methods section.

The sequencing of all red colonies ever obtained only revealed a second-site revertant for the single mutant D354C. D354C is the variants which displays the difference spectrum with the lowest intensity of all loop 10-11 mutants. Moreover, the residue possesses the lowest expression rate among the loop-comprising amino acids. Surprisingly, the mutation responsible for the formation of the second site mutation is I22S. This isoleucine-serine substitution occurred for all Lys-377 substitutions. Hence, the Ile-22 apparently is a crucial amino acid either for the transporter stability, the transport activity or both.

In the case of the single mutants D351C and R363C, dozens of red colonies indicating a recovered sugar transport appeared. Unfortunately, all sequencing data demonstrated the absence of the first-site mutation. The original genetic background, C-less, was recovered again by replacing the cysteine with an aspartic acid in position 351 (Asp-351) or with an arginine in position 363 (Arg-363).

The charged residues might not participate in a charged pair construct, as it is possible in their location in a reentrant loop structure. A second explanation could be that the mutation of these amino acids is too severe for the transporter function demonstrated by quite low expression rates and eliminated transport activities. Hence, for salvation of the function the replacement of the cysteine by the original mutation is employed to guarantee transport activity.

A third tendency is the rather rare probability of a second site mutation. Even though that 100% of the observed colonies were tested negatively, it does not necessarily implicate an absence of a charged pair interaction of Asp-351 and Arg-363.

Fig. 8.2 gives rise for a provisional hypothesis. Even though all the mutants evidently

## RESULTS

interact with the sodium ion overseeing their intensities, it is certain to state that the loop is somehow involved in the binding process of the cation. Reflected by the relative low spectral similarity of loop-located residues compared to the C-less background, the mutants affect the transporters interaction with the sodium. Especially startling are the amide regions between 1700 and 1500  $\text{cm}^{-1}$  where all mutants present similar conformational changes, but completely different from the C-less reference.

The peak at 1550  $\text{cm}^{-1}$  is negative whereas in the C-less reference spectrum this peak is positive. The differences in the protein-sensitive bands cause the large drop in spectral similarity of the mutants. The quantification of the spectra enhanced this speculation since the similarity is somehow equal at a value of just 25% even the double mutant D354C/I22S.

The cation binding affinity is represented by the intensity. The mutants D351C, D354C and R363C couple the cation with less affinity whereas the mutants E357C and E365C and the spontaneous revertant D354C/I22S demonstrate a sodium-induced difference spectrum with reasonable intensity.

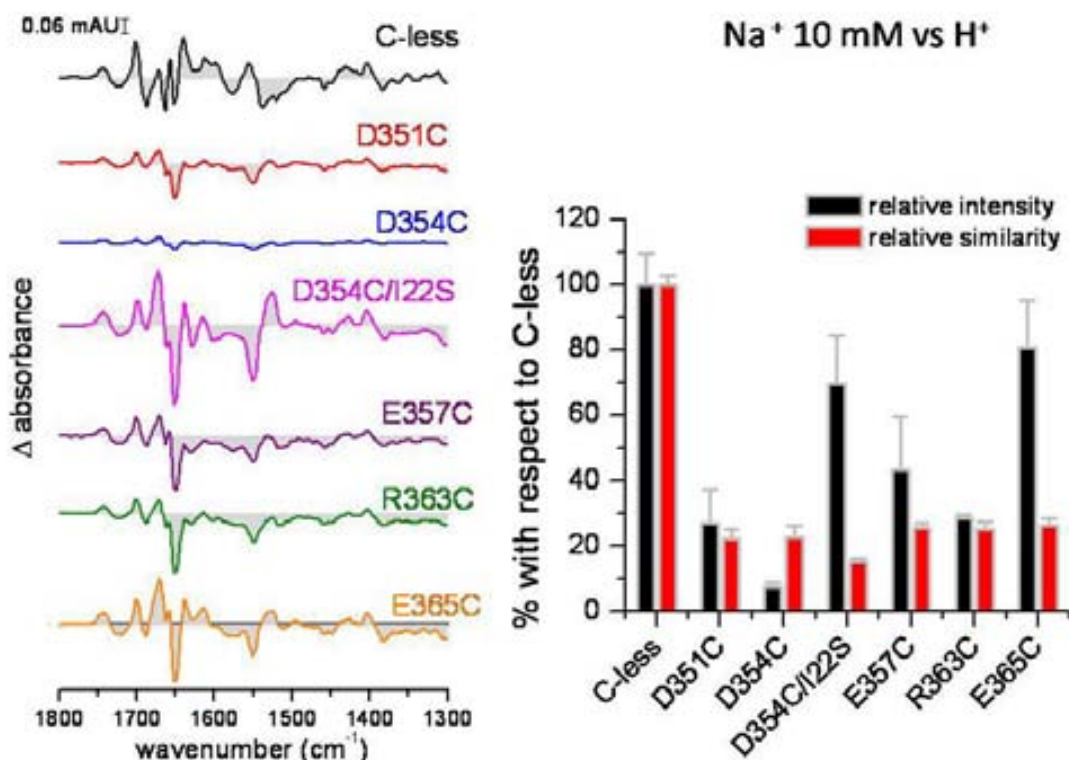


Figure 8.2 Na-induced (10 mM Na)  $\text{IR}_{\text{diff}}$  spectra of crucial residues in the cytoplasmic loop between the helices X and XI. In the left panel: difference spectra of the MelB mutants, in black: C-less as reference spectrum, in red: D351C mutant, in blue: D354C mutant, in pink: D354C/I22S mutant (spontaneous revertant), in purple: E357C mutant, in green: R363C mutant, in orange: E365C mutant; in the right panel: comparison using the first derivative of mutant spectra with C-less as reference spectrum. The error bars indicate the variation depending on at least two independent data acquisitions.

By validating the difference spectrum of the D354C, the I22S mutation definitely restores the carriers' capacity to bind the cation. The transport-defective mutations of Asp-351, Asp-354 and Arg-363 to cysteine exhibit a reduced cation binding affinity of just 20% compared to the C-less reference. Even saturating concentrations of 50 mM sodium induce no further conformational changes in the mutants. The spectral intensities remain low compared to C-less.

## 8.2. *The effect of melibiose binding*

The sugar-induced difference spectrum gives further insights of how MelB is eventually influenced by the replacement of the crucial charged amino acids in the cytoplasmic loop 10-11. From the difference spectra, it can be stated that the interaction with melibiose in the presence of sodium is affected in all mutants. The sugar binding is most conserved by the E357C mutant which has a relatively high spectrum intensity of almost 50% compared to the C-less porter. Because of the high spectral intensity, comparison between the spectra can be made. Two severe alterations occur considering the protein-sensitive region between 1700 -1500  $\text{cm}^{-1}$ . The negative peak at 1650  $\text{cm}^{-1}$  from the C-less protein appears to be positive for E357C. Moreover, the negative peak at around 1550  $\text{cm}^{-1}$  is much less intense in E357C than it is in the C-less control.

R363C and E365C interact modestly with melibiose by retaining an intensity of their sugar-induced spectrum of just 20% related to C-less. The capacity to bind the sugar molecule is therefore reduced.

The mutations of Asp-351 and Asp-354 to cysteine which completely lost the ability to transport, display only remnants of a sugar-induced difference spectrum (Fig. 8.3). Their spectral intensities diminished to just 10% and 5%, respectively. All difference spectra of the single mutants still maintain their similarity compared to C-less of around 80%. The high similarities conduct the idea of similar fashion of melibiose binding in the mutants although with different affinities.

Aside the single site replacements, the spontaneous double mutant D354C/I22S denies the expectation of a recovered sugar binding. In the presence of sodium, the mutant is unable to demonstrate a sugar-induced  $\text{IR}_{\text{diff}}$  spectrum. Above all, this result corresponds well to the previously shown results for the revertants of Lys-377 containing the I22S replacement. These spontaneous double mutants failed to recover sugar binding in the presence of the cation as well.

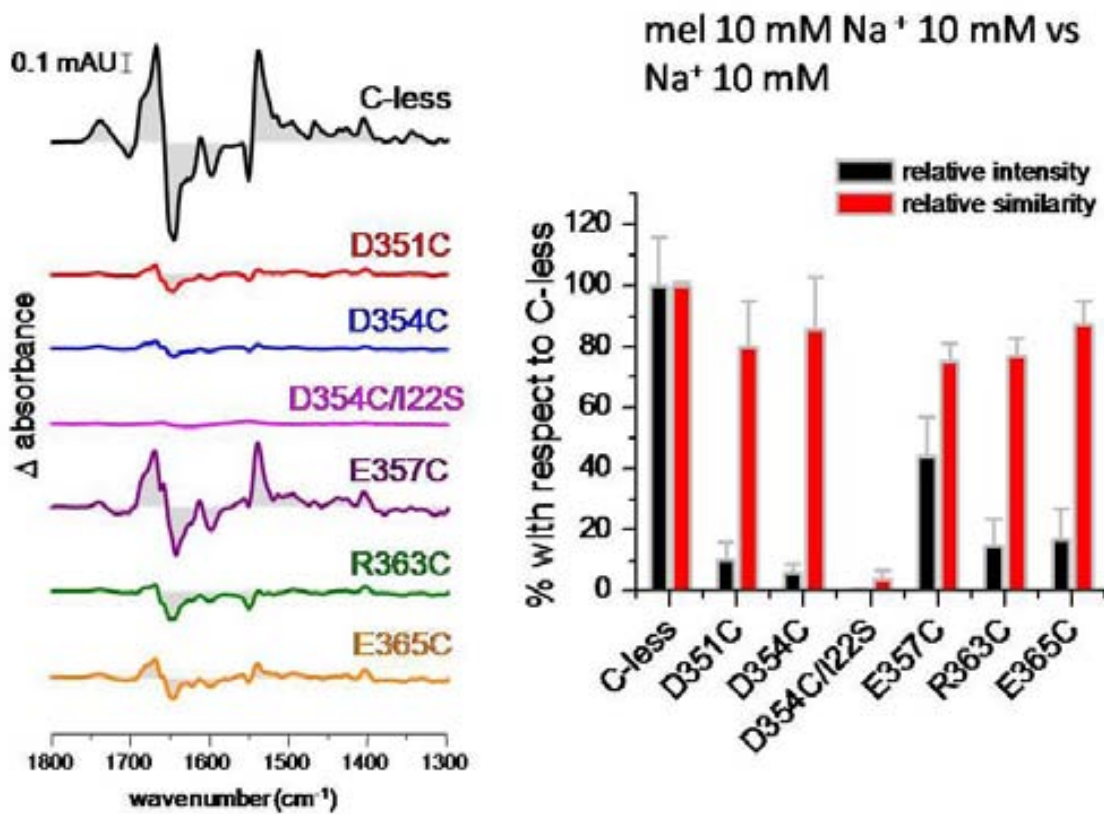


Figure 8.3 IR<sub>diff</sub> spectra induced by 10 mM melibiose in the presence of the cation sodium. In the left panel: difference spectra of the MelB variants, in black: C-less as reference spectrum, in red: D351C mutant, in blue: D354C mutant, in pink: D354C/I22S mutant (spontaneous revertant), in purple: E357C mutant, in green: R363C mutant, in orange: E365C mutant; in the right panel: comparison using the first derivative of mutant spectra with C-less as reference spectrum. The error bars indicate the variation depending on at least two independent data acquisitions.

The melibiose/ $H^+$  difference spectra for the loop mutants match well with the results from melibiose/ $Na^+$  data. The Glu-357 mutant possesses an equivalent affinity for the sugar like the C-less transporter considering its spectral intensity of almost 100%. The E357C melibiose-induced IR<sub>diff</sub> in the presence of the proton displays similar characteristics as the spectrum in the presence of sodium. The negative peak at  $1650\text{ cm}^{-1}$  from C-less is replaced by a positive peak in the melibiose-induced IR<sub>diff</sub> of E357C. Furthermore, the negative peak at  $1550\text{ cm}^{-1}$  appears less intense, but simultaneously the consecutive positive peak at  $1540\text{ cm}^{-1}$  possesses more intensity than in the cysteine-less IR<sub>diff</sub>.

The other transporting mutant E365C similarly binds melibiose with high affinity by displaying around 60% spectral intensity. This confirms that Glu-365 is not essential for the transport mechanism like the other negatively charged residue Glu-357.

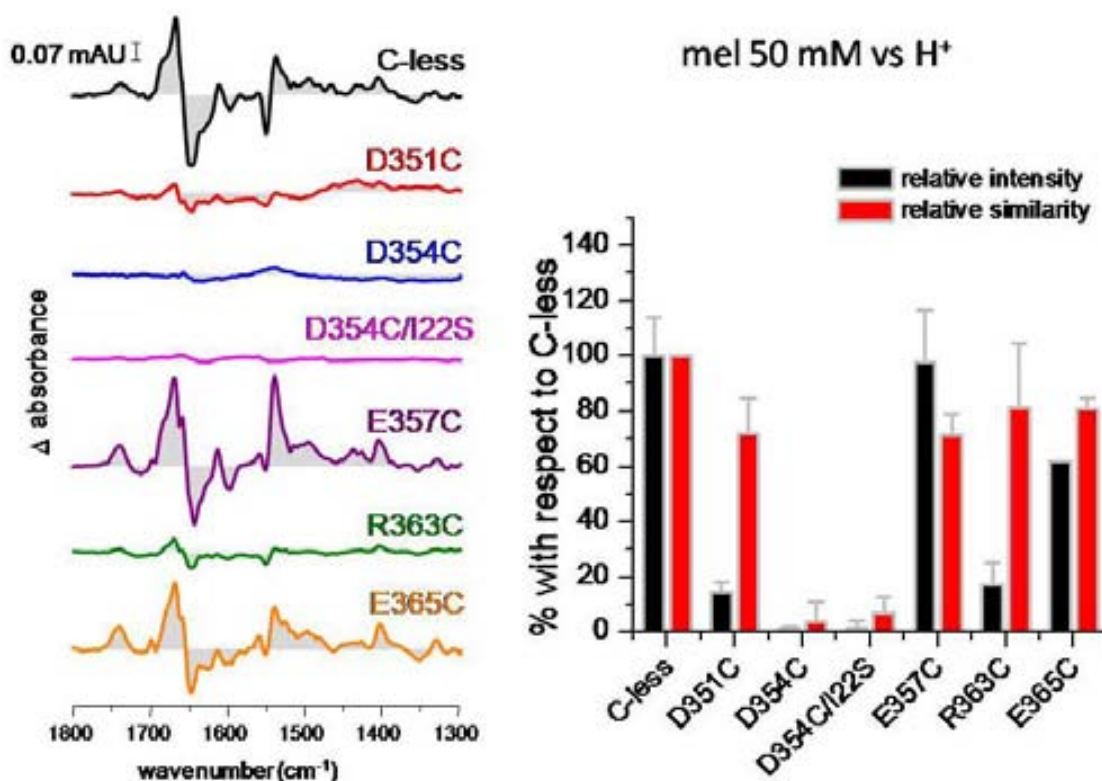


Figure 8.4 IR<sub>diff</sub> spectra of the charged mutants of the loop 10-11 induced by 50 mM melibiose. In the left panel: difference spectra of the MelB variants, in black: C-less as reference spectrum, in red: D351C mutant, in blue: D354C mutant, in pink: D354C/I22S mutant (spontaneous revertant), in purple: E357C mutant, in green: R363C mutant, in orange: E365C mutant; in the right panel: comparison using the first derivative of mutant spectra with C-less as reference spectrum. The error bars indicate the variation depending on at least two independent data acquisitions.

The difference spectra of R363C and D351C show analogous features. The spectra of the mutants D351C and R363C have an intensity of only 15% and 17% respectively in the range from  $1700\text{ to }1500\text{ cm}^{-1}$  compared to C-less. The other negatively charged residue D354C, which also impedes transport, shows no difference spectra in the presence of the proton.

The recruited double mutant containing the I22S exchange as a second site mutation clearly does not improve the binding of the sugar in the presence of the proton or sodium as visible in Fig. 8.3 and 8.4. No evidences for melibiose binding were detected.

The reason for the ambivalent occurrence of this residues exchange remains therefore rather speculative. Furthermore, the data of the IR<sub>diff</sub> spectra at a saturating concentration of 50 mM melibiose in the presence of the proton are in agreement with the results obtained for sodium as the co-substrate. Only D354C shows partial coupling with the sugar molecule in the presence of sodium whereas the substrates melibiose and H<sup>+</sup> could not trigger any conformational changes in the mutant.

As commented before, the absorbance spectrum for each cysteine mutant can give evidences for secondary structure alteration caused principally by the single residue substitution. The mutant D354C triggers very little to no difference spectrum for both substrates. Beyond that, the mutant is unable to accumulate the melibiose intracellularly. The second derivative of the absorbance spectrum elucidates small alterations of the protein (Fig. 8.5).

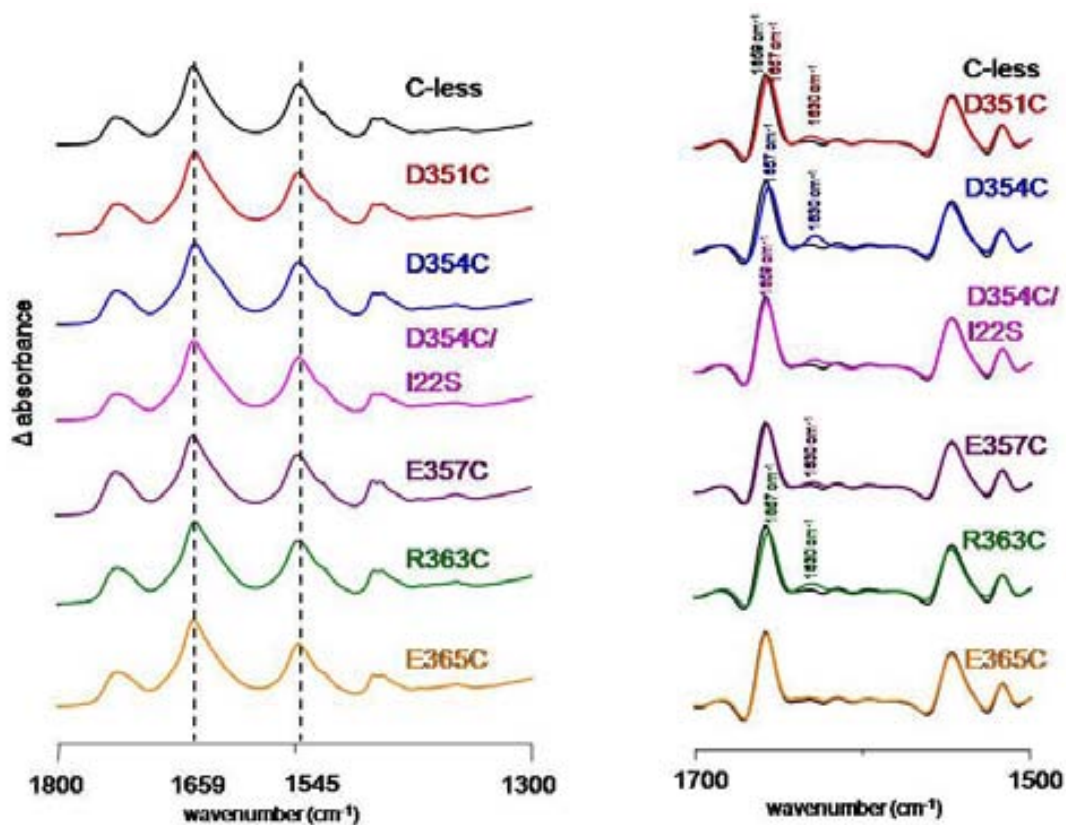


Figure 8.5 Absorbance spectra comparison between mutants of loop 10-11 and the C-less reference. Left panel: absorbance spectra of the wet protein film between 1800 and 1300 cm<sup>-1</sup>, right panel: second derivative of the absorbance spectra in the amide region between 1700 and 1500 cm<sup>-1</sup>.

Worth mentioning is the effect of the mutation I22S in the D354C/I22S revertant. Whereas in the amide I region the single mutant D354C displays a shifted peak to 1657 cm<sup>-1</sup>, the revertant D354C/I22S recovers almost entirely the C-less pattern by relocating the large peak to its original

position at  $1659\text{ cm}^{-1}$ . In parallel the second site mutation reduces the intensity of the peak at  $1630\text{ cm}^{-1}$ . Since the I22S mutation realizes a comparable rearrangement for the K377C mutant, the protein apparently tolerates conformational adjustments when mutated in unfavorable positions.

The two glutamic acids mutants still catalyzing transport activity also show structure-sensitive bands which resembles the C-less reference (see Fig. 8.5).

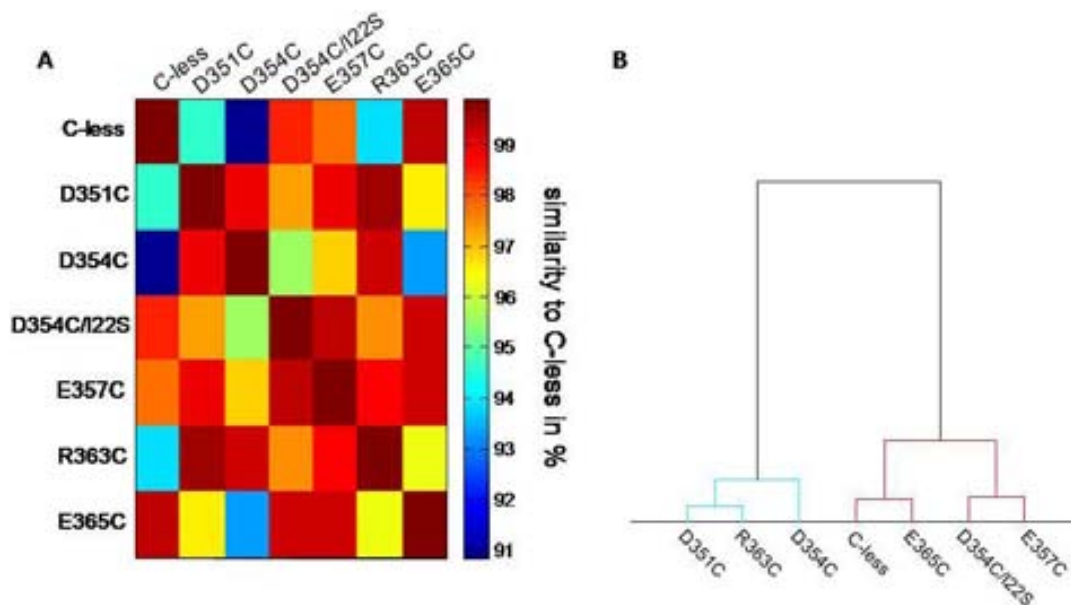


Figure 8.6 Quantitative absorbance comparison of the mutants of the cytoplasmic loop 10-11 using C-less as reference spectrum, **A** pictogram of the absorbance spectra similarity expressed in a color scheme, **B** dendrogram of the MelB mutants of the cytosolic loop 10-11 representing the spectral differences between the mutants compared to C-less; calculated as  $(1-R^2) \times 100$ .

The qualitative comparison of the absorbance spectra is accompanied by a quantification of the similarity expressed by a color scheme in Fig. 8.6 A. The mutant D354C appears to be the one most affecting the protein structure by displaying only around 90% similarity with the parental C-less protein. This difference is reflected by the abolished transport as well as the almost vanished substrate binding.

The revertant D354C/I22S clearly improves the structural issue from the defective single mutant D354C by showing around 98% resemblance to C-less. Therefore, it can be stated that also in this case the I22S second site mutation apparently compensates for the loss of structural order in the protein.

E365C and E357C demonstrate a high amount of absorbance spectrum similarity of 99% and 97% respectively. R363C and D351C are associated not only by comparable  $IR_{\text{diff}}$  spectra features but also by an almost identical similitude of their amide region.

### 8.3. Fluorescence spectroscopy

#### 8.3.1. Trp response in the presence of the substrates

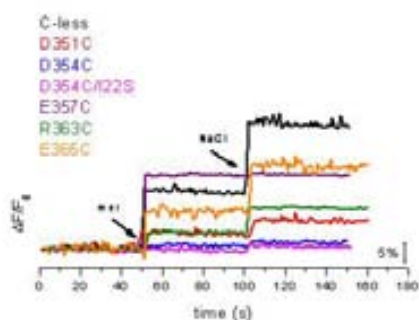


Figure 8.7 Trp fluorescence using 290 nm as excitation and 325 nm as emission wavelength. Black line: C-less, red line: D351C, blue line: D354C, magenta line: D354C/I22S, purple line: E357C, olive line: R363C, orange line: E365C;

The result from the Trp fluorescence points out a  $\Delta F/F_0$  increase of only 2%. Nevertheless, both mutants also display tryptophanyl response in the presence of the melibiose and the cation.

By assessing the fluorescence changes of the MelB variants in the cytoplasmic loop 10-11 (Fig. 8.7), it is evident that the substrate addition provokes conformational changes in all the mutants.

Expectingly, the mutations of Glu-357 and Glu-365 have the smallest impact on the fluorescence changes mediated by the transporter substrates. In the case of the E357C mutant, the  $\Delta F/F_0$  is even larger for the tertiary complex consisting of MelB·sugar·H<sup>+</sup> in the C-less control. The sodium cation causes just a small increase in intrinsic fluorescence. The mutations of D351C and R363C display a modest fluorescence increase as expected from earlier data from the infrared difference spectra. The mutant D354C along with its double mutant D354C/I22S hardly

#### 8.3.2. FRET analysis of the residues in the cytoplasmic loop 10-11 in proteoliposomes

The energy transfer between D<sup>2</sup>G and Trp's elucidate primarily the ability of  $\beta$ -sugar binding but at the same time information about distances between the sugar molecule and the intrinsic tryptophans can be deduced from the FRET analysis (Fig. 8.8).

Certainly elucidating is that the sugar analog binds to all cysteine mutants. But the intensity of FRET signal varies immensely among the mutants. D354C alongside with its spontaneous double mutant D354C/I22S displays a very small signal at the D<sup>2</sup>G emission maximum at 465 nm. The charged residue substitutions of Asp-351 and Arg-363 with cysteine affect the transfer intensity as well.

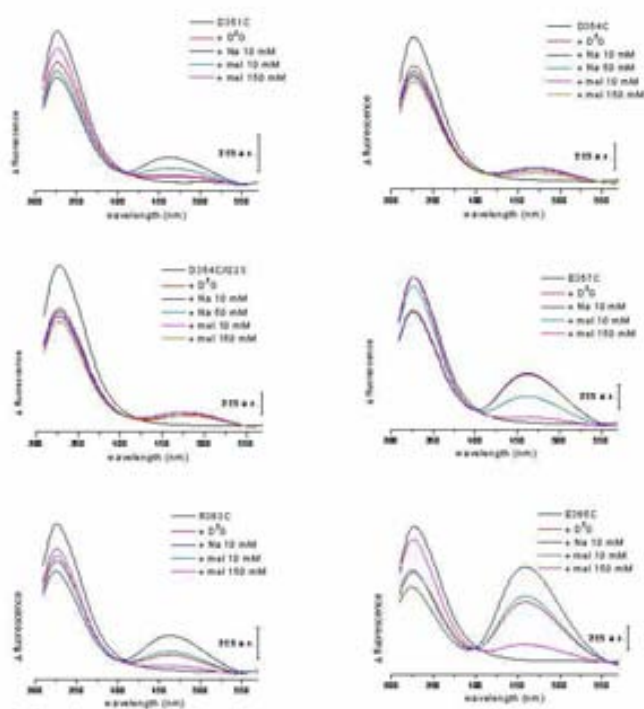


Figure 8.8 FRET analysis of the mutants in loop 10-11. Listed in zigg-zagg-fashion: D351C (upper left corner), D354C (upper right corner), D354C/I22S (centre left), E357C (centre right), R363C (lower left corner) and E365C (lower right corner).

addition causes only a slight increase in Trp fluorescence. This might be related to the reduced conformational changes of the transporter carrying the mutation E357C after sodium addition. The presence of the hydrogen and the melibiose provoke hypothetically most of the structural changes upon substrate binding.

Conclusively, the mutations D351C, D354C and R363C which after all failed to accumulate the sugar intracellularly, in parallel either inhibit or weaken a convenient binding of the ligands. Considering the Arg-363 and the Asp-351, both ligands provoke minute but significant alterations of the transporter structure. D354C on the other side obviously neglects similar access for the substrates to their particular binding sides.

#### 8.4. ISO and RSO FRET data of the mutants of the loop 10-11

The big advantage of the analyses by vesicles is the fact that during the preparation the protein remains intact in the membrane. The unfavorable condition of membrane extraction by a detergent is avoided in the preparation process.

For the mutations of the re-entrant loop 10-11, the validation of the vesicles suits as well as

The two glutamic residues mutations E365C and E357C show a normal behavior in the presence of D<sup>2</sup>G. In E365C the intensity of energy transfer even increases compared to C-less (see Fig. 8.8). This extended response must be related to the different configuration of the sugar, because former results were obtained with the  $\alpha$ -galactoside melibiose whereas for the FRET experiments the  $\beta$ -galactoside D<sup>2</sup>G was utilized. E357C on the other side interacts strongly with the sugar derivative but the sodium-induced FRET response almost is not increased. The result strengthens the intrinsic fluorescence data from E357C (Fig. 8.8) where sodium

## RESULTS

control of the obtained results from the proteoliposomes. The purified MelB variants indicated the importance of several residues in this interhelical segment.

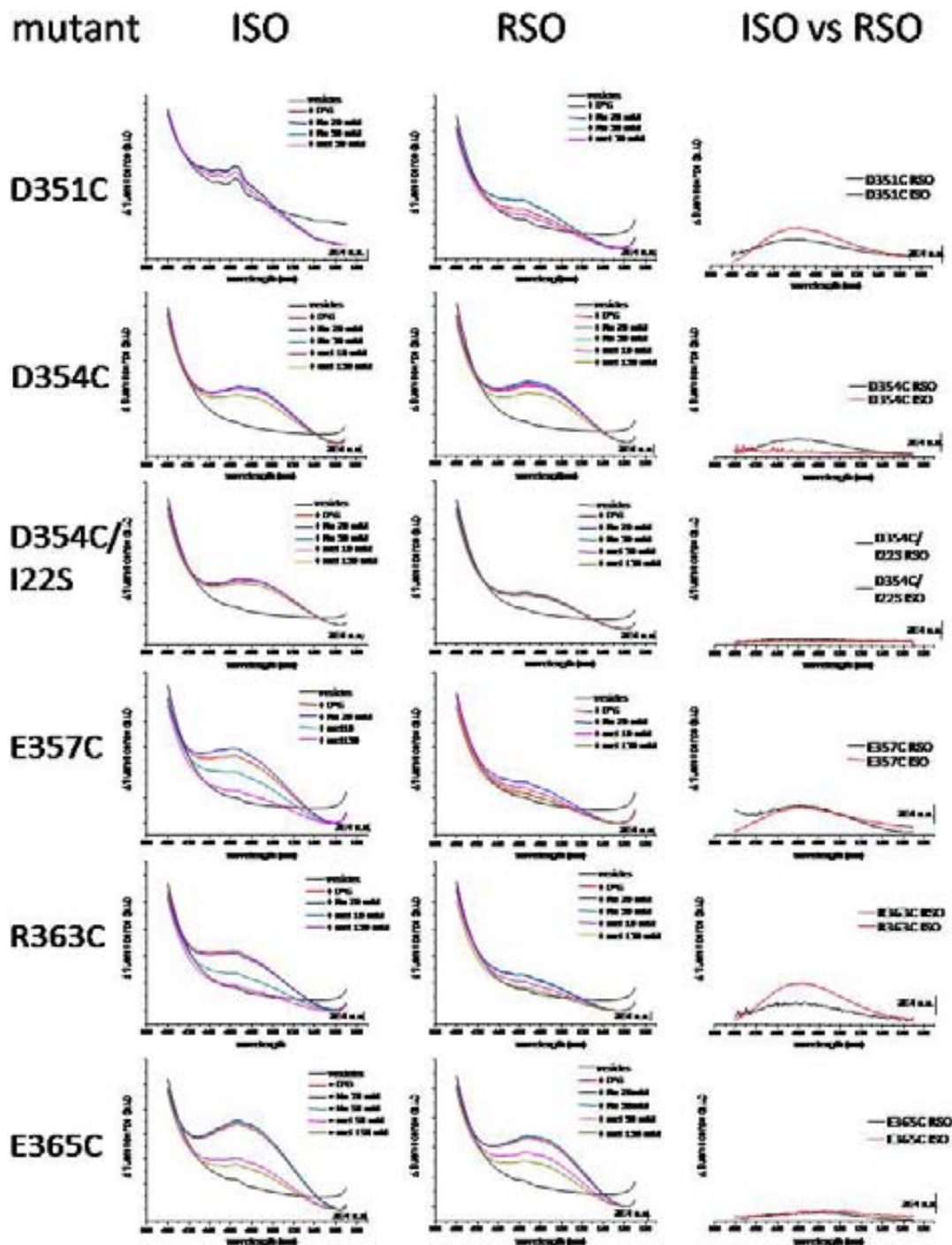


Figure 8.9 Qualitative examination of the membrane vesicles obtained from the different mutations of the cytoplasmic loop 10-11 from the melibiose permease (MelB). On the right side: inside-out (ISO) vesicles, in the centre: right-side-out (RSO) vesicles, on the left side: comparison between the sodium-mediated FRET difference in the ISO and RSO vesicles from all the cysteine-replaced mutants in the loop 10-11. In all conditions the buffer for the fluorescence spectroscopy analyses was composed of 0.1 M KPi and 0.1 M KCl, pH 7.0. Excitation at 290 nm, emission from 400 – 570 nm. The displayed results are the mean of at least to independent scans for each mutant.

As expected, the majority of the mutants point out an expected ratio ISO/RSO (or the other way around) of around 1, as already manifested for the cysteine-less transporter in chapter 7.9. The transport-defective single amino acid replacements D351C and R363C exhibit a higher FRET signal intensity in ISO vesicles than in the comparable right-side-out vesicles under equal experimental conditions. The ISO and RSO were always prepared from the same batch of cell culture excluding variations in protein expression eventually affecting the results. D351C and R363C demonstrate two-fold higher signal intensity in the ISO membrane vesicles. The mutant E357C as already established from the purified membrane transporter binds both substrates in a C-less like fashion which could be confirmed from the both vesicles populations (Fig. 8.9). The Na-dependent increase in fluorescence is similarly small as in the proteoliposomes.

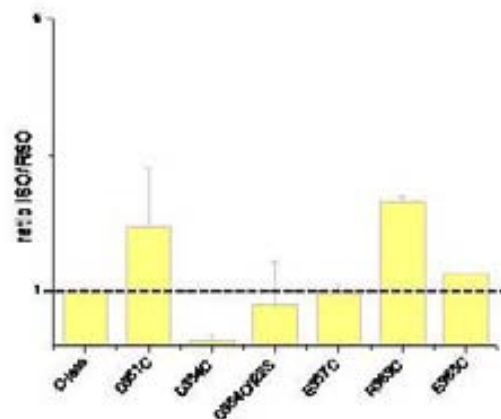


Figure 8.10 Na-dependent FRET ratio between ISO and RSO vesicles for the mutants in the extramembranal loop 10-11. All data are the mean of at least two independent scans for each type of vesicle.

Overall the ratio of the sodium-dependent increase in fluorescence in both vesicles types is equal by matching factor 1. Considering the single amino acid substitution of Glu-365 to cysteine, ISO and RSO point out a relatively large increase in fluorescence in the presence of the fluorescent sugar D<sup>2</sup>G. Contrarily to the data from the proteoliposomes, the presence of the co-substrate sodium did not provoke an increase of the fluorescence signal around 465 nm. Nevertheless, both vesicles forms present similar fluorescence signals and thus the ISO/RSO-factor is close to 1.

Although both vesicles types rely on the same batch of culture, the preparation of the vesicles differ from another. For a convenient conclusion, the amounts of protein in the vesicles were detected by using a specific reagent against the histidine-Tag of the protein. This way the probed amount of total protein could be correlated to the detected fluorescence change.

The conclusion drawn from the ISO and RSO fluorescence spectra of the cysteine mutation Asp-354 differs from the rest of the cytoplasmic loop 10-11.

First of all, the ISO vesicles clearly indicate a D<sup>2</sup>G binding which has only been partially demonstrated in the purified and reconstituted MelB mutants. The co-substrate however does not trigger an increase in fluorescence energy transfer between the intrinsic tryptophans and the D<sup>2</sup>G sugar analog.

In the RSO vesicles the D<sup>2</sup>G-mediated fluorescence signal enhances in the presence of the sodium cation which differs from the inside-out form. The sodium-dependent ratio ISO/RSO therefore is 0.1. Or calculating the other way around, the relative sodium-triggered FRET increase in RSO is 10-fold the relative signal in the ISO vesicles. An explanation for the discrepancy between the



Figure 8.11 vesicles from the loop 10-11 mutants detected by His. lane 1: C-less control (proteoliposomes – 250 ng), lane 2: D351C ISO (5 µg total protein), lane 3: D351C RSO (10 µg), lane 4: D354C ISO (30 µg), lane 5: D354C RSO (10 µg), lane 6: R363C ISO (5 µg), lane 7: R363C RSO (10 µg), lane 8: D354C/I22S ISO (8 µg), lane 9: D354C/I22S RSO (8 µg).

ISO and RSO vesicles is delivered in fig. 8.11. The ISO vesicles of the D354C/I22S contain fewer MelB than the RSO counterpart. This explains the failure of D<sup>2</sup>G signal detection in the ISO vesicles. The vesicles from the spontaneous double mutant D354C/I22S however, distribute analogous results as the purified equivalent embedded into proteoliposomes. The D<sup>2</sup>G sugar might cause a FRET signal which can be related to low affinity interaction with the transporter.

Nevertheless, the addition of the co-substrate fails to enhance the D<sup>2</sup>G-mediated FRET signal.

## 9. Elucidating the importance of residues in helix XI

The C-terminal transmembrane segment XI was hypothesized as a contributor during the transport mechanism. Based on previous assumptions several residues display sensitivity for replacement by site-specific mutagenesis. Cysteine scanning already emphasized meticulously crucial amino acids for the MelB transport activity<sup>63</sup>. Considering the absence of a dependable three-dimensional structure for MelB, the amount of residues encompassing transmembrane segments remain putative based on biochemical, biophysical and modeling approaches. Therefore, the length of the putative  $\alpha$ -helix XI was modified over time.

Relying on the latest MelB-model as the reference for tertiary structure arrangement, besides the majority being embedded into the putative helix, three residues termed as Ile-394, Gly-395 and Tyr-396 are located in the periplasmic loop 11-12. Earlier topological maps of the transporter described the residues as part of the helix and were included in the characterization.

To point out all important residues, the Lys-377 must be named forefront and was already discussed in detail. But apart from this single charged residue, mutations of several apolar amino acids abolish the intracellular sugar accumulation in the membrane-transversing region.

Gly-379, Phe-385 and Tyr-396 replaced by cysteine failed to accumulate sugar intracellular. Cysteine substitution of Ala-383 inhibited the transport activity greatly. Gly-395 and Leu-391 substitutions also reduced the catalytic activity of the carrier although less severe<sup>63</sup>. The mutation of the glutamine in position 372 to cysteine retains the accessibility by aqueous solutions through the aqueous channel. Thus, this site obviously is located in the crucial moiety of the transporter.

With the help of the infrared difference spectrum, the different mutants of the helix XI were characterized considering the ability to interact with the ligands, sodium and melibiose.

Since earlier transport assays pointed out, that cysteine mutations of several residues

eliminate the transporter activity, the question remains if the replacements directly affect the mandatory substrate binding. Apart from the above mentioned mutants, the Gly-379 was additionally substituted by valine to assess a similar hydrophobic residue with a prolonged side chain.

### *9.1. IR<sub>diff</sub> triggered by the cation*

The sodium-induced difference spectra demonstrate a diverse effect on the binding capability for each mutant (Fig. 9.1). The mutants Q372C, G379C, F385C, L391C, G395C and Y396C retain a C-less-like signal in the crucial region between 1500 and 1700 cm<sup>-1</sup>, although the level of intensity varies. The IR<sub>diff</sub> spectra reveal variations in the sodium-protein interaction indicated by the relative intensity. The mutant A383C compiles the lowest intensity of around 10% of the cysteine substitutions.

The mutants Q372C, G379C and F385C display a difference spectrum induced by the sodium with relative high intensity compared to C-less. These amino acids are definitely not essential for the cation binding site. The three residues in the putative periplasmic end to the helix or already part of the loop, L391C, G395C and Y396C demonstrate a significant reduction in their spectral intensity. Overall, the spectral features are conserved by all mutants shown by the high amount of spectral similarity between 70 and 90% in respect to the C-less.

Apart from G379C, the glycine was also replaced by a valine with maintains the hydrophobicity but applies a larger side chain in this particular position of the transporter. Evidently, G379V is no more able to bind the cation since it has lost the characteristic features of the difference spectrum.

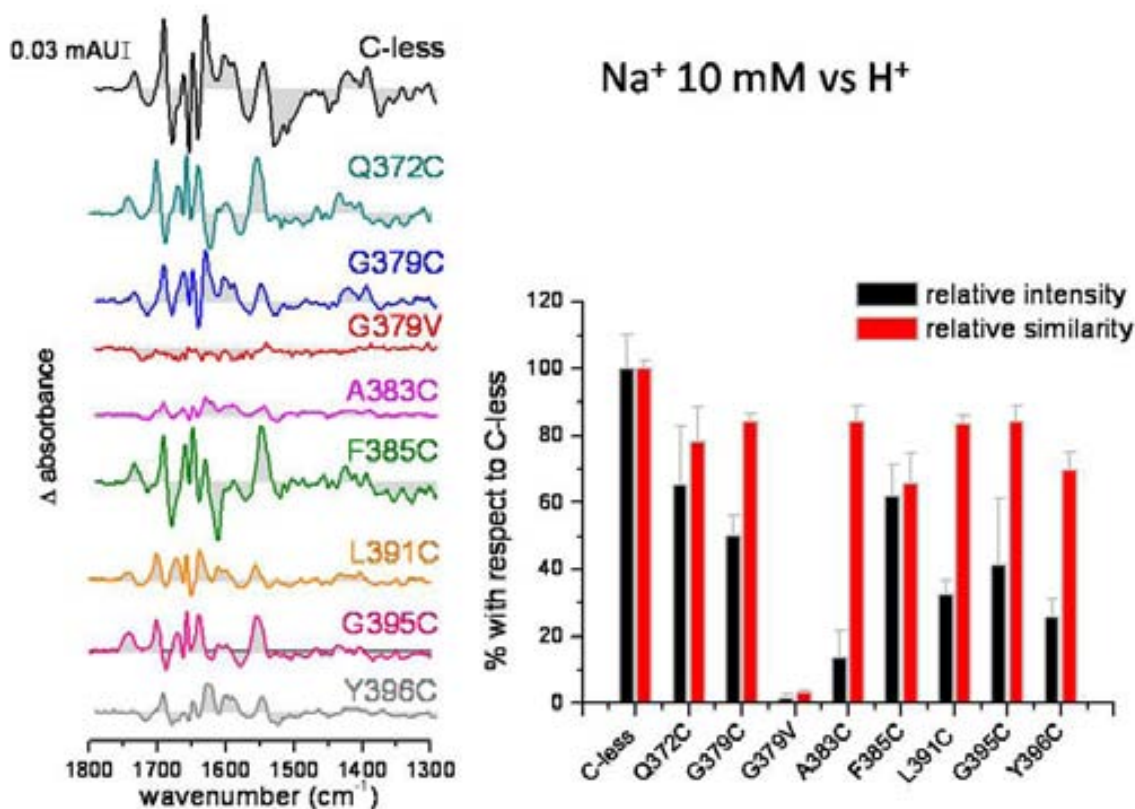


Figure 9.1 IR<sub>diff</sub> spectra mediated by the co-substrate sodium of the mutants of the transmembrane segment XI. In the left panel: difference spectra of all the mutants: C-less (black line), Q372C (cyan line), G379C (blue line), G379V (red line), A383C (magenta line) F385C (olive line), L391C (orange line), G395C (pink line), Y396C (light grey line); in the right panel: difference spectra evaluation using the spectra's first derivative. The displayed spectrum for each mutant is the mean of at least two independent experiments.

## 9.2. Melibiose-mediated IR<sub>diff</sub> of helix XI mutants

The infrared difference spectra for the residue substitutions of helix XI gives a pronounced idea of the modification of sugar binding corroborated by the spectral differences. By evaluating the intensities for the mutant spectra, the substitutions had a much larger impact on the melibiose binding (Fig. 9.2).

Only the Phe-385 can be substituted for a cysteine without reducing the sugar affinity for the transporter. F385C has a difference spectrum with an intensity of about two thirds of the C-less reference. The MelB mutants Q372C and G395C as well as G379C mediate sugar binding even though largely affecting the intensity in the protein-sensitive bands amide I and II.

Ala-383, Leu-391 and Tyr-396 are unfavorable for cysteine replacements. Ding and Wilson already verified the loss of transport<sup>63</sup>. In our study similar conclusions can be drawn by considering that cysteine substitution highly reduces the sugar binding within those mutants.

Above all, the G379V MelB variant is unable to interact with the melibiose in the presence of the cation. Apart from G379V, all other helix XI mutants corroborate a high similarity to the C-less difference spectra of almost 90%. In G379V a melibiose difference spectrum is absent.

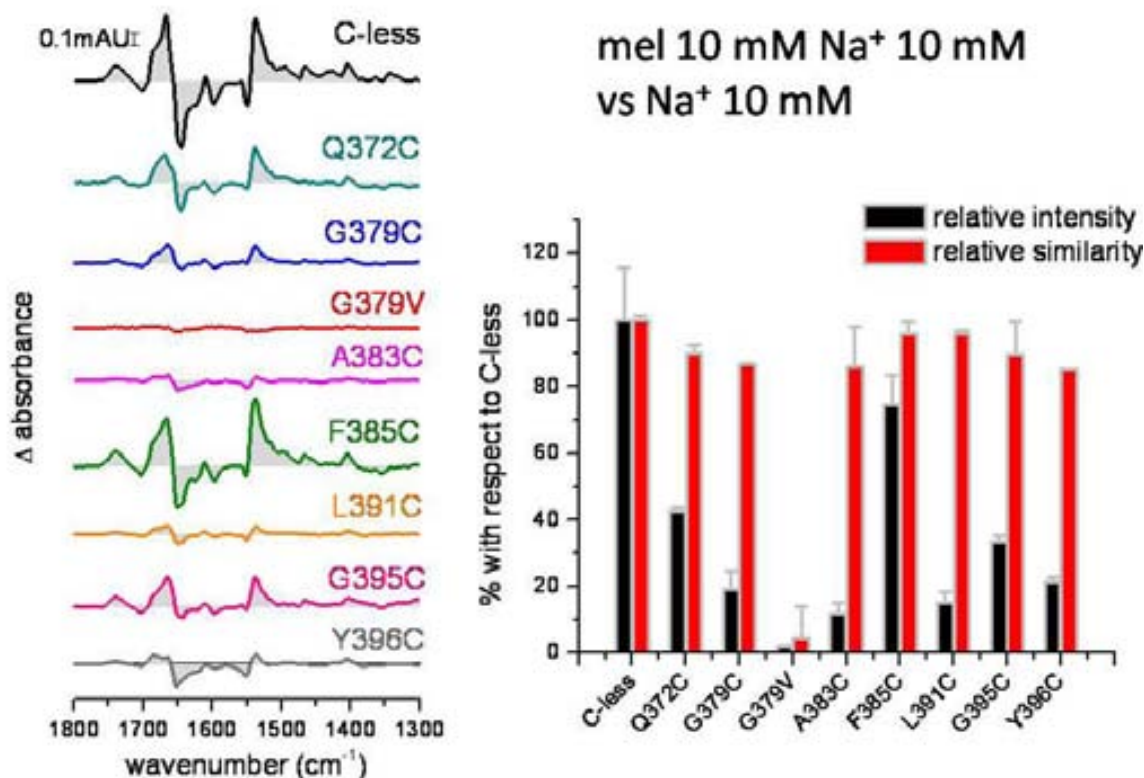


Figure 9.2 Melibiose-induced  $IR_{diff}$  in the presence of the co-substrate sodium of the helix XI mutants. In the left panel: difference spectra of all the mutants: C-less (black line), Q372C (cyan line), G379C (blue line), G379V (red line), A383C (magenta line) F385C (olive line), L391C (orange line), G395C (pink line), Y396C (light grey line); in the right panel: difference spectra evaluation using the spectra's first derivative. The displayed spectra are the mean of at least two independent experiments

By validating the sugar binding in the presence of the proton, it must be stated that the cysteine mutants in helix XI couple the sugar, but the  $IR_{diff}$  spectra vary in their intensities.

The mutant F385C even binds the melibiose with a higher affinity than the control of C-less (Fig. 9.3). The rest of the mutations of the helix XI residues display a reduction of the spectral intensity. Q372C, L391C, G395C and Y396C demonstrate a spectral intensity of around 40-50%. In the case for L391C and Y396C the higher sugar concentration of 50 mM in the presence of the proton enhances the binding affinity compared to the data from the melibiose-induced difference spectra in the presence of the sodium.

The substitutions A383C and G379C demonstrated to low intensity difference spectra triggered by the sugar. The intensity accounts for 25% for the G379C mutant and 15% for the A383C mutant. By regarding all cysteine replacements the  $IR_{diff}$  spectra in the presence of the proton have a large spectral similarity between 70 and 80% like the previous  $IR_{diff}$  spectra in the presence of sodium.

Also the higher amount of melibiose cannot induce sugar binding in the G379V mutant.

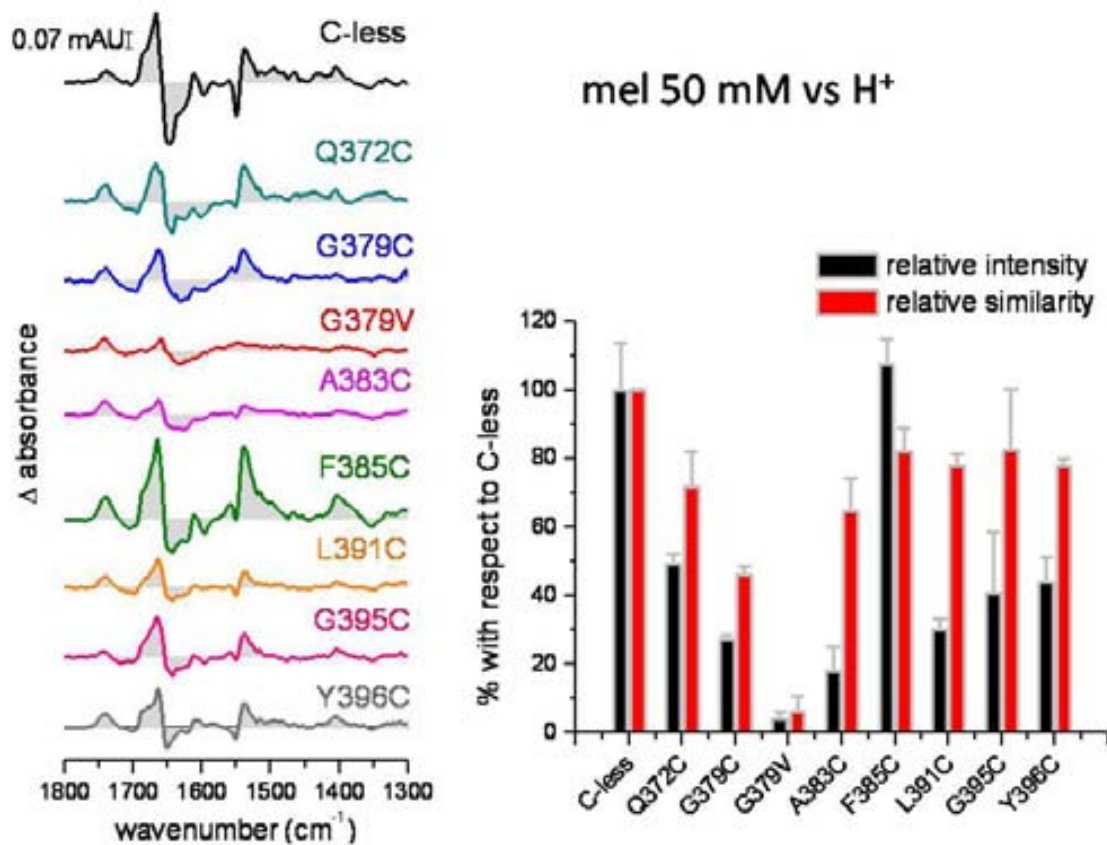


Figure 9.3 Melibiose-induced  $\text{IR}_{\text{diff}}$  in the presence of the proton of the helix XI mutants. In the left panel: difference spectra of all the mutants: C-less (black line), Q372C (cyan line), G379C (blue line), G379V (red line), A383C (magenta line) F385C (olive line), L391C (orange line), G395C (pink line), Y396C (light grey line); in the right panel: difference spectra evaluation using the spectra's first derivative. The displayed spectra are the mean of at least two independent experiments

Only the mutant G379V displays no difference spectrum for the MelB substrates indicating the loss of substrate interaction. All other residues bind the substrates although with less affinity. The phenylalanine is position 385 is neither essential for the sodium nor for the sugar binding, however the mutant is transport defective. The most severe reduction in ligand binding was observed for the A383C mutant. Both substrates bind to MelB but with highly reduced affinity.

The analysis of the absorbance spectrum might aid explaining the reduced liganding. The absorbance spectra of the wet protein film containing the protein-characteristic bands amide I and II have been further investigated by calculating the 2<sup>nd</sup> derivative of the spectrum (Fig. 9.4). This method exposes hidden structural alterations of the MelB protein exclusively based on the single amino acid substitution.

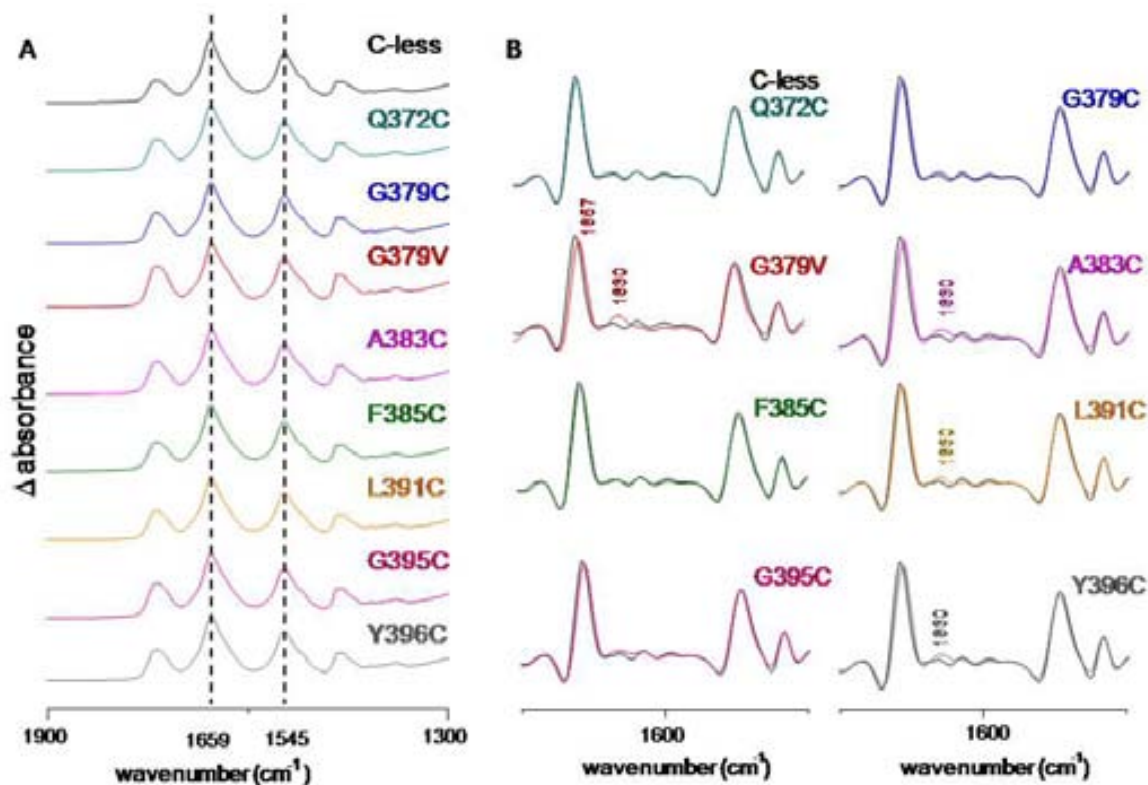


Figure 9.4 Absorbance spectrum comparison between the crucial mutations of helix XI and the C-less reference. In panel A absorbance spectra of the mutants illustrated between the wavenumber 1900 and 1300 cm<sup>-1</sup>. In panel B second derivative of the equivalent absorbance spectra depicted in panel A (truncate for evaluation between 1700 and 1500 cm<sup>-1</sup>). The color scheme is equal for panel A and B. Black line: C-less, cyan line: Q372C, blue line: G379C, red line: G379V, magenta line: A383C, olive line: F385C, orange line: L391C, pink line: G395C and grey line: Y396C.

In Figure 9.4 the qualitative approach of comparing the absorbance spectra of the mutants with the C-less reference demonstrate that the mutants Q372C, G379C, F385C and G395C almost overlap with the C-less spectrum. The mutations do not affect the proportion between  $\alpha$ - and  $\beta$ -structures as it was the case with earlier shown mutants.

Figure 9.5 distributes a quantitative comparison of absorbance spectra of helix XI mutants. The results imply that the band deformation in the region amide I and II correlates perfectly with the obtained IR<sub>diff</sub> results. The mutations of the MelB transporter least affecting the binding of the substrates are Q372C, F385C and G395C. By comparing the differentiated average of the

absorbance spectrum depending on all conditions (melibiose vs H<sup>+</sup>, Na<sup>+</sup> vs H<sup>+</sup> and melibiose·Na<sup>+</sup>

vs Na<sup>+</sup>), it is obvious that the structure retains a similar conformation as the C-less porter.

The mutant G379V in which the substrates sodium and melibiose are not provoking changes of the porter (Fig. 9.1, 9.2 and 9.3) uncover in parallel a distorted structural formation. Especially the pronounced shoulder at

1630 cm<sup>-1</sup> and the shifted peak at 1657cm<sup>-1</sup> align well with former detections of mutations of the melibiose carrier unable to bind its ligands (Lys-377 mutants, see section 1). The peak displacement is associated with an alteration of  $\alpha$ -helical structure, whereas the spectral feature at 1630 cm<sup>-1</sup> is related to a higher amount of  $\beta$ -sheet contexture obviously formed in correlation to the single amino acid substitution.

Apart from the Gly-379-Val mutant, the A383C exhibits similar but slightly less prominent changes of the MelB structure with in turn also explain the highly reduced capacity to bind and further transport the ligands. A383C has an overall similarity of around 92%, whereas G379V resembles less than 90% with the C-less reference.

The most conservative mutations of the helix XI are the Phe-385 and Gln-372 replacements to cysteine. The quantitative analysis states than more 98% of their spectrum matches the control from the fully functional C-less carrier agreeing perfectly well with the visual impression. The ancestral tree in Fig. 9.4 B groups the mutants according to their spectral similarity. Basically, the mutations F385C, Q372C, G395C, L391C and G379C differ only in small details from the expected helical arrangement of the protein, whereas the second group composed of Y396C, A383C and above all G379V display major changes considering the amide region between 1500 and 1700 cm<sup>-1</sup>.

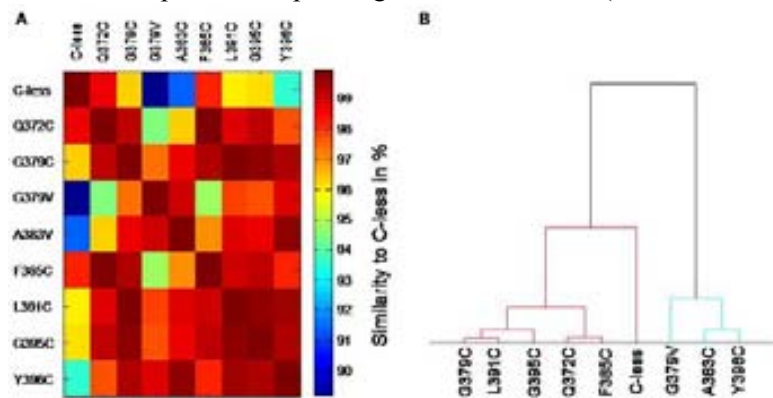


Figure 9.5 comparison of the quantitative comparison of the absorbance spectra between C-less and the mutants. **A** array of the absorbance spectrum similarity using C-less as the reference. **B** dendrogram clustering the helix XI mutants in accordance to their resemblance.

### 9.3. Fluorescence experiments of the helix XI mutants

#### 9.3.1. Intrinsic fluorescence

The data retrieved from the intrinsic fluorescence were assessed for their content regarding the response of the protein's tryptophans upon substrate addition. As the wild-type and the cysteine devoid protein display a characteristic effect, it could be used to draw conclusions for the intrinsic protein alteration due to conformational changes induced by the ligands. Normally, the carrier shows an increase in fluorescence intensity after the addition of the sugar in an aqueous environment. By supplementing further sodium cations, the absolute fluorescence change is even larger than in the presence of protons.

For the mutants of the hydrophobic membrane segment XI, the change in fluorescence is also a suitable control for the previously demonstrated difference spectra generated by the proteins ligands (Fig. 9.6).

For the G379V mutant neither melibiose nor the successive addition of sodium causes an increase in fluorescence emission of the Trp's. Therefore the earlier drawn conclusion from the ATR-FTIR is confirmed that G379V lacks interaction with the substrates.

Extracted from fluorescence data, it can be stated that the mutants L391C and Y396C have a relatively small increase of the intrinsic fluorescence while forming the tertiary complex consisting of the  $\alpha$ -galactoside sugar, the cation and MelB.

The mutants F385C, Q372C and G395C corroborate a normal binding mode with the sugar and the cation in the infrared spectroscopy. The data also prove this outcome to be valid by their similar fluorescence response in the presence of the substrates (Fig. 9.6). Only the result for the single mutant A383C varies from the difference spectra data. Exhibiting only traces of substrate binding by  $IR_{diff}$ , the signal mediated by the tryptophans is much more significant by reaching almost half the  $\Delta F/F_0$  value as from the control protein, C-less.

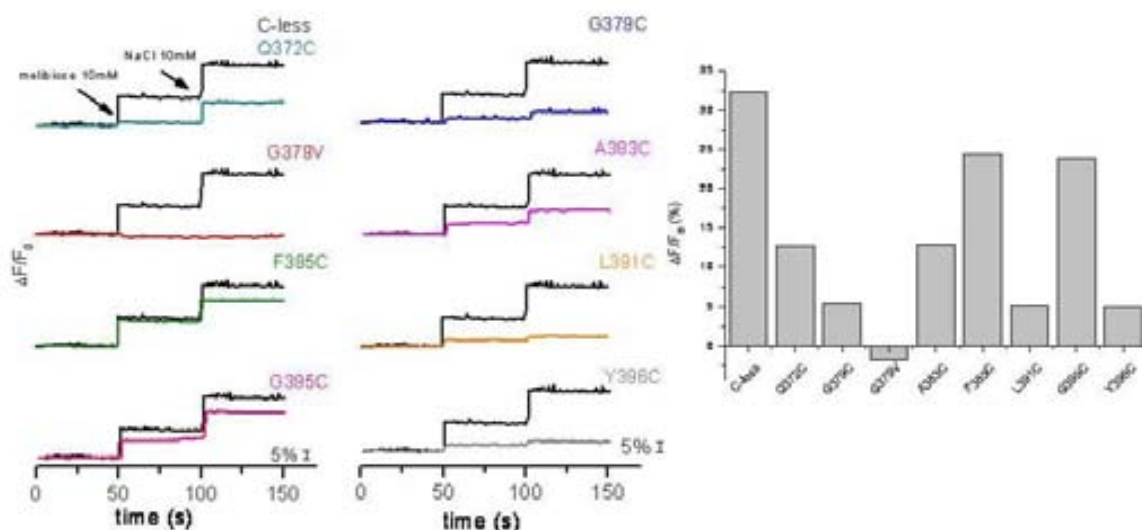


Figure 9.6 Intrinsic fluorescence using an excitation wavelength of 290 nm and acquiring the tryptophanyl response at 325 nm (emission maximum). On the left side: kinetic fluorescence spectra of the mutants of the helix XI. On the right side bar graph implementing the emission change based on substrate binding to the MelB mutants. As indicated only in the upper left corner by the arrows: for all mutants after 50 sec addition of 10 mM melibiose and after further 50 sec addition of 10 mM sodium.

### 9.3.2. FRET experiments

The  $D^2G$  sugar energy transfer verifies our expectations that most of the mutants of helix XI bind the sugar analog, although with different affinities.

In Figure 9.7 the FRET data are in agreement with the obtained results. Even the  $D^2G$  possesses unlike the melibiose a beta configuration, MelB recognizes the sugar analog. Nevertheless, the dansylated sugar is not transported and is a competitive inhibitor of the sugar binding site. Regarding the FRET data, F385C and G395C are the only 2 mutants exemplifying an energy transfer between the intrinsic Trp's and the dansyl group that is comparable to C-less in its intensity (Fig. 9.7).

A reduced FRET was detected in the mutants G379C, L391C and Q372C. The data for G379C and L391C are in agreement with the previous results from infrared difference and fluorescence spectroscopy. The mutant Q372C binds the fluorescent sugar  $D^2G$ , but however the addition of sodium does not induce further FRET signal augmentation at 465 nm as expected. The preference might be related to the different enantiomeric configuration of the sugar molecule.

The mutants Y396C and A383C demonstrate insignificant interaction between the transporter and the fluorescent acceptor molecule D<sup>2</sup>G which is in line of the data collected in the combination with melibiose as primer conformational trigger.

The mutant G379V is the only MelB variant where the FRET is entirely absent. This result is not surprising since in ATR-FTIR the difference spectra were feature-less and in the fluorescence time-course a substrate-induced signal increase was not detectable. Only hints of difference spectrum were detected at 50 melibiose in the presence of the proton. A massively reduced sugar affinity might be the reason in the G379V mutant.

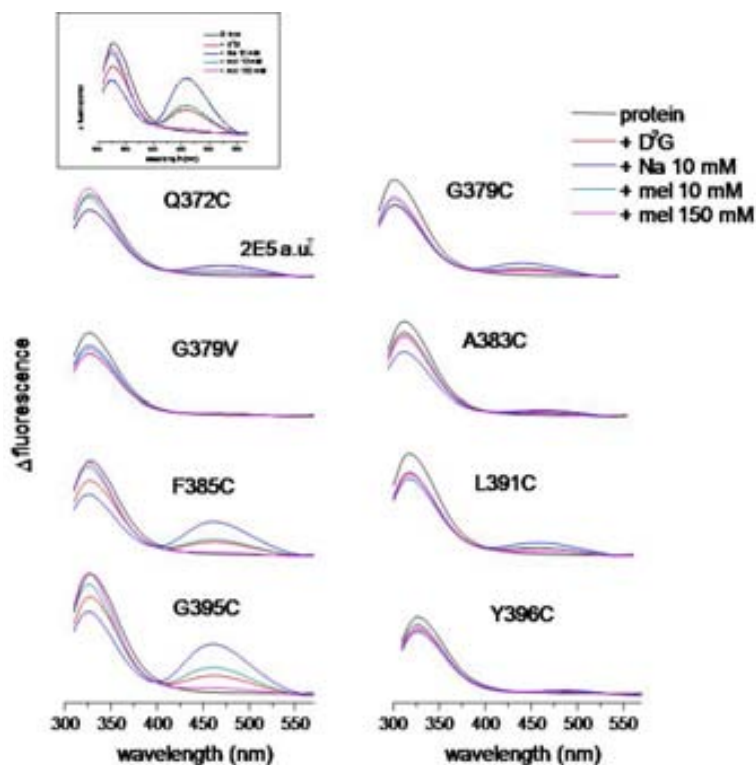


Figure 9.7 FRET analysis of the helix XI mutants. squared Figure in the top left corner exemplifies the FRET of the C-less mutant as a positive reference. Legend on the right explains that the black line demonstrates the sole MelB mutant protein, the red line: MelB mutant + 16  $\mu$ M D<sup>2</sup>G, blue line: MelB mutant + 16  $\mu$ M D<sup>2</sup>G + 10 mM NaCl, cyan line: MelB mutant + 16  $\mu$ M D<sup>2</sup>G + 10 mM NaCl + melibiose 10 mM, magenta line: MelB mutant + 16  $\mu$ M D<sup>2</sup>G + 10 mM NaCl + melibiose 150 mM

#### *9.4. Labeling of cysteines in helix XI with the fluorescent probe MIANS*

The fluorescent probe MIANS (2-(4'-maleimidylanilino)naphthalene-6- sulfonic acid) specifically detects the cysteine residues of the carrier protein. Apart from G379V, all other generated mutants are composed of one cysteine. This individual cysteine contains the only reactive sulfhydryl side chain for the interaction with the MIANS probe. The fluorescence probe can be excited directly when present in aqueous solution together with the MelB-proteoliposomes.

Its fluorescence only increases when bound to a cysteine. The time-course data can be validated by comparing the interaction between MIANS and MelB in different states. Different buffer compositions describe the reactivity of the fluorescent probe with the cysteine. MIANS

prefers an apolar surrounding.

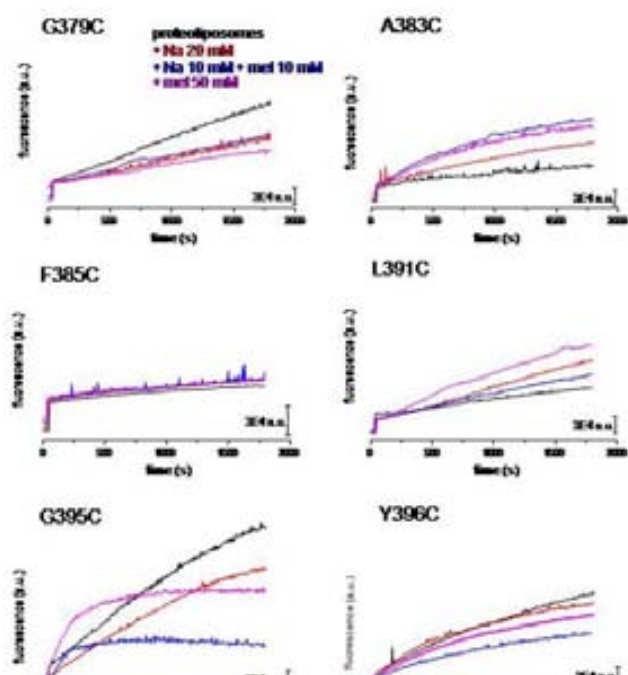


Figure 9.8 MIANS data of the cysteine mutants of helix XI.

in the presence of the sugar. For the co-substrate and substrate-less sample the interaction is slower manifested by a linear curve (Fig. 9.8 A383C).

The F385C mutant propagates a C-less like behavior under all conditions. The cysteine seems to be enclosed in a polar surrounding manifesting that F385C might be facing the aqueous channel relatively close to the substrate binding sites. Neither the presence of the sugar nor the sodium modifies the interaction between MIANS and the transporter in terms of intensity and reactivity rate. The results obtained for the mutant L391C are difficult to interpret. Under all conditions the reaction follows a linear behavior like G379C. The data demonstrates a reduced reactivity between the fluorescent probe and the cysteine. The residue may reside in a more polar environment like L391C. The fluorescent probe MIANS exhibits much higher susceptibility for G395C for interacting with the probe in the presence of the sugar. A relatively slow alkylation occurs in the empty and cation loaded state, whereas the sugar initiates a fast reaction which might be due to an altered accessibility or a tilting in the helix. The tilting of the helix could induce a change in the microenvironment from a hydrophilic to a more apolar surrounding. After adding melibiose, the cysteine-MIANS complex is almost entirely formed after just 500 sec. The reactivity of the empty transporter or in the presence of sodium is much more reduced (Fig. 9.8).

The empty transporter in the mutant Y396C does not interact quickly with the MIANS probe. Each substrate reduces the level of fluorescence intensity stepwise. When both substrates are present, the binding of MIANS with the Y396C cysteine is relatively slow and compared to the other conditions to low signal intensity.

MIANS time course experiments were acquired in four different conditions to assess if the substrates affect the reactivity of the fluorescent probe with the transporter; without substrates, with just sodium or melibiose and finally with sodium and melibiose as the main substrates together. The MIANS data of G379C are similar for all conditions. Remarkably the interaction of MIANS with the cysteine is relatively slow which might indicate that the cysteine is embedded in a polar environment.

A383C demonstrates a faster interaction with the probe where plateau phase is reached after 30 min

## 9.5. Examining the FRET in membrane vesicles of the mutants from helix XI

For the mutants in the transmembrane helix XI the vesicle approach could strengthen the results from the purified MelB transporter. The interpretation of the FRET data is not straightforward. The vesicles contain apart from the overexpressed melibiose permease several other membrane-bound proteins and polypeptides which could ultimately interfere by enhancing the background.

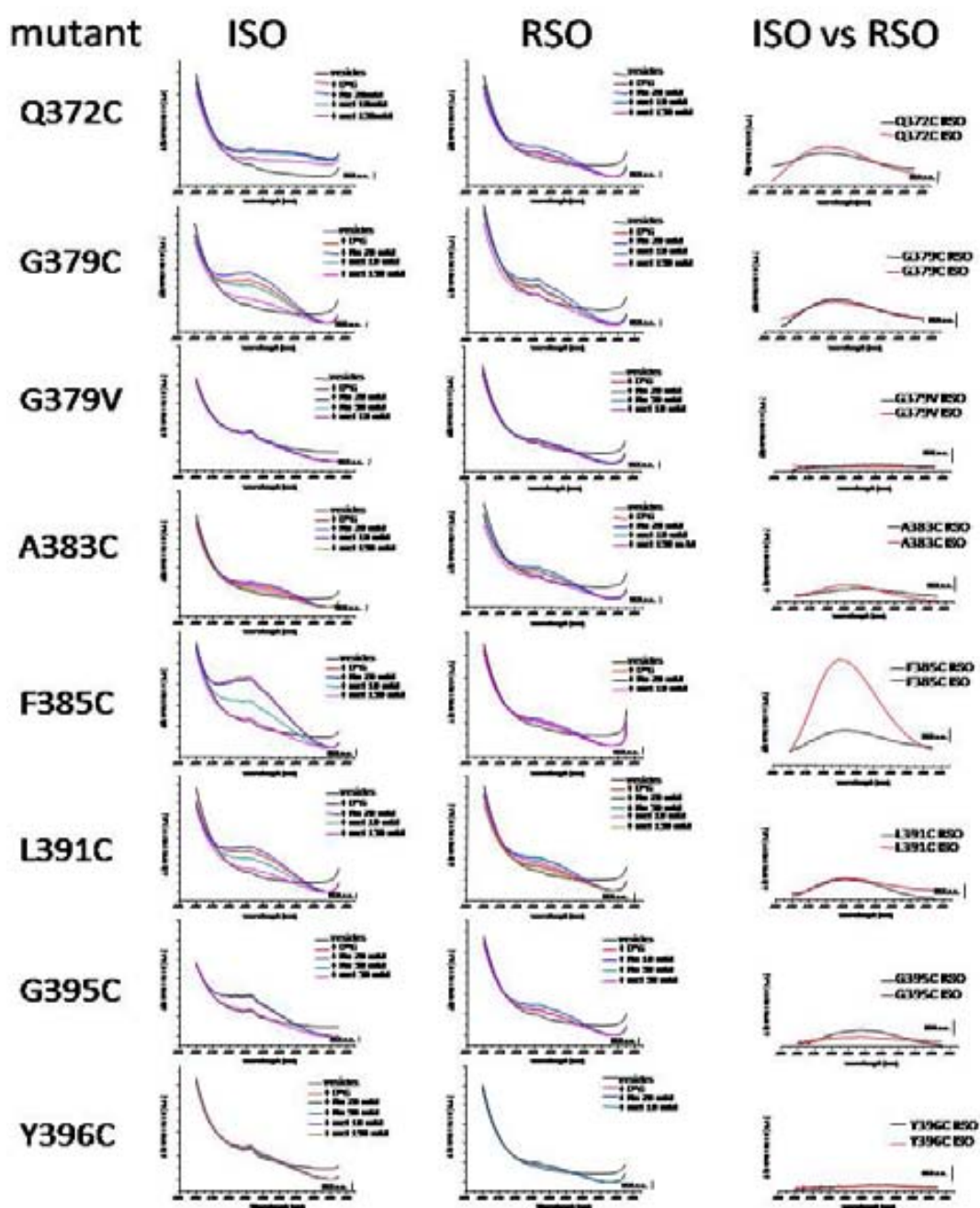


Figure 9.9 Vesicles of the helix XI mutants, first column illustrates the inside-out (ISO) vesicles, the second

## RESULTS

column depicts the right-side-out (RSO) form, the last column describes the fluorescence increase after adding 20 mM sodium to the vesicles-D<sup>2</sup>G-complex. The scaling bar in the last column is identical for the rest of the vesicles from the same mutant ordered by rows. The result is the mean of two independent experiments.

These FRET data suit as well for a qualitative comparison of the mutant in the unpurified form in a polymorph membrane environment versus the reconstituted pure membrane transporter after protein purification. By comparing the FRET data of the proteoliposomes from chapter 9.3 to the proteoliposomes, the mutants G379C, L391C and Q372C exhibit a similar FRET signal in both types of vesicles. The co-substrate sodium mediates a relatively small increase in the fluorescence emission of D<sup>2</sup>G.

No fluorescence energy transfer was detected in the ISO and RSO membrane fractions of mutant G379V which is in line with the results from the mutant re-embedded into the liposomes. Hence, the mutant lacks the interaction with the sugar per se and not because of structural alterations during the purification process.

The vesicles of the mutant A383C demonstrate a small energy transfer in the presence of the co-substrate and the D<sup>2</sup>G fluorescent sugar. This result in turn confirms the A383C data acquired by ATR-FTIR, where the sugar only provokes a tiny difference spectrum.

The Y396C MelB variant which is defective in accumulating the  $\alpha$ -galactoside sugar, fails to show evidences for a sodium-dependent FRET in the prepared vesicles. In both types of vesicles the calculated rise in fluorescence after adding the co-substrate resulted in a feature-less line similar to the non-binding G379V mutant.

The mutant G395C manifested a C-less like behavior in its LAPAO-purified form.

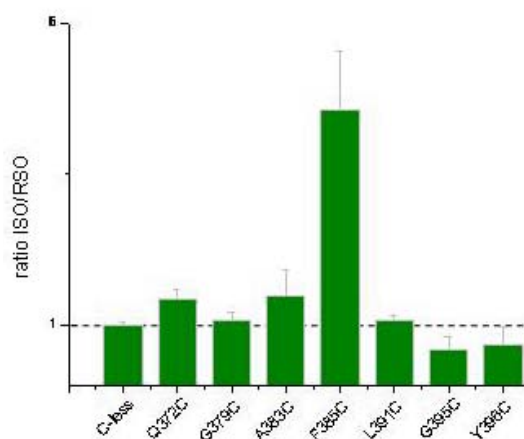


Figure 9.10 ISO/RSO ratio of the mutants from the helix XI using the maximum of the D<sup>2</sup>G emission at 465 nm. The Data is based on at least two independent acquisitions for each vesicle form.

the mutant presents a rigid FRET signal alike the one obtained from the purified protein. On the other side, the right side out form of this mutant produce only minor differences after exciting the tryptophan residues.

Extraordinarily, the FRET from the vesicles does not correspond to the proteoliposomes. Especially, the inside-out vesicles hardly provide any sodium-dependent FRET signal, although from the data it seems that the dansyl-sugar grants a significant increase in fluorescence (Fig. 9.8 G395C ISO graph) which does not amplify after adding 20 mM sodium. The reason for that might be manifold. Many parameters influence the fluorescence spectroscopy and even more in membrane vesicles.

The most striking result delivers the mutant F385C. In the inside-out vesicle form

To better correlate the obtained results with each other, the fluorescence increment was calculated at the D<sup>2</sup>G maximum for ISO and RSO respectively. As mentioned beforehand, the ratio between ISO and RSO should generate normally a value close to 1. Figure 9.9 points out that apart from some smaller alterations the majority of the mutants display an expected ratio. Only the MelB mutant F385C stands out by having a larger fluorescence change in the inside-out compared to the right-side-out membrane vesicles. The calculation generates an almost five-fold higher signal increase in the ISO than in the RSO vesicles. The results for the mutant G379V has been excluded from the Figure, because this mutant denies an indication of binding of the fluorescent sugar in the vesicles.

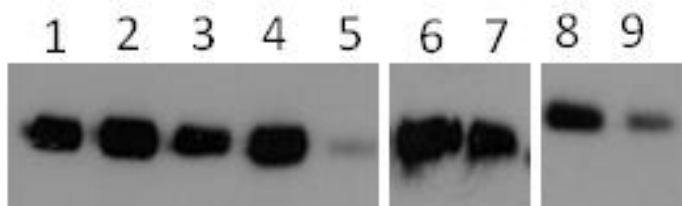


Figure 9.11 Vesicles from helix XI mutants labeled by His-Probe<sup>TM</sup>-HRP. lane 1: C-less control (proteoliposomes – 250 ng), lane 2: A383C ISO (5 µg total protein), lane 3: A383C RSO (5 µg), lane 4: Y396C ISO (5 µg), lane 5: Y396C RSO (5 µg), lane 6: F385C ISO (1.5 µg), lane 7: F385C RSO (5 µg), lane 8: G379V ISO (10 µg), lane 9: G379V RSO (10 µg).

The mutants G395C and Y396C offer a value that is lower than 1. In the case of the Y396C mutant, the variability of the signal in relatively low intensity range might explain the reduced ratio. In the case of the Gly-395, the detected signal in the ISO vesicles is considerably lower than in the corresponding RSO vesicles. The reason has not been established yet. Another aspect that needs clarification is the amount of

expression for each mutant. Therefore, the data were not intercorrelated between the mutants because of this variability in expression.

In Fig. 9.11, we used the specific reagent His-Probe<sup>TM</sup>-HRP for the detection of the MelB protein in each vesicle form of the mutants G379V, A383C, F385C and Y396C. For the mutants G379V, A383C and Y396C, the lack of FRET in the vesicles is related to the single amino acid replacement. A low protein expression can be excluded since all mutated MelB transporters are expressed fairly well in the vesicles. Only Y396C in the RSO vesicles was detected as a faint band which is related to the preparation variability.

## 10. Trp-342, a suggested participant in sugar binding

### 10.1. Phenotype of W342C

The tryptophanyl residue from the MelB porter was described as a residue closely residing the sugar binding site. First fluorescence approaches replacing Trp-342 by the related phenylalanine led to a misplaced FRET signal indicating a more hydrophilic surrounding.

In our experiments W342 was replaced by cysteine to verify the effect of substrate binding.

After plating the MelB variant on a MacConkey agar plate,



Figure 10.2 W342C mutant on a MacConkey agar plate supplemented with 10 mM melibiose.

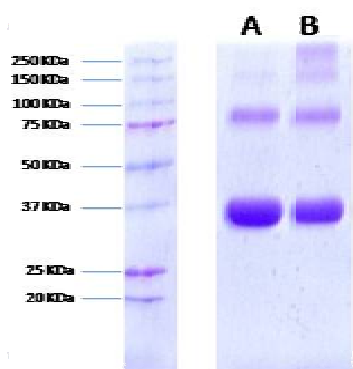


Figure 10.1 **A** W342C soluble protein purified from Ni-NTA resin; **B** W342C reconstituted into proteoliposomes from *E.coli* total lipid extract

the grown colonies exhibit a red color indicating a pH change due to metabolisation of the melibiose (Fig. 10.2). This mutant was never validated

considering the level of protein expression but the preparation of a 4 L culture delivered a sufficient amount for reconstitution and subsequent analysis. The purification of that mutant was performed under normal circumstances by LAPAO as the solubilizing surfactant. Apart from the common oligomer formation, Detergent-solubilised and reconstituted protein exhibit a highly pure monomer fraction without observable cleavage pattern due to protease activity (Fig. 10.1). Upper bands at a molecular weight of 75, 150 and around 300 KDa occur due to oligomer formation of the MelB transporter.

## 10.2. W342C – $IR_{diff}$ spectra

### 10.2.1. Sodium-induced difference spectrum

By assessing the difference spectrum obtained for W342C for 10 mM  $Na^+$  in the presence of the proton, it is obvious that the MelB variant retains sodium binding. The cation binding although differs from the C-less reference spectrum. Arguably, the amide I region demonstrates various alterations. The most prominent is the strong enhancement of the negative peak at  $1650\text{ cm}^{-1}$  (Fig. 10.3) which was shown for loop 10-11 mutants in the chapter 2 to the results section.

Beyond that, the former positive peaks at  $1660\text{ cm}^{-1}$  (amide I) and  $1550\text{ cm}^{-1}$  (amide II) totally disappeared. And even the positive peak at  $1640\text{ cm}^{-1}$  lost dramatically in intensity. The quantification was

performed by using the first derivative of the sodium-induced spectrum and correlate the spectrum to the C-less reference spectrum. This result gives a more convenient determination of the spectral resemblance between W342C and C-less and its sodium binding fashion.

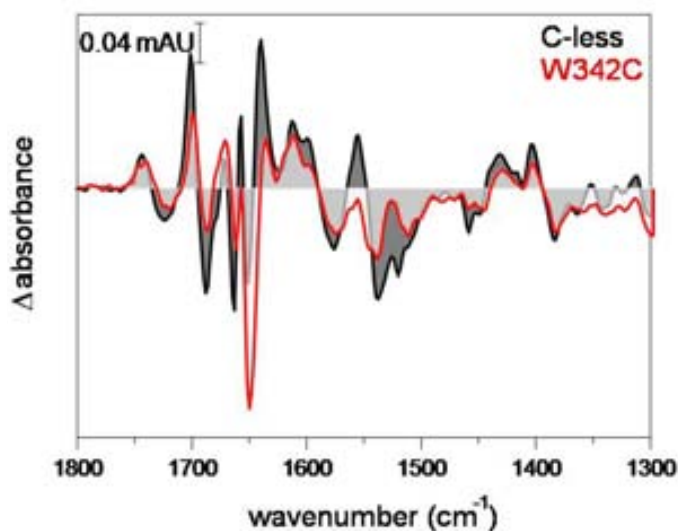


Figure 10.3 sodium-induced  $IR_{diff}$  of C-less (black line) and W342 (red line). Protein films of MelB variants in 20 mM MES, 100 mM KCl, 10 mM NaCl, pH 6.6 minus the same films in 20 mM MES, 110 mM KCl, pH 6.6

### 10.2.2. melibiose-induced IR<sub>diff</sub> spectrum

The melibiose-induced difference spectrum has been examined in the presence of sodium and the proton. In the case of the melibiose-dependent difference spectrum in the presence of sodium, W342C signal intensity decreases drastically to 44% (Fig. 10.4) in reference to the spectrum for the wild-type-like C-less MelB. Especially, the positive peaks at 1660 (amide I) and 1540 cm<sup>-1</sup> are greatly reduced in intensity (Fig. 10.4).

Strikingly, the melibiose binding efficiency enhances when mediated only by the proton. W342C has been reported to presumably reside close to the sugar binding side. ATR-FTIR experiments done using the melibiose·H<sup>+</sup>·MelB tertiary complex pronounce the

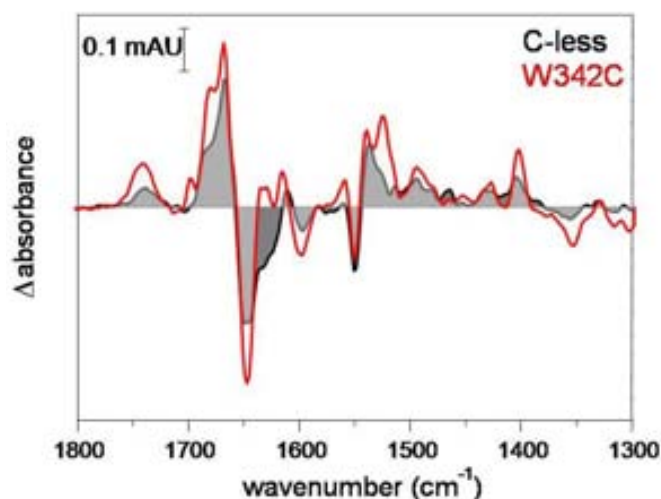


Figure 10.5 Difference spectrum due to melibiose binding (50 mM), in the presence of the proton. Dark grey with black line: C-less and light grey with red line: W342C, buffer composition with substrate: 20 mM MES, 100 mM KCl, 50 mM melibiose, pH 6.6; reference buffer: 20 mM MES, 100 mM KCl, pH 6.6.

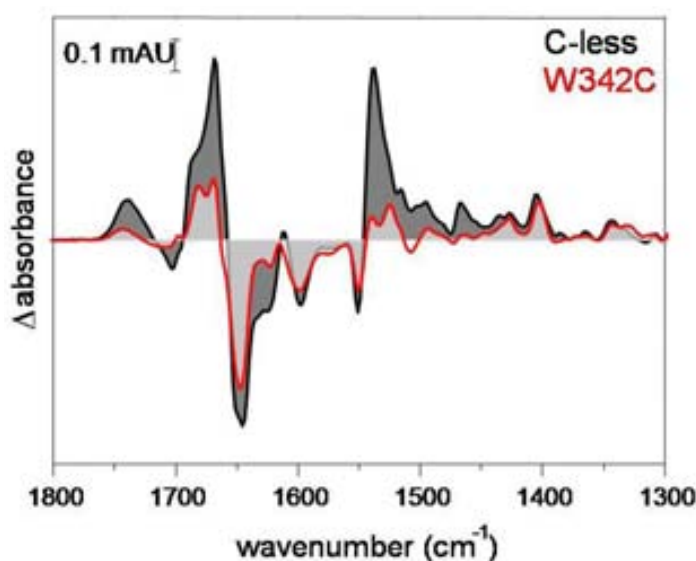


Figure 10.4 melibiose-induced IR<sub>diff</sub> in the presence of sodium. In dark grey with black line: ATR-FTIR difference spectrum of C-less, in light grey with red line: W342C difference spectrum due to melibiose interaction. Substrate buffer contains 20 mM MES, 100 mM KCl, 10 mM NaCl, 10 mM melibiose, pH 6.6 whereas the reference buffer is composed of 20 mM MES, 100 mM KCl, 10 mM NaCl, pH 6.6.

slightly increase melibiose binding in the W342C compared to the referential C-less spectrum. Pronounced alterations occur in the amide I region (Fig. 10.5). At 1699 cm<sup>-1</sup> a new positive peak appears which is not present in the C-less background spectrum. Furthermore, the peaks at 1680 (+) cm<sup>-1</sup> and at 1647 (-) cm<sup>-1</sup> are more intense. The peak at 1633 and 1631 cm<sup>-1</sup> respectively are positive whereas in the melibiose-induced IR<sub>diff</sub> of C-less these peaks are negatively oriented.

Considering the amide II region, the biggest change occurs for the peak at

1524 (+)  $\text{cm}^{-1}$ . This peak is much more pronounced in the W342C mutant than it is in the C-less control.

Apart from the qualitative analysis of the infrared difference spectra induced by the substrates of MelB, a more discrete approach has been undermined by comparing quantitatively the spectral features using the first derivative of both MelB variants as shown before.

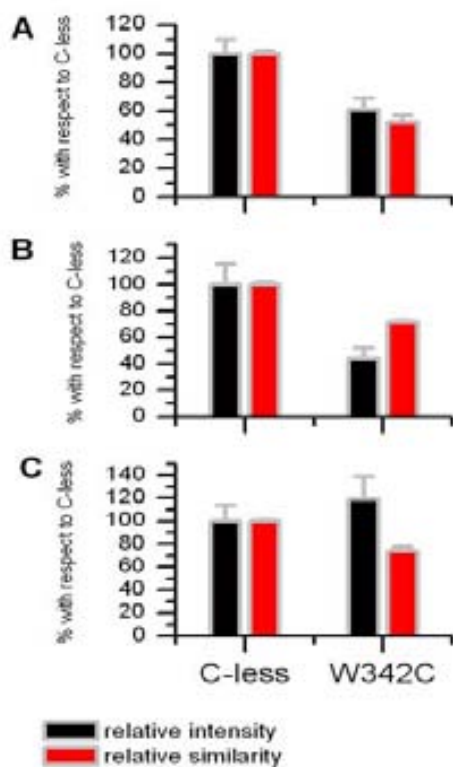


Figure 10.6 intensity and similarity comparison of the  $\text{IR}_{\text{diff}}$  of C-less and W342C. **A** data evaluation using the difference spectra induced by sodium (10 mM), see fig. 3.3; **B** data evaluation using the difference spectra induced by melibiose (10 mM) in the presence of sodium (10 mM), see fig. 3.4; **C** data evaluation using the difference spectra induced by melibiose (50 mM) in the presence of the proton, see fig. 3.5.

### 10.3. Fluorescence spectra of W342C

The fluorescence spectroscopy suits as a valuable technique to prove tryptophanyl response due to substrate interaction with the membrane protein. For W342C, the supplementation of both substrates (sodium and melibiose) results in a signal increase ( $\Delta F/F_0$ ) of approximately 10%. This increase relates well to the ~30% change occurring for C-less.

Kinetics obtained for W342C can be matched to the melibiose-dependent  $\text{IR}_{\text{diff}}$  spectrum in the presence of sodium which gives a similar signal intensity of around 40% compared to C-less.

Comparing the melibiose-mediated increase of the intrinsic fluorescence in the presence of the proton to the  $\text{IR}_{\text{diff}}$  spectrum, it is obvious that W342C exhibits a smaller signal in fluorescence spectroscopy. The reason is the lower concentration of just 10 mM melibiose addition in the fluorescence experiment, whereas  $\text{IR}_{\text{diff}}$  spectra were acquired for 50 mM

melibiose. The small signal indicates a reduced affinity for the substrate whereas 50 mM substrate causes the same intensity in the  $IR_{diff}$  as the C-less control.

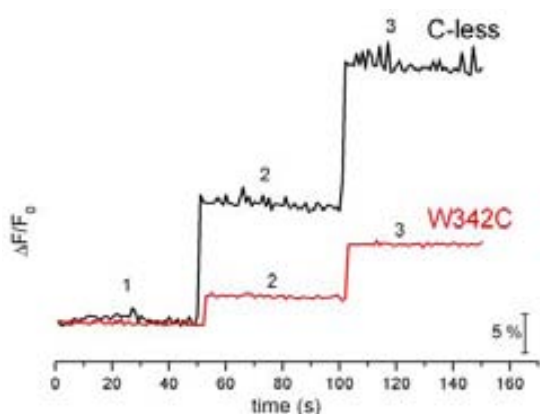


Figure 10.7 kinetic intrinsic Trp fluorescence emission of W342C (red line) compared to C-less (black line) measured at excitation of 290 nm and emission at 310 nm; Buffer composition 0.1 M KPi, 0.1 M KCl, pH 7.0; 1 MelB mutants proteoliposomes, 2 addition of 10 mM melibiose; 3 addition of 10 mM NaCl.  $F_0$  is the maximum emission of the intrinsic Trp fluorescence in an unbound state of MelB.

#### 10.4. Fluorescence energy transfer mediated by fluorescent sugar

FRET analyses of W342C confirmed the results obtained from infrared difference spectra.

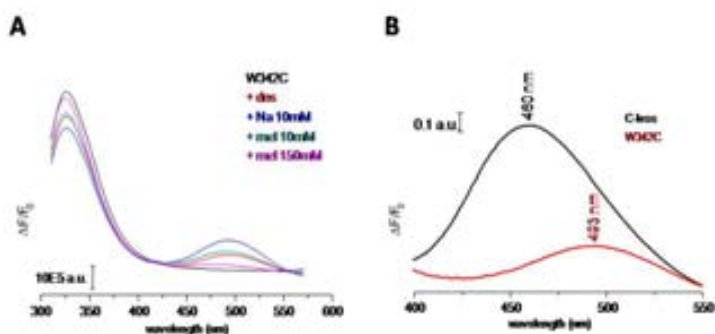


Figure 10.8 **A** FRET signal from W342C; in black: W342C proteoliposomes, in red: after adding 15  $\mu$ M Dns<sup>2</sup>-S-Gal, in blue: after adding 10 mM NaCl, in cyan: after adding 10 mM melibiose, in pink: after adding 150 mM melibiose. **B** amplified FRET spectra of W342C (red) and C-less (black) proteoliposomes after supplementation of 15  $\mu$ M Dns<sup>2</sup>-S-Gal and 10 mM NaCl. The buffer composition in all cases was 0.1 M KPi, 0.1 M KCl, pH 7.0. The spectra were corrected for the influence of the free fluorescent sugar in solution.

The sugar derivative D<sup>2</sup>G binds to the protein verified by energy transfer from the tryptophanyl residues towards the dansyl group of the fluorescence probe. Additionally, sodium binding induces further energy transfer (Fig. 10.8 A). The FRET signal overall is less intense than in the cysteine-less protein confirming the result from  $IR_{diff}$  and intrinsic fluorescence. Strikingly, by comparing the maxima of the D<sup>2</sup>G-dependent FRET signal of

W342C and C-less, it is obvious that the residue replacement of Trp-342 causes a shift towards higher wavelengths (Fig. 10.8 B). This variation indicates that the sugar molecule is embedded in a more hydrophilic moiety within the protein. A similar observation was already revealed when Trp-342 was replaced by the aromatic amino acid phenylalanine<sup>126</sup>.

The reduced hydrophobicity in proximity of W342C indicates that this residue is probably located near the aqueous channel of the transporter. On the other hand, the W342C mutant binds the substrates fairly well but with a potentially reduced affinity for the sugar. The sugar-induced difference spectrum in the presence of the proton ( $\text{mel}\cdot\text{H}^+$  vs  $\text{H}^+$ ) indicates a similar binding as in the C-less reference. For the sodium, the spectral intensity is reduced to just 40% compared to the MelB without cysteines.

#### 10.4.1. Fluorescence probe

##### - MIANS

The fluorescence probe MIANS represents a useful tool to study the interaction with cysteinyl thiol groups. The sole compound emits very little fluorescence. Only when reacted with a cyteineyl residue.

Obviously, W342C interacts with MIANS indicated by the increase in fluorescence intensity. But the velocity of the reaction is reduced and leads to linear rather than exponential curve. The presence of the substrates has no effect of the accessibility of the cysteine residues. One must take into account that the fluorescent probe prefers hydrophobic surroundings. As demonstrated by a shifted FRET maximum, the residue in position 342 apparently possesses a hydrophilic microenvironment. Under these circumstances, one might expect, the proximity to the aqueous channel which in turn deteriorates the accessibility by MIANS.

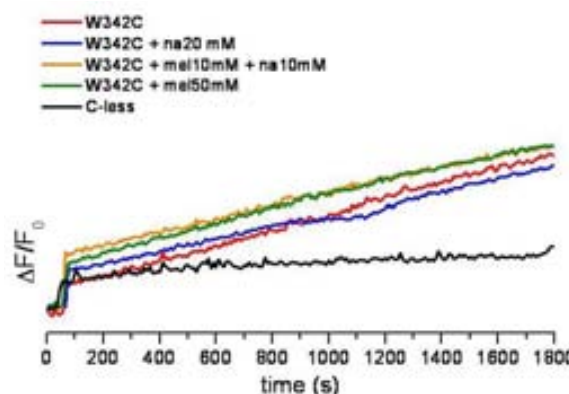


Figure 10.9 MIANS reactivity with W342C MelB mutant with different substrate composition. All conditions are the mean of two independent experiments.



## DISCUSSION

### 11. Proteoliposomes vs vesicles – chances and boundaries

The sugar co-transporter melibiose permease from *E. coli* symbolizes an ideal carrier protein for the study of the secondary active transport. A major benefit of this prokaryotic symporter is the relatively straightforward sample preparation based on the high expression yield. The well-established purification delivers large amounts of functional protein compared to eukaryotic membrane protein where post-translational modifications complicate the process. The solubilization of MelB from the membrane is done in principle by LAPAO and the presence of a high concentration of sodium ions ensures the stability of MelB.

The data presented in the previous sections are foremost based on biophysical and biochemical methodologies. The generated point mutations of the membrane transporter MelB from *Escherichia coli* were extensively studied by ATR-FTIR and fluorescence spectroscopy. The data set was acquired from proteoliposomes containing the purified transport protein and from membrane vesicles corresponding to each MelB mutant.

The main advantage of the proteoliposomes is the purity of the transporter, since it is the only protein contained into the proteoliposomes. Being able to reconstitute MelB, the protein has to be extracted from the membrane by hydrophobic agents called detergents. Depending on the type of detergent, the solubilization efficiency varies vastly. Some surfactants cause a complete solubilization of the entire lipid bilayer<sup>195</sup>. Other milder detergents solubilize the membrane in larger fragments and generate also bicelles; a mixture of detergent and lipid. Usually, the detergent micelles protect the membrane proteins from the hydrophilic surrounding which can cause unfolding or precipitation of the polypeptides.

After solubilization from the membrane, the nickel-affinity chromatography is the selective step during the purification of MelB. The genetically engineered C-terminal six histidines attach the protein to a polymer matrix of nickel-ions. Several washing steps with different buffers gradually reduce the contamination with other membrane proteins.

In the final reconstitution, the hydrophobic polypeptide protected by micelles is re-embedded into an amphiphilic liposome, hence proteoliposome. In the case of the wild-type carrier, the reconstitution process into natural *E. coli* lipids generates a fully functional MelB transporter. The crucial process of insertion into the lipid bilayer can be validated by using the absorbance spectrum of either the dry or the wet protein film in infrared spectroscopy (ATR-FTIR). The wet proteoliposome film represents the physiological conditions and is therefore preferential.

The only part of the purification which cannot be assessed is the effect of the solubilization of the protein with the detergent.

Pourcher *et al.* validated the efficiency of different classes of detergents during extraction from the membrane. LAPAO alongside with SB12 exhibit the highest efficiency for MelB extraction<sup>40</sup>. But for LAPAO, only the presence of a high concentration of NaCl or LiCl conserved the function of wild-type MelB. The zwitter-ionic detergent SB12 inactivates the transporter completely in all probed conditions and therefore is undesirable. Since LAPAO retains the activity of MelB in the presence of a high sodium concentration of 600 mM and simultaneously achieves a high rate of solubilization, the detergent was used as the standard surfactant during the preparation of the MelB mutants.

The second approach for mutant characterization uses only polymorphous membrane vesicles with multiple membrane proteins or membrane-attached proteins.

The preparation of those vesicles offers several advantages. First, the methodology is relatively straightforward based on well-established protocols used for several decades<sup>156</sup>. The time consumption to obtain the pure vesicles is considerably small and simultaneously less materials is required.

The biggest advantage however, is the absence of the protein solubilization. The extraction of the protein from the membrane by detergent might affect the protein conformation. Depending on the chemical composition of the detergent, the lipid bilayer is completely degenerated<sup>195</sup> and the protein conserved in amphiphilic micelles adopts an intermediate conformation inconvenient in terms of functionality. The two types of membrane vesicles, Inside-out (ISO) and right-side-out (RSO) vesicles differ from each other considering the orientation of the cytosol-facing membrane side. Both types were prepared originating from the same batch of cell culture to avoid influential parameters as the protein expression and growth rate. Aside the different size between RSO and ISO vesicles, both forms also contain different quantities of proteins on their surfaces. ISO vesicles usually contain a larger amount of protein in the surface than the RSO form, because of the crucial class of membrane-attached proteins mediating signals from the exterior towards the nucleus by phosphorylation.

The assessment of the vesicles however bears some limitations. The easily prepared vesicles are comprised of a bulk of membrane proteins. Techniques for the specifically detecting vesicles are limited. Western blotting and labeling with specific dyes are used as quantification methods for protein expression yields. Transport assays using radioactive labeled sugars were used to validate catalytic activities of the MelB transporter in vesicles.

The approach using the ATR difference spectroscopy for MelB vesicles seems an attractive alternative to study the substrate interaction directly without purification.

The melibiose sugar is a rare substrate of membrane proteins, whereas sodium is targeted by many proteins as a potential ligand. Since LacY is deleted in our experimental *E. coli* strain, the only melibiose-transporter is MelB. But even though MelB is transiently overexpressed and inserted into the membrane, the quantity of the transporter appears to be insufficient for specific

detection of melibiose-induced signals by infrared techniques.

Melibiose-induced difference spectra from C-less ISO vesicles failed to demonstrate a difference signal. The main reason must be related to the extensive quantity of membrane proteins in the vesicles which unspecifically increase the background noise. Although ISO vesicles must contain more protein on their surface than the larger RSO counterparts, this aspect is not affecting the difference spectrum. The vesicles tend to break on the surface of the ATR crystal and hence accessibility for the substrate-containing buffer solution is given for both sides for the membrane.

Moreover, the buffer system for the difference spectrum acquisition contains a large amount of  $K^+$  ions. Since the membrane vesicles reflect the entire cell membrane of the bacterium, a large quantity of membrane proteins in the vesicles are ion channels filtering selectively different ions like potassium. Those proteins might interact with the potassium and surpass the melibiose binding signal of MelB.

The same conclusions could be drawn for the  $Na^+$ -induced  $IR_{diff}$ . There, the explanation is even more rational. Aside MelB, countless membrane proteins interact with the sodium and dilute the expected sodium difference spectrum of MelB.

For proving specifically the MelB protein, the sensitive fluorescent-sugar derivative  $D^2G$  was applied to the vesicles. This sugar contains a galactoside-group alike melibiose. Hence,  $D^2G$  exclusively binds to the sugar moiety of MelB and LacY<sup>127,190-192</sup>. But since the bacterial strain is depleted of the *lacY* gene, the data obtained from the FRET of the vesicles can be entirely assigned to the melibiose transporter.

Nevertheless, the data shown for each mutant contain an uncertainty. The amount of MelB embedded in the membrane varies depending on the expression rate of mutant and the preparation of the vesicles. Therefore, the results from the vesicles were compared only for the preparations for ISO and RSO vesicles, but not with different MelB mutants.

## **12. Lys-377 – the significance of the positively charged residue**

The residue Lys-377 has been announced as a crucial residue considering the transport activity of MelB. As the only charged amino acid in the transmembrane helix XI, transport assays done on a cysteine replacement mutant expresses the significance of the residue in position 377 of MelB. An alignment of melibiose transporter from several other prokaryotic organisms emphasizes the conservation of this particular lysine among other species. The GPH-family, where MelB is grouped into, is comprised of other sugar transporter, like the raffinose permease RafP from *Pedococcus pentosaceus* or the xylose transporter XylP from *Lactobacillus pentosus*. The characterized transporters from the GPH subfamily were included into the sequence alignment as well (Fig. 2.1). Remarkably, even these related transporters contain a positively

charged lysine residue in the same position. This result strengthens the notion of a highly conserved residue. Only the included MFS transporter LeuT, PutP and LacY possess other residues in the same protein loci after alignment calculations.

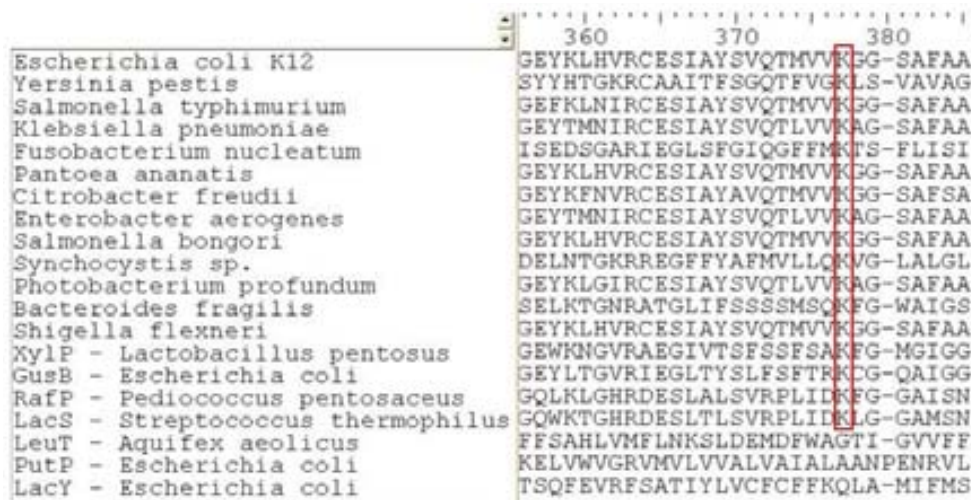


Figure 12.1 Sequence alignment of proteins from different prokaryotic organisms; MelB protein from *Escherichia coli* K12, *Yersinia pestis*, *Salmonella typhimurium*, *Klebsiella pneumoniae*, *Fusobacterium nucleatum*, *Pantoea ananatis*, *Citrobacter freundii*, *Enterobacter aerogenes*, *Salmonella bongori*, *Syncocystis sp.*, *Photobacterium profundum*, *Bacteroides fragilis*, *Shigella flexneri*;; GPH proteins: XylP from *Lactobacillus pentosus*, GusB from *Escherichia coli*, RafP from *Pediococcus pentosaceus*, LacS from *Streptococcus thermophilus*; other MFS protein: LeuT from *Aquifex aeolicus*, PutP from *Escherichia coli* and LacY from *Escherichia coli*. Alignments were done with ClustalW and BioEdit software. The numbers above the alignment are designated to the number of the amino acid sequence corresponding to MelB from *E. coli* K-12.

The FTIR as well as the fluorescence data point out the absence of substrate binding in the Lys-377 replacements with cysteine, aspartic acid, histidine, arginine and valine in all tested conditions. K377C, K377R and K377H display remnants of melibiose binding at a concentration of 50 mM melibiose using the proton as co-substrate. The evaluation of the spectra revealed a melibiose-induced difference spectrum although with extraordinarily small intensity.

The mutant K377R is the only lysine replacement indicating a small partial melibiose binding, already detectable at 10 mM melibiose in the presence of sodium. But sodium binding is still not recognizable in this charge conserving mutant. The data from the fluorescence spectroscopy confirms the data from infrared difference spectrum.

The fluorescent sugar D<sup>2</sup>G binds to the MelB mutant K377R and the addition of 10 mM sodium provokes a signal increase of the FRET signal around 465 nm. In the four other replacements of the Lys-377, a detectable FRET signal was absent. Considering the results of the proteoliposomes for the single amino acid replacements, the positive charge in position 377 of MelB is of major importance but apparently it is not the only contributing factor for the substrates binding activity of the transporter, because of the absence of the sodium-induced difference

spectrum and the reduced response in the presence of melibiose.

Concerning the particular mutant K377R, the transporter obviously conserved partially the sugar binding as it is indicated by the spectroscopic data. But apparently also this mutant lost its original conformation during the purification process as the absorbance spectra reveals. This interpretation might be valid for all Lys-377 replacements. Lysine as a charged residue is unlikely to be localized in close contact to the lipid bilayer without interacting with other charged residues.

A sugar transporter expressed in mammalian cells demonstrated a high sequence similarity to the melibiose transporter. Interestingly, sequence alignment between the mammalian transporter MFSD2A and MelB revealed a large amount of sequence identity. Especially, the residues Asp-93, Asp-97 and Lys-436 from MFSD2A and Asp-55, Asp-59 and Lys-377 for MelB corroborate a high similarity after sequence alignment. As well as in MelB, the sugar transport vanishes after mutating Asp-97 and Lys-436. Staining detection of the mutant K436A (aligns well with Lys-377 of MelB) emphasizes the localization of the MFSD2A transporter in other cell compartments rather than embedded into the membrane bilayer<sup>21</sup>. The MFSD2A Lys-436 mutant was not properly integrated into the membrane which seems likely for the MelB Lys-377 mutants as well. Apparently, the mutation of Lys-436 is crucial for proper membrane insertion in the case for this sugar transporter.

First postulated by Honig and Hubbell, charged amino acids could provoke instability in membrane segments. Though thermodynamically far less concerning are charged residues involved in a charged pair or salt bridge<sup>197</sup>. Therefore, it has been assumed for the Lys-377 to form a charged pair with negatively charged residues<sup>65</sup>. Concluded from the MelB model based on the refined 3D-structure using the lactose permease as a template, the aspartic acids 55 and 59 as well as the lysine are positioned in proximity. One has to remember that the distributed distances from Figure 2.2 are based on a putative MelB structure modeled after LacY. In the lactose symporter, a similar interaction has been described for a lysine and two negatively charged residues<sup>198</sup>. Designed double mutants implementing a switch of charges between amino acids 55 and 377 as well as 59 and 377 respectively ought to strengthen the idea of a stabilizing salt bridge (Fig. 12.2). Other membrane proteins have been previously described containing lysines as part of salt bridges for structural and functional purposes<sup>67,68</sup>.

Unfortunately, the results undermine the possibility of charged pairs between the two aspartic

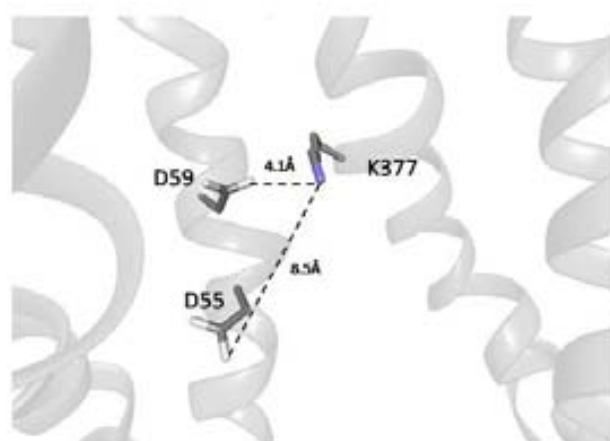


Figure 12.2 Calculated distances between Lys-377 and Asp-55 and Asp-59, respectively. Model from Guan used for distance estimation<sup>50</sup>. The Figure was generated by BALLView 1.3.2<sup>196</sup>.

acids and the lysine for MelB. By assessing the structural alterations marked by the absorbance spectrum, the similar changes have been observed for the two double mutants like for the single Lys-377 mutants. A direct correlation has been found between the absorbance spectrum changes and the lack of substrate binding. By examining the second derivative of the infrared absorbance spectrum of the mutants where the binding is affected, the peak positioned normally at  $1659\text{ cm}^{-1}$  is shifted slightly to  $1657\text{ cm}^{-1}$ . In parallel the intensity of the shoulder at  $1630\text{ cm}^{-1}$  rises in mutants with a distorted coupling of the sugar and the co-substrate. These features correlate well considering all purified mutants from the melibiose permease.

The use of MTS-reagents carrying a positive charge could not restore the binding characteristics of the transporter. This result strengthens the hypothesis that the additional charge alone cannot restore sodium/melibiose-binding.

Another fact worth mentioning is that Lys-377 might have the same structural implications as the Lys-358 of the related lactose/ $\text{H}^+$ -symporter. As cysteine and alanine scanning revealed, the Lys-358 has a reduced transport activity rate. An uncompensated charge of Asp-237 causes an instable transporter which is opted for a low insertion into the membrane bilayer. It forms a charged pair with Asp-237<sup>199</sup>. When in parallel to the Lys-358 mutations, also Asp-237 is substituted with a non-charged residues, the transporter is less vulnerable. But also a charge switch D237K/K358D is applicable in terms of transport activity for the lactose permease. The same rescue of activity was detected for the charged pair D59K/K377D in MelB<sup>65</sup>. But our approach failed to demonstrate a coupling of the ligands by spectroscopic methods. Therefore, by examining the data from Franco *et al.*, it is difficult to find an explanation for the significant transport activity detected using the proton-motive force for the double mutant D59K/K377D with no detected substrate binding by spectroscopy<sup>65</sup>.

One option to examine whether Asp-59 and Lys-377 are close to each other is to replace them with neutral cysteines. Either spontaneous cross-linking or forced formation of a cysteine-cysteine linker might substantiate the hypothesized proximity of the charged residues.

### **13. Lys-377 and its “revertants”**

As described as a powerful tool by different authors, revertants restoring the function of a defective mutant might elucidate the significance of special amino acid. For the Lys-377 mutants, the Ile-22 replacement by serine appeared spontaneously as a second site mutation inducing a red-colored colony after incubating the bacteria over 5 – 10 days on a MacConkey agar plate. Located in the transmembrane helix I of the transporter, this residue resides far away (around 14 Å in the model) from the lysine and a direct interaction of the two amino acids therefore seems implausible. Strikingly, the substitution I22S occurred in combination with all the Lys-377 mutations. K377C, K377R, K377V and K377H all established the second site mutation I22S. The results from the proteoliposomes reveal however, that the replacements fail to rescue the binding

with the sugar.

The question appears which effect would have the I22S mutation in the MelB transporter?

For the revertant K377C/I22S a sodium-induced difference spectrum had been obtained. It differs from the C-less spectra, but still indicates a partial binding of the cation. Even though also detectable at 10 mM sodium, the higher concentration of 50 mM intensifies the interaction between the sodium ligand and the MelB mutant. Peculiarly, none of the two other tested mutants K377R/I22S and K377V/I22S exhibit similar binding capacities for the co-ion. Beyond the detected coupling, K377C/I22S rescues the malformation of the MelB structure. This might explain in parallel the restored sodium binding even though different from the control.

Spectroscopic data of the I22S mutant exhibits interesting results. The sodium binding is not affected at all by this mutation demonstrating an almost identical C-less like spectrum. The melibiose coupling on the contrary is completely absent in I22S like in the double mutants containing the replacement of the Lys-377. In this case the hydrophobic isoleucine is been replaced by a polar serine which might indicate a clash of hydrophobic and hydrophilic

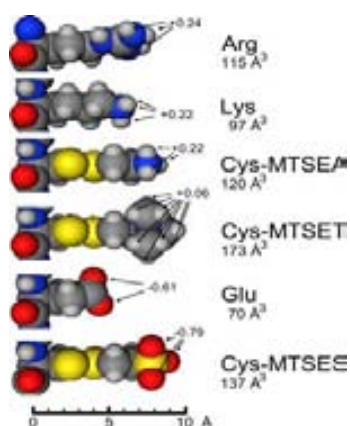


Figure 13.1 from Ma et al.<sup>200</sup> focusing on the length and volume of the thiol-reagents compared to charged amino acids. Used for sulfhydryl group interaction

microenvironments. Thus, suitable as a control for the different side chain characteristics, a second single mutant I22A resolve the problem of hydrophobicity. But even I22A declines the interaction with the sugar molecule, whereas the cation is bound alike I22S. Hence, this result states that the isoleucine is either near or part of the direct interaction with the melibiose molecule.

A supporting factor derives from the conclusions of the mutant D19C. Formerly considered as a residue scaffolding the sodium binding, Granell et al. convincingly proved that this hypothesis was not correct<sup>61</sup>. Nevertheless, D19C demonstrates its importance for the interaction with the melibiose. Even at higher sugar concentrations of 50 mM, the difference spectrum triggered by the sugar was not detectable.

Thus, Asp-19 and Ile-22 form a part of the melibiose binding either directly by interaction with the molecule or indirectly in its translocation.

Interestingly, the vesicles of the double mutant K377R/I22S clearly bind the fluorescent sugar D<sup>2</sup>G; however after the purification with the standard detergent, substrate binding is lost. The vesicles from the second double mutant K377C/I22S and the single mutant I22S could not demonstrate similar FRET signal in the vesicles. The recovered binding in K377R/I22S might be related to the positive charge in combination with the second site substitution.

The screening of mutation in combination with Lys-377 mutants uncovered also the replacement of Leu-236 by a phenylalanine.

The purification process increases suppositions of a possible interference of the detergent in the protein conformation, especially in the case of the double mutant K377R/L236F. The usual applied detergent caused apparently a dramatic loss in substrate recognition. Direct purification using  $\beta$ -DDM might better conserve the protein conformation. The same mutant purified in two different detergents caused an immense improvement in the binding characteristics of the spontaneous double mutant in proteoliposomes. The motivation for the change of detergent for the protein extraction was based on the data from the vesicles. Compared to the poorly binding proteoliposomes, the FRET signal from the vesicles of the mutant K377R/L236F had the same or even a larger signal intensity after sodium addition as the C-less reference.

The proteoliposomes of the double mutant K377R/L236F purified with  $\beta$ -DDM bind both substrates, although the sodium difference spectrum varies in greater parts from the C-less control spectrum. The conformation is conserved in the presence of DDM whereas the LAPAO-purified mutant displays broader structural alterations.

A control mutant K377C/L236F was included to test the hypothesis of the significance of the charge in position 377. The PCR-generated mutant K377C/L236F demonstrated red colonies on the MacConkey-agar plates similar to K377R/L236F. The FRET of vesicles on the other side lacks similar signal intensities. Adopting the direct DDM purification for K377C/L236F, FTIR and fluorescence spectroscopy confirmed the absence of substrate coupling in the generated mutant K377C/L236F compared to the spontaneous mutant K377R/L236F.

The effect of the detergents on membrane proteins during the extraction from the membrane is still understudied. For the related GPH transporter LacS, also member of the GPH family like MelB, distinctive detergents affect the protein activity during the reconstitution. Whereas one detergent favors the insertion of LacS in a unidirectional manner, another detergent favors the insertion of the transporter more randomly causing a highly reduced activity<sup>201</sup>.

To gain additional information whether the charge of the residue 377 is important, thiol reagents carrying a compensative charge were reacted with the sulfhydryl group of cysteine.

The MelB-mutant K377C/L236F interacting with MTS-reagent (MTSEA) carrying a positive charge induced a small but significant sodium-induced FRET signal. Therefore, it can be claimed that in the presence of a positive charge the K377C double mutant is able to bind D<sup>2</sup>G and sodium. For the K377C single mutant a similar approach in the vesicles failed to demonstrate substrate binding. Surprisingly, the other positive charge containing reagent MTSET did not induce similar fluorescence changes. This might be related to the reagent volume. MTSEA is more compact than MTSET (Fig. 13.1). This result further proves that besides the significance of the charge also other parameters like side chain length contribute.

The L236F mutation was previously detected as a lithium-sustaining site<sup>194</sup>, occurring spontaneously in Agar plates supplemented with a non-physiological lithium concentration.

Alternatively, the mutation occurred in combination with a defective mutant in helix I. The second site mutation L236F recovered the transporter function in the Y31C mutant<sup>57</sup>. It has therefore been postulated that helix VII is in proximity to helix I. The residue Leu-236 in helix

VII was not yet established as a crucial residue for substrate coupling.

The single mutant L236F exhibits C-less like substrate binding for the sodium and the melibiose.

The discovery of the substrate-binding double mutant points out the likelihood of proximity of the helices VII and XI in MelB which has not been established so far. The impact of the substitution of Leu-236 by Phe on substrate binding must be minimal as exemplified by the C-less like IR<sub>diff</sub> spectra.

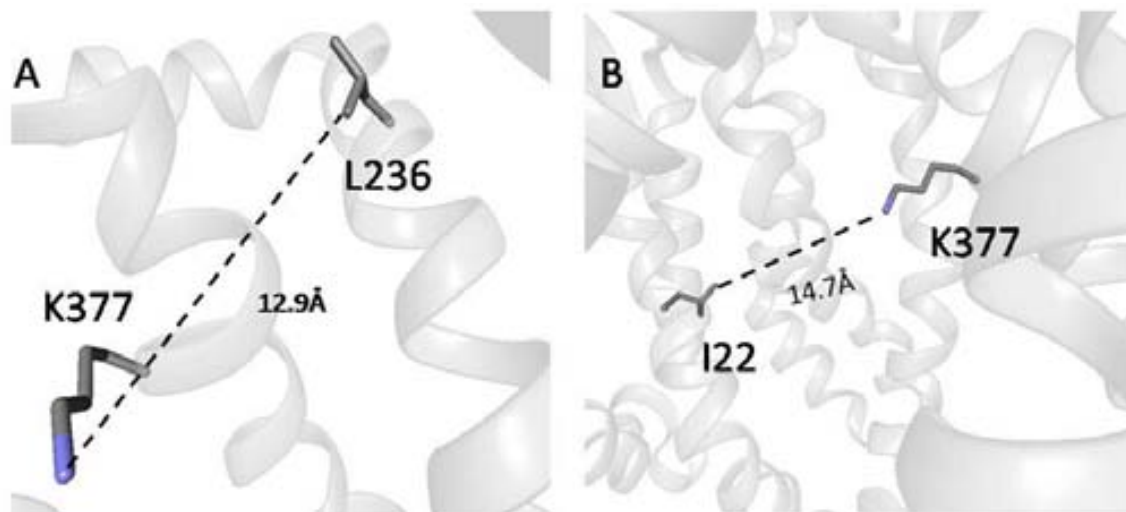


Figure 13.2 Calculated distances from Yousef model<sup>50</sup> calculated distances between Lys-377 and its second site mutations from Yousef model. **A** Ile-22 is located 12.9 Å away, whereas **B** Leu-236 is around 14.7 Å further apart from the lysine. It seems implausible that both residues directly affecting the lysine replacement. The images were generated by BALLView 1.3.2<sup>196</sup>.

Furthermore, our data strengthen the idea that the positive charge in position 377 is mandatory for the transporter but not enough to ensure substrate coupling<sup>64</sup>. The side chain length might be important as well. The replacement of L236F apparently drives minute conformational changes of the transporter beneficial in combination with a positive charge in position 377. A structural clash might explain the supportive effect of MTSEA whereas MTSET failed to enhance the fluorescence of D<sup>2</sup>G in the presence of sodium.

Considering the K377R/I22S FRET data, the revertant obviously recovered substrate binding as well. The FRET signal for the mutant K377R/L236F was more intense in comparison.

Also this double mutant offers the possibility for purification with a different detergent like DDM. K377R/L236F demonstrates a smaller FRET signal after purification and reconstitution compared to C-less. Nevertheless, the sodium and melibiose binding is evidently recovered. The same might occur for the double mutant K377R/I22S. For the double mutants carrying the I22S replacement as the second site replacement, the affinity was as low as the parental mutant of Lys-377. However it was hypothesized that their  $v_{\max}$  has substantially increased allowing a fast turnover rate<sup>69</sup>. The MelB mutant can be interpreted as a channel. This fast influx obviously causes the red colored colonies. An attractive idea is the stabilization of the substrate binding site implemented by the replacements I22S and L236F. Especially, I22 substitutions were already

obtained for several mutants<sup>69,74</sup>.

Nevertheless, the obtained double mutants emphasize the interaction of the crucial helices I – XI (K377/I22S) and VII – XI (K377R/L236F). Since the earlier double mutant Y31C/L236F describes a potential proximity between I – VII, the three helices obviously lie close to each other and perhaps forming a major part of the substrate moiety in the aqueous channel. The discovered interaction of helix VII and XI emphasizes helical proximity.

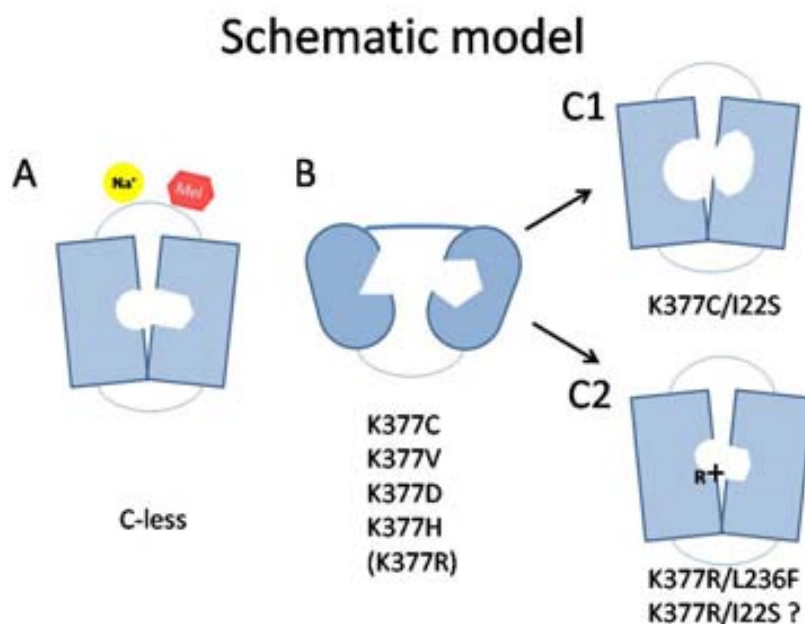


Figure 13.3 Schematic model of the effect of the Lys-377 mutations on the MelB transporter. A C-less structure, B global structural alterations caused by Lys-377 mutations, also affecting the binding sites (K377R in braces, because less severe), C1 recovered structure by K377C/I22S with partial sodium moiety, but still lacking melibiose binding indicated by misfitting binding pocket, C2 recovered structure by K377R/L236F with low affinity binding of both substrates. Indicated importance of the positive charge introduced by arginine. The double mutant K377R/I22S exposes D<sup>2</sup>G and sodium binding in the vesicles, similar to K377R/L236F, but no coupling in the proteoliposomes. Substrates: sodium ion as yellow ball; melibiose molecule as hexagonal shape

## 14. loop 10-11 as a functional domain?

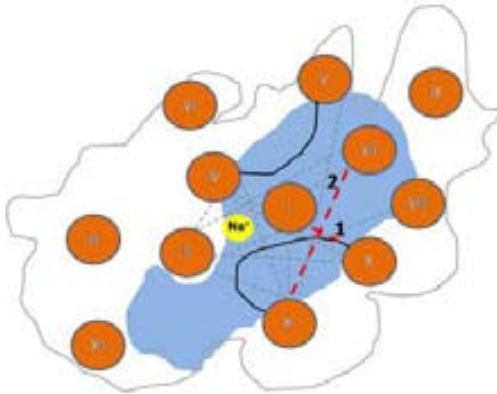


Figure 14.1 scheme of interactions between the helices. **1** newly found interactions between loop 10-11 and helix I (D354C/I22S) and **2** new interaction of helix XI with helix VII (K377R/L236F). Figure after Pao et al.<sup>14</sup> and Meyer-Lipp<sup>102</sup>.

The cytoplasmic loop between the helices 10 and 11 is considered to be involved in the transport mechanism of the melibiose permease. Because of its predicted length the extramembrane segment might even be considered to form a re-entrant loop as described mainly for ion channels<sup>202,203</sup>. Reasons to believe so are the amount of charged residues located in this loop. Re-entrant loops are defined as large amino acid sequences associated to membrane helices and entering the lipid bilayer. Because these motifs possess numerous polar and charged residues, they usually intrude sites with lower hydrophobicity, like aqueous channels.

Site-directed mutagenesis studies uncovered several charged residues which ultimately affect the transport activity of MelB when mutated. In the past, such loops have been described to be an essential part for catalytic activities for several membrane proteins<sup>80,204,205</sup>.



Figure 14.2 Protein sequence alignment from prokaryotic organisms. MelB protein from *Escherichia coli* K12, *Yersinia pestis*, *Salmonella typhimurium*, *Klebsiella pneumoniae*, *Fusobacterium nucleatum*, *Pantoea ananatis*, *Citrobacter freundii*, *Enterobacter aerogenes*, *Salmonella bongori*, *Synchronocystis sp.*, *Photobacterium profundum*, *Bacteroides fragilis*, *Shigella flexneri*; GPH proteins: XylP from *Lactobacillus pentosus*, GusB from *Escherichia coli*, RafP from *Pediococcus pentosaceus*, LacS from *Streptococcus thermophilus*; other MFS protein: LeuT from *Aquifex aeolicus*, PutP from *Escherichia coli* and LacY from *Escherichia coli*. Alignments calculated with ClustalW<sup>206</sup> and BioEdit software. Encircled in dark blue: aspartic acids, in sky blue: glutamic acids and in red: arginine. The numbers above the alignment are designated to the number of the amino acid sequence corresponding to MelB from *E. coli* K-12.

The sequence alignment of permeases from distinctive archaea and prokaryotic organisms clearly demonstrates the significance of residues in the cytoplasmic loop 10-11. Especially, Asp-351 and Arg-363 are highly conserved among the melibiose permeases. Only the archaea *Fusobacterium nucleatum* possess a glutamate instead of the aspartate; however, the negative charged is conserved. All of the GPH member proteins behold aspartic acid and arginine in similar positions. Even the MFS transporter PutP contains an arginine in the similar domain displayed after ClustalW alignment (Fig. 14.2).

Also the Asp-354 as well as Glu-357 and Glu-365 exhibit a vast conservation among the orthologous proteins. Other membrane proteins display equally well conserved domains, especially consisting of charged amino acids<sup>207,208</sup>.

Cysteine mutagenesis pointed out Asp-351, Asp-354 and Arg-363 as potentially crucial residues for the transport mechanism in MelB. The mutations D351C, D354C and R363C abolish completely the transport activity.

Our obtained spectroscopic data indicate a highly reduced binding capacity in the mutants D351C, D354C and R363C for the ligands, melibiose and sodium. Glu-357 and Glu-365C on the contrary seem to be less essential for the permease. The mutants bind the sodium and the sugar to a certain extent in a C-less manner. Also, assays showed previously that E357C and E365C cause

only minor reductions of the transport activity<sup>82</sup>. Sery reported that E357C causes instability of the protein<sup>64</sup>. The function of Glu-365 in the first place was attributed to the reorientation mechanism<sup>209</sup>. The negative charge of the amino acid side chain is not essential for the transport. Besides, the E365A mutant causes a temperature-sensitive transporter<sup>209</sup>.

The search for transport-rescuing mutations of the mutants D351C, D354C and R363C unfortunately exhibit only a second site mutation in D354C. D351C and R363C revealed only the recovery of the genetic background of C-less in the presence of both substrates in the MacConkey-agar plates. Nevertheless, it is not improbable that these residues have interactions partners within the transporter under different conditions with only one or no substrates at all. This outcome suggests on the other hand that a mutation (cysteine) affecting the two residues have severe impact of the transporter function and /or stability.

Incubation of the mutant D354C also caused the appearance of red colonies. Surprisingly, the second site location was the again the I22S mutation.

The mutant D354C/I22S binds the sodium with much higher affinity compared to D354C. On the contrary, the melibiose binding compared to D354C is completely lost, like for the double mutants concerning Lys-377. Because the spontaneous I22S mutation already appeared for the Lys-377 mutants, the isoleucine-serine replacement does not seem to be a site specific. Moreover, this mutation obviously alters the transporters general characteristics. The reason to believe so is based on the structural changes caused by I22S. This spreads the notion that the isoleucine is directly involved in the sugar binding. In all mutants containing a substitution of I22, the sodium couples in a C-less manner, the melibiose binding however is completely absent. Concluding this result and bearing in mind the finding for the mutant D19C, the sugar obviously binds partially with the helix I of MelB. Interestingly, the second site-mutation was generated in mutants where at least remnants of sugar accumulation were detected. In mutants where transport activity is completely lost (like Asp-351, Asp-354, Arg-363, Tyr-396), this second site mutation has not been described.

The conclusions drawn from the vesicles are miscellaneous. The finding earlier commented that D354C obviously binds D<sup>2</sup>G and sodium well in the right-side-out form, but not in the ISO vesicles. The reason for the lack of D<sup>2</sup>G and Sodium binding in the ISO vesicles is the reduced expression of the transporter. The RSO vesicles demonstrate the expected sodium-dependent increase in fluorescence. Nevertheless, the combination of an expression rate of around 12% compared to C-less<sup>73</sup>, the higher amount of contaminating protein in ISO vesicles compared to RSO vesicles and variation during vesicle preparation are parameters to be considered of while interpreting the data from the FRET in the membrane vesicles. Especially the MelB band labeled with the His-Probe<sup>TM</sup>-HRP against the C-terminal His-tag exhibit the low amount of D354C MelB in the ISO vesicles. The mutant is defective in active transport and furthermore its expression is extremely low<sup>73,82</sup>.

Also the mutants D351C and R363C demonstrated a ratio ISO/RSO above the expected factor 1. But, after the labeling of the prepared vesicles, RSO vesicles of both mutants contain

around 50% less MelB than the ISO counterpart. This in turn explains the weaker FRET signal in the RSO vesicles and suggests eventually an accessible MelB transporter from both side of the membrane.

Described by Pourcher *et al.*, Glu-365 is considered to be close to the thermo-sensitive site of the transporter and mutations to glycine and aspartic acid fail to catalyze the transport activity. The authors also concluded that Glu-365 might be involved in the reorientation mechanism<sup>209,210</sup>.

Glu-365 and Glu-357 are two negatively charged residues which are non-essential for MelB also their charge is not significant in terms of active sugar transport. Glu-365 is definitely not essential for the substrate binding in MelB confirming the conclusion drawn in the thesis by Meyer-Lipp<sup>102</sup>. For the Glu-357, Séry pointed out that the mutation causes modifications in the sugar recognition pattern. In the unstable mutant E357C disaccharides containing an  $\alpha$ -linker still bind to the carrier. But dimeric sugar molecules in which both monomers are connected by a  $\beta$ -linkage are not recognized anymore<sup>64</sup>. Contradictory to the result from Séry, Glu-357 binds D<sup>2</sup>G in proteoliposomes very well.

Still our result cannot intensify the strict significance of this interhelix loop for the transport mechanism. Although considerably reduced in their expression, the mutations D351C, D354C and R363C affect the substrate binding. Our results confirm that the residues possibly not be involved directly in the substrate binding process but obviously play a crucial role during the translocation or release of the substrates.

Perhaps, this motif mediates similarly to Q loops of primary active transporters conformational changes on the entire protein upon substrate binding<sup>208,211</sup>. In a recent work investigating the extracellular loop from the human organic cation transporter (OCT), a loop domain is found to be primarily responsible for the insertion into the plasma membrane. The substrate affinity is affected as well<sup>212</sup>.

From the acquired results, it seems difficult to envision the role of the putative loop 10-11 during the transport cycle. A functional importance of helix-connecting loop domains has been described already in the literature. The sodium-glutamate transporter GltS apparently uses its reentrant loop 9-10 for the glutamate accumulation<sup>213</sup>. Further a functional role of reentrant loops or loops in general have been elucidated as well for the sodium,-citrate transporter<sup>213</sup>, the human di-/tri-peptide porter hPEPT1<sup>214</sup>, the serotonin transporter<sup>215</sup> and the dopamine transporter<sup>216</sup>.

## 15. Helix XI as mainly hydrophobic segment facing the aqueous channel in MelB

In the final part of the discussion, the transmembrane helix XI should be discussed considering the effect of substitutions of crucial amino acids for the transport mechanism.

Transport assays published by Ding *et al.* already identified critical residues in this C-terminal segment<sup>63</sup>. During the study of the melibiose permease, this segment has been changed in terms of distributing amino acids. The latest putative model predicts a length of 25 amino acids<sup>50</sup>. This helix encompasses the residue from 370 to 394. But since, it is a only putative prediction based on biophysical and biochemical data combined with the three-dimensional structure of LacY, the amount of amino acids might differ. Previous cysteine-scanning assays also include residues 394 to 396 to the membrane-spanning segment.

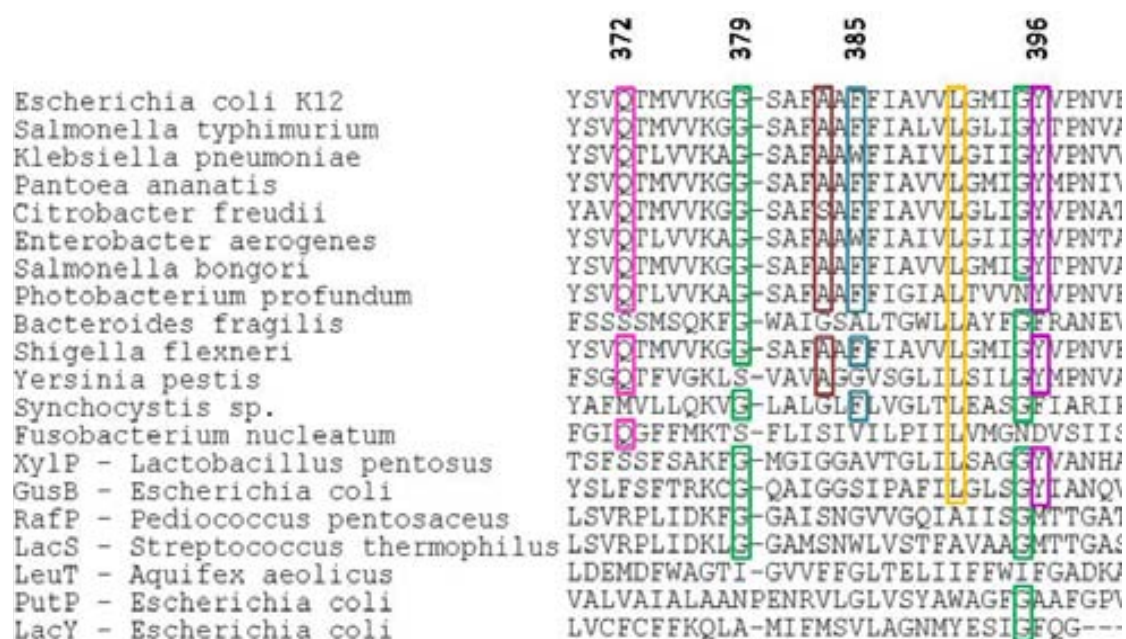


Figure 15.1 Sequence alignment of the melibiose permeases from various organisms plus GPH proteins (XylP, GusB, RafP and LacS) and three MFS proteins with known 3D structure. Sequences in order from *Escherichia coli* K12, *Yersinia pestis*, *Salmonella typhimurium*, *Klebsiella pneumoniae*, *Fusobacterium nucleatum*, *Pantoea ananatis*, *Citrobacter freundii*, *Enterobacter aerogenes*, *Salmonella bongori*, *Synchocystis sp.*, *Photobacterium profundum*, *Bacteroides fragilis*, *Shigella flexneri*; GPH proteins: XylP from *Lactobacillus pentosus*, GusB from *Escherichia coli*, RafP from *Pediococcus pentosaceus*, LacS from *Streptococcus thermophilus*; other MFS protein: LeuT from *Aquifex aeolicus*, PutP from *Escherichia coli* and LacY from *Escherichia coli*. Alignments calculated with ClustalW and BioEdit software. marked in magenta: glutamine, in green: glycine, in brown: alanine, in blue: phenylalanine, in orange: leucine and in purple: tyrosine. The numbers above the alignment are designated to the number of the amino acid sequence corresponding to MelB from *E. coli* K-12.

The conservation of amino acids of the helix XI is not as stringent as for the Lys-377 or for the charged residues in the loop 10-11. The Leu-391 is best conserved among the amino acids from the transmembrane segment. Even in the GPH subfamily, GusB and XlyP hold leucine in the corresponding position. RafP and LacS, two other members of the GPH family, maintain the hydrophobic character with an alanine instead of leucine.

The Gly-379 and Gly-395 are similarly conserved like the Leu-391 which also emphasizes their significance for MelB. The amino acids Ala-383 and Phe-385 are less abundant among the melibiose symporters of different species. However, their replacement by cysteine impairs the transport activity.

From the 23 characterized amino acids, three residues displayed a lack of sugar transport and several other residues demonstrated a drastic decrease in intracellular melibiose accumulation<sup>63</sup>. Hence, we focused on the substrate binding capacities of these substitutions. G379C, F385C and Y396C were published to show a defective activity, whereas A383C, L391C and G395C caused either a dramatic or substantial reduction in sugar transport. Furthermore, the replacement Q372C was included into our screening of crucial residues, because of its proposed significance for the sodium binding characteristics<sup>82</sup>, significant lack of melibiose accumulation and the inhibitory affect by water-soluble agents<sup>82</sup>. G379V is the only mutation which has not been examined in terms of expression rate and transport activity.

The spectroscopic results point out that especially A383C and Y396C affect sodium and melibiose binding characteristics. The conformational changes are diminished evidently, while still expressed at considerable levels<sup>63</sup>. Y396C lies either at the periplasmic end of the helix or already in the short extramembrane loop connecting helices XI and XII. Therefore, it is rather improbable that Tyr-396 is directly involved in the binding process. However, since transport assays outlined an abolished sugar accumulation in Y396C, the tyrosine might be involved in conformational changes upon substrate binding. Ala-383 is more likely to affect the substrate binding. This amino acid lays half-way in the membrane. The binding sites of the substrates are supposed to be centered somewhere in the aqueous channel half-way through the membrane. The 2D projection map by Hacksell *et al.* envisioned a possible arrangement of the protein domains<sup>101</sup>. Ding *et al.* hypothesized that Helix XI lines up the aqueous channel.

Considering earlier results, the color of the mutant F385C in MacConkey-agar plate was contradictory to published results. F385C was announced by Ding and Wilson<sup>69</sup> as a mutant forming white colonies with no transport activity. In our study, this particular mutant clearly displays red colonies similar to the C-less control (Fig. 5.1). An explanation for this diverse phenotype is rather speculative. The sugar concentration tested in the previous publication was with 29 mM even higher than our 10 mM melibiose which excluded the reasoning for reduced affinity. A red colony usually appears when



Figure 15.2 F385C mutant on MacConkey-agar plate supplemented with 10 mM melibiose grown at 30°C.

the intracellular pH changes. A more acidic pH occurs during the metabolism of the melibiose which indicates accumulation of the sugar. As one possibility, the sugar might enter the cell rapidly as forced by the gradient. The strain DW2-R transformed with the pK95ΔAHB expresses the  $\alpha$ -galactosidase which cleaves melibiose into galactose and glucose and, hence provokes the change in the pH. The strain in the publication was DW2. It differs from DW2-R only in the possession of *recA*. Usually, *recA* is deleted for molecular biological purposes. Without this gene, extrachromosomal DNA remains intact in the cytosol. In the DW2 strain harboring the plasmid with the F385C mutation might be altered unspecifically by the cell. All publications after that were done with the strain DW2-R *E. coli* strain.

The results from the proteoliposomes of the F385C mutation suggest a mutation which does not affect the binding of the substrates at all. Deduced from the FRET experiments in the vesicles, the binding of the fluorescent sugar derivative seem to be reduced in the RSO vesicles. The ISO form on the contrary binds D<sup>2</sup>G with very high affinity. Therefore, it was assumed that the mutation F385C might be involved in the conformational changes after the substrate binding from the outside oriented transporter to the inward-facing side.

The evaluation of the amount of MelB in each vesicle type revealed a 1.8 times higher MelB concentration in ISO vesicles compared to the RSO form. This in turn argues in favor for a correct reorientation mechanism which is either not influenced by the Phe-385 or to a lesser extent.

The equilibrium between the substrate-bound outward facing and the inward-facing MelB is shifted in the mutant R149C. The inward-facing MelB apparently is thermodynamically preferred.

The Na-dependent D<sup>2</sup>G signal in ISO is a staggering 25 times the RSO signal in the same conditions. For the F385C mutant, this ratio is only around 5 times higher in the ISO vesicles than in the RSO form. Regarding the higher amount of detected transporter protein in ISO, the ratio ISO/RSO is reduced to 2.8. However, the conformational change might be affected by the F385C mutant.

Transport assays also show that the mutants G379C and Y396C completely lost their catalytic activity. For G379C the substrate binding is only slightly affected for the sugar, but not for the co-substrate. The glycine is located in proximity to the Lys-377, a predicted ligand for the sugar molecule. Hence, minor alterations in the direct surrounding might structural shifts.

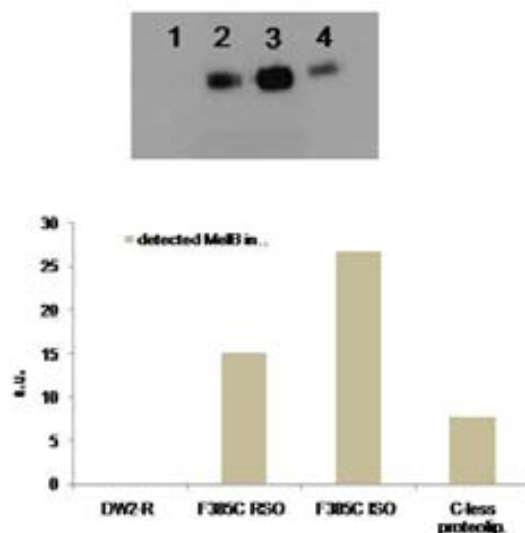


Figure 15.3 MelB detection in the ISO and RSO vesicles. 1 DW2-R as a negative control not expression MelB, 2 F385C RSO, 3 F385C ISO, 4 C-less proteoliposome as positive control.

Moreover, Gly-379 is accompanied by another Gly-380. In the predicted centre of a transmembrane segment these small-volume residues cause some steric flexibility. This might as well explain the result for the mutant G379V. The valine substitution, albeit being a hydrophobic amino acid like glycine, obviously impedes the coupling of melibiose as well as sodium. Since the defective glycine mutant binds the substrates relatively well, it can be assumed that either the greater hydrophobicity of the valine compared the glycine alters the microenvironment around this domain. Or secondly, the proximity of the sugar and/or sodium binding site is sterically distorted by the larger side chain volume of the valine substitution. In the case of the Tyr-396, the cysteine replacement definitely generates a major impact on the coupling characteristics for both substrates.

Considering the predicted MelB helix arrangement, the oxalate-formate antiporter (OxIT) has a similar structural composition. OxIT and MelB share the same categorization into the major facilitator superfamily (MFS). The substrates oxalate and formate are exchanged by this transport protein. The C-terminal domain governs the substrate binding sites. The two aromatic residues Arg-272 (helix VIII) and Lys-355 (helix XI) enable substrate binding as they are positively charged liganding the opposite charged organic salts.

Another important MFS transporter is the sodium/proton-antiporter NhaA. As one of the first published three-dimensional structures, this antiporter allows broad assumptions of the function of prokaryotic transport<sup>113</sup>. Although catalyzing accumulation of two cations in opposite directions, the structural similarities to MelB are evident. One of the most important features during the transport mechanism is the fast assembly between the helices IV and XI. Both helices are split into two small helical segments connected by a loop sequence. This loop serves as a hinge for fast conformational changes upon substrate binding.

Conclusions can be drawn also from publications dedicated to revertants from the helix XI mutations. The transport-affecting mutants K377C, A383C, L391C and G395C demonstrate their interaction with the transmembrane segment I. Strikingly; all four residues when replaced by cysteine establish over time (incubation on MacConkey plate) revertants almost exclusively replacing residues from helix I. Especially, the apolar Ile-22 is a major target for substitutions by polar amino acids like asparagine, threonine or as in our case with serine. But in none of the revertants, this second-site mutation completely recovers the melibiose transport activity. On the contrary, only for L391C/I22T the transport activity mediate by the proton improves compared to the single mutant. In all other mutants, the transport rate is lower than in the original single mutant<sup>69</sup>. This agrees well with our conclusions from the double mutants K377C/I22S and D354C/I22S. The second site does not improve the affinity for the sugar. But it appeared to enhance the binding capacity for the co-ion sodium. This outcome might be related directly to the alterations of the MelB structure.

The F385C mutant also test for the appearance of second-site revertants in the mentioned study only displayed interaction partners within helix XI or the C-terminal part. Considering the result from the alkylation with the fluorescence probe MIANS, an interpretation is not

straightforward. Intrinsic Trps may quench the signal also known as static quenching<sup>217</sup>. Considering helix XI and its position based on the 2D-crystals of MelB, the closest Trp's are located in position 342 (helix X), 54 and 64 (helix II). Trp-342 is one of the main contributors of the fluorescence signal in MelB. If after the addition of the sugar, the Trp's move closer to the bound fluorophore, the signal quenching increases and the fluorescence is reduced in parallel<sup>102</sup>. For the interaction of MIANS with some helix XI cysteine replacements this might be the case, like G395C.

Another explanation for the change in the fluorescence for G395C is that the melibiose binding provokes conformational changes redirecting parts of the domain into a less hydrophobic environment. This causes the reduced fluorescence since MIANS prefers a less polar surrounding. This scenario is possible since Ding and Wilson reported the putative helix XI as partially lining the aqueous channel<sup>69</sup>.

## 16. Outlook

For a better understanding of the entire mechanism a more profound evaluation of the mutations is needed. The Lys-377 offers still plenty of opportunities to investigate its function as a potential key residue for the melibiose permease.

As already partially exploited, IR dichroism might be utilized in terms of elucidating the correct insertion of the purified protein qualitatively as well as quantitatively. Especially, the positive charge maintained in the mutant K377R and the spontaneous revertants suggest that the positive charge in position 377 is crucial in combination with the correct position.

The charge switch between Lys-377 and Asp-55 and Asp-59 could not elucidate a potential salt bridge formed by the charged residues. Nevertheless, cysteine cross-linking between these residues might emphasize their proximity giving strength to the putative model of MelB.

The obtained second site mutations of K377R and D354C must be characterized considering their transport activity. So far, we just measured substrate binding, but not the sugar accumulation inside the cells. These data will deliver conclusive data about their ability to recover active transport. Especially, the K377R double mutants containing the second site replacements L236F and to a lesser extent I22S indicate D<sup>2</sup>G binding in the vesicles. As for the double mutants K377R/L236F, a variation in the purification process by extracting MelB directly with DDM might explain the D<sup>2</sup>G signal difference between the proteoliposomes and the vesicles of the double mutant K377R/I22S. Therefore, protein purification using DDM instead of LAPAO might conserve the protein structure of the double mutant as well like for K377R/L236F.

The main goal is to reveal amino acids forming the binding site for the sugar molecule. Preliminary data are already available describing Asp-19, Ile-22, Ser-153, Ala-155, Thr-159 and Lys-377 as possible liganding residues.

For the detailed explanation of the protein mechanism, it is of essential significance to

understand each step during the transport process. Nowadays, the most useful technique to gain insights of structural alterations is the protein crystallography. Although difficult to accomplish, a solved three-dimensional structure would elucidate several issues of the process. Even more desirable would be to get protein crystals in different stages of the transport process. Eventually, those data would enhance a broad understanding of the transport mechanism.

So far, structural biology relies majorly on solved 3D-protein structures or to a lesser extent on structural modeling. Such information can be helpful to predict possible mechanisms for membrane transporter.

Considering the study of MelB, prokaryotic sugar transporter can assist to delineate the structure-function relationship of co-substrate mediated transport mechanisms for the more complex eukaryotic transporter as well. As a perfect example of the study of bacterial secondary sugar transporter suits the lactose permease from *E. coli*, termed as LacY. Throughout the last two decades LacY has been studied extensively. Not only biochemical and biophysical but also crystallographic studies revealed extraordinary insights of the transport mechanism of this exemplary secondary active transporter. The Kaback lab was also the first to successfully crystallize a protein form the MFS family<sup>218</sup> at low resolution and to solve the structure afterwards.

For the melibiose permease a solved three-dimensional structure would definitely boost the understanding of yet unsolved structural issues. Also protein domains or even side chains which are involved in the substrate coupling might be revealed by the protein structure.

## SUMMARY OF THE THESIS

This doctoral thesis was dedicated to the study of the secondary transporter, the melibiose permease (MelB) from *Escherichia coli* with biochemical and biophysical methodologies. The main objective was to obtain insights of the symport mechanism of MelB. This prokaryotic transporter uses the downhill translocation of a cation to transport the disaccharide melibiose against its concentration gradient into the cell. Although MelB possess the highest affinity for Na<sup>+</sup> cations, the transporter can couple the transport process also to the smaller Li<sup>+</sup> and H<sup>+</sup> ions. Apart from melibiose, MelB transports a variety of  $\alpha$ - and  $\beta$ -galactosides making it versatile carrier. The transporter comprises 70% of hydrophobic amino acids and is organized in 12 transmembrane spanning helices connected by hydrophilic loops.

As preliminary studies already reveal, the C-terminal domains of MelB has been proven to play a crucial role in the active transport mechanism. The focus in this doctoral thesis lies especially on the helices X and XI as well as the interconnecting cytoplasmic loop 10-11. Site-directed mutagenesis delivered valuable information about important amino acids which might participate in the active transport by forming part of the binding sites or taking part in the translocation and release of the substrates.

During our study, numerous MelB mutants have been extracted from the membrane by using the detergents LAPAO and  $\beta$ -DDM. Subsequently, the solubilized transporter was reconstituted into liposomes composed of lipids from *E. coli* mimicking MelB's original habitat.

As the only charged residue residing in the transmembrane segment XI, Lys-377 was replaced by cysteine, valine, arginine, histidine and aspartic acid. None of these MelB mutants interacts with sodium concluded from infrared difference spectra (IR<sub>diff</sub>) induced by the cation Na<sup>+</sup>. The melibiose binding is only remotely detectable in K377R, K377H and K377C in the presence of the proton. K377V and K377D lost the interaction with the sugar molecule. The charge in the particular position in MelB is important but not sufficient to conserve the substrate binding.

The amino acid substitutions of Lys-377 appear as white colonies on a MacConkey agar plate. This color indicates the absence of hydrolysis of the melibiose into the monosaccharides, glucose and galactose. A metabolisation of the sugar is indicated by a red colony. In these colored bacteria, the sugar hydrolysis causes an acidification of the medium indicated by the MacConkey agar which stains the bacterial colonies.

The screening of potential revertants, second site mutations which allow sugar influx, demonstrate the appearance of a unique second site mutation I22S which turn the former white colonies of the Lys-377 mutants into a red phenotype. Another red-colored phenotype appeared only for the mutant K377R, in which Leu-236 is replaced by a phenylalanine.

All K377/I22S revertants are not able to restore the melibiose binding in proteoliposomes and only the revertant K377C/I22S recovered a partial sodium binding. The absorbance spectra of the single Lys-mutants as well as the corresponding revertants indicate a correlation between the absence of sodium binding and conformational changes of the MelB transporter. These structural changes are identical to previously examined MelB mutants D55C, D59C and D124C which also demonstrated a detrimental impact on the Na<sup>+</sup> binding.

The single mutants I22S and I22A exhibit a clear response of the structure in the presence of Na<sup>+</sup>. The interaction with melibiose on the contrary is lost in these MelB mutants. This outlines Ile-22 as a potential amino acid participating in the binding process of the melibiose molecule in MelB.

The second revertant K377R/L236F demonstrates only minor interaction with the Na<sup>+</sup> as well with the melibiose in proteoliposomes. Measurements using membrane vesicles of this mutant demonstrate however a large Förster energy transfer (FRET) signal mediated by the fluorescent sugar analog, D<sup>2</sup>G. By extracting the mutant K377R/L236F with  $\beta$ -DDM instead of LAPAO, the solubilised and then reconstituted transporter exhibits a clear improvement considering the conservation of the MelB structure. IR<sub>diff</sub> spectroscopy results concluded that the K377R/L236F mutant binds melibiose and Na<sup>+</sup>, although the cation-induced difference spectra differs from the C-less reference.

The PCR-generated double mutant K377C/L236F failed to demonstrate similar interactions with the substrates in proteoliposomes as well as in membrane vesicles. The positive charge in position 377 is essential for the MelB transporter, but the sole charge is not sufficient for the substrate binding. The charge requires also structural arrangement to interact with the sugar and the co-ion.

In the second part of the PhD thesis, cysteine mutants replacing charged residue in the cytoplasmic loop 10-11 were characterized for their ability of substrate binding. The transport-defective mutants D351C, D354C and R363C couple sodium with reduced affinity indicated by their low intense IR<sub>diff</sub> spectra. The melibiose binding is even further reduced in these MelB mutants. Appearing as white colonies on MacConkey agar plate, the screening of potential revertants only revealed a second site mutation for D354C. Interestingly, Ile-22 was substituted for a serine like in the Lys-377 mutants. Congruent results with the K377/I22S mutants indicate for D354C/I22S the loss of sugar binding. However, the sodium triggers a difference spectrum similar to C-less and much more intense than in the D354C single mutant. This indicates a tight interaction of the cation with the MelB mutant D354C/I22S.

In the third part of this thesis, eight mutants were generated by replacing crucial residues in the C-terminal helix XI of MelB with cysteine. The mutants Q372C, G379C, F385C, L391C and G395C show an almost normal interaction with Na<sup>+</sup>. A383C and Y396C on the other side display a Na<sup>+</sup>-induced IR<sub>diff</sub> with low intensity indicating their impaired cation binding.

Considering the interaction with melibiose, all helix XI mutants bind the sugar in the presence of either the proton or  $\text{Na}^+$ . The MelB mutants A383C, L391C and Y396C exhibit a melibiose-induced difference spectrum with very low intensity indicating their importance for the binding process. Tested in vesicles and proteoliposomes, G379V is the only characterised mutant which lacks sodium and sugar binding making this mutant a potential candidate for crystallography trials to obtain the structure of the empty MelB transporter.



## RESUMEN DE LA TESIS

En este trabajo, el objetivo principal ha sido el estudio del mecanismo del co-transporte de la permeasa de melibiosa (MelB) de *Escherichia coli*. Esta proteína de membrana realiza co-transporte activo de varios oligosacáridos utilizando la fuerza electroquímica de cationes. Una característica remarcable de este transportador es el hecho que permite utilizar tres diferentes cationes, el protón, el sodio y el litio. Los sustratos con mayor afinidad a la proteína son el sodio y la melibiosa.

Para cumplir nuestro objetivo principal se llevó a cabo el estudio de los dominios C-terminales de la proteína reconstituida como proteoliposomas. El bucle existente entre las hélices 10 y 11 así como la hélice XI del transportador se revelaron como dominios fundamentales para el funcionamiento del transporte activo. Estudios previos indican que la sustitución de diversos amino ácidos por una cisteína impide el transporte. Con la técnica de mutagénesis dirigida se obtuvieron sustituciones de amino ácidos en la proteína MelB, generando así múltiples mutantes con diferentes propiedades de unión, de translocación y de liberación de los sustratos. La solubilización de los mutantes generados se realizó con los detergentes LAPAO y DDM. Después de varios pasos de purificación, los mutantes de la MelB se reconstituyeron en liposomas de *Escherichia coli* para simular así el hábitat natural del transportador.

Con técnicas espectroscópicas (infrarrojo y fluorescencia) se analizaron la unión de diferentes mutantes de MelB a los sustratos

Este estudio puso de manifiesto el papel crucial del amino ácido Lys-377 en el transportador MelB. Sustituciones de dicho amino ácido por cisteína, valina, histidina, arginina y ácido aspártico mostraron como el transportador perdía completamente la unión a sodio y pasaba a acoplar el azúcar sólo en presencia del protón pero de manera disminuida. La carga en posición 377 de la MelB destaca por mantener el acoplamiento a los sustratos. Otra característica importante de la MelB es el volumen de cadena lateral que influye en la unión a sodio y melibiosa.

La búsqueda de revertantes se realizó a través de un fenotipo diferente de la cepa, haciéndola crecer en placas de agar suplementadas de melibiosa. Los mutantes con un defecto de transporte, como es el caso de los mutantes de Lys-377, eran reconocidos al formar éstos colonias blancas, a diferencia de los revertantes, que generaban colonias rojas, indicando este color un pH dentro de la célula distinto en ambos casos. El cambio rojo en los revertantes es debido a la hidrólisis de la melibiosa en dos monosacáridos, glucosa y galactosa. La hidrólisis disminuye el pH que es detectado por el indicador suplementado en la placa.

La secuenciación de estas subcolonias rojas reveló sustituciones de los amino ácidos Ile-22 por serina y Leu-236 por fenilalanina. La mutación I22S ocurre en todos mutantes singulares de Lys-377, pero el desplazamiento de Leu-236 por fenilalanina sólo se detectó en el mutante K377R.

Ninguno de los revertantes de K377/I22S recuperó la unión al azúcar en proteoliposomas y únicamente K377C/I22S fue capaz de unir el sodio pero con una afinidad menor. Los espectros de absorbancia de los revertantes indicaron que existe una cierta correlación entre cambios conformacionales de la MelB y la ausencia de señales en espectros de diferencia provocada por sodio.

Como controles se usaron los mutantes singulares I22S y I22A que como revelan los espectros de diferencia, mantienen la capacidad de unión a el sodio pero no al azúcar. La isoleucina en posición 22 podría formar parte del sitio de unión de la melibiosa en MelB.

Solubilizando el revertante K377R/L236F con LAPAO, detergente común para la purificación de MelB, demostró que dicho mutante tiene una afinidad disminuida a sus sustratos, tal y como demuestran los espectros de diferencia y fluorescencia. Sin embargo, las vesículas del mutante K377R/L236F tienen la capacidad de unir un análogo fluorescente de azúcar similar al C-less, la wild-type permeasa sin cisteínas.

La solubilización del mutante con DDM unía los sustratos con mucha más afinidad que el mismo mutante solubilizado con LAPAO y mantenía la estructura similar a C-less. La prueba con K377C/L236F, un doble mutante generado por PCR, no reveló interacciones con los sustratos. Este resultado indica la importancia de la carga positiva conservada de la arginina en combinación con cambios estructurales para mantener la capacidad de unión de los sustratos.

En la segunda parte se examinaron mutaciones con cisteínas de varios amino ácidos cargados colocados en el bucle entre las hélices transmembranales X y XI.

Estudios previos del transporte activo indican que tres amino ácidos perdían la capacidad de acumular melibiosa contra el gradiente.

Los residuos Asp-351, Asp-354 y Arg-363 estudiados a través de IR<sub>diff</sub> y fluorescencia, demostraron la persistencia de unión a sodio aunque reducida. Los tres mutantes de MelB unían el azúcar también pero de una forma drásticamente reducida. Sólo en un revertante se descubrió un desplazamiento también en Ile-22 por una serina como en el caso de Lys-377. El revertante D354C/I22S demostró un incremento de la unión a sodio, pero una pérdida total de la unión a melibiosa.

En el parte final de la tesis, se generaron ocho mutantes. Cada mutante con una mutación en un amino ácido diferente colocados todos ellos en la hélice XI de la MelB. Q372C, G379C, F385C, L391C y G395C mantuvieron la unión de sodio de manera equivalente a C-less. A383C y Y396C mostraron una cierta reducción de la señal mediada por sodio. El mutante G379V fue el único mutante que perdió totalmente la interacción con el catión.

Los espectros de IR<sub>diff</sub> inducido por melibiosa demostraron en A383C, L391C y Y396C una afinidad muy baja al azúcar. G379V tampoco fue capaz de unir la melibiosa.



---

## BIBLIOGRAPHY

- 1 Ahram, M., Litou, Z. I., Fang, R. & Al-Tawallbeh, G. Estimation of membrane proteins in the human proteome. *In Silico Biol* **6**, 379-386, (2006).
- 2 Stevens, T. J. & Arkin, I. T. Do more complex organisms have a greater proportion of membrane proteins in their genomes? *Proteins* **39**, 417-420, (2000).
- 3 Jiang, Y. *et al.* Crystal structure and mechanism of a calcium-gated potassium channel. *Nature* **417**, 515-522, (2002).
- 4 Haga, K. *et al.* Structure of the human M2 muscarinic acetylcholine receptor bound to an antagonist. *Nature*, (2012).
- 5 Teplyakov, A. *et al.* Structure of phosphorylated enzyme I, the phosphoenolpyruvate:sugar phosphotransferase system sugar translocation signal protein. *Proceedings of the National Academy of Sciences* **103**, 16218-16223, (2006).
- 6 Paulsen, I. T., Nguyen, L., Sliwinski, M. K., Rabus, R. & Saier Jr, M. H. Microbial genome analyses: comparative transport capabilities in eighteen prokaryotes. *Journal of Molecular Biology* **301**, 75-100, (2000).
- 7 Giacomini, K. M. *et al.* Membrane transporters in drug development. *Nat Rev Drug Discov* **9**, 215-236, (2010).
- 8 Reizer, J., Reizer, A. & Saier, M. H., Jr. A functional superfamily of sodium/solute symporters. *Biochim Biophys Acta* **1197**, 133-166, (1994).
- 9 Baker, M. Making membrane proteins for structures: a trillion tiny tweaks. *Nat Methods* **7**, 429-434, (2010).
- 10 Garneau, L., Klein, H., Parent, L. & Sauve, R. Toward the rational design of constitutively active KCa3.1 mutant channels. *Methods Enzymol* **485**, 437-457, (2010).
- 11 D'Avanzo, N., Hyrc, K., Enkvetchakul, D., Covey, D. F. & Nichols, C. G. Enantioselective protein-sterol interactions mediate regulation of both prokaryotic and eukaryotic inward rectifier K<sup>+</sup> channels by cholesterol. *PLoS ONE* **6**, e19393, (2011).
- 12 Ren, Q., Chen, K. & Paulsen, I. T. TransportDB: a comprehensive database resource for cytoplasmic membrane transport systems and outer membrane channels. *Nucleic Acids Res* **35**, D274-279, (2007).
- 13 Ren, Q., Kang, K. H. & Paulsen, I. T. TransportDB: a relational database of cellular membrane transport systems. *Nucleic Acids Res* **32**, D284-288, (2004).
- 14 Pao, S. S., Paulsen, I. T. & Saier, M. H., Jr. Major facilitator superfamily. *Microbiol Mol Biol Rev* **62**, 1-34, (1998).
- 15 Saier, M. H., Jr. Families of transmembrane sugar transport proteins. *Mol Microbiol* **35**, 699-710, (2000).
- 16 West, I. C. Ligand conduction and the gated-pore mechanism of transmembrane transport. *Biochim Biophys Acta* **1331**, 213-234, (1997).
- 17 Saier, M. H., Jr. Tracing pathways of transport protein evolution. *Mol Microbiol* **48**, 1145-1156, (2003).

- 18 Saier, M. H., Jr. *et al.* The major facilitator superfamily. *J Mol Microbiol Biotechnol* **1**, 257-279, (1999).
- 19 Naderi, S. & Saier, M. H., Jr. Plant sucrose:H<sup>+</sup> symporters are homologous to the melibiose permease of Escherichia coli. *Mol Microbiol* **22**, 390-391, (1996).
- 20 Poolman, B. *et al.* Cation and sugar selectivity determinants in a novel family of transport proteins. *Mol Microbiol* **19**, 911-922, (1996).
- 21 Reiling, J. H. *et al.* A haploid genetic screen identifies the major facilitator domain containing 2A (MFSD2A) transporter as a key mediator in the response to tunicamycin. *Proceedings of the National Academy of Sciences* **108**, 11756-11765, (2011).
- 22 Meyer, S. *et al.* AtSUC3, a gene encoding a new Arabidopsis sucrose transporter, is expressed in cells adjacent to the vascular tissue and in a carpel cell layer. *Plant J* **24**, 869-882, (2000).
- 23 Reinders, A. & Ward, J. M. Functional characterization of the  $\alpha$ -glucoside transporter Sut1p from Schizosaccharomyces pombe, the first fungal homologue of plant sucrose transporters. *Molecular Microbiology* **39**, 445-455, (2001).
- 24 Shimokawa, N. *et al.* Past-A, a novel proton-associated sugar transporter, regulates glucose homeostasis in the brain. *J Neurosci* **22**, 9160-9165, (2002).
- 25 Veenhoff, L. M., Heuberger, E. H. & Poolman, B. The lactose transport protein is a cooperative dimer with two sugar translocation pathways. *EMBO J* **20**, 3056-3062, (2001).
- 26 Pardee, A. B. An inducible mechanism for accumulation of melibiose in Escherichia coli. *J Bacteriol* **73**, 376-385, (1957).
- 27 Prestidge, L. S. & Pardee, A. B. A Second Permease for Methyl-Thio-Beta-D-Galactoside in Escherichia Coli. *Biochim Biophys Acta* **100**, 591-593, (1965).
- 28 Stock, J. & Roseman, S. A sodium-dependent sugar co-transport system in bacteria. *Biochem Biophys Res Commun* **44**, 132-138, (1971).
- 29 Hama, H. & Wilson, T. H. Primary structure and characteristics of the melibiose carrier of Klebsiella pneumoniae. *J Biol Chem* **267**, 18371-18376, (1992).
- 30 Poolman, B., Royer, T. J., Mainzer, S. E. & Schmidt, B. F. Lactose transport system of Streptococcus thermophilus: a hybrid protein with homology to the melibiose carrier and enzyme III of phosphoenolpyruvate-dependent phosphotransferase systems. *J Bacteriol* **171**, 244-253, (1989).
- 31 Levinthal, M. Biochemical studies of melibiose metabolism in wild type and mel mutant strains of Salmonella typhimurium. *J Bacteriol* **105**, 1047-1052, (1971).
- 32 Lopilato, J., Tsuchiya, T. & Wilson, T. H. Role of Na<sup>+</sup> and Li<sup>+</sup> in thiomethylgalactoside transport by the melibiose transport system of Escherichia coli. *Journal of Bacteriology* **134**, 147-156, (1978).
- 33 Tsuchiya, T., Lopilato, J. & Wilson, T. H. Effect of lithium ion on melibiose transport in Escherichia coli. *J Membr Biol* **42**, 45-59, (1978).
- 34 Bassilana, M., Pourcher, T. & Leblanc, G. Facilitated diffusion properties of melibiose permease in Escherichia coli membrane vesicles. Release of co-substrates is rate limiting for permease cycling. *J Biol Chem* **262**, 16865-16870, (1987).
- 35 Padan, E., Bibi, E., Ito, M. & Krulwich, T. A. Alkaline pH homeostasis in bacteria: new insights. *Biochim Biophys Acta* **1717**, 67-88, (2005).
- 36 Geertsma, E. R. What lies between: Functional interfaces in a dimeric transporter. (2005).
- 37 Yazyu, H. *et al.* Nucleotide sequence of the melB gene and characteristics of deduced amino acid sequence of the melibiose carrier in Escherichia coli. *J Biol Chem* **259**, 4320-4326, (1984).

- 38 Hanatani, M. *et al.* Physical and genetic characterization of the melibiose operon and identification of the gene products in *Escherichia coli*. *J Biol Chem* **259**, 1807-1812, (1984).
- 39 Wade, J. T., Belyaeva, T. A., Hyde, E. I. & Busby, S. J. Repression of the *Escherichia coli* melR promoter by MelR: evidence that efficient repression requires the formation of a repression loop. *Mol Microbiol* **36**, 223-229, (2000).
- 40 Pourcher, T., Leclercq, S., Brandolin, G. & Leblanc, G. Melibiose permease of *Escherichia coli*: large scale purification and evidence that H<sup>+</sup>, Na<sup>+</sup>, and Li<sup>+</sup> sugar symport is catalyzed by a single polypeptide. *Biochemistry* **34**, 4412-4420, (1995).
- 41 Zani, M. L., Pourcher, T. & Leblanc, G. Mutation of polar and charged residues in the hydrophobic NH<sub>2</sub>-terminal domains of the melibiose permease of *Escherichia coli*. *J Biol Chem* **269**, 24883-24889, (1994).
- 42 Wilson, D. M. & Wilson, T. H. Cation specificity for sugar substrates of the melibiose carrier in *Escherichia coli*. *Biochim Biophys Acta* **904**, 191-200, (1987).
- 43 Tsuchiya, T. & Wilson, T. H. Cation-sugar cotransport in the melibiose transport system of *Escherichia coli*. *Membr Biochem* **2**, 63-79, (1978).
- 44 Heuberger, E. H. Unraveling structural and functional features of secondary transport proteins. (2001).
- 45 Guan, L. & Kaback, H. R. Lessons from lactose permease. *Annu Rev Biophys Biomol Struct* **35**, 67-91, (2006).
- 46 Zani, M. L., Pourcher, T. & Leblanc, G. Mutagenesis of acidic residues in putative membrane-spanning segments of the melibiose permease of *Escherichia coli*. II. Effect on cationic selectivity and coupling properties. *J Biol Chem* **268**, 3216-3221, (1993).
- 47 Gwizdek, C., Leblanc, G. & Bassilana, M. Proteolytic mapping and substrate protection of the *Escherichia coli* melibiose permease. *Biochemistry* **36**, 8522-8529, (1997).
- 48 Botfield, M. C., Naguchi, K., Tsuchiya, T. & Wilson, T. H. Membrane topology of the melibiose carrier of *Escherichia coli*. *J Biol Chem* **267**, 1818-1822, (1992).
- 49 Purhonen, P., Lundback, A. K., Lemonnier, R., Leblanc, G. & Hebert, H. Three-dimensional structure of the sugar symporter melibiose permease from cryo-electron microscopy. *J Struct Biol* **152**, 76-83, (2005).
- 50 Yousef, M. S. & Guan, L. A 3D structure model of the melibiose permease of *Escherichia coli* represents a distinctive fold for Na<sup>+</sup> symporters. *Proc Natl Acad Sci U S A* **106**, 15291-15296, (2009).
- 51 Mitchell, P. A General Theory of Membrane Transport From Studies of Bacteria. *Nature* **180**, 134-136, (1957).
- 52 Jardetzky, O. Simple allosteric model for membrane pumps. *Nature* **211**, 969-970, (1966).
- 53 Doyle, D. A. *et al.* The structure of the potassium channel: molecular basis of K<sup>+</sup> conduction and selectivity. *Science* **280**, 69-77, (1998).
- 54 Vanni, S., Campomanes, P., Marcia, M. & Rothlisberger, U. Ion Binding and Internal Hydration in the Multidrug Resistance Secondary Active Transporter NorM Investigated by Molecular Dynamics Simulations. *Biochemistry* **51**, 1281-1287, (2012).
- 55 Pourcher, T. B., M; Sarkar, HK; Kaback, HR; Leblanc, G. The Melibiose/Na symporter of *Escherichia coli*: Kinetic and Molecular Properties. *Phil. Trans. R. Soc. Lond.* **326**, 411-423, (1990).
- 56 Franco, P. J. & Wilson, T. H. Arg-52 in the melibiose carrier of *Escherichia coli* is important for cation-coupled sugar transport and participates in an intrahelical salt bridge. *J Bacteriol* **181**,

- 6377-6386, (1999).
- 57 Ding, P. Z. & Wilson, T. H. Cysteine mutagenesis of the amino acid residues of transmembrane helix I in the melibiose carrier of *Escherichia coli*. *Biochemistry* **40**, 5506-5510, (2001).
- 58 Ding, P. Z., Botfield, M. C. & Wilson, T. H. Sugar recognition mutants of the melibiose carrier of *Escherichia coli*: possible structural information concerning the arrangement of membrane-bound helices and sugar/cation recognition site. *Biochim Biophys Acta* **1509**, 123-130, (2000).
- 59 le Coutre, J., Narasimhan, L. R., Patel, C. K. & Kaback, H. R. The lipid bilayer determines helical tilt angle and function in lactose permease of *Escherichia coli*. *Proc Natl Acad Sci U S A* **94**, 10167-10171, (1997).
- 60 Locher, K. P., Bass, R. B. & Rees, D. C. Breaching the Barrier. *Science* **301**, 603-604, (2003).
- 61 Granell, M., Leon, X., Leblanc, G., Padros, E. & Lorenz-Fonfria, V. A. Structural insights into the activation mechanism of melibiose permease by sodium binding. *Proc Natl Acad Sci U S A* **107**, 22078-22083, (2010).
- 62 Ganea, C. *et al.* G117C MelB, a mutant melibiose permease with a changed conformational equilibrium. *Biochim Biophys Acta* **1808**, 2508-2516, (2011).
- 63 Ding, P. Z. & Wilson, T. H. The melibiose carrier of *Escherichia coli*: cysteine substitutions for individual residues in helix XI. *J Membr Biol* **174**, 135-140, (2000).
- 64 Séry, N. Roles fonctionnelles des boucles cytoplasmique d'un co-transporteur Na<sup>+</sup>/sucre d'*Escherichia coli*, la melibiose permease. *DEA*, (2002).
- 65 Franco, P. J., Jena, A. B. & Wilson, T. H. Physiological evidence for an interaction between helices II and XI in the melibiose carrier of *Escherichia coli*. *Biochim Biophys Acta* **1510**, 231-242, (2001).
- 66 Dunten, R. L., Sahin-Toth, M. & Kaback, H. R. Role of the charge pair aspartic acid-237-lysine-358 in the lactose permease of *Escherichia coli*. *Biochemistry* **32**, 3139-3145, (1993).
- 67 Dürr, K. L., Seuffert, I. & Friedrich, T. Deceleration of the E1P-E2P Transition and Ion Transport by Mutation of Potentially Salt Bridge-forming Residues Lys-791 and Glu-820 in Gastric H<sup>+</sup>/K<sup>+</sup>-ATPase. *Journal of Biological Chemistry* **285**, 39366-39379, (2010).
- 68 Zhang, Y., Buchko, G. W., Qin, L., Robinson, H. & Varnum, S. M. Crystal structure of the receptor binding domain of the botulinum C-D mosaic neurotoxin reveals potential roles of lysines 1118 and 1136 in membrane interactions. *Biochemical and Biophysical Research Communications* **404**, 407-412, (2011).
- 69 Ding, P. Z. & Wilson, T. H. Physiological evidence for an interaction between helix XI and helices I, II, and V in the melibiose carrier of *Escherichia coli*. *Biochem Biophys Res Commun* **268**, 409-413, (2000).
- 70 Cordat, E., Leblanc, G. & Mus-Veteau, I. Evidence for a role of helix IV in connecting cation- and sugar-binding sites of *Escherichia coli* melibiose permease. *Biochemistry* **39**, 4493-4499, (2000).
- 71 Wilson, T. H. & Ding, P. Z. Sodium-substrate cotransport in bacteria. *Biochim Biophys Acta* **1505**, 121-130, (2001).
- 72 Hastings Wilson, T. & Wilson, D. M. Evidence for a close association between helix IV and helix XI in the melibiose carrier of *Escherichia coli*. *Biochim Biophys Acta* **1374**, 77-82, (1998).
- 73 Ding, P. Z. An investigation of cysteine mutants on the cytoplasmic loop X/XI in the melibiose transporter of *Escherichia coli* by using thiol reagents: implication of structural conservation of charged residues. *Biochem Biophys Res Commun* **307**, 864-869, (2003).
- 74 Meyer-Lipp, K. *et al.* The inner interhelix loop 4-5 of the melibiose permease from *Escherichia*

- coli takes part in conformational changes after sugar binding. *J Biol Chem* **281**, 25882-25892, (2006).
- 75 Abdel-Dayem, M., Basquin, C., Pourcher, T., Cordat, E. & Leblanc, G. Cytoplasmic loop connecting helices IV and V of the melibiose permease from *Escherichia coli* is involved in the process of Na<sup>+</sup>-coupled sugar translocation. *J Biol Chem* **278**, 1518-1524, (2003).
- 76 Ganea, C. & Fendler, K. Bacterial transporters: charge translocation and mechanism. *Biochim Biophys Acta* **1787**, 706-713, (2009).
- 77 Spooner, P. J. R., Veenhoff, L. M., Watts, A. & Poolman, B. Structural Information on a Membrane Transport Protein from Nuclear Magnetic Resonance Spectroscopy Using Sequence-Selective Nitroxide Labeling†. *Biochemistry* **38**, 9634-9639, (1999).
- 78 Veenhoff, L. M., Geertsma, E. R., Knol, J. & Poolman, B. Close Approximation of Putative  $\alpha$ -Helices II, IV, VII, X, and XI in the Translocation Pathway of the Lactose Transport Protein of *Streptococcus thermophilus*. *Journal of Biological Chemistry* **275**, 23834-23840, (2000).
- 79 Ehnes, C. *et al.* Structure-function relations of the first and fourth extracellular linkers of the type IIa Na<sup>+</sup>/Pi cotransporter: II. Substrate interaction and voltage dependency of two functionally important sites. *J Gen Physiol* **124**, 489-503, (2004).
- 80 Krupnik, T., Sobczak-Elbourne, I. & Lolkema, J. S. Turnover and accessibility of a reentrant loop of the Na<sup>+</sup>-glutamate transporter GltS are modulated by the central cytoplasmic loop. *Mol Membr Biol* **28**, 462-472, (2011).
- 81 Yan, C. & Luo, J. An analysis of reentrant loops. *Protein J* **29**, 350-354, (2010).
- 82 Ding, P. Z. Loop X/XI, the largest cytoplasmic loop in the membrane-bound melibiose carrier of *Escherichia coli*, is a functional re-entrant loop. *Biochim Biophys Acta* **1660**, 106-117, (2004).
- 83 Ding, P. Z. & Wilson, T. H. The proximity between helix I and helix XI in the melibiose carrier of *Escherichia coli* as determined by cross-linking. *Biochim Biophys Acta* **1514**, 230-238, (2001).
- 84 Ding, P. Z. & Wilson, T. H. The effect of modifications of the charged residues in the transmembrane helices on the transport activity of the melibiose carrier of *Escherichia coli*. *Biochem Biophys Res Commun* **285**, 348-354, (2001).
- 85 Damiano-Forano, E., Bassilana, M. & Leblanc, G. Sugar binding properties of the melibiose permease in *Escherichia coli* membrane vesicles. Effects of Na<sup>+</sup> and H<sup>+</sup> concentrations. *J Biol Chem* **261**, 6893-6899, (1986).
- 86 Mus-Veteau, I., Pourcher, T. & Leblanc, G. Melibiose permease of *Escherichia coli*: substrate-induced conformational changes monitored by tryptophan fluorescence spectroscopy. *Biochemistry* **34**, 6775-6783, (1995).
- 87 Pourcher, T., Deckert, M., Bassilana, M. & Leblanc, G. Melibiose permease of *Escherichia coli*: mutation of aspartic acid 55 in putative helix II abolishes activation of sugar binding by Na<sup>+</sup> ions. *Biochem Biophys Res Commun* **178**, 1176-1181, (1991).
- 88 Pourcher, T., Zani, M. L. & Leblanc, G. Mutagenesis of acidic residues in putative membrane-spanning segments of the melibiose permease of *Escherichia coli*. I. Effect on Na<sup>(+)</sup>-dependent transport and binding properties. *J Biol Chem* **268**, 3209-3215, (1993).
- 89 Wilson, D. M. & Wilson, T. H. Asp-51 and Asp-120 are important for the transport function of the *Escherichia coli* melibiose carrier. *J Bacteriol* **174**, 3083-3086, (1992).
- 90 Hama, H. & Wilson, T. H. Replacement of alanine 58 by asparagine enables the melibiose carrier of *Klebsiella pneumoniae* to couple sugar transport to Na<sup>+</sup>. *J Biol Chem* **269**, 1063-1067, (1994).
- 91 Hama, H. & Wilson, T. H. Cation-coupling in chimeric melibiose carriers derived from *Escherichia coli* and *Klebsiella pneumoniae*. The amino-terminal portion is crucial for Na<sup>+</sup>

- recognition in melibiose transport. *J Biol Chem* **268**, 10060-10065, (1993).
- 92 Abramson, J. *et al.* The lactose permease of *Escherichia coli*: overall structure, the sugar-binding site and the alternating access model for transport. *FEBS Lett* **555**, 96-101, (2003).
- 93 Guan, L., Jakkula, S. V., Hodkoff, A. A. & Su, Y. Role of Gly117 in the cation/melibiose symport of MelB of *Salmonella typhimurium*. *Biochemistry*, (2012).
- 94 Guan, L., Sahin-Toth, M. & Kaback, H. R. Changing the lactose permease of *Escherichia coli* into a galactose-specific symporter. *Proc Natl Acad Sci U S A* **99**, 6613-6618, (2002).
- 95 Johnson, J. L. & Brooker, R. J. Role of glutamate-126 and arginine-144 in the lactose permease of *Escherichia coli*. *Biochemistry* **42**, 1095-1100, (2003).
- 96 Fu, D., Sarker, R. I., Abe, K., Bolton, E. & Maloney, P. C. Structure/function relationships in OxIT, the oxalate-formate transporter of *Oxalobacter formigenes*. Assignment of transmembrane helix 11 to the translocation pathway. *J Biol Chem* **276**, 8753-8760, (2001).
- 97 Koenderink, J. B., Swarts, H. G. P., Willems, P. H. G. M., Krieger, E. & De Pont, J. J. H. H. M. A conformation-specific interhelical salt bridge in the K<sup>+</sup>-binding site of gastric H,K-ATPase. *J. Biol. Chem.*, M400020200, (2004).
- 98 Cao, Y. *et al.* Crystal structure of a phosphorylation-coupled saccharide transporter. *Nature* **473**, 50-54, (2011).
- 99 Karpowich, N. K. & Wang, D. N. Structural biology. Symmetric transporters for asymmetric transport. *Science* **321**, 781-782, (2008).
- 100 Faham, S. *et al.* The Crystal Structure of a Sodium Galactose Transporter Reveals Mechanistic Insights into Na<sup>+</sup>/Sugar Symport. *Science* **321**, 810-814, (2008).
- 101 Hacksell, I. *et al.* Projection structure at 8 Å resolution of the melibiose permease, an Na-sugar co-transporter from *Escherichia coli*. *EMBO J* **21**, 3569-3574, (2002).
- 102 Meyer-Lipp, K. Time-resolved measurements of sugar-binding-induced conformational changes in the Melibiose Permease from *Escherichia coli*. (2005).
- 103 Heymann, J. A. W. *et al.* Projection structure and molecular architecture of OxIT, a bacterial membrane transporter. *EMBO J* **20**, 4408-4413, (2001).
- 104 Williams, K. A. Three-dimensional structure of the ion-coupled transport protein NhaA. *Nature* **403**, 112-115, (2000).
- 105 Deisenhofer, J., Epp, O., Miki, K., Huber, R. & Michel, H. X-ray structure analysis of a membrane protein complex. Electron density map at 3 Å resolution and a model of the chromophores of the photosynthetic reaction center from *Rhodospseudomonas viridis*. *J Mol Biol* **180**, 385-398, (1984).
- 106 Frillingos, S., Sahin-tóth, M., Wu, J. & Kaback, H. R. Cys-scanning mutagenesis: a novel approach to structure–function relationships in polytopic membrane proteins. *The FASEB Journal* **12**, 1281-1299, (1998).
- 107 Hirai, T. & Subramaniam, S. Structure and Transport Mechanism of the Bacterial Oxalate Transporter OxIT. *Biophysical Journal* **87**, 3600-3607, (2004).
- 108 Dang, S. *et al.* Structure of a fucose transporter in an outward-open conformation. *Nature* **467**, 734-738, (2010).
- 109 Yin, Y., He, X., Szewczyk, P., Nguyen, T. & Chang, G. Structure of the Multidrug Transporter EmrD from *Escherichia coli*. *Science* **312**, 741-744, (2006).
- 110 Newstead, S. *et al.* Crystal structure of a prokaryotic homologue of the mammalian oligopeptide-proton symporters, PepT1 and PepT2. *EMBO J* **30**, 417-426, (2011).
- 111 Abramson, J., Kaback, H. R. & Iwata, S. Structural comparison of lactose permease and the glycerol-3-phosphate antiporter: members of the major facilitator superfamily. *Curr Opin Struct*

- Biol* **14**, 413-419, (2004).
- 112 Padan, E. The enlightening encounter between structure and function in the NhaA Na<sup>+</sup>-H<sup>+</sup> antiporter. *Trends Biochem Sci* **33**, 435-443, (2008).
- 113 Hunte, C. *et al.* Structure of a Na<sup>+</sup>/H<sup>+</sup> antiporter and insights into mechanism of action and regulation by pH. *Nature* **435**, 1197-1202, (2005).
- 114 Liao, J. *et al.* Structural insight into the ion-exchange mechanism of the sodium/calcium exchanger. *Science* **335**, 686-690, (2012).
- 115 Shimamura, T. *et al.* Molecular basis of alternating access membrane transport by the sodium-hydantoin transporter Mhp1. *Science* **328**, 470-473, (2010).
- 116 Singh, S. K., Piscitelli, C. L., Yamashita, A. & Gouaux, E. A competitive inhibitor traps LeuT in an open-to-out conformation. *Science* **322**, 1655-1661, (2008).
- 117 Watanabe, A. *et al.* The mechanism of sodium and substrate release from the binding pocket of vSGLT. *Nature* **468**, 988-991, (2010).
- 118 Faham, S. *et al.* The crystal structure of a sodium galactose transporter reveals mechanistic insights into Na<sup>+</sup>/sugar symport. *Science* **321**, 810-814, (2008).
- 119 Ressler, S., Terwisscha van Scheltinga, A. C., Vonrhein, C., Ott, V. & Ziegler, C. Molecular basis of transport and regulation in the Na<sup>(+)</sup>/betaine symporter BetP. *Nature* **458**, 47-52, (2009).
- 120 Gao, X. *et al.* Mechanism of substrate recognition and transport by an amino acid antiporter. *Nature* **463**, 828-832, (2010).
- 121 Kowalczyk, L. *et al.* Molecular basis of substrate-induced permeation by an amino acid antiporter. *Proceedings of the National Academy of Sciences* **108**, 3935-3940, (2011).
- 122 Shaffer, P. L., Goehring, A., Shankaranarayanan, A. & Gouaux, E. Structure and Mechanism of a Na<sup>+</sup>-Independent Amino Acid Transporter. *Science* **325**, 1010-1014, (2009).
- 123 Martineau, P., Szmelcman, S., Spurlino, J. C., Quiocho, F. A. & Hofnung, M. Genetic approach to the role of tryptophan residues in the activities and fluorescence of a bacterial periplasmic maltose-binding protein. *J Mol Biol* **214**, 337-352, (1990).
- 124 Mus-Veteau, I. & Leblanc, G. Melibiose permease of Escherichia coli: structural organization of cosubstrate binding sites as deduced from tryptophan fluorescence analyses. *Biochemistry* **35**, 12053-12060, (1996).
- 125 Chang, A. B., Lin, R., Keith Studley, W., Tran, C. V. & Saier, M. H., Jr. Phylogeny as a guide to structure and function of membrane transport proteins. *Mol Membr Biol* **21**, 171-181, (2004).
- 126 Cordat, E., Mus-Veteau, I. & Leblanc, G. Structural studies of the melibiose permease of Escherichia coli by fluorescence resonance energy transfer. II. Identification of the tryptophan residues acting as energy donors. *J Biol Chem* **273**, 33198-33202, (1998).
- 127 Maehrel, C., Cordat, E., Mus-Veteau, I. & Leblanc, G. Structural studies of the melibiose permease of Escherichia coli by fluorescence resonance energy transfer. I. Evidence for ion-induced conformational change. *J Biol Chem* **273**, 33192-33197, (1998).
- 128 Overath, P., Teather, R. M., Simoni, R. D., Aichele, G. & Wilhelm, U. Lactose carrier protein of Escherichia coli. Transport and binding of 2'-(N-dansyl)aminoethyl beta-D-thiogalactopyranoside and p-nitrophenyl alpha-d-galactopyranoside. *Biochemistry* **18**, 1-11, (1979).
- 129 Dave, N. *et al.* Secondary structure components and properties of the melibiose permease from Escherichia coli: a fourier transform infrared spectroscopy analysis. *Biophys J* **79**, 747-755, (2000).
- 130 Tatulian, S. A., Cortes, D. M. & Perozo, E. Structural dynamics of the Streptomyces lividans K<sup>+</sup> channel (SKC1): secondary structure characterization from FTIR spectroscopy. *FEBS Letters* **423**,

- 205-212, (1998).
- 131 Kendrick, B. S. *et al.* Aggregation of recombinant human interferon gamma: Kinetics and structural transitions. (1998).
- 132 Dave, N. *et al.* Study of amide-proton exchange of Escherichia coli melibiose permease by attenuated total reflection-Fourier transform infrared spectroscopy: evidence of structure modulation by substrate binding. *J Biol Chem* **277**, 3380-3387, (2002).
- 133 Lórenz, V. A. *et al.* The Secondary Structure of the Inhibited Mitochondrial ADP/ATP Transporter from Yeast Analyzed by FTIR Spectroscopy†. *Biochemistry* **40**, 8821-8833, (2001).
- 134 Leon, X., Lemonnier, R., Leblanc, G. & Padros, E. Changes in secondary structures and acidic side chains of melibiose permease upon cosubstrates binding. *Biophys J* **91**, 4440-4449, (2006).
- 135 Leon, X., Leblanc, G. & Padros, E. Alteration of sugar-induced conformational changes of the melibiose permease by mutating Arg141 in loop 4-5. *Biophys J* **96**, 4877-4886, (2009).
- 136 Dave, N., Lorenz-Fonfria, V. A., Leblanc, G. & Padros, E. FTIR spectroscopy of secondary-structure reorientation of melibiose permease modulated by substrate binding. *Biophys J* **94**, 3659-3670, (2008).
- 137 Leon, X., Lorenz-Fonfria, V. A., Lemonnier, R., Leblanc, G. & Padros, E. Substrate-induced conformational changes of melibiose permease from Escherichia coli studied by infrared difference spectroscopy. *Biochemistry* **44**, 3506-3514, (2005).
- 138 Lórenz-Fonfria, V. A. & Padrós, E. Maximum Entropy Deconvolution of Infrared Spectra: Use of a Novel Entropy Expression Without Sign Restriction. *Appl. Spectrosc.* **59**, 474-486, (2005).
- 139 Granell, M. Estudi del lloc d'unió del sodi de la permeasa de melibiosa d'*Escherichia coli*. (2009).
- 140 Botfield, M. C. & Wilson, T. H. Mutations that simultaneously alter both sugar and cation specificity in the melibiose carrier of Escherichia coli. *J Biol Chem* **263**, 12909-12915, (1988).
- 141 Hanahan, D. Studies on transformation of Escherichia coli with plasmids. *J Mol Biol* **166**, 557-580, (1983).
- 142 Edelheit, O., Hanukoglu, A. & Hanukoglu, I. Simple and efficient site-directed mutagenesis using two single-primer reactions in parallel to generate mutants for protein structure-function studies. *BMC Biotechnol* **9**, 61, (2009).
- 143 Kushner, S. An improved method for transformation of Escherichia coli with ColEI-derived plasmids. *Genetic engineering*, (1978).
- 144 Mandel, M. & Higa, A. Calcium-dependent bacteriophage DNA infection. *Journal of Molecular Biology* **53**, 159-162, (1970).
- 145 Inoue, H., Nojima, H. & Okayama, H. High efficiency transformation of Escherichia coli with plasmids. *Gene* **96**, 23-28, (1990).
- 146 MacConkey, A. Lactose-fermenting bacteria in feces. *J. Hyg.* **3**, (1905).
- 147 Farmer, J. J., 3rd & Davis, B. R. H7 antiserum-sorbitol fermentation medium: a single tube screening medium for detecting Escherichia coli O157:H7 associated with hemorrhagic colitis. *J Clin Microbiol* **22**, 620-625, (1985).
- 148 Syldatk, C., Lang, S., Matulovic, U. & Wagner, F. Production of four interfacial active rhamnolipids from n-alkanes or glycerol by resting cells of Pseudomonas species DSM 2874. *Z Naturforsch C* **40**, 61-67, (1985).
- 149 Scheidle, M. *et al.* Controlling pH in shake flasks using polymer-based controlled-release discs with pre-determined release kinetics. *BMC Biotechnol* **11**, 25, (2011).
- 150 Tamai, E., Shimamoto, T., Tsuda, M., Mizushima, T. & Tsuchiya, T. Conversion of Temperature-sensitive to -resistant Gene Expression Due to Mutations in the Promoter Region of

- the Melibiose Operon in *Escherichia coli*. *Journal of Biological Chemistry* **273**, 16860-16864, (1998).
- 151 Brandolin, G. D., J; Gulik, A; Gulik-Krzywicki, T; Lauquin, GJ and Vignais PV. Kinetic, binding and ultrastructural properties of the beef heart adenine nucleotide carrier protein after incorporation into phospholipid vesicles. *Biochim. Biophys. Acta* **592**, 592-614, (1980).
- 152 Allen, T. M., Romans, A. Y., Kercret, H. & Segrest, J. P. Detergent removal during membrane reconstitution. *Biochimica et Biophysica Acta (BBA) - Biomembranes* **601**, 328-342, (1980).
- 153 Hertzberg, E. L. & Hinkle, P. C. Oxidative phosphorylation and proton translocation in membrane vesicles prepared from *Escherichia coli*. *Biochemical and Biophysical Research Communications* **58**, 178-184, (1974).
- 154 Reenstra, W. W., Patel, L., Rottenberg, H. & Kaback, H. R. Electrochemical proton gradient in inverted membrane vesicles from *Escherichia coli*. *Biochemistry* **19**, 1-9, (1980).
- 155 Short, S. A., Kaback, H. R. & Kohn, L. D. Localization of D-lactate dehydrogenase in native and reconstituted *Escherichia coli* membrane vesicles. *Journal of Biological Chemistry* **250**, 4291-4296, (1975).
- 156 Kaback, H. R. & Barnes, E. M. Mechanisms of Active Transport in Isolated Membrane Vesicles. *Journal of Biological Chemistry* **246**, 5523-5531, (1971).
- 157 Laemmli, U. K. Cleavage of structural proteins during the assembly of the head of bacteriophage T4. *Nature* **227**, 680-685, (1970).
- 158 Lowry, O. H., Rosebrough, N. J., Farr, A. L. & Randall, R. J. PROTEIN MEASUREMENT WITH THE FOLIN PHENOL REAGENT. *Journal of Biological Chemistry* **193**, 265-275, (1951).
- 159 Goormaghtigh, E., Cabiaux, V. & Ruysschaert, J. M. Determination of soluble and membrane protein structure by Fourier transform infrared spectroscopy. I. Assignments and model compounds. *Subcell Biochem* **23**, 329-362, (1994).
- 160 Arrondo, J. L. R. & Goñi, F. M. Structure and dynamics of membrane proteins as studied by infrared spectroscopy. *Progress in Biophysics and Molecular Biology* **72**, 367-405, (1999).
- 161 Barth, A. & Zscherp, C. What vibrations tell us about proteins. *Q Rev Biophys* **35**, 369-430, (2002).
- 162 Tatulian, S. A. Attenuated total reflection Fourier transform infrared spectroscopy: a method of choice for studying membrane proteins and lipids. *Biochemistry* **42**, 11898-11907, (2003).
- 163 Lorenz-Fonfria, V. A. *et al.* Structural and functional implications of the instability of the ADP/ATP transporter purified from mitochondria as revealed by FTIR spectroscopy. *Biophys J* **85**, 255-266, (2003).
- 164 Torres, J. & Padrós, E. Spectroscopic studies of bacteriorhodopsin fragments dissolved in organic solution. *Biophysical Journal* **68**, 2049-2055, (1995).
- 165 Barth, A. & Zscherp, C. Substrate binding and enzyme function investigated by infrared spectroscopy. *FEBS Letters* **477**, 151-156, (2000).
- 166 Rothschild, K. J. *et al.* Asp96 deprotonation and transmembrane alpha-helical structural changes in bacteriorhodopsin. *Journal of Biological Chemistry* **268**, 27046-27052, (1993).
- 167 Rothschild, K. J. FTIR difference spectroscopy of bacteriorhodopsin: toward a molecular model. *J Bioenerg Biomembr* **24**, 147-167, (1992).
- 168 Goormaghtigh, E., Cabiaux, V. & Ruysschaert, J. M. Determination of soluble and membrane protein structure by Fourier transform infrared spectroscopy. II. Experimental aspects, side chain structure, and H/D exchange. *Subcell Biochem* **23**, 363-403, (1994).
- 169 Goormaghtigh, E., Cabiaux, V. & Ruysschaert, J. M. Determination of soluble and membrane

- protein structure by Fourier transform infrared spectroscopy. III. Secondary structures. *Subcell Biochem* **23**, 405-450, (1994).
- 170 Barth, A. Infrared spectroscopy of proteins. *Biochimica et Biophysica Acta (BBA) - Bioenergetics* **1767**, 1073-1101, (2007).
- 171 Furutani, Y., Murata, T. & Kandori, H. Sodium or Lithium Ion-Binding-Induced Structural Changes in the K-Ring of V-ATPase from *Enterococcus hirae* Revealed by ATR-FTIR Spectroscopy. *Journal of the American Chemical Society* **133**, 2860-2863, (2011).
- 172 Griffiths, P. d. H., JA. *Transform Infrared Spectrometry*. Vol. 2 (Wiley, 2007).
- 173 Pike Technologies. ATR - Theory and Applications. *PIKE Technologies technical bulletin*, (2005).
- 174 de Jongh, H. H. J., Goormaghtigh, E. & Ruyschaert, J.-M. The Different Molar Absorptivities of the Secondary Structure Types in the Amide I Region: An Attenuated Total Reflection Infrared Study on Globular Proteins. *Analytical Biochemistry* **242**, 95-103, (1996).
- 175 Scheirlinckx, F., Raussens, V., Ruyschaert, J. M. & Goormaghtigh, E. Conformational changes in gastric H<sup>+</sup>/K<sup>+</sup>-ATPase monitored by difference Fourier-transform infrared spectroscopy and hydrogen/deuterium exchange. *Biochem J* **382**, 121-129, (2004).
- 176 Vasilescu, V. & Katona, E. Deuteration as a tool in investigating the role of water in the structure and function of excitable membranes. *Methods Enzymol* **127**, 662-678, (1986).
- 177 Heimburg, T. & Marsh, D. Investigation of secondary and tertiary structural changes of cytochrome c in complexes with anionic lipids using amide hydrogen exchange measurements: an FTIR study. *Biophys J* **65**, 2408-2417, (1993).
- 178 Marsh, D. Spin-label electron spin resonance and Fourier transform infrared spectroscopy for structural/dynamic measurements on ion channels. *Methods Enzymol* **294**, 59-92, (1999).
- 179 Marsh, D., Muller, M. & Schmitt, F. J. Orientation of the infrared transition moments for an alpha-helix. *Biophys J* **78**, 2499-2510, (2000).
- 180 Goormaghtigh, E., Raussens, V. & Ruyschaert, J. M. Attenuated total reflection infrared spectroscopy of proteins and lipids in biological membranes. *Biochim Biophys Acta* **1422**, 105-185, (1999).
- 181 Steele, D. in *Handbook of Vibrational Spectroscopy* (John Wiley & Sons, Ltd, 2006).
- 182 Gross, P. C. & Zeppezauer, M. Infrared spectroscopy for biopharmaceutical protein analysis. *J Pharm Biomed Anal* **53**, 29-36, (2010).
- 183 Jackson, M. & Mantsch, H. H. Beware of proteins in DMSO. *Biochim Biophys Acta* **1078**, 231-235, (1991).
- 184 Jackson, M., Haris, P. I. & Chapman, D. Fourier transform infrared spectroscopic studies of Ca(2<sup>+</sup>)-binding proteins. *Biochemistry* **30**, 9681-9686, (1991).
- 185 Lórenz-Fonfría, V. c. A. & Padrós, E. Curve-fitting of Fourier manipulated spectra comprising apodization, smoothing, derivation and deconvolution. *Spectrochimica Acta Part A: Molecular and Biomolecular Spectroscopy* **60**, 2703-2710, (2004).
- 186 Lakowicz, J. Principles of Fluorescence Spectroscopy. **2nd**, (1999).
- 187 Haugland, R. Handbook of fluorescent probes and research products. (2002).
- 188 Ganea, C., Pourcher, T., Leblanc, G. & Fendler, K. Evidence for intraprotein charge transfer during the transport activity of the melibiose permease from *Escherichia coli*. *Biochemistry* **40**, 13744-13752, (2001).
- 189 Merrick, M. F. & Pardue, H. L. Evaluation of absorption and first- and second-derivative spectra for simultaneous quantification of bilirubin and hemoglobin. *Clin Chem* **32**, 598-602, (1986).
- 190 Schuldiner, S., Kerwar, G. K., Kaback, H. R. & Weil, R. Energy-dependent binding of

- dansylgalactosides to the beta-galactoside carrier protein. *J Biol Chem* **250**, 1361-1370, (1975).
- 191 Schuldiner, S., Kung, H., Kaback, H. R. & Weil, R. Differentiation between binding and transport of dansylgalactosides in Escherichia coli. *J Biol Chem* **250**, 3679-3682, (1975).
- 192 Schuldiner, S. & Kaback, H. R. Fluorescent galactosides as probes for the lac carrier protein. *Biochim Biophys Acta* **472**, 399-418, (1977).
- 193 Kaback, H. R. Active transport in Escherichia coli: passage to permease. *Annu Rev Biophys Chem* **15**, 279-319, (1986).
- 194 Kawakami, T. *et al.* Amino acid substitutions and alteration in cation specificity in the melibiose carrier of Escherichia coli. *J Biol Chem* **263**, 14276-14280, (1988).
- 195 Lórenz-Fonfría, V., Perálvarez-Marín, A., Padrós, E. & Lazarova, T. in *Production of Membrane Proteins* 317-360 (Wiley-VCH Verlag GmbH & Co. KGaA, 2011).
- 196 Moll, A. H., A.; Lenhof, H.P.; Kohlbacher, O. . BALLView: an object-oriented molecular visualization and modeling framework. *J Comput Aided Mol Des.* **19**, 791-800, (2005).
- 197 Honig, B. H. & Hubbell, W. L. Stability of "salt bridges" in membrane proteins. *Proc Natl Acad Sci U S A* **81**, 5412-5416, (1984).
- 198 Lee, J. I., Hwang, P. P. & Wilson, T. H. Lysine 319 interacts with both glutamic acid 269 and aspartic acid 240 in the lactose carrier of Escherichia coli. *J Biol Chem* **268**, 20007-20015, (1993).
- 199 Frillingos, S. & Kaback, H. R. Chemical rescue of Asp237-->Ala and Lys358-->Ala mutants in the lactose permease of Escherichia coli. *Biochemistry* **35**, 13363-13367, (1996).
- 200 Ma, C. *et al.* Identification of the substrate binding sites within the yeast mitochondrial citrate transport protein. *J Biol Chem* **282**, 17210-17220, (2007).
- 201 Knol, J., Sjollem, K. & Poolman, B. Detergent-Mediated Reconstitution of Membrane Proteins<sup>†</sup>. *Biochemistry* **37**, 16410-16415, (1998).
- 202 Billman, G. *Novel therapeutic targets for antiarrhythmic drugs.* (Wiley, 2010).
- 203 Craven, K. B. & Zagotta, W. N. CNG and HCN channels: two peas, one pod. *Annu Rev Physiol* **68**, 375-401, (2006).
- 204 Murer, H., Forster, I. C. & Biber, J. The sodium phosphate cotransport family SLC34. *Eur J Physiol*, 763, (2004).
- 205 Grunewald, M. & Kanner, B. I. The Accessibility of a Novel Reentrant Loop of the Glutamate Transporter GLT-1 Is Restricted by Its Substrate. *Journal of Biological Chemistry* **275**, 9684-9689, (2000).
- 206 Chenna, R. S., H; Koike, T; Lopez, R; Gibson, TJ; Higgins, DG; Thompson, JD. Multiple sequence alignment with the Clustal series of programs. *Nucleic Acids Res.* **31**, 3497-3500, (2003).
- 207 Conseil, G., Rothnie, A. J., Deeley, R. G. & Cole, S. P. C. Multiple Roles of Charged Amino Acids in Cytoplasmic Loop 7 for Expression and Function of the Multidrug and Organic Anion Transporter MRP1 (ABCC1). *Molecular Pharmacology* **75**, 397-406, (2009).
- 208 Okuda, K. *et al.* Functional significance of the E loop, a novel motif conserved in the lantibiotic immunity ATP-binding cassette transport systems. *J Bacteriol* **192**, 2801-2808, (2010).
- 209 Pourcher, T., Bassilana, M., Sarkar, H. K., Kaback, H. R. & Leblanc, G. The melibiose/Na<sup>+</sup> symporter of Escherichia coli: kinetic and molecular properties. *Philos Trans R Soc Lond B Biol Sci* **326**, 411-423, (1990).
- 210 Pourcher, T., Sarkar, H. K., Bassilana, M., Kaback, H. R. & Leblanc, G. Histidine-94 is the only important histidine residue in the melibiose permease of Escherichia coli. *Proc Natl Acad Sci U S A* **87**, 468-472, (1990).
- 211 Jones, P. M. & George, A. M. Mechanism of ABC transporters: a molecular dynamics simulation

- of a well characterized nucleotide-binding subunit. *Proc Natl Acad Sci U S A* **99**, 12639-12644, (2002).
- 212 Keller, T. *et al.* The large extracellular loop of organic cation transporter 1 influences substrate affinity and is pivotal for oligomerization. *Journal of Biological Chemistry*, (2011).
- 213 Dobrowolski, A. & Lolkema, J. S. Functional Importance of GGXG Sequence Motifs in Putative Reentrant Loops of 2HCT and ESS Transport Proteins. *Biochemistry* **48**, 7448-7456, (2009).
- 214 Xu, L., Li, Y., Haworth, I. S. & Davies, D. L. Functional role of the intracellular loop linking transmembrane domains 6 and 7 of the human dipeptide transporter hPEPT1. *J Membr Biol* **238**, 43-49, (2010).
- 215 Zhang, Y.-W. & Rudnick, G. Cysteine scanning mutagenesis of serotonin transporter intracellular loop 2 suggests an alpha-helical conformation. *Journal of Biological Chemistry*, (2005).
- 216 Chen, N., Ferrer, J. V., Javitch, J. A. & Justice, J. B., Jr. Transport-dependent Accessibility of a Cytoplasmic Loop Cysteine in the Human Dopamine Transporter. *J. Biol. Chem.* **275**, 1608-1614, (2000).
- 217 Marmé, N., Knemeyer, J.-P., Sauer, M. & Wolfrum, J. Inter- and Intramolecular Fluorescence Quenching of Organic Dyes by Tryptophan. *Bioconjugate Chemistry* **14**, 1133-1139, (2003).
- 218 Abramson, J. *et al.* Structure and mechanism of the lactose permease of *Escherichia coli*. *Science* **301**, 610-615, (2003).

## ACKNOWLEDGEMENTS

Reflecting the last four year, I spend one of the best times of my life doing my PhD at the Unitat de Biofísica at the autonomous University of Barcelona. I remember my arrival on September the 15<sup>th</sup> in 2008 as it was yesterday. After an endless journey by car that started in Devon, UK, I arrived at the campus from the UAB in Bellaterra. Throughout the 2-days-trip, I was crossing my fingers half-way through France. Near Clermont-Ferrand my exhaust was literally falling into pieces. But eventually I made just in time.

Well to start with, I want to express my gratitude to Prof. Esteve Padrós Morell for his personal tutoring and mentoring of the thesis, for his help and advice during these four years especially in terms of spectroscopy and physics in general. He was the decisive factor to start a PhD in Catalunya in the first place. Without him as a director of the work, I would not have conceded the fellowship from the Spanish government. I also want to thank him for the flexibility of my working hours. Moltes gracies!

Dr. Victor Lórenz-Fonfria deserves a very special dedication. Even though, he had to leave the unit before I could have finished my work, I deeply admire his spectroscopic knowledge, his accuracy for data analysis and skills in writing scientifically. I am honestly grateful about the numerous suggestions he gave me to get insights of the MelB mutants by infrared difference spectroscopy. Also his home-made matlab programs were basic parts of my PhD thesis. Thanks a lot.

Yibin, a special thanks goes directly to you. I am grateful for the fruitful discussion we had so many times. Your dedication for the crystallization of MelB resulted in the first protein crystals in October 2010 and subsequently we were able to reduce the resolution from 20 Å to 8 Å. Also the established protocol for the preparation of membrane vesicles was very helpful. Together with the two Jordi, we had so much fun on the trips to the Synchrotron in Grenoble which I will certainly remember. For the future as a Post-Doc, I wish you all the best, wherever it may be. We were a great team.

Elodia, muchísimas gracias por tu ayuda en pedir productos de laboratorio de nuestro grupo. Seguramente, no me voy a olvidar cuantas veces nosotros hemos buscado nitrógeno líquido para infrarojo. También en los llamados a técnicos o empresas eran cosas que me has facilitado la vida profundamente. Gracias!

Neusita, tu mereces unas palabras especiales aquí. MUCHÍSIMAS GRACIAS por toda tu trabajo en el laboratorio durante este tiempo. No me acuerdo cuantos litros de medios has preparado o los tampones de infrarojo o de la purificación y muchas cosas más. Gracias por tu apollo cuando no salían las cosas o cuando no he conseguido proteína después de una purificación muy larga.

My buddy, Asrar!!! I guess I lost count of the occasions we went for coffee together. Most of

the times, we just shared the lab myseries when the experiments were as expected. Thanks for the intellectual speeches you have given so many times. I am going to miss them.

Moltes gracies a la gent del laboratori. Especialment al grup dels catenines amb Bea, Gabriela, Montse, Erito i Txell. Els millors!

Thanks as well to my labmates Arash, Pablo, Rosana, Meritxell, Dr. Alejandro Peralvarez-Marin and Dr. Jose Luis Vasquez-Ibar, it was always a pleasure to spend time with you in the lab and struggle for a place on the bench.

Con mis compañeros del despacho Mijael, Oksana, Guillem y Silvia era siempre una atmosfera muy tranquilo que te dar fuerzas para trabajo concentrado. Muchas gracias a vosotros!

Edu y Marta, mis estudiantes!!! Cuantas veces he intentado de explicar infrarojo

An dieser Stelle ganz besonders bedanken möchte ich mich bei meiner Familie. Meiner Mama Marietta und ihrem Heinz witme ich diese Arbeit in ganz besonderer Weise.

Auch wenn wir diese vier Jahre getrennt voneinander gelebt haben, so konnten wir uns trotzdem jeden Sonntag per Skype unterhalten. Ihr habt mir viel Zuversicht und Vertrauen geschenkt. Wenn ich enttäuscht über die aktuellen Experimente und Ergebnisse war, habt ihr mich wieder ermuntert weiter zumachen. Das hat wieder neue Kräfte freigesetzt die mich bis hier haben kommen lassen.

Auch mein Schwesterherz Antje, mein Schwager Oliver, meine Nichte Lisann und vorallem mein Patentkind Maximilian haben großen Anteil am erfolgreichen Abschluss dieser Arbeit. Im halbjährlichen Deutschland-Aufenthalt war es mir immer wichtig Zeit mit Euch in Kassel zu verbringen um auf andere Gedanken zu kommen. Vielen Dank für den Besuch im vergangenen Oktober. Der tolle Strandtag in Sitges, die Spaziergänge mit leckerem Eis durch Barcelona und vor allem das Spiel von Barca gegen Santander waren sicherlich nicht nur für mich besondere Momente. Dieser Kurzurlaub in Barcelona war eine kleine Ablenkung, während der schwierigen Behandlung von Max' Erkrankung. Zum Glück ist der Heilungsprozess gut verlaufen und wir können auf bessere Tag hoffen.

Muchas Gracias quiero decir tambien a Modesto, Conchita, Paula y Fulgencia. Vosotros me habeis ayudado tanto durante los últimos años cuando mi Anna no estaba a mi lado y yo tenia que "sobrevivir" solo en Barcelona. Conchi, más paella por favor! Y Paula, cuando te queda un tiempo libre, podemos jugar a tenis otra vez.

The last chapter is dedicated to you, Anna, mein Mäuschen. If it wouldn't have been for you, nothing else could have kept me going all the way to the end of the thesis. Thanks a million for your patience, your criticism, your kindness and above all your love. Because of a common friend, la Mercé, I got to know you almost three years ago. The best that ever happened to me. We share already a lot of memories of trips to Germany, Amsterdam and Montreal and I hope many more are about to come. After your departure last year to Montreal, we had to suffer not being close to each other every day and both were suffering in that long distance relationship in different time zones. Thanks to "Skype", I could tell what you had for breakfast on a Sunday morning and you have seen me sleepy at night in front of the screen while you were seated close to the confocal

microscope. I cannot imagine how we would have made it without the daily chatting. That is why I am looking forward to a bright future for us together in Canada.

**Oliver Fürst**  
**CEB – Centre d'Estudis en**  
**Biofísica**  
**Universitat Autònoma de**  
**Barcelona**